



HAL
open science

Mathematical modelling of tsunami waves

Denys Dutykh

► **To cite this version:**

Denys Dutykh. Mathematical modelling of tsunami waves. Mathematics [math]. École normale supérieure de Cachan - ENS Cachan, 2007. English. NNT: . tel-00194763v2

HAL Id: tel-00194763

<https://theses.hal.science/tel-00194763v2>

Submitted on 21 Jan 2008

HAL is a multi-disciplinary open access archive for the deposit and dissemination of scientific research documents, whether they are published or not. The documents may come from teaching and research institutions in France or abroad, or from public or private research centers.

L'archive ouverte pluridisciplinaire **HAL**, est destinée au dépôt et à la diffusion de documents scientifiques de niveau recherche, publiés ou non, émanant des établissements d'enseignement et de recherche français ou étrangers, des laboratoires publics ou privés.



N° ENSC-2007/76



**THÈSE DE DOCTORAT
DE L'ÉCOLE NORMALE SUPÉRIEURE DE CACHAN**

Présentée par

Denys DUTYKH

pour obtenir le grade de

**DOCTEUR DE L'ÉCOLE NORMALE SUPÉRIEURE DE
CACHAN**

Domaine:

Mathématiques Appliquées

Sujet de la thèse:

MODÉLISATION MATHÉMATIQUE DES TSUNAMIS

Thèse présentée et soutenue à Cachan le 3 décembre 2007 devant le jury composé de:

M. Jean-Michel GHIDAGLIA	Examineur
M. Jean-Claude SAUT	Rapporteur et Président
M. Didier BRESCH	Rapporteur
M. Costas SYNOLAKIS	Examineur
M. Vassilios DOUGALIS	Examineur
M. Daniel BOUCHE	Membre invité
M. Frédéric DIAS	Directeur de thèse

Centre de Mathématiques et de Leurs Applications
ENS CACHAN/CNRS/UMR 8536
61, avenue du Président Wilson, 94235 CACHAN CEDEX (France)

To my parents, my sister and A.M.

Remerciements

Je tiens à remercier, en tout premier lieu, Frédéric Dias qui a encadré ce travail. Il m'a beaucoup soutenu et encouragé au cours de ces magnifiques années de recherche. Je lui en suis très profondément reconnaissant.

Je remercie tout particulièrement Jean-Michel Ghidaglia qui m'a beaucoup guidé dans mes recherches. Je tiens à souligner que par sa grande disponibilité, j'ai pu bénéficier de ses très grandes compétences scientifiques tout au long de mes investigations. Enfin, c'est un honneur pour moi qu'il ait accepté de présider le jury de cette thèse.

J'exprime ma gratitude aux Professeurs Jean-Claude Saut et Didier Bresch, qui ont accepté d'être les rapporteurs, ainsi qu'aux Professeurs Costas Synolakis et Vassilios Dougalis pour leur intérêt qu'ils ont porté à mon travail en ayant accepté de faire partie du jury.

Mes trois années de thèse se sont déroulées dans un contexte scientifique de grande qualité au Centre de Mathématiques et de Leurs Applications de l'ENS Cachan. Je remercie son directeur Laurent Desvillettes de m'avoir accueilli et d'avoir créé d'excellentes conditions de travail. Parmi tout le personnel de ce laboratoire je voudrais plus particulièrement remercier Micheline Brunetti pour son aimabilité et efficacité dans le traitement des questions administratives.

Je remercie Frédéric Pascal pour son tutorat pédagogique. Ses conseils m'ont beaucoup servis lors de trois ans d'enseignement du calcul scientifique aux agrégatifs de l'ENS Cachan. J'en profite aussi pour remercier tous mes élèves de leur assiduité et intelligence.

J'exprime mes plus vifs remerciements à Daniel Bouche de m'avoir accueilli au sein de LRC CEA/CMLA. Ses remarques pertinentes et conseils avisés, sa gentillesse m'ont beaucoup aidé et motivé durant le DEA MN2MC et plus particulièrement pendant la réalisation de cette thèse.

Parmi tous mes collègues de LRC, Christophe Fochesato, Jean-Michel Rovarch et Denis Gueyffier ont occupé une place très particulière: en plus de leur amitié, ils m'ont offert de nombreux conseils amicaux et professionnels. Je vous en remercie très sincèrement.

Parmi les personnes qui ont contribué à ma formation, je suis tout particulièrement reconnaissant envers Vladimir Lamzyuk qui m'a fait découvrir le monde de la modélisation mathématique et des mathématiques appliquées en général. Il m'a soutenu constamment durant mes études à l'Université Nationale de Dnipropétrovsk.

Mes pensées vont également à tous mes concurrents qui m'ont constamment poussé dans mes recherches et m'ont donné les forces pour continuer ce travail.

Je dis grand merci à Yann, Joachim, Lavinia, Serge, Nanthilde, Thomas, Alexandra et aux autres doctorants du LMT pour leur amitié et tous les instants de détente partagés ensemble. Je tiens à remercier particulièrement Alexandra Pradeau de nos discussions passionnantes ainsi qu'enrichissantes. Sans ces personnes cette thèse n'aurait pas eu la même saveur.

Je remercie ma famille et leur dédie cette thèse pour leurs encouragements permanents et toutes autres raisons qui s'imposent.

Je conclurai en remerciant de tout coeur Anna Maria pour la patience et le soutien sans limite dont elle fait preuve quotidiennement.

Résumé

Cette thèse est consacrée à la modélisation des tsunamis. La vie de ces vagues peut être conditionnellement divisée en trois parties: génération, propagation et inondation. Dans un premier temps, nous nous intéressons à la génération de ces vagues extrêmes. Dans cette partie du mémoire, nous examinons les différentes approches existantes pour la modélisation, puis nous en proposons d'autres. La conclusion principale à laquelle nous sommes arrivés est que le couplage entre la sismologie et l'hydrodynamique est actuellement assez mal compris.

Le deuxième chapitre est dédié essentiellement aux équations de Boussinesq qui sont souvent utilisées pour modéliser la propagation d'un tsunami. Certains auteurs les utilisent même pour modéliser le processus d'inondation (le run-up). Plus précisément, nous discutons de l'importance, de la nature et de l'inclusion des effets dissipatifs dans les modèles d'ondes longues.

Dans le troisième chapitre, nous changeons de sujet et nous nous tournons vers les écoulements diphasiques. Le but de ce chapitre est de proposer un modèle simple et opérationnel pour la modélisation de l'impact d'une vague sur les structures côtières. Ensuite, nous discutons de la discrétisation numérique de ces équations avec un schéma de type volumes finis sur des maillages non structurés.

Finalement, le mémoire se termine par un sujet qui devrait être présent dans tous les manuels classiques d'hydrodynamique mais qui ne l'est pas. Nous parlons des écoulements viscopotentiels. Nous proposons une nouvelle approche simplifiée pour les écoulements faiblement visqueux. Nous conservons la simplicité des écoulements potentiels tout en ajoutant la dissipation. Dans le cas de la profondeur finie nous incluons un terme correcteur dû à la présence de la couche limite au fond. Cette correction s'avère être non locale en temps. Donc, la couche limite au fond apporte un certain effet de mémoire à l'écoulement.

Mots clés: Ondes de surface, génération des tsunamis, équations de Boussinesq, écoulements diphasiques, écoulements viscopotentiels, volumes finis

Abstract

This thesis is devoted to tsunami wave modelling. The life of tsunami waves can be conditionally divided into three parts: generation, propagation and inundation (or run-up). In the first part of the manuscript we consider the generation process of such extreme waves. We examine various existing approaches to its modelling. Then we propose a few alternatives. The main conclusion is that the seismology/hydrodynamics coupling is poorly understood at the present time.

The second chapter essentially deals with Boussinesq equations which are often used to model tsunami propagation and sometimes even run-up. More precisely, we discuss the importance, nature and inclusion of dissipative effects in long wave models.

In the third chapter we slightly change the subject and turn to two-phase flows. The main purpose of this chapter is to propose an operational and simple set of equations in order to model wave impacts on coastal structures. Another important application includes wave sloshing in liquified natural gas carriers. Then, we discuss the numerical discretization of governing equations in the finite volume framework on unstructured meshes.

Finally, this thesis deals with a topic which should be present in any textbook on hydrodynamics but it is not. We mean visco-potential flows. We propose a novel and sufficiently simple approach for weakly viscous flow modelling. We succeeded in keeping the simplicity of the classical potential flow formulation with the addition of viscous effects. In the case of finite depth we derive a correction term due to the presence of the bottom boundary layer. This term is nonlocal in time. Hence, the bottom boundary layer introduces a memory effect to the governing equations.

Keywords: Water waves, tsunami generation, Boussinesq equations, two-phase flows, visco-potential flows, finite volumes

Contents

Remerciements	i
Contents	vii
List of Figures	xiii
List of Tables	xv
Introduction	xvii
Propagation of tsunamis	xviii
Classical formulation	xx
Dimensionless equations	xxi
Shallow-water equations	xxi
Boussinesq equations	xxiii
Korteweg–de Vries equation	xxvi
Energy of a tsunami	xxvi
Tsunami run-up	xxvii
1 Tsunami generation	1
1.1 Waves generated by a moving bottom	2
1.1.1 Source model	4
1.1.2 Volterra’s theory of dislocations	5
1.1.3 Dislocations in elastic half-space	6
1.1.3.1 Finite rectangular source	10
1.1.3.2 Curvilinear fault	12
1.1.4 Solution in fluid domain	16
1.1.5 Free-surface elevation	21
1.1.6 Velocity field	25
1.1.6.1 Pressure on the bottom	28
1.1.7 Asymptotic analysis of integral solutions	29

1.1.8	Numerical results	31
1.2	Comparison of tsunami generation models	36
1.2.1	Physical problem description	37
1.2.2	Linear theory	43
1.2.3	Active generation	44
1.2.4	Passive generation	44
1.2.4.1	Numerical method for the linear problem	47
1.2.5	Nonlinear shallow water equations	47
1.2.6	Mathematical model	48
1.2.7	Numerical method	50
1.2.8	Numerical method for the full equations	50
1.2.9	Comparisons and discussion	51
1.2.10	Conclusions	64
1.3	Tsunami generation by dynamic displacement of sea bed	64
1.3.1	Introduction	64
1.3.2	Mathematical models	67
1.3.2.1	Dynamic fault model	67
1.3.2.2	Fluid layer model	69
1.3.3	Numerical methods	70
1.3.3.1	Discretization of the viscoelastodynamic equations	70
1.3.3.2	Finite-volume scheme	71
1.3.4	Validation of the numerical method	72
1.3.5	Results of the simulation	73
1.3.6	Conclusions	78
2	Dissipative Boussinesq equations	81
2.1	Introduction	82
2.2	Derivation of the Boussinesq equations	85
2.2.1	Asymptotic expansion	89
2.3	Analysis of the linear dispersion relations	93
2.3.1	Linearized potential flow equations	93
2.3.2	Dissipative Boussinesq equations	95
2.3.3	Discussion	99
2.4	Alternative version of the Boussinesq equations	99
2.4.1	Derivation of the equations	100
2.5	Improvement of the linear dispersion relations	104
2.6	Regularization of Boussinesq equations	105
2.7	Bottom friction	107

2.8	Spectral Fourier method	108
2.8.1	Validation of the numerical method	110
2.9	Numerical results	113
2.9.1	Construction of the initial condition	113
2.9.2	Comparison between the dissipative models	115
2.10	Conclusions	119
3	Two phase flows	121
3.1	Introduction	122
3.2	Mathematical model	125
3.2.1	Sound speed in the mixture	126
3.2.2	Equation of state	127
3.3	Formal limit in barotropic case	129
3.4	Finite volume scheme on unstructured meshes	131
3.4.1	Sign matrix computation	136
3.4.2	Second order scheme	137
3.4.2.1	Historical remark	137
3.4.3	TVD and MUSCL schemes	138
3.4.3.1	Green-Gauss gradient reconstruction	140
3.4.3.2	Least-squares gradient reconstruction method	141
3.4.3.3	Slope limiter	143
3.4.4	Diffusive fluxes computation	144
3.4.5	Solution interpolation to mesh nodes	146
3.4.6	Time stepping methods	148
3.4.7	Boundary conditions treatment	151
3.5	Numerical results	153
3.5.1	Convergence test	154
3.5.2	Falling water column	157
3.5.3	Water drop test case	157
3.6	Conclusions	162
4	Viscous potential flows	169
4.1	Introduction	169
4.2	Anatomy of dissipation	172
4.3	Derivation	174
4.3.1	Dissipative KdV equation	179
4.4	Dispersion relation	180
4.4.1	Discussion	182

4.5	Attenuation of linear progressive waves	182
4.6	Numerical results	187
4.6.1	Approximate solitary wave solution	187
4.6.2	Discussion	189
4.7	Conclusion	192
	Direction for future research	195
A	VFFC scheme	197
A.1	Discretization in the finite volume framework	198
A.1.1	The one dimensional case	198
A.1.2	Extension to the multidimensional case	201
A.1.3	On the discretization of source terms	202
A.2	On the discretization of boundary conditions	204
	Bibliography	206

List of Figures

1.1	Coordinate system adopted in this study.	7
1.2	Illustration for strike angle definition.	8
1.3	Geometry of the source model.	11
1.4	Dip-slip fault	13
1.5	Strike-slip fault	14
1.6	Tensile fault	14
1.7	Geometry of a fault with elliptical shape	15
1.8	Free-surface deformation due to curvilinear faulting	17
1.9	Definition of the fluid domain and coordinate system	17
1.10	Plot of the frequency $\omega(m)$ and its derivatives $d\omega/dm, d^2\omega/dm^2$	21
1.11	Typical graphs of $T_e(t)$ and $T_c(t)$	24
1.12	Free-surface elevation at $t = 0.01, 0.6, 3, 5$ in dimensionless time	33
1.13	Velocity field computed along the free surface at $t = 0.01$	34
1.14	Bottom pressure at $t = 0.01, 0.6, 3, 5$ in dimensionless time	35
1.15	Typical seafloor deformation due to dip-slip faulting	39
1.16	Initial net volume V of the seafloor displacement	39
1.17	Wave profiles at different times for the case of a normal fault	41
1.18	Comparisons of the free-surface elevation for $S = 5$	53
1.19	Comparisons of the free-surface elevation for $S = 0.04$	54
1.20	Top view of the initial free surface deformation	55
1.21	Transient waves generated by an underwater earthquake	56
1.22	Comparisons of the free-surface elevation for $S = 0.005$	58
1.23	Same as Figure 1.22 for later times ($t = 150$ s, $t = 200$ s).	59
1.24	Transient waves generated by an underwater earthquake	60
1.25	Transient waves, the water depth is $h = 500$ m	61
1.26	Same as Figure 1.25, $h = 1$ km	62
1.27	Relative difference between the two solutions - I	63
1.28	Relative difference between the two solutions - II	63

1.29	Geometry of the source model.	66
1.30	Comparison between analytical and numerical solutions	73
1.31	Static deformation due to the dislocation.	74
1.32	Water free surface at the beginning of the earthquake ($t = 2s$).	76
1.33	Same as Figure 1.32 for times $t = 4s$ and $t = 6s$	76
1.34	Same as Figure 1.32 for times $t = 7s$ and $t = 10s$	77
1.35	Same as Figure 1.32 for times $t = 150s$ and $t = 250s$	77
1.36	Same as Figure 1.35 (left plot) for two rupture velocities.	77
1.37	Same as Figure 1.36 at time $t = 250s$	78
1.38	Water free surface at $t = 150s$ for a longer earthquake.	78
2.1	Sketch of the fluid domain	86
2.2	Dissipation model I. Real part of the phase velocity.	96
2.3	Dissipation model I. Zoom on long waves	96
2.4	Dissipation model I. Imaginary part of the frequency.	97
2.5	Dissipation model II. Real part of the phase velocity.	97
2.6	Dissipation model II. Imaginary part of the frequency.	98
2.7	Dissipation model II. Zoom on long waves	98
2.8	Regularized dispersion relation	107
2.9	Error of the numerical method	113
2.10	Solitary wave and a step interaction	116
2.11	Free-surface snapshot before the interaction	116
2.12	Free surface just before the interaction	117
2.13	Beginning of the solitary wave deformation	117
2.14	Initiation of the reflected wave separation	118
2.15	Separation of the reflected wave	118
2.16	Two separate waves moving in opposite directions	119
3.1	Example of water/air mixture after wave breaking.	123
3.2	Sound speed c_s in the water/air mixture at normal conditions.	124
3.3	Sketch of the flow	130
3.4	An example of control volume K	132
3.5	Illustration for cell-centered finite volume method	133
3.6	Illustration for vertex-centered finite volume method	134
3.7	Illustration for Green-Gauss gradient reconstruction	140
3.8	Illustration for least-squares gradient reconstruction.	141
3.9	Diamond cell constructed around face f	144
3.10	Triangles sharing the same vertex N	146

3.11	Linear absolute stability regions	150
3.12	Nonlinear absolute stability regions	150
3.13	Control volume sharing a face with boundary $\partial\Omega$	152
3.14	Shock tube of Sod. This plot represents the density.	153
3.15	Numerical method error in L_∞ norm.	155
3.16	CPU time for different finite volume schemes.	156
3.17	Geometry and initial condition for falling water	157
3.18	The beginning of column dropping process	158
3.19	Splash creation due to the interaction with step	158
3.20	Water strikes the wall - I	159
3.21	Water strikes the wall - II	159
3.22	Splash is climbing the wall	160
3.23	Turbulent mixing process	160
3.24	Maximal pressure on the right wall. Heavy gas case.	161
3.25	Maximal pressure on the right wall as a function of time. Light gas.	162
3.26	Geometry and initial condition for water drop test case	163
3.27	Initial configuration and the beginning of the fall	163
3.28	Drop approaching container bottom	164
3.29	Drop/bottom compressible interaction	164
3.30	Water drop test case. Vertical jets formation	165
3.31	Water drop test case. Side jets crossing	165
3.32	Water drop test case. Side jets interflow at the center	166
3.33	Central jet reflection from the bottom	166
3.34	Water drop test case. Maximal bottom pressure as a function of time.	167
4.1	Conventional partition of the flow region	172
4.2	Real and imaginary part of dispersion curve at $t = 0$	183
4.3	Phase velocity at $t = 1$	184
4.4	Phase velocity at $t = 2$	184
4.5	Phase velocity at $t = 4$	185
4.6	Real part of the phase velocity at $t = 4$	185
4.7	Amplitude of linear progressive waves	188
4.8	Snapshots of the free surface at $t = 0.5$	190
4.9	Snapshots of the free surface at $t = 1.0$	190
4.10	Snapshots of the free surface at $t = 2.0$	191
4.11	Zoom on the soliton crest at $t = 2.0$	191
4.12	Amplitude of the solitary wave as function of time	192

List of Tables

1.1	Parameter set	13
1.2	Parameter set used in Figure 1.8.	16
1.3	Laplace transforms of different time-dependencies	24
1.4	Physical parameters used in the numerical computations	32
1.5	Parameters set for the source model	38
1.6	Typical physical parameters used in the numerical computations.	74
2.1	Typical parameters in tsunami applications	89
2.2	Soliton-step interaction parameters	114
3.1	Parameters for an air/water mixture under normal conditions	128
4.1	Parameters of the linear progressive waves	187
4.2	Parameters used in the numerical computations	188

Introduction

*An expert is a man who has made all the mistakes,
which can be made, in a very narrow field.*

Niels Henrik David Bohr (1885 – 1962)

Contents

Propagation of tsunamis	xviii
Classical formulation	xx
Dimensionless equations	xxi
Shallow-water equations	xxi
Boussinesq equations	xxiii
Korteweg–de Vries equation	xxvi
Energy of a tsunami	xxvi
Tsunami run-up	xxvii

Given the broadness of the topic of tsunamis [DD06], our purpose here is to recall some of the basics of tsunami modeling and to emphasize some general aspects, which are sometimes overlooked. The life of a tsunami is usually divided into three phases: the generation (tsunami source), the propagation and the inundation. The third and most difficult phase of the dynamics of tsunami waves deals with their breaking as they approach the shore. This phase depends greatly on the bottom bathymetry and on the coastline type. The breaking can be progressive. Then the inundation process is relatively slow and can last for several minutes. Structural damages are mainly caused by inundation. The breaking can also be explosive and lead to the formation of a plunging jet. The impact on the coast is then very rapid. In very shallow water, the amplitude of tsunami waves grows to such an extent that typically an undulation appears on the long wave, which develops into a progressive bore [Cha05]. This turbulent front, similar to the wave that occurs when a dam breaks, can be quite high and travel onto the beach at great speed. Then the front and the turbulent current behind it move onto the shore, past buildings and vegetation

until they are finally stopped by rising ground. The water level can rise rapidly, typically from 0 to 3 meters in 90 seconds.

The trajectory of these currents and their velocity are quite unpredictable, especially in the final stages because they are sensitive to small changes in the topography, and to the stochastic patterns of the collapse of buildings, and to the accumulation of debris such as trees, cars, logs, furniture. The dynamics of this final stage of tsunami waves is somewhat similar to the dynamics of flood waves caused by dam breaking, dyke breaking or overtopping of dykes (cf. the recent tragedy of hurricane Katrina in August 2005). Hence research on flooding events and measures to deal with them may be able to contribute to improved warning and damage reduction systems for tsunami waves in the areas of the world where these waves are likely to occur as shallow surge waves (cf. the recent tragedy of the Indian Ocean tsunami in December 2004).

Civil engineers who visited the damage area following the Boxing day tsunami came up with several basic conclusions. Buildings that had been constructed to satisfy modern safety standards offered a satisfactory resistance, in particular those with reinforced concrete beams properly integrated in the frame structure. These were able to withstand pressure associated with the leading front of the order of 1 atmosphere (recall that an equivalent pressure p is obtained with a windspeed U of about 450 m/s, since $p = \rho_{\text{air}}U^2/2$). By contrast brick buildings collapsed and were washed away. Highly porous or open structures survived. Buildings further away from the beach survived the front in some cases, but they were then destroyed by the erosion of the ground around the buildings by the water currents [HB05].

Propagation of tsunamis

The problem of tsunami propagation is a special case of the general water-wave problem. The study of water waves relies on several common assumptions. Some are obvious while some others are questionable under certain circumstances. The water is assumed to be incompressible. Dissipation is not often included. However there are three main sources of dissipation for water waves: bottom friction, surface dissipation and body dissipation. For tsunamis, bottom friction is the most important one, especially in the later stages, and is sometimes included in the computations in an ad-hoc way. In most theoretical analyses, it is not included. The question of dissipation in potential flows and long waves equations is thoroughly investigated in Chapter 4.

A brief description of the common mathematical model used to study water waves follows. The horizontal coordinates are denoted by x and y , and the vertical coordinate

by z . The horizontal gradient is denoted by

$$\nabla := \left(\frac{\partial}{\partial x}, \frac{\partial}{\partial y} \right).$$

The horizontal velocity is denoted by

$$\mathbf{u}(x, y, z, t) = (u, v)$$

and the vertical velocity by $w(x, y, z, t)$. The three-dimensional flow of an inviscid and incompressible fluid is governed by the conservation of mass

$$\nabla \cdot \mathbf{u} + \frac{\partial w}{\partial z} = 0 \quad (1)$$

and by the conservation of momentum

$$\rho \frac{D\mathbf{u}}{Dt} = -\nabla p, \quad \rho \frac{Dw}{Dt} = -\rho g - \frac{\partial p}{\partial z}, \quad (2)$$

where $\frac{Df}{Dt}$ is the material derivative defined as $\frac{Df}{Dt} := \frac{\partial f}{\partial t} + \vec{u} \cdot \nabla f$, $\vec{u} = (\mathbf{u}, w) = (u, v, w)$. In (2), ρ is the density of water (assumed to be constant throughout the fluid domain), g is the acceleration due to gravity and $p(x, y, z, t)$ the pressure field.

The assumption that the flow is irrotational is commonly made to analyze surface waves. Then there exists a scalar function $\phi(x, y, z, t)$ (the velocity potential) such that

$$\mathbf{u} = \nabla \phi, \quad w = \frac{\partial \phi}{\partial z}.$$

The continuity equation (1) becomes

$$\nabla^2 \phi + \frac{\partial^2 \phi}{\partial z^2} = 0. \quad (3)$$

The equation of momentum conservation (2) can be integrated into Bernoulli's equation

$$\frac{\partial \phi}{\partial t} + \frac{1}{2} |\nabla \phi|^2 + \frac{1}{2} \left(\frac{\partial \phi}{\partial z} \right)^2 + gz + \frac{p - p_0}{\rho} = 0, \quad (4)$$

which is valid everywhere in the fluid. The constant p_0 is a pressure of reference, for example the atmospheric pressure. The effects of surface tension are not important for tsunami propagation.

Classical formulation

The surface wave problem consists in solving Laplace's equation (3) in a domain $\Omega(t)$ bounded above by a moving free surface (the interface between air and water) and below by a fixed solid boundary (the bottom).¹ The free surface is represented by $F(x, y, z, t) := \eta(x, y, t) - z = 0$. The shape of the bottom is given by $z = -h(x, y)$. The main driving force is gravity.

The free surface must be found as part of the solution. Two boundary conditions are required. The first one is the kinematic condition. It can be stated as $DF/Dt = 0$ (the material derivative of F vanishes), which leads to

$$\eta_t + \nabla\phi \cdot \nabla\eta - \phi_z = 0 \quad \text{at } z = \eta(x, y, t). \quad (5)$$

The second boundary condition is the dynamic condition which states that the normal stresses must be in balance at the free surface. The normal stress at the free surface is given by the difference in pressure. Bernoulli's equation (4) evaluated on the free surface $z = \eta$ gives

$$\phi_t + \frac{1}{2}|\nabla\phi|^2 + \frac{1}{2}\phi_z^2 + g\eta = 0 \quad \text{at } z = \eta(x, y, t). \quad (6)$$

Finally, the boundary condition at the bottom is

$$\nabla\phi \cdot \nabla h + \phi_z = 0 \quad \text{at } z = -h(x, y). \quad (7)$$

To summarize, the goal is to solve the set of equations (3), (5), (6) and (7) for $\eta(x, y, t)$ and $\phi(x, y, z, t)$. When the initial value problem is integrated, the fields $\eta(x, y, 0)$ and $\phi(x, y, z, 0)$ must be specified at $t = 0$. The conservation of momentum equation (2) is not required in the solution procedure; it is used *a posteriori* to find the pressure p once η and ϕ have been found.

In the following subsections, we will consider various approximations of the full water-wave equations. One is the system of Boussinesq equations, that retains nonlinearity and dispersion up to a certain order. Another one is the system of nonlinear shallow-water equations that retains nonlinearity but no dispersion. The simplest one is the system of linear shallow-water equations. The concept of shallow water is based on the smallness of the ratio between water depth and wavelength. In the case of tsunamis propagating on the surface of deep oceans, one can consider that shallow-water theory is appropriate because the water depth (typically several kilometers) is much smaller than the wavelength (typically several hundred kilometers).

¹The surface wave problem can be easily extended to the case of a moving bottom. This extension may be needed to model tsunami generation if the bottom deformation is relatively slow.

Dimensionless equations

The derivation of shallow-water type equations is a classical topic. Two dimensionless numbers, which are supposed to be small, are introduced:

$$\alpha = \frac{a}{d} \ll 1, \quad \beta = \frac{d^2}{\ell^2} \ll 1, \quad (8)$$

where d is a typical water depth, a a typical wave amplitude and ℓ a typical wavelength. The assumptions on the smallness of these two numbers are satisfied for the Indian Ocean tsunami. Indeed the satellite altimetry observations of the tsunami waves obtained by two satellites that passed over the Indian Ocean a couple of hours after the rupture occurred give an amplitude a of roughly 60 cm in the open ocean. The typical wavelength estimated from the width of the segments that experienced slip is between 160 and 240 km [LKA⁺05]. The water depth ranges from 4 km towards the west of the rupture to 1 km towards the east. These values give the following ranges for the two dimensionless numbers:

$$1.5 \times 10^{-4} < \alpha < 6 \times 10^{-4}, \quad 1.7 \times 10^{-5} < \beta < 6.25 \times 10^{-4}. \quad (9)$$

The equations are more transparent when written in dimensionless variables. The new independent variables are

$$x = \ell \tilde{x}, \quad y = \ell \tilde{y}, \quad z = d \tilde{z}, \quad t = \ell \tilde{t} / c_0, \quad (10)$$

where $c_0 = \sqrt{gd}$, the famous speed of propagation of tsunamis in the open ocean ranging from 356 km/h for a 1 km water depth to 712 km/h for a 4 km water depth. The new dependent variables are

$$\eta = a \tilde{\eta}, \quad h = d \tilde{h}, \quad \phi = g a \ell \tilde{\phi} / c_0. \quad (11)$$

In dimensionless form, and after dropping the tildes, the equations become

$$\beta \nabla^2 \phi + \phi_{zz} = 0, \quad (12)$$

$$\beta \nabla \phi \cdot \nabla h + \phi_z = 0 \quad \text{at } z = -h(x, y), \quad (13)$$

$$\beta \eta_t + \alpha \beta \nabla \phi \cdot \nabla \eta = \phi_z \quad \text{at } z = \alpha \eta(x, y, t), \quad (14)$$

$$\beta \phi_t + \frac{1}{2} \alpha \beta |\nabla \phi|^2 + \frac{1}{2} \alpha \phi_z^2 + \beta \eta = 0 \quad \text{at } z = \alpha \eta(x, y, t). \quad (15)$$

So far, no approximation has been made. In particular, we have not used the fact that the numbers α and β are small.

Shallow-water equations

When β is small, the water is considered to be shallow. The linearized theory of water waves is recovered by letting α go to zero. For the shallow water-wave theory, one assumes

that β is small and expand ϕ in terms of β :

$$\phi = \phi_0 + \beta\phi_1 + \beta^2\phi_2 + \dots$$

This expansion is substituted into the governing equation and the boundary conditions. The lowest-order term in Laplace's equation is

$$\phi_{0zz} = 0. \quad (16)$$

The boundary conditions imply that $\phi_0 = \phi_0(x, y, t)$. Thus the vertical velocity component is zero and the horizontal velocity components are independent of the vertical coordinate z at lowest order. Let $\phi_{0x} = u(x, y, t)$ and $\phi_{0y} = v(x, y, t)$. Assume now for simplicity that the water depth is constant ($h = 1$). Solving Laplace's equation and taking into account the bottom kinematic condition yields the following expressions for ϕ_1 and ϕ_2 :

$$\phi_1(x, y, z, t) = -\frac{1}{2}(1+z)^2(u_x + v_y), \quad (17)$$

$$\phi_2(x, y, z, t) = \frac{1}{24}(1+z)^4[(\nabla^2 u)_x + (\nabla^2 v)_y]. \quad (18)$$

The next step consists in retaining terms of requested order in the free-surface boundary conditions. Powers of α will appear when expanding in Taylor series the free-surface conditions around $z = 0$. For example, if one keeps terms of order $\alpha\beta$ and β^2 in the dynamic boundary condition (15) and in the kinematic boundary condition (14), one obtains

$$\beta\phi_{0t} - \frac{1}{2}\beta^2(u_{tx} + v_{ty}) + \beta\eta + \frac{1}{2}\alpha\beta(u^2 + v^2) = 0, \quad (19)$$

$$\beta[\eta_t + \alpha(u\eta_x + v\eta_y) + (1 + \alpha\eta)(u_x + v_y)] = \frac{1}{6}\beta^2[(\nabla^2 u)_x + (\nabla^2 v)_y]. \quad (20)$$

Differentiating (19) first with respect to x and then to respect to y gives a set of two equations:

$$u_t + \alpha(uu_x + vv_x) + \eta_x - \frac{1}{2}\beta(u_{txx} + v_{txy}) = 0, \quad (21)$$

$$v_t + \alpha(uu_y + vv_y) + \eta_y - \frac{1}{2}\beta(u_{txy} + v_{tyy}) = 0. \quad (22)$$

The kinematic condition (20) can be rewritten as

$$\eta_t + [u(1 + \alpha\eta)]_x + [v(1 + \alpha\eta)]_y = \frac{1}{6}\beta[(\nabla^2 u)_x + (\nabla^2 v)_y]. \quad (23)$$

Equations (21)–(23) contain in fact various shallow-water models. The so-called fundamental shallow-water equations are obtained by neglecting the terms of order β :

$$u_t + \alpha(uu_x + vv_x) + \eta_x = 0, \quad (24)$$

$$v_t + \alpha(uv_x + vv_y) + \eta_y = 0, \quad (25)$$

$$\eta_t + [u(1 + \alpha\eta)]_x + [v(1 + \alpha\eta)]_y = 0. \quad (26)$$

Recall that we assumed h to be constant for the derivation. Going back to an arbitrary water depth and to dimensional variables, the system of nonlinear shallow water equations reads

$$u_t + uu_x + vv_y + g\eta_x = 0, \quad (27)$$

$$v_t + uv_x + vv_y + g\eta_y = 0, \quad (28)$$

$$\eta_t + [u(h + \eta)]_x + [v(h + \eta)]_y = 0. \quad (29)$$

This system of equations has been used for example by Titov and Synolakis for the numerical computation of tidal wave run-up [TS98]. Note that this model does not include any bottom friction terms. To solve the problem of tsunami generation caused by bottom displacement, the motion of the seafloor obtained from seismological models [Oka85] can be prescribed during a time t_0 . Usually t_0 is assumed to be small, so that the bottom displacement is considered as an instantaneous vertical displacement. This assumption may not be appropriate for slow events.

The satellite altimetry observations of the Indian Ocean tsunami clearly show dispersive effects. The question of dispersive effects in tsunamis is open. Most propagation codes ignore dispersion. A few propagation codes that include dispersion have been developed [DGK06]. A well-known code is FUNWAVE, developed at the University of Delaware over the past ten years [KWC+98]. Dispersive shallow water-wave models are presented next.

Boussinesq equations

An additional dimensionless number, sometimes called the Stokes number (in other references it is called Ursell number as well), is introduced:

$$S = \frac{\alpha}{\beta}. \quad (30)$$

For the Indian Ocean tsunami, one finds

$$0.24 < S < 46. \quad (31)$$

Therefore the additional assumption that $S \approx 1$ may be realistic.

In this subsection, we provide the guidelines to derive Boussinesq-type systems of equations [BCS02]. Of course, the variation of bathymetry is essential for the propagation of tsunamis, but for the derivation the water depth will be assumed to be constant. Some notation is introduced. The potential evaluated along the free surface is denoted by $\Phi(x, y, t) := \phi(x, y, \eta, t)$. The derivatives of the velocity potential evaluated on the free surface are denoted by $\Phi_{(*)}(x, y, t) := \phi_{*}(x, y, \eta, t)$, where the star stands for x , y , z or t .

Consequently, Φ_* (defined for $* \neq z$) and $\Phi_{(*)}$ have different meanings. They are however related since

$$\Phi_* = \Phi_{(*)} + \Phi_{(z)}\eta_*.$$

The vertical velocity at the free surface is denoted by $W(x, y, t) := \phi_z(x, y, \eta, t)$.

The boundary conditions on the free surface (5) and (6) become

$$\eta_t + \nabla\Phi \cdot \nabla\eta - W(1 + \nabla\eta \cdot \nabla\eta) = 0, \quad (32)$$

$$\Phi_t + g\eta + \frac{1}{2}|\nabla\Phi|^2 - \frac{1}{2}W^2(1 + \nabla\eta \cdot \nabla\eta) = 0. \quad (33)$$

These two nonlinear equations provide time-stepping for η and Φ . In addition, Laplace's equation as well as the kinematic condition on the bottom must be satisfied. In order to relate the free-surface variables with the bottom variables, one must solve Laplace's equation in the whole water column. In Boussinesq-type models, the velocity potential is represented as a formal expansion,

$$\phi(x, y, z, t) = \sum_{n=0}^{\infty} \phi^{(n)}(x, y, t) z^n. \quad (34)$$

Here the expansion is about $z = 0$, which is the location of the free surface at rest. Demanding that ϕ formally satisfy Laplace's equation leads to a recurrence relation between $\phi^{(n)}$ and $\phi^{(n+2)}$. Let ϕ_o denote the velocity potential at $z = 0$, \mathbf{u}_o the horizontal velocity at $z = 0$, and w_o the vertical velocity at $z = 0$. Note that ϕ_o and w_o are nothing else than $\phi^{(0)}$ and $\phi^{(1)}$. The potential ϕ can be expressed in terms of ϕ_o and w_o only. Finally, one obtains the velocity field in the whole water column ($-h \leq z \leq \eta$) [MBS03]:

$$\mathbf{u}(x, y, z, t) = \cos(z\nabla)\mathbf{u}_o + \sin(z\nabla)w_o, \quad (35)$$

$$w(x, y, z, t) = \cos(z\nabla)w_o - \sin(z\nabla)\mathbf{u}_o. \quad (36)$$

Here the cosine and sine operators are infinite Taylor series operators defined by

$$\cos(z\nabla) = \sum_{n=0}^{\infty} (-1)^n \frac{z^{2n}}{(2n)!} \nabla^{2n}, \quad \sin(z\nabla) = \sum_{n=0}^{\infty} (-1)^n \frac{z^{2n+1}}{(2n+1)!} \nabla^{2n+1}.$$

Then one can substitute the representation (35)-(36) into the kinematic bottom condition and use successive approximations to obtain an explicit recursive expression for w_o in terms of \mathbf{u}_o to infinite order in $h\nabla$.

A wide variety of Boussinesq systems can be derived [MBS03]. One can generalize the expansions to an arbitrary z -level, instead of the $z = 0$ level. The Taylor series for the cosine and sine operators can be truncated, Padé approximants can be used in operators at $z = -h$ and/or at $z = 0$.

The classical Boussinesq equations are more transparent when written in the dimensionless variables used in the previous subsection. We further assume that h is constant, drop the tildes, and write the equations for one spatial dimension (x). Performing the expansion about $z = 0$ leads to the vanishing of the odd terms in the velocity potential. Substituting the expression for ϕ into the free-surface boundary conditions evaluated at $z = 1 + \alpha\eta(x, t)$ leads to two equations in η and ϕ_o with terms of various order in α and β . The small parameters α and β are of the same order, while η and ϕ_o as well as their partial derivatives are of order one.

Classical Boussinesq equations

The classical Boussinesq equations are obtained by keeping all terms that are at most linear in α or β . In the derivation of the fundamental nonlinear shallow-water equations (24)–(26), the terms in β were neglected. It is therefore implicitly assumed that the Stokes number is large. Since the cube of the water depth appears in the denominator of the Stokes number ($S = \alpha/\beta = al^2/d^3$), it means that the Stokes number is 64 times larger in a 1 km depth than in a 4 km depth! Based on these arguments, dispersion is more important to the west of the rupture. Considering the Stokes number to be of order one leads to the following system in dimensional form²:

$$u_t + uu_x + g\eta_x - \frac{1}{2}h^2u_{txx} = 0, \quad (37)$$

$$\eta_t + [u(h + \eta)]_x - \frac{1}{6}h^3u_{xxx} = 0. \quad (38)$$

The classical Boussinesq equations are in fact slightly different. They are obtained by replacing u with the depth averaged velocity

$$\frac{1}{h} \int_{-h}^{\eta} u dz.$$

They read

$$u_t + uu_x + g\eta_x - \frac{1}{3}h^2u_{txx} = 0, \quad (39)$$

$$\eta_t + [u(h + \eta)]_x = 0. \quad (40)$$

A number of variants of the classical Boussinesq system were studied by Bona et al. [BCS02], who in particular showed that depending on the modeling of dispersion the linearization about the rest state may or may not be well-posed.

²Equations (37) and (38) could have been obtained from equations (21) and (23).

Korteweg–de Vries equation

The previous system allows the propagation of waves in both the positive and negative x -directions. Seeking solutions travelling in only one direction, for example the positive x -direction, leads to a single equation for η , the Korteweg–de Vries equation:

$$\eta_t + c_0 \left(1 + \frac{3\eta}{2d} \right) \eta_x + \frac{1}{6} c_0 d^2 \eta_{xxx} = 0, \quad (41)$$

where d is the water depth. It admits solitary wave solutions travelling at speed V in the form

$$\eta(x, t) = a \operatorname{sech}^2 \left(\sqrt{\frac{3a}{4d^3}} (x - Vt) \right), \quad \text{with } V = c_0 \left(1 + \frac{a}{2d} \right).$$

The solitary wave solutions of the Korteweg–de Vries equation are of elevation ($a > 0$) and travel faster than c_0 . Their speed increases with amplitude. Note that a natural length scale appears:

$$\ell = \sqrt{\frac{4d^3}{3a}}.$$

For the Indian Ocean tsunami, it gives roughly $\ell = 377$ km. It is of the order of magnitude of the wavelength estimated from the width of the segments that experienced slip.

Solitary waves exist for more general nonlinear dispersive equations such as KdV-KdV, and Bona-Smith systems. Their existence was recently studied in [FDG05, DM04]. Numerical methods (based on Galerkin discretization) for the approximation of solutions to KdV-KdV systems are discussed in [BDM07].

Energy of a tsunami

The energy of the earthquake is measured via the strain energy released by the faulting. The part of the energy transmitted to the tsunami wave is less than one percent Lay et al. [LKA⁺05]. They estimate the tsunami energy to be 4.2×10^{15} J. They do not give details on how they obtained this estimate. However, a simple calculation based on considering the tsunami as a soliton

$$\eta(x) = a \operatorname{sech}^2 \left(\frac{x}{\ell} \right), \quad u(x) = \alpha c_0 \operatorname{sech}^2 \left(\frac{x}{\ell} \right),$$

gives for the energy

$$E = \frac{1}{\sqrt{3}} \alpha^{3/2} \rho d^2 (c_0^2 + gd) \int_{-\infty}^{\infty} \operatorname{sech}^4 x \, dx + O(\alpha^2).$$

The value for the integral is $4/3$. The numerical estimate for E is close to that of Lay et al. (2005) [LKA⁺05]. Incidentally, at this level of approximation, there is equipartition between kinetic and potential energy. It is also important to point out that a tsunami being a shallow water wave, the whole water column is moving as the wave propagates. For the parameter values used so far, the maximum horizontal current is 3 cm/s. However, as the water depth decreases, the current increases and becomes important when the depth becomes less than 500 m. Additional properties of solitary waves can be found for example in [LH74].

Tsunami run-up

The last phase of a tsunami is its run-up and inundation. Although in some cases it may be important to consider the coupling between fluid and structures, we restrict ourselves to the description of the fluid flow. The problem of waves climbing a beach is a classical one [CG58]. The transformations used by Carrier and Greenspan are still used nowadays. The basis of their analysis is the one-dimensional counterpart of the system (27)–(29). In addition, they assume the depth to be of uniform slope: $h = -x \tan \theta$. Introduce the following dimensionless quantities, where ℓ is a characteristic length³:

$$x = \ell \tilde{x}, \quad \eta = \ell \tilde{\eta}, \quad u = \sqrt{g\ell} \tilde{u}, \quad t = \sqrt{\ell/g} \tilde{t}, \quad c^2 = (h + \eta)/\ell.$$

After dropping the tildes, the dimensionless system of equations (27)–(29) becomes

$$\begin{aligned} u_t + uu_x + \eta_x &= 0, \\ \eta_t + [u(-x \tan \theta + \eta)]_x &= 0. \end{aligned}$$

In terms of the variable c , these equations become

$$\begin{aligned} u_t + uu_x + 2cc_x + \tan \theta &= 0, \\ 2c_t + cu_x + 2uc_x &= 0. \end{aligned}$$

The equations written in characteristic form are

$$\begin{aligned} \left[\frac{\partial}{\partial t} + (u + c) \frac{\partial}{\partial x} \right] (u + 2c + t \tan \theta) &= 0, \\ \left[\frac{\partial}{\partial t} + (u - c) \frac{\partial}{\partial x} \right] (u - 2c + t \tan \theta) &= 0. \end{aligned}$$

³In fact there is no obvious characteristic length in this idealized problem. Some authors simply say at this point that ℓ is specific to the problem under consideration.

The characteristic curves C^+ and C^- as well as the Riemann invariants are

$$\begin{aligned} C^+ &: \frac{dx}{dt} = u + c, & u + 2c + t \tan \theta = r, \\ C^- &: \frac{dx}{dt} = u - c, & u - 2c + t \tan \theta = s. \end{aligned}$$

Next one can rewrite the hyperbolic equations in terms of the new variables λ and σ defined as follows:

$$\begin{aligned} \frac{\lambda}{2} &= \frac{1}{2}(r + s) = u + t \tan \theta, \\ \frac{\sigma}{4} &= \frac{1}{4}(r - s) = c. \end{aligned}$$

One obtains

$$\begin{aligned} x_s - \left[\frac{1}{4}(3r + s) - t \tan \theta \right] t_s &= 0, \\ x_r - \left[\frac{1}{4}(r + 3s) - t \tan \theta \right] t_r &= 0. \end{aligned}$$

The elimination of x results in the *linear* second-order equation for t

$$\sigma(t_{\lambda\lambda} - t_{\sigma\sigma}) - 3t_{\sigma} = 0. \quad (42)$$

Since $u + t \tan \theta = \lambda/2$, u must also satisfy (42). Introducing the potential $\phi(\sigma, \lambda)$ such that

$$u = \frac{\phi_{\sigma}}{\sigma},$$

one obtains the equation

$$(\sigma\phi_{\sigma})_{\sigma} - \sigma\phi_{\lambda\lambda} = 0$$

after integrating once. Two major simplifications have been obtained. The nonlinear set of equations have been reduced to a linear equation for u or ϕ and the free boundary is now the fixed line $\sigma = 0$ in the (σ, λ) -plane. The free boundary is the instantaneous shoreline $c = 0$, which moves as a wave climbs a beach.

The above formulation has been used by several authors to study the run-up of various types of waves on sloping beaches [Syn87, TS94, CWY03, TT05]. Synolakis [Syn87] validated analytical results by comparing them with experiments on the run-up of a solitary wave on a plane beach. He used Carrier-Greenspan transformation and linear theory solutions to draw several important conclusions:

- A law predicting the maximum run-up of non-breaking waves was given;

- The author found different run-up variations for breaking and non-breaking solitary waves;
- Nonlinear theory models adequately describe surface profiles of non-breaking waves;
- Different criteria were considered whether a solitary wave with given height/depth ratio will break or not as it climbs up a sloping beach.

Later, it was shown that leading depression N -waves run-up higher than leading elevation N -waves, suggesting that perhaps the solitary wave model may not be adequate for predicting an upper limit for the run-up of near-shore generated tsunamis. In [KS06] it was shown that there is a difference in the maximum run-up by a factor 2 in shoreline motions with and without initial velocity. This difference suggests strong implications for the run-up predictions and tsunami warning system [GBM⁺05] if the appropriate initial velocity is not specified.

There is a rule of thumb that says that the run-up does not usually exceed twice the fault slip. Since run-ups of 30 meters were observed in Sumatra during the Boxing Day tsunami, the slip might have been of 15 meters or even more.

Analytical models are useful, especially to perform parametric studies. However, the breaking of tsunami waves as well as the subsequent floodings must be studied numerically. The most natural methods that can be used are the free surface capturing methods based on a finite volume discretisation, such as the Volume Of Fluid (VOF) or the Level Set methods, and the family of Smoothed Particle Hydrodynamics methods (SPH), applied to free-surface flow problems [Mon94, GGD04, GGCCD05]. Such methods allow a study of flood wave dynamics, of wave breaking on the land behind beaches, and of the flow over rising ground with and without the presence of obstacles. This task is an essential part of tsunami modelling, since it allows the determination of the level of risk due to major flooding, the prediction of the resulting water levels in the flooded areas, the determination of security zones. It also provides some help in the conception and validation of protection systems in the most exposed areas.

The present manuscript is organized as follows. In Chapter 1 we extensively investigate the tsunami generation process (see Sections 1.1 and 1.3) and the first minutes of propagation (Section 1.2) using different mathematical models. Several important conclusions about the physics of tsunami waves were drawn out. Chapter 2 discusses different possibilities of introducing dissipative effects into Boussinesq equations. Pros and cons of two models under consideration are revealed. In Chapter 3 our attention is attracted by two-phase flows and wave impact problem. An efficient numerical method based on a finite volume scheme is described and a few numerical results are presented. In the last Chapter 4 we return to the investigation of dissipative effects onto water waves. Novel bottom

boundary layer correction is derived and the new set of governing equations is thoroughly analysed.

Chapter 1

Tsunami generation modelling

From a drop of water a logician could predict an Atlantic or a Niagara.

Sir Arthur Conan Doyle

Contents

1.1	Waves generated by a moving bottom	2
1.1.1	Source model	4
1.1.2	Volterra's theory of dislocations	5
1.1.3	Dislocations in elastic half-space	6
1.1.4	Solution in fluid domain	16
1.1.5	Free-surface elevation	21
1.1.6	Velocity field	25
1.1.7	Asymptotic analysis of integral solutions	29
1.1.8	Numerical results	31
1.2	Comparison of tsunami generation models	36
1.2.1	Physical problem description	37
1.2.2	Linear theory	43
1.2.3	Active generation	44
1.2.4	Passive generation	44
1.2.5	Nonlinear shallow water equations	47
1.2.6	Mathematical model	48
1.2.7	Numerical method	50
1.2.8	Numerical method for the full equations	50

1.2.9	Comparisons and discussion	51
1.2.10	Conclusions	64
1.3	Tsunami generation by dynamic displacement of sea bed . .	64
1.3.1	Introduction	64
1.3.2	Mathematical models	67
1.3.3	Numerical methods	70
1.3.4	Validation of the numerical method	72
1.3.5	Results of the simulation	73
1.3.6	Conclusions	78

1.1 Waves generated by a moving bottom

Waves at the surface of a liquid can be generated by various mechanisms: wind blowing on the free surface, wavemaker, moving disturbance on the bottom or the surface, or even inside the liquid, fall of an object into the liquid, liquid inside a moving container, etc. In this chapter, we concentrate on the case where the waves are created by a given motion of the bottom. One example is the generation of tsunamis by a sudden seafloor deformation.

There are different natural phenomena that can lead to a tsunami. For example, one can mention submarine slumps, slides, volcanic explosions, etc. In this chapter we use a submarine faulting generation mechanism as tsunami source. The resulting waves have some well-known features. For example, characteristic wavelengths are large and wave amplitudes are small compared with water depth.

Two factors are usually necessary for an accurate modelling of tsunamis: information on the magnitude and distribution of the displacements caused by the earthquake, and a model of surface gravity waves generation resulting from this motion of the seafloor. Most studies of tsunami generation assume that the initial free-surface deformation is equal to the vertical displacement of the ocean bottom. The details of wave motion are neglected during the time that the source operates. While this is often justified because the earthquake rupture occurs very rapidly, there are some specific cases where the time scale of the bottom deformation may become an important factor. This was emphasized for example by Trifunac and Todorovska [TT01], who considered the generation of tsunamis by a slowly spreading uplift of the seafloor and were able to explain some observations. During the 26 December 2004 Sumatra-Andaman event, there was in the northern extent of the source a relatively slow faulting motion that led to significant vertical bottom motion but left little record in the seismic data. It is interesting to point out that it is the inversion

of tide-gauge data from Paradip, the northernmost of the Indian east-coast stations, that led Neetu et al. [NSS⁺05] to conclude that the source length was greater by roughly 30% than the initial estimate of Lay et al. [LKA⁺05]. Incidentally, the generation time is also longer for landslide tsunamis.

Our study is restricted to the water region where the incompressible Euler equations for potential flow can be linearized. The wave propagation away from the source can be investigated by shallow water models which may or may not take into account nonlinear effects and frequency dispersion. Such models include the Korteweg-de Vries equation [KdV95] for unidirectional propagation, nonlinear shallow-water equations and Boussinesq-type models [Bou71b, Per66, BBM72].

Several authors have modeled the incompressible fluid layer as a special case of an elastic medium [Pod68, Kaj63, Gus72, AG73, Gus76]. In our opinion it may be convenient to model the liquid by an elastic material from a mathematical point of view, but it is questionable from a physical point of view. The crust was modeled as an elastic isotropic half-space. This assumption will also be adopted in the present study.

The problem of tsunami generation has been considered by a number of authors: see for example [Car71, vdD72, BvdDP73]. The models discussed in these papers lack flexibility in terms of modelling the source due to the earthquake. The present study provides some extensions. A good review on the subject is [Sab86].

Here we essentially follow the framework proposed by Hammack [Ham73] and others. The tsunami generation problem is reduced to a Cauchy-Poisson boundary value problem in a region of constant depth. The main extensions given in the present work consist in three-dimensional modelling and more realistic source models. This approach was followed recently in [TT01, THT02], where the mathematical model was the same as in [Ham73] but the source was different.

Most analytical studies of linearized wave motion use integral transform methods. The complexity of the integral solutions forced many authors [Kaj63, Kel63] to use asymptotic methods such as the method of stationary phase to estimate the far-field behaviour of the solutions. In the present study we have also obtained asymptotic formulas for integral solutions. They are useful from a qualitative point of view, but in practice it is better to use numerical integration formulas [Fil28] that take into account the oscillatory nature of the integrals. All the numerical results presented in this section were obtained in this manner.

One should use asymptotic solutions with caution since they approximate exact solutions of the linearized problem. The relative importance of linear and nonlinear effects can

be measured by the Stokes (or Ursell) number [Urs53]:

$$U := \frac{a/h}{(kh)^2} = \frac{a}{k^2 h^3},$$

where k is a wave number, a a typical wave amplitude and h the water depth. For $U \gg 1$, the nonlinear effects control wave propagation and only nonlinear models are applicable. Ursell [Urs53] proved that near the wave front U behaves like

$$U \sim t^{\frac{1}{3}}.$$

Hence, regardless of how small nonlinear effects are initially, they will become important.

Recently, the methodology used in this thesis for tsunami generation was applied in the framework of the Boussinesq equations [Mit07] over uneven bottom. These equations have the advantage of being two-dimensional while the physical problem and, consequently, the potential flow formulation are 3D. On the other hand, Boussinesq equations represent a long wave approximation to the complete water-wave problem.

1.1.1 Source model

The inversion of seismic wave data allows the reconstruction of permanent deformations of the sea bottom following earthquakes. In spite of the complexity of the seismic source and of the internal structure of the earth, scientists have been relatively successful in using simple models for the source. One of these models is Okada's model [Oka85]. Its description follows.

The fracture zones, along which the foci of earthquakes are to be found, have been described in various papers. For example, it has been suggested that Volterra's theory of dislocations might be the proper tool for a quantitative description of these fracture zones [Ste58]. This suggestion was made for the following reason. If the mechanism involved in earthquakes and the fracture zones is indeed one of fracture, discontinuities in the displacement components across the fractured surface will exist. As dislocation theory may be described as that part of the theory of elasticity dealing with surfaces across which the displacement field is discontinuous, the suggestion makes sense.

As is often done in mathematical physics, it is necessary for simplicity's sake to make some assumptions. Here we neglect the curvature of the earth, its gravity, temperature, magnetism, non-homogeneity, and consider a semi-infinite medium, which is homogeneous and isotropic. We further assume that the laws of classical linear elasticity theory hold.

Several studies showed that the effect of earth curvature is negligible for shallow events at distances of less than 20° [BMSS69, BMSS70, SM71]. The sensitivity to earth topography, homogeneity, isotropy and half-space assumptions was studied and discussed recently

[Mas03]. A commercially available code, ABACUS, which is based on a finite element model (FEM), was used. Six FEMs were constructed to test the sensitivity of deformation predictions to each assumption. The author came to the conclusion that the vertical layering of lateral inhomogeneity can sometimes cause considerable effects on the deformation fields.

The usual boundary conditions for dealing with earth problems require that the surface of the elastic medium (the earth) shall be free from forces. The resulting mixed boundary-value problem was solved a century ago [Vol07]. Later, Steketee proposed an alternative method to solve this problem using Green's functions [Ste58].

1.1.2 Volterra's theory of dislocations

In order to introduce the concept of dislocation and for simplicity's sake, this section is devoted to the case of an entire elastic space, as was done in the original paper by Volterra [Vol07].

Let O be the origin of a Cartesian coordinate system in an infinite elastic medium, x_i the Cartesian coordinates ($i = 1, 2, 3$), and \mathbf{e}_i a unit vector in the positive x_i -direction. A force $\mathbf{F} = F\mathbf{e}_k$ at O generates a displacement field $u_i^k(P, O)$ at point P , which is determined by the well-known Somigliana tensor

$$u_i^k(P, O) = \frac{F}{8\pi\mu} (\delta_{ik} r_{,nn} - \alpha r_{,ik}), \quad \text{with } \alpha = \frac{\lambda + \mu}{\lambda + 2\mu}. \quad (1.1)$$

In this relation δ_{ik} is the Kronecker delta, λ and μ are Lamé's constants, and r is the distance from P to O . The coefficient α can be rewritten as $\alpha = 1/2(1 - \nu)$, where ν is Poisson's ratio. Later we will also use Young's modulus E , which is defined as

$$E = \frac{\mu(3\lambda + 2\mu)}{\lambda + \mu}.$$

The notation $r_{,i}$ means $\partial r / \partial x_i$ and the summation convention applies.

The stresses due to the displacement field (1.1) are easily computed from Hooke's law:

$$\sigma_{ij} = \lambda \delta_{ij} u_{k,k} + \mu (u_{i,j} + u_{j,i}). \quad (1.2)$$

One finds

$$\sigma_{ij}^k(P, O) = -\frac{\alpha F}{4\pi} \left(\frac{3x_i x_j x_k}{r^5} + \frac{\mu}{\lambda + \mu} \frac{\delta_{ki} x_j + \delta_{kj} x_i - \delta_{ij} x_k}{r^3} \right).$$

The components of the force per unit area on a surface element are denoted as follows:

$$T_i^k = \sigma_{ij}^k \nu_j,$$

where the ν_j 's are the components of the normal to the surface element. A Volterra dislocation is defined as a surface Σ in the elastic medium across which there is a discontinuity Δu_i in the displacement fields of the type

$$\Delta u_i = u_i^+ - u_i^- = U_i + \Omega_{ij}x_j, \quad (1.3)$$

$$\Omega_{ij} = -\Omega_{ji}. \quad (1.4)$$

Equation (1.3) in which U_i and Ω_{ij} are constants is the well-known Weingarten relation which states that the discontinuity Δu_i should be of the type of a rigid body displacement, thereby maintaining continuity of the components of stress and strain across Σ .

The displacement field in an infinite elastic medium due to the dislocation is then determined by Volterra's formula [Vol07]

$$u_k(Q) = \frac{1}{F} \iint_{\Sigma} \Delta u_i T_i^k dS. \quad (1.5)$$

Once the surface Σ is given, the dislocation is essentially determined by the six constants U_i and Ω_{ij} . Therefore we also write

$$u_k(Q) = \frac{U_i}{F} \iint_{\Sigma} \sigma_{ij}^k(P, Q) \nu_j dS + \frac{\Omega_{ij}}{F} \iint_{\Sigma} \{x_j \sigma_{il}^k(P, Q) - x_i \sigma_{jl}^k(P, Q)\} \nu_l dS, \quad (1.6)$$

where Ω_{ij} takes only the values Ω_{12} , Ω_{23} , Ω_{31} . Following Volterra [Vol07] and Love [Lov44] we call each of the six integrals in (1.6) an elementary dislocation.

It is clear from (1.5) and (1.6) that the computation of the displacement field $u_k(Q)$ is performed as follows. A force $F\mathbf{e}_k$ is applied at Q , and the stresses $\sigma_{ij}^k(P, Q)$ that this force generates are computed at the points $P(x_i)$ on Σ . In particular the components of the force on Σ are computed. After multiplication with prescribed weights of magnitude Δu_i these forces are integrated over Σ to give the displacement component in Q due to the dislocation on Σ .

1.1.3 Dislocations in elastic half-space

When the case of an elastic half-space is considered, equation (1.5) remains valid, but we have to replace σ_{ij}^k in T_i^k by another tensor ω_{ij}^k . This can be explained by the fact that the elementary solutions for a half-space are different from Somigliana solution (1.1).

The ω_{ij}^k can be obtained from the displacements corresponding to nuclei of strain in a half-space through relation (1.2). Steketee showed a method of obtaining the six ω_{ij}^k fields by using a Green's function and derived ω_{12}^k , which is relevant to a vertical strike-slip fault (see below). Maruyama derived the remaining five functions [Mar64].

It is interesting to mention here that historically these solutions were first derived in a straightforward manner by Mindlin [Min36, MC50], who gave explicit expressions of the displacement and stress fields for half-space nuclei of strain consisting of single forces with and without moment. It is only necessary to write the single force results since the other forms can be obtained by taking appropriate derivatives. The method consists in finding the displacement field in Westergaard's form of the Galerkin vector [Wes35]. This vector is then determined by taking a linear combination of some biharmonic elementary solutions. The coefficients are chosen to satisfy boundary and equilibrium conditions. These solutions were also derived by Press in a slightly different manner [Pre65].

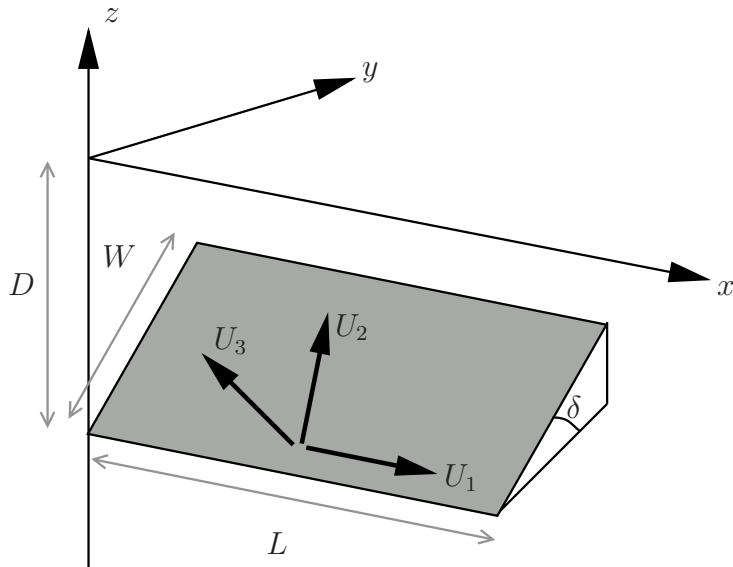


Figure 1.1: Coordinate system adopted in this study and geometry of the source model.

Here, we take the Cartesian coordinate system shown in Figure 1.1. The elastic medium occupies the region $x_3 \leq 0$ and the x_1 -axis is taken to be parallel to the strike direction of the fault. In this coordinate system, $u_i^j(x_1, x_2, x_3; \xi_1, \xi_2, \xi_3)$ is the i th component of the displacement at (x_1, x_2, x_3) due to the j th direction point force of magnitude F at (ξ_1, ξ_2, ξ_3) . It can be expressed as follows [Oka85, Min36, Pre65, Oka92]:

$$\begin{aligned}
 u_i^j(x_1, x_2, x_3) &= u_{iA}^j(x_1, x_2, -x_3) - u_{iA}^j(x_1, x_2, x_3) \\
 &\quad + u_{iB}^j(x_1, x_2, x_3) + x_3 u_{iC}^j(x_1, x_2, x_3),
 \end{aligned}
 \tag{1.7}$$

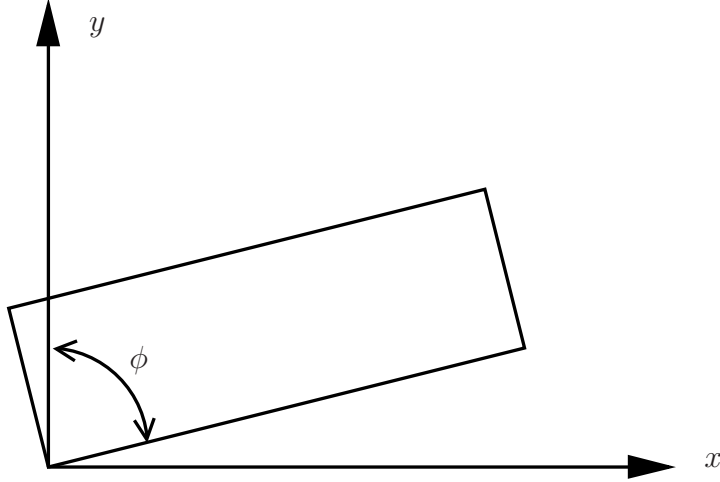


Figure 1.2: Illustration for strike angle definition.

where

$$\begin{aligned}
 u_{iA}^j &= \frac{F}{8\pi\mu} \left((2 - \alpha) \frac{\delta_{ij}}{R} + \alpha \frac{R_i R_j}{R^3} \right), \\
 u_{iB}^j &= \frac{F}{4\pi\mu} \left(\frac{\delta_{ij}}{R} + \frac{R_i R_j}{R^3} + \frac{1 - \alpha}{\alpha} \left[\frac{\delta_{ij}}{R + R_3} + \right. \right. \\
 &\quad \left. \left. + \frac{R_i \delta_{j3} - R_j \delta_{i3} (1 - \delta_{j3})}{R(R + R_3)} - \frac{R_i R_j}{R(R + R_3)^2} (1 - \delta_{i3})(1 - \delta_{j3}) \right] \right), \\
 u_{iC}^j &= \frac{F}{4\pi\mu} (1 - 2\delta_{i3}) \left((2 - \alpha) \frac{R_i \delta_{j3} - R_j \delta_{i3}}{R^3} + \alpha \xi_3 \left[\frac{\delta_{ij}}{R^3} - 3 \frac{R_i R_j}{R^5} \right] \right).
 \end{aligned}$$

In these expressions $R_1 = x_1 - \xi_1$, $R_2 = x_2 - \xi_2$, $R_3 = -x_3 - \xi_3$ and $R^2 = R_1^2 + R_2^2 + R_3^2$.

The first term in equation (1.7), $u_{iA}^j(x_1, x_2, -x_3)$, is the well-known Somigliana tensor, which represents the displacement field due to a single force placed at (ξ_1, ξ_2, ξ_3) in an infinite medium [Lov44]. The second term also looks like a Somigliana tensor. This term corresponds to a contribution from an image source of the given point force placed at $(\xi_1, \xi_2, -\xi_3)$ in the infinite medium. The third term, $u_{iB}^j(x_1, x_2, x_3)$, and $u_{iC}^j(x_1, x_2, x_3)$ in the fourth term are naturally depth dependent. When x_3 is set equal to zero in equation (1.7), the first and the second terms cancel each other, and the fourth term vanishes. The remaining term, $u_{iB}^j(x_1, x_2, 0)$, reduces to the formula for the surface displacement field

due to a point force in a half-space [Oka85]:

$$\begin{cases} u_1^1 = \frac{F}{4\pi\mu} \left(\frac{1}{R} + \frac{(x_1 - \xi_1)^2}{R^3} + \frac{\mu}{\lambda + \mu} \left[\frac{1}{R - \xi_3} - \frac{(x_1 - \xi_1)^2}{R(R - \xi_3)^2} \right] \right), \\ u_2^1 = \frac{F}{4\pi\mu} (x_1 - \xi_1)(x_2 - \xi_2) \left(\frac{1}{R^3} - \frac{\mu}{\lambda + \mu} \frac{1}{R(R - \xi_3)^2} \right), \\ u_3^1 = \frac{F}{4\pi\mu} (x_1 - \xi_1) \left(-\frac{\xi_3}{R^3} - \frac{\mu}{\lambda + \mu} \frac{1}{R(R - \xi_3)} \right), \end{cases}$$

$$\begin{cases} u_1^2 = \frac{F}{4\pi\mu} (x_1 - \xi_1)(x_2 - \xi_2) \left(\frac{1}{R^3} - \frac{\mu}{\lambda + \mu} \frac{1}{R(R - \xi_3)^2} \right), \\ u_2^2 = \frac{F}{4\pi\mu} \left(\frac{1}{R} + \frac{(x_2 - \xi_2)^2}{R^3} + \frac{\mu}{\lambda + \mu} \left[\frac{1}{R - \xi_3} - \frac{(x_2 - \xi_2)^2}{R(R - \xi_3)^2} \right] \right), \\ u_3^2 = \frac{F}{4\pi\mu} (x_2 - \xi_2) \left(-\frac{\xi_3}{R^3} - \frac{\mu}{\lambda + \mu} \frac{1}{R(R - \xi_3)} \right), \end{cases}$$

$$\begin{cases} u_1^3 = \frac{F}{4\pi\mu} (x_1 - \xi_1) \left(-\frac{\xi_3}{R^3} + \frac{\mu}{\lambda + \mu} \frac{1}{R(R - \xi_3)} \right), \\ u_2^3 = \frac{F}{4\pi\mu} (x_2 - \xi_2) \left(-\frac{\xi_3}{R^3} + \frac{\mu}{\lambda + \mu} \frac{1}{R(R - \xi_3)} \right), \\ u_3^3 = \frac{F}{4\pi\mu} \left(\frac{1}{R} + \frac{\xi_3^2}{R^3} + \frac{\mu}{\lambda + \mu} \frac{1}{R} \right). \end{cases}$$

In these formulas $R^2 = (x_1 - \xi_1)^2 + (x_2 - \xi_2)^2 + \xi_3^2$.

In order to obtain the displacements due to the dislocation we need to calculate the corresponding ξ_k -derivatives of the point force solution (1.7) and to insert them in Volterra's formula (1.5)

$$u_i = \frac{1}{F} \iint_{\Sigma} \Delta u_j \left[\lambda \delta_{jk} \frac{\partial u_i^n}{\partial \xi_n} + \mu \left(\frac{\partial u_i^j}{\partial \xi_k} + \frac{\partial u_i^k}{\partial \xi_j} \right) \right] \nu_k dS.$$

The ξ_k -derivatives are expressed as follows:

$$\begin{aligned} \frac{\partial u_i^j}{\partial \xi_k}(x_1, x_2, x_3) &= \frac{\partial u_{iA}^j}{\partial \xi_k}(x_1, x_2, -x_3) - \frac{\partial u_{iA}^j}{\partial \xi_k}(x_1, x_2, x_3) + \\ &+ \frac{\partial u_{iB}^j}{\partial \xi_k}(x_1, x_2, x_3) + x_3 \frac{\partial u_{iC}^j}{\partial \xi_k}(x_1, x_2, x_3), \end{aligned}$$

with

$$\begin{aligned}
\frac{\partial u_{iA}^j}{\partial \xi_k} &= \frac{F}{8\pi\mu} \left((2 - \alpha) \frac{R_k}{R^3} \delta_{ij} - \alpha \frac{R_i \delta_{jk} + R_j \delta_{ik}}{R^3} + 3\alpha \frac{R_i R_j R_k}{R^5} \right), \\
\frac{\partial u_{iB}^j}{\partial \xi_k} &= \frac{F}{4\pi\mu} \left(-\frac{R_i \delta_{jk} + R_j \delta_{ik} - R_k \delta_{ij}}{R^3} + 3 \frac{R_i R_j R_k}{R^5} + \right. \\
&\quad + \frac{1 - \alpha}{\alpha} \left[\frac{\delta_{3k} R + R_k}{R(R + R_3)^2} \delta_{ij} - \frac{\delta_{ik} \delta_{j3} - \delta_{jk} \delta_{i3} (1 - \delta_{j3})}{R(R + R_3)} + \right. \\
&\quad + (R_i \delta_{j3} - R_j \delta_{i3} (1 - \delta_{j3})) \frac{\delta_{3k} R^2 + R_k (2R + R_3)}{R^3 (R + R_3)^2} + \\
&\quad \left. \left. + (1 - \delta_{i3})(1 - \delta_{j3}) \left(\frac{R_i \delta_{jk} + R_j \delta_{ik}}{R(R + R_3)^2} - R_i R_j \frac{2\delta_{3k} R^2 + R_k (3R + R_3)}{R^3 (R + R_3)^3} \right) \right] \right), \\
\frac{\partial u_{iC}^j}{\partial \xi_k} &= \frac{F}{4\pi\mu} (1 - 2\delta_{i3}) \left((2 - \alpha) \left[\frac{\delta_{jk} \delta_{i3} - \delta_{ik} \delta_{j3}}{R^3} + \frac{3R_k (R_i \delta_{j3} - R_j \delta_{i3})}{R^5} \right] + \right. \\
&\quad \left. + \alpha \delta_{3k} \left[\frac{\delta_{ij}}{R^3} - \frac{3R_i R_j}{R^5} \right] + 3\alpha \xi_3 \left[\frac{R_i \delta_{jk} + R_j \delta_{ik} + R_k \delta_{ij}}{R^5} - \frac{5R_i R_j R_k}{R^7} \right] \right).
\end{aligned}$$

1.1.3.1 Finite rectangular source

Let us now consider a more practical problem. We define the elementary dislocations U_1 , U_2 and U_3 , corresponding to the strike-slip, dip-slip and tensile components of an arbitrary dislocation. In Figure 1.1 each vector represents the direction of the elementary faults. The vector \mathbf{D} is the so-called Burger's vector, which shows how both sides of the fault are spread out: $\mathbf{D} = \mathbf{u}^+ - \mathbf{u}^-$.

A general dislocation can be determined by three angles: the dip angle δ of the fault ($0 \leq \delta \leq \pi$), the slip or rake angle θ ($0 \leq \theta \leq \pi$), and the angle ϕ between the fault plane and Burger's vector \mathbf{D} . When dealing with a geophysical application, an additional angle, the azimuth or strike (see Figure 1.2 for strike angle definition), is introduced in order to provide an orientation of the fault. The general situation is schematically described in Figure 1.3.

For a finite rectangular fault with length L and width W occurring at depth d (Figure 1.3), the deformation field can be evaluated analytically by a change of variables and by integrating over the rectangle. This was done by several authors [Oka85, Oka92, Chi63, SM74, IS79]. Here we give the results of their computations. The final results are represented below in compact form, using Chinnery's notation $\|$ to represent the substitution

$$f(\xi, \eta)\| = f(x, p) - f(x, p - W) - f(x - L, p) + f(x - L, p - W),$$

where $p = y \cos \delta + d \sin \delta$. Next we introduce the notation

$$q = y \sin \delta - d \cos \delta, \quad \tilde{y} = \eta \cos \delta + q \sin \delta, \quad \tilde{d} = \eta \sin \delta - q \cos \delta$$

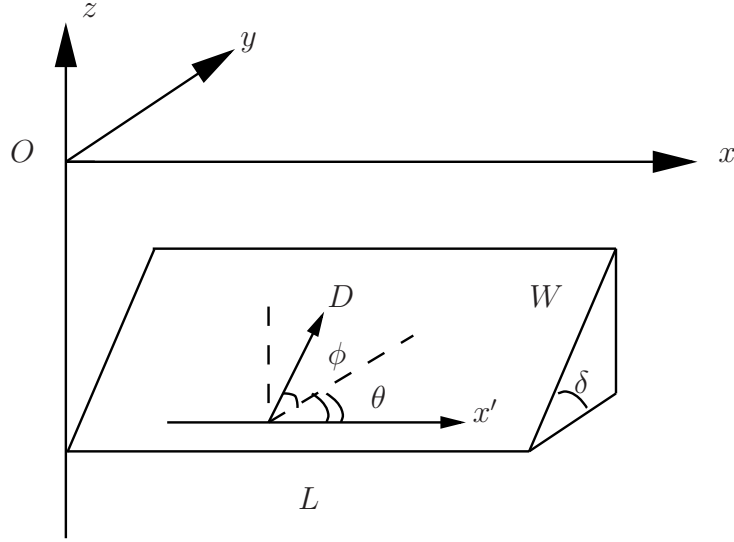


Figure 1.3: Geometry of the source model (dip angle δ , depth d_f , length L , width W) and orientation of Burger's vector \mathbf{D} (rake angle θ , angle ϕ between the fault plane and Burger's vector).

and

$$R^2 = \xi^2 + \eta^2 + q^2 = \xi^2 + \tilde{y}^2 + \tilde{d}^2, \quad X^2 = \xi^2 + q^2.$$

The quantities U_1 , U_2 and U_3 are linked to Burger's vector through the identities

$$U_1 = |\mathbf{D}| \cos \phi \cos \theta, \quad U_2 = |\mathbf{D}| \cos \phi \sin \theta, \quad U_3 = |\mathbf{D}| \sin \phi.$$

For a strike-slip dislocation, one has

$$\begin{aligned} u_1 &= -\frac{U_1}{2\pi} \left(\frac{\xi q}{R(R+\eta)} + \arctan \frac{\xi \eta}{qR} + I_1 \sin \delta \right) \Big\|, \\ u_2 &= -\frac{U_1}{2\pi} \left(\frac{\tilde{y} q}{R(R+\eta)} + \frac{q \cos \delta}{R+\eta} + I_2 \sin \delta \right) \Big\|, \\ u_3 &= -\frac{U_1}{2\pi} \left(\frac{\tilde{d} q}{R(R+\eta)} + \frac{q \sin \delta}{R+\eta} + I_4 \sin \delta \right) \Big\|. \end{aligned}$$

For a dip-slip dislocation, one has

$$\begin{aligned} u_1 &= -\frac{U_2}{2\pi} \left(\frac{q}{R} - I_3 \sin \delta \cos \delta \right) \Big\|, \\ u_2 &= -\frac{U_2}{2\pi} \left(\frac{\tilde{y} q}{R(R+\xi)} + \cos \delta \arctan \frac{\xi \eta}{qR} - I_1 \sin \delta \cos \delta \right) \Big\|, \\ u_3 &= -\frac{U_2}{2\pi} \left(\frac{\tilde{d} q}{R(R+\xi)} + \sin \delta \arctan \frac{\xi \eta}{qR} - I_5 \sin \delta \cos \delta \right) \Big\|. \end{aligned}$$

For a tensile fault dislocation, one has

$$\begin{aligned} u_1 &= \frac{U_3}{2\pi} \left(\frac{q^2}{R(R+\eta)} - I_3 \sin^2 \delta \right) \Big\|, \\ u_2 &= \frac{U_3}{2\pi} \left(\frac{-\tilde{d}q}{R(R+\xi)} - \sin \delta \left[\frac{\xi q}{R(R+\eta)} - \arctan \frac{\xi \eta}{qR} \right] - I_1 \sin^2 \delta \right) \Big\|, \\ u_3 &= \frac{U_3}{2\pi} \left(\frac{\tilde{y}q}{R(R+\xi)} + \cos \delta \left[\frac{\xi q}{R(R+\eta)} - \arctan \frac{\xi \eta}{qR} \right] - I_5 \sin^2 \delta \right) \Big\|. \end{aligned}$$

The terms I_1, \dots, I_5 are given by

$$\begin{aligned} I_1 &= -\frac{\mu}{\lambda + \mu} \frac{\xi}{(R + \tilde{d}) \cos \delta} - \tan \delta I_5, \\ I_2 &= -\frac{\mu}{\lambda + \mu} \log(R + \eta) - I_3, \\ I_3 &= \frac{\mu}{\lambda + \mu} \left[\frac{1}{\cos \delta} \frac{\tilde{y}}{R + \tilde{d}} - \log(R + \eta) \right] + \tan \delta I_4, \\ I_4 &= \frac{\mu}{\mu + \lambda \cos \delta} \left(\log(R + \tilde{d}) - \sin \delta \log(R + \eta) \right), \\ I_5 &= \frac{\mu}{\lambda + \mu \cos \delta} \arctan \frac{\eta(X + q \cos \delta) + X(R + X) \sin \delta}{\xi(R + X) \cos \delta}, \end{aligned}$$

and if $\cos \delta = 0$,

$$\begin{aligned} I_1 &= -\frac{\mu}{2(\lambda + \mu)} \frac{\xi q}{(R + \tilde{d})^2}, \\ I_3 &= \frac{\mu}{2(\lambda + \mu)} \left[\frac{\eta}{R + \tilde{d}} + \frac{\tilde{y}q}{(R + \tilde{d})^2} - \log(R + \eta) \right], \\ I_4 &= -\frac{\mu}{\lambda + \mu} \frac{q}{R + \tilde{d}}, \\ I_5 &= -\frac{\mu}{\lambda + \mu} \frac{\xi \sin \delta}{R + \tilde{d}}. \end{aligned}$$

Figures 1.4, 1.5, and 1.6 show the free-surface deformation due to the three elementary dislocations. The values of the parameters are given in Table 1.1.

1.1.3.2 Curvilinear fault

In the previous subsection analytical formulas for the free-surface deformation in the special case of a rectangular fault were given. In fact, Volterra's formula (1.5) allows to evaluate the displacement field that accompanies fault events with much more general geometry. The shape of the fault and Burger's vector are suggested by seismologists and

<i>parameter</i>	<i>value</i>
Dip angle δ	13°
Fault depth d , km	25
Fault length L , km	220
Fault width W , km	90
U_i , m	15
Young modulus E , GPa	9.5
Poisson's ratio ν	0.23

Table 1.1: Parameter set used in Figures 1.4, 1.5, and 1.6.

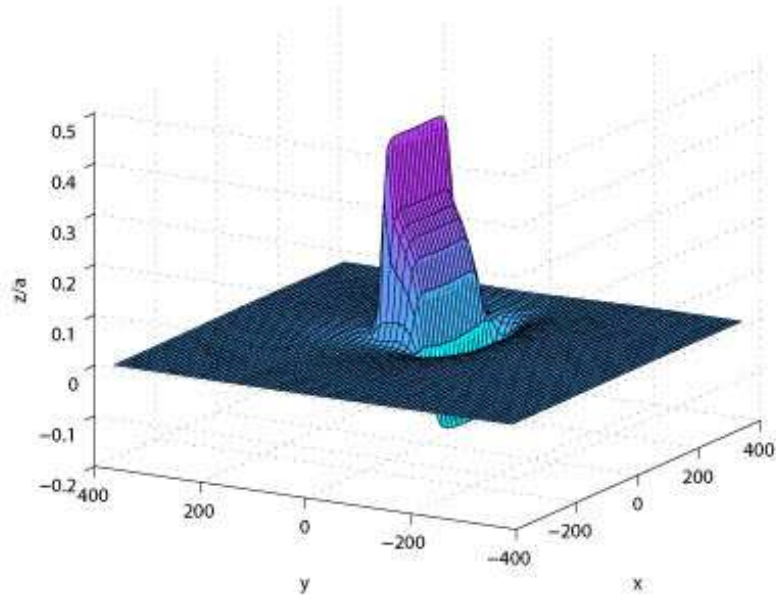


Figure 1.4: Dimensionless free-surface deformation z/a due to dip-slip faulting: $\phi = 0$, $\theta = \pi/2$, $\mathbf{D} = (0, U_2, 0)$. Here a is $|\mathbf{D}|$ (15 m in the present application). The horizontal distances x and y are expressed in kilometers.

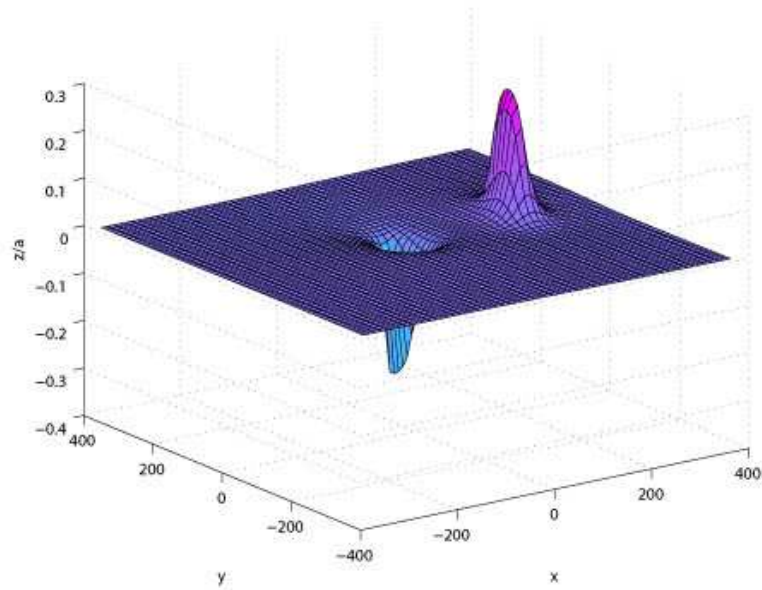


Figure 1.5: Dimensionless free-surface deformation z/a due to strike-slip faulting: $\phi = 0$, $\theta = 0$, $\mathbf{D} = (U_1, 0, 0)$. Here a is $|\mathbf{D}|$ (15 m in the present application). The horizontal distances x and y are expressed in kilometers.

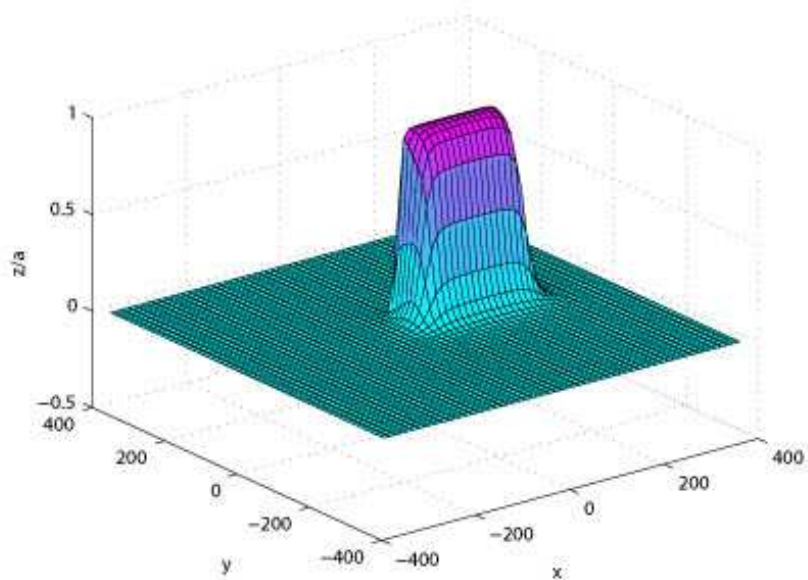


Figure 1.6: Dimensionless free-surface deformation z/a due to tensile faulting: $\phi = \pi/2$, $\mathbf{D} = (0, 0, U_3)$. Here a is $|\mathbf{D}|$. The horizontal distances x and y are expressed in kilometers.

after numerical integration one can obtain the deformation of the seafloor for more general types of events as well.

Here we will consider the case of a fault whose geometry is described by an elliptical arc (see Figure 1.7).

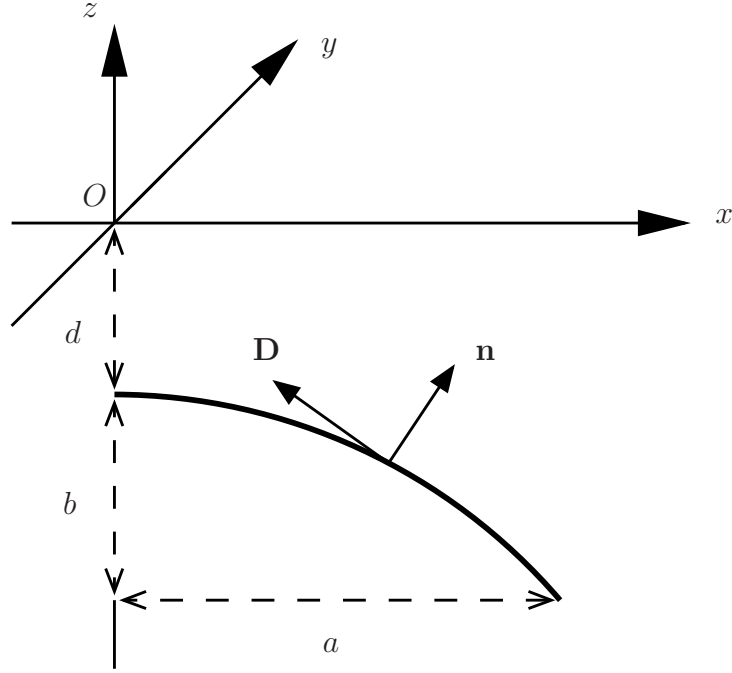


Figure 1.7: Geometry of a fault with elliptical shape

The parametric equations of this surface are given by

$$x(\xi, \eta) = \xi, \quad 0 \leq \xi \leq a, \quad y(\xi, \eta) = \eta, \quad -\frac{c}{2} \leq \eta \leq \frac{c}{2},$$

$$z(\xi, \eta) = -(b + d) + \frac{b}{a} \sqrt{a^2 - \xi^2}.$$

Then the unit normal to this surface can be easily calculated:

$$\mathbf{n} = \left(\frac{b\xi}{\sqrt{a^4 + (b^2 - a^2)\xi^2}}, 0, \frac{a\sqrt{a^2 - \xi^2}}{\sqrt{a^4 + (b^2 - a^2)\xi^2}} \right).$$

We also need to compute the coefficients of the first fundamental form in order to reduce the surface integral in (1.5) to a double Riemann integral. These coefficients are

$$E = \frac{a^4 + \xi^2(b^2 - a^2)}{a^2(a^2 - \xi^2)}, \quad F = 0, \quad G = 1$$

<i>parameter</i>	<i>value</i>
Depth event d , km	20
Ellipse semiminor axis a , km	17
Ellipse semimajor axis b , km	6
Fault width c , km	15
Young modulus E , GPa	9.5
Poisson's ratio ν	0.23

Table 1.2: Parameter set used in Figure 1.8.

and the surface element dS is

$$dS = \sqrt{EG - F^2} d\xi d\eta = \frac{1}{a} \frac{\sqrt{a^4 + \xi^2(b^2 - a^2)}}{\sqrt{a^2 - \xi^2}} d\xi d\eta.$$

Since in the crust the hydrostatic pressure is very large, it is natural to impose the condition that $\mathbf{D} \cdot \mathbf{n} = 0$. The physical meaning of this condition is that both sides of the fault slide and do not detach. This condition is obviously satisfied if we take Burger's vector as

$$\mathbf{D} = D \left(\frac{a\sqrt{a^2 - \xi^2}}{\sqrt{a^4 + \xi^2(b^2 - a^2)}}, 0, -\frac{b\xi}{\sqrt{a^4 + \xi^2(b^2 - a^2)}} \right).$$

It is evident that $D = |\mathbf{D}|$.

The numerical integration was performed using a 9-point two-dimensional Gauss-type integration formula. The result is presented on Figure 1.8. The parameter values are given in Table 1.2.

The example considered in this subsection may not be physically relevant. However it shows how Okada's solution can be extended. For a more precise modeling of the faulting event we need to have more information about the earthquake source and its related parameters.

After having reviewed the description of the source, we now switch to the deformation of the ocean surface following a submarine earthquake. The traditional approach for hydrodynamic modelers is to use elastic models similar to the model we just described with the seismic parameters as input in order to evaluate the details of the seafloor deformation. Then this deformation is translated to the free surface of the ocean and serves as initial condition of the evolution problem described in the next section.

1.1.4 Solution in fluid domain

The fluid domain is supposed to represent the ocean above the fault area. Let us consider the fluid domain Ω shown in Figure 1.9. It is bounded above by the free surface of

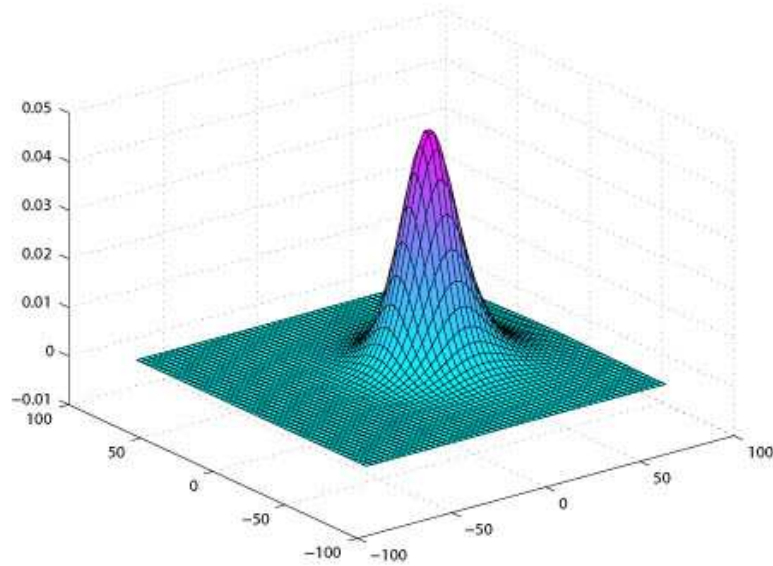


Figure 1.8: Free-surface deformation due to curvilinear faulting. The horizontal distances x and y are expressed in kilometers.

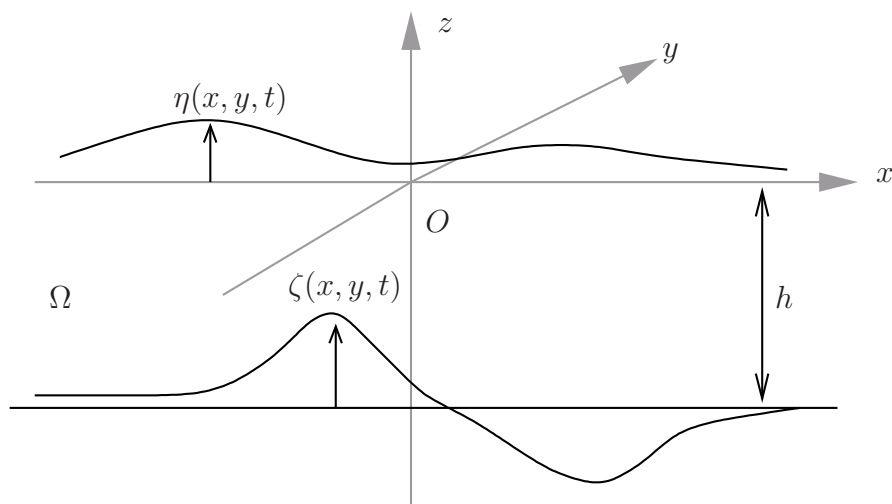


Figure 1.9: Definition of the fluid domain and coordinate system

the ocean and below by the rigid ocean floor. The domain Ω is unbounded in the horizontal directions x and y , and can be written as

$$\Omega = \mathbb{R}^2 \times [-h + \zeta(x, y, t), \eta(x, y, t)].$$

Initially the fluid is assumed to be at rest and the sea bottom to be horizontal. Thus, at time $t = 0$, the free surface and the sea bottom are defined by $z = 0$ and $z = -h$, respectively. For time $t > 0$ the bottom boundary moves in a prescribed manner which is given by

$$z = -h + \zeta(x, y, t).$$

The displacement of the sea bottom is assumed to have all the properties required to compute its Fourier transform in x, y and its Laplace transform in t . The resulting deformation of the free surface $z = \eta(x, y, t)$ must be found. It is also assumed that the fluid is incompressible and the flow is irrotational. The latter implies the existence of a velocity potential $\phi(x, y, z, t)$ which completely describes this flow. By definition of ϕ , the fluid velocity vector can be expressed as $\mathbf{q} = \nabla\phi$. Thus, the continuity equation becomes

$$\nabla \cdot \mathbf{q} = \Delta\phi = 0, \quad (x, y, z) \in \Omega. \quad (1.8)$$

The potential $\phi(x, y, z, t)$ must also satisfy the following kinematic boundary conditions on the free-surface and the solid boundary, respectively:

$$\frac{\partial\phi}{\partial z} = \frac{\partial\eta}{\partial t} + \frac{\partial\phi}{\partial x} \frac{\partial\eta}{\partial x} + \frac{\partial\phi}{\partial y} \frac{\partial\eta}{\partial y}, \quad z = \eta(x, y, t), \quad (1.9)$$

$$\frac{\partial\phi}{\partial z} = \frac{\partial\zeta}{\partial t} + \frac{\partial\phi}{\partial x} \frac{\partial\zeta}{\partial x} + \frac{\partial\phi}{\partial y} \frac{\partial\zeta}{\partial y}, \quad z = -h + \zeta(x, y, t). \quad (1.10)$$

Assuming that viscous effects as well as capillary effects can be neglected, the dynamic condition to be satisfied on the free surface reads

$$\frac{\partial\phi}{\partial t} + \frac{1}{2}|\nabla\phi|^2 + g\eta = 0, \quad z = \eta(x, y, t). \quad (1.11)$$

As described above, the initial conditions are given by

$$\eta(x, y, 0) = 0 \quad \text{and} \quad \zeta(x, y, 0) = 0. \quad (1.12)$$

The significance of the various terms in the equations is more transparent when the equations are written in dimensionless variables. The new independent variables are

$$\tilde{x} = \kappa x, \quad \tilde{y} = \kappa y, \quad \tilde{z} = \kappa z, \quad \tilde{t} = \sigma t,$$

where κ is a wavenumber and σ is a typical frequency. Note that here the same unit length is used in the horizontal and vertical directions, as opposed to shallow-water theory.

The new dependent variables are

$$\tilde{\eta} = \frac{\eta}{a}, \quad \tilde{\zeta} = \frac{\zeta}{a}, \quad \tilde{\phi} = \frac{\kappa}{a\sigma}\phi,$$

where a is a characteristic wave amplitude. A dimensionless water depth is also introduced:

$$\tilde{h} = \kappa h.$$

In dimensionless form, and after dropping the tildes, equations (1.8–1.11) become

$$\Delta\phi = 0, \quad (x, y, z) \in \Omega,$$

$$\begin{aligned} \frac{\partial\phi}{\partial z} &= \frac{\partial\eta}{\partial t} + \kappa a \left(\frac{\partial\phi}{\partial x} \frac{\partial\eta}{\partial x} + \frac{\partial\phi}{\partial y} \frac{\partial\eta}{\partial y} \right), & z &= \kappa a \eta(x, y, t), \\ \frac{\partial\phi}{\partial z} &= \frac{\partial\zeta}{\partial t} + \kappa a \left(\frac{\partial\phi}{\partial x} \frac{\partial\zeta}{\partial x} + \frac{\partial\phi}{\partial y} \frac{\partial\zeta}{\partial y} \right), & z &= -h + \kappa a \zeta(x, y, t), \end{aligned}$$

$$\frac{\partial\phi}{\partial t} + \frac{1}{2}\kappa a |\nabla\phi|^2 + \frac{g\kappa}{\sigma^2}\eta = 0, \quad z = \kappa a \eta(x, y, t).$$

Finding the solution to this problem is quite a difficult task due to the nonlinearities and the a priori unknown free surface. In this study we linearize the equations and the boundary conditions by taking the limit as $\kappa a \rightarrow 0$. In fact, the linearized problem can be found by expanding the unknown functions as power series of a small parameter $\varepsilon := \kappa a$. Collecting the lowest order terms in ε yields the linear approximation. For the sake of convenience, we now switch back to the physical variables. The linearized problem in dimensional variables reads

$$\Delta\phi = 0, \quad (x, y, z) \in \mathbb{R}^2 \times [-h, 0], \quad (1.13)$$

$$\frac{\partial\phi}{\partial z} = \frac{\partial\eta}{\partial t}, \quad z = 0, \quad (1.14)$$

$$\frac{\partial\phi}{\partial z} = \frac{\partial\zeta}{\partial t}, \quad z = -h, \quad (1.15)$$

$$\frac{\partial\phi}{\partial t} + g\eta = 0, \quad z = 0. \quad (1.16)$$

Combining equations (1.14) and (1.16) yields the single free-surface condition

$$\frac{\partial^2\phi}{\partial t^2} + g\frac{\partial\phi}{\partial z} = 0, \quad z = 0. \quad (1.17)$$

This problem will be solved by using the method of integral transforms. We apply the Fourier transform in (x, y) :

$$\begin{aligned}\mathbb{F}[f] &= \widehat{f}(k, \ell) = \int_{\mathbb{R}^2} f(x, y) e^{-i(kx+\ell y)} dx dy, \\ \mathbb{F}^{-1}[\widehat{f}] &= f(x, y) = \frac{1}{(2\pi)^2} \int_{\mathbb{R}^2} \widehat{f}(k, \ell) e^{i(kx+\ell y)} dk d\ell,\end{aligned}$$

and the Laplace transform in time t :

$$\mathfrak{L}[g] = \mathbf{g}(s) = \int_0^{+\infty} g(t) e^{-st} dt.$$

For the combined Fourier and Laplace transforms, the following notation is introduced:

$$\mathbb{F}\mathfrak{L}[F(x, y, t)] = \overline{F}(k, \ell, s) = \int_{\mathbb{R}^2} e^{-i(kx+\ell y)} dx dy \int_0^{+\infty} F(x, y, t) e^{-st} dt.$$

After applying the transforms, equations (1.13), (1.15) and (1.17) become

$$\frac{d^2 \overline{\phi}}{dz^2} - (k^2 + \ell^2) \overline{\phi} = 0, \quad (1.18)$$

$$\frac{d\overline{\phi}}{dz}(k, \ell, -h, s) = s \overline{\zeta}(k, \ell, s), \quad (1.19)$$

$$s^2 \overline{\phi}(k, \ell, 0, s) + g \frac{d\overline{\phi}}{dz}(k, \ell, 0, s) = 0. \quad (1.20)$$

The transformed free-surface elevation can be obtained from (1.16):

$$\overline{\eta}(k, \ell, s) = -\frac{s}{g} \overline{\phi}(k, \ell, 0, s). \quad (1.21)$$

A general solution of equation (1.18) is given by

$$\overline{\phi}(k, \ell, z, s) = A(k, \ell, s) \cosh(mz) + B(k, \ell, s) \sinh(mz), \quad (1.22)$$

where $m = \sqrt{k^2 + \ell^2}$. The functions $A(k, \ell, s)$ and $B(k, \ell, s)$ can be easily found from the boundary conditions (1.19) and (1.20):

$$\begin{aligned}A(k, \ell, s) &= -\frac{gs \overline{\zeta}(k, \ell, s)}{\cosh(mh)[s^2 + gm \tanh(mh)]}, \\ B(k, \ell, s) &= \frac{s^3 \overline{\zeta}(k, \ell, s)}{m \cosh(mh)[s^2 + gm \tanh(mh)]}.\end{aligned}$$

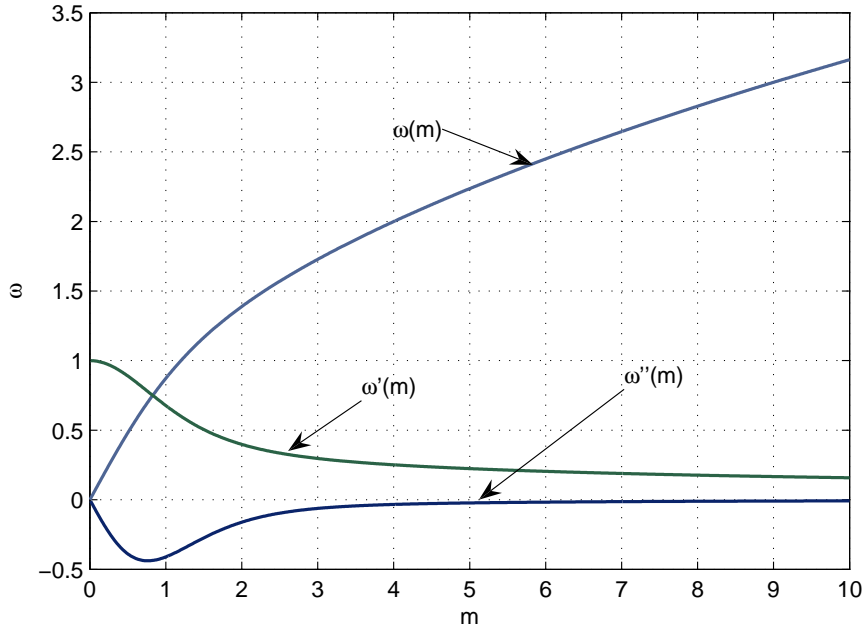


Figure 1.10: Plot of the frequency $\omega(m) = \sqrt{gm \tanh(mh)}$ and its derivatives $d\omega/dm$, $d^2\omega/dm^2$. The acceleration due to gravity g and the water depth h have been set equal to 1.

From now on, the notation

$$\omega = \sqrt{gm \tanh(mh)} \quad (1.23)$$

will be used. The graphs of $\omega(m)$, $\omega'(m)$ and $\omega''(m)$ are shown in Figure 1.10.

Substituting the expressions for the functions A , B in (1.22) yields

$$\bar{\phi}(k, \ell, z, s) = -\frac{gs\bar{\zeta}(k, \ell, s)}{\cosh(mh)(s^2 + \omega^2)} \left(\cosh(mz) - \frac{s^2}{gm} \sinh(mz) \right). \quad (1.24)$$

1.1.5 Free-surface elevation

From (1.21), the free-surface elevation becomes

$$\bar{\eta}(k, \ell, s) = \frac{s^2 \bar{\zeta}(k, \ell, s)}{\cosh(mh)(s^2 + \omega^2)}.$$

Inverting the Laplace and Fourier transforms provides the general integral solution

$$\eta(x, y, t) = \frac{1}{(2\pi)^2} \iint_{\mathbb{R}^2} \frac{e^{i(kx+\ell y)}}{\cosh(mh)} \frac{1}{2\pi i} \int_{\mu-i\infty}^{\mu+i\infty} \frac{s^2 \bar{\zeta}(k, \ell, s)}{s^2 + \omega^2} e^{st} ds \, dk d\ell. \quad (1.25)$$

One can evaluate the Laplace integral in (1.25) using the convolution theorem:

$$\mathfrak{L}[f_1(t) * f_2(t)] = \mathbf{f}_1(s)\mathbf{f}_2(s).$$

It yields

$$\eta(x, y, t) = \frac{1}{(2\pi)^2} \iint_{\mathbb{R}^2} \frac{e^{i(kx+\ell y)}}{\cosh(mh)} \int_0^t (1 - \omega \sin \omega\tau) \bar{\zeta}(k, \ell, t - \tau) d\tau dk d\ell.$$

This general solution contains as a special case the solution for an axisymmetric problem, which we now describe in detail. Assume that the initial solid boundary deformation is axisymmetric:

$$\zeta(x, y) = \zeta(r), \quad r = \sqrt{x^2 + y^2}.$$

The Fourier transform $\mathbb{F}[\zeta(x, y)] = \widehat{\zeta}(k, \ell)$ of an axisymmetric function is also axisymmetric with respect to transformation parameters, i.e.

$$\widehat{\zeta}(k, \ell) = \widehat{\zeta}(m), \quad m := \sqrt{k^2 + \ell^2}.$$

In the following calculation, we use the notation $\psi = \arctan(\ell/k)$. One has

$$\begin{aligned} \widehat{\zeta}(k, \ell) &= \iint_{\mathbb{R}^2} \zeta(r) e^{-i(kx+\ell y)} dx dy = \int_0^{2\pi} d\phi \int_0^\infty \zeta(r) e^{-ir(k \cos \phi + \ell \sin \phi)} r dr = \\ &= \int_0^{2\pi} d\phi \int_0^\infty r \zeta(r) e^{-irm \cos(\phi-\psi)} dr = \int_0^\infty r \zeta(r) dr \int_0^\pi (e^{-irm \cos \phi} + e^{irm \cos \phi}) d\phi. \end{aligned}$$

Using an integral representation of Bessel functions [GR00] finally yields

$$\widehat{\zeta}(k, \ell) = 2\pi \int_0^\infty r \zeta(r) J_0(mr) dr \equiv \widehat{\zeta}(m).$$

It follows that

$$\begin{aligned} \eta(r, t) &= \frac{1}{(2\pi)^2} \int_0^{2\pi} d\psi \int_0^{+\infty} \frac{m e^{imr \cos(\phi-\psi)}}{\cosh(mh)} dm \int_0^t (1 - \omega \sin \omega\tau) \bar{\zeta}(m, t - \tau) d\tau \\ &= \frac{1}{2\pi} \int_0^{+\infty} m \frac{J_0(mr)}{\cosh(mh)} dm \int_0^t (1 - \omega \sin \omega\tau) \bar{\zeta}(m, t - \tau) d\tau. \end{aligned}$$

The last equation gives the general integral solution of the problem in the case of an axisymmetric seabed deformation. Below we no longer make this assumption since Okada's solution does not have this property.

In the present study we consider seabed deformations with the following structure:

$$\zeta(x, y, t) := \zeta(x, y)T(t). \quad (1.26)$$

Mathematically we separate the time dependence from the spatial coordinates. There are two main reasons for doing this. First of all we want to be able to invert analytically the Laplace transform. The second reason is more fundamental. In fact, dynamic source models are not easily available. Okada's solution, which was described in the previous section, provides the static sea-bed deformation $\zeta_0(x, y)$ and we will consider different time dependencies $T(t)$ to model the time evolution of the source. Four scenarios will be considered:

1. **Instantaneous:** $T_i(t) = H(t)$, where $H(t)$ denotes the Heaviside step function,

2. **Exponential:**

$$T_e(t) = \begin{cases} 0, & t < 0, \\ 1 - e^{-\alpha t}, & t \geq 0, \end{cases} \quad \text{with } \alpha > 0,$$

3. **Trigonometric:** $T_c(t) = H(t - t_0) + \frac{1}{2}[1 - \cos(\pi t/t_0)]H(t_0 - t)$,

4. **Linear:**

$$T_l(t) = \begin{cases} 0, & t < 0, \\ t/t_0, & 0 \leq t \leq t_0, \\ 1, & t > t_0. \end{cases}$$

The typical graphs of $T_c(t)$ and $T_e(t)$ are shown in Figure 1.11. Inserting (1.26) into (1.25) yields

$$\eta(x, y, t) = \frac{1}{(2\pi)^2} \iint_{\mathbb{R}^2} \frac{\widehat{\zeta}(k, \ell) e^{i(kx + \ell y)}}{\cosh(mh)} \frac{1}{2\pi i} \int_{\mu - i\infty}^{\mu + i\infty} \frac{s^2 \mathbf{T}(s)}{s^2 + \omega^2} e^{st} ds dk d\ell. \quad (1.27)$$

Clearly, $\eta(x, y, t)$ depends continuously on the source $\zeta(x, y)$. Physically it means that small variations of ζ (in a reasonable space of functions such as L^2) yield small variations of η . Mathematically this problem is said to be well-posed, and this property is essential for modelling the physical processes, since it means that small modifications of the ground motion (for example, the error in measurements) do not induce huge modifications of the wave patterns.

Using the special representation (1.26) of seabed deformation and prescribed time-dependencies, one can compute analytically the Laplace integral in (1.27). To perform this

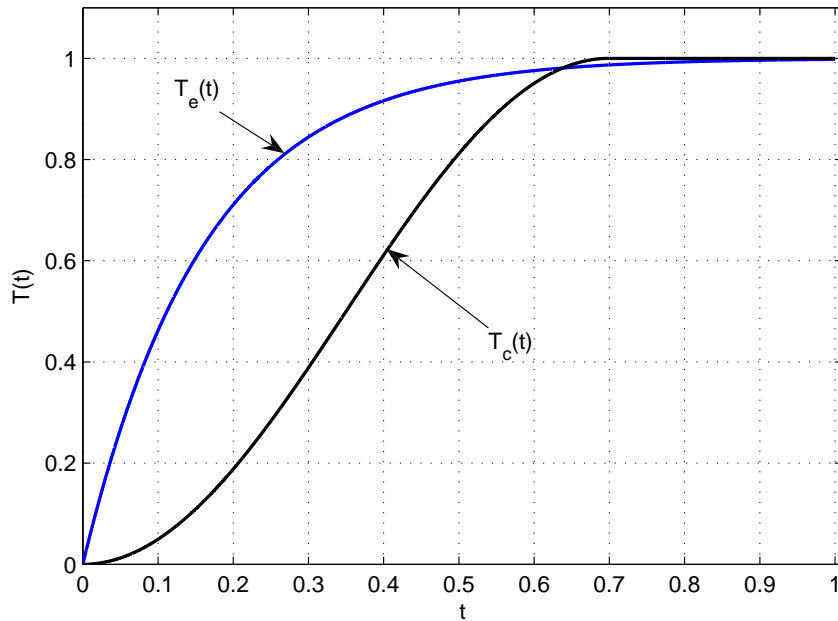


Figure 1.11: Typical graphs of $T_e(t)$ and $T_c(t)$. Here we have set $\alpha = 6.2$, $t_0 = 0.7$.

integration, we first have to compute the Laplace transform of $T_{i,e,c,l}(t)$. The results of these computations are given in Table 1.3.

<i>scenario</i>	<i>Laplace transform</i>
Instantaneous	$\mathcal{L}[T_i] = \frac{1}{s}$
Exponential	$\mathcal{L}[T_e] = \frac{\alpha}{s(\alpha+s)}$
Trigonometric	$\mathcal{L}[T_c] = \frac{\gamma^2}{2s(s^2+\gamma^2)}(1 + e^{-st_0})$ with $\gamma = \frac{\pi}{t_0}$
Linear	$\mathcal{L}[T_l] = \frac{1-e^{-st_0}}{t_0s^2}$

Table 1.3: Laplace transforms of different time-dependencies for prescribed bottom motion.

Inserting these formulas into the inverse Laplace integral yields

$$\begin{aligned} \frac{1}{2\pi i} \int_{\mu-i\infty}^{\mu+i\infty} \frac{e^{st} s^2 \mathbf{T}_i(s)}{s^2 + \omega^2} ds &= \cos \omega t, \\ \frac{1}{2\pi i} \int_{\mu-i\infty}^{\mu+i\infty} \frac{e^{st} s^2 \mathbf{T}_e(s)}{s^2 + \omega^2} ds &= -\frac{\alpha^2}{\alpha^2 + \omega^2} \left(e^{-\alpha t} - \cos \omega t - \frac{\omega}{\alpha} \sin \omega t \right), \\ \frac{1}{2\pi i} \int_{\mu-i\infty}^{\mu+i\infty} \frac{e^{st} s^2 \mathbf{T}_c(s)}{s^2 + \omega^2} ds &= \frac{\gamma^2}{2(\gamma^2 - \omega^2)} \\ &\quad (\cos \omega t - \cos \gamma t + H(t - t_0)[\cos \omega(t - t_0) + \cos \gamma t]), \\ \frac{1}{2\pi i} \int_{\mu-i\infty}^{\mu+i\infty} \frac{e^{st} s^2 \mathbf{T}_1(s)}{s^2 + \omega^2} ds &= \frac{\sin \omega t - H(t - t_0) \sin \omega(t - t_0)}{\omega t_0}. \end{aligned}$$

The final integral formulas for the free-surface elevations with different time dependencies are as follows:

$$\begin{aligned} \eta_i(x, y, t) &= \frac{1}{(2\pi)^2} \iint_{\mathbb{R}^2} \frac{\widehat{\zeta}(k, \ell) e^{i(kx + \ell y)}}{\cosh(mh)} \cos \omega t \, dk d\ell, \\ \eta_e(x, y, t) &= \frac{-\alpha^2}{(2\pi)^2} \iint_{\mathbb{R}^2} \frac{\widehat{\zeta}(k, \ell) e^{i(kx + \ell y)}}{\cosh(mh)} \left(\frac{e^{-\alpha t} - \cos \omega t - \frac{\omega}{\alpha} \sin \omega t}{\alpha^2 + \omega^2} \right) dk d\ell, \\ \eta_c(x, y, t) &= \frac{\gamma^2}{(2\pi)^2} \iint_{\mathbb{R}^2} \frac{\widehat{\zeta}(k, \ell) e^{i(kx + \ell y)}}{2(\gamma^2 - \omega^2) \cosh(mh)} \\ &\quad (\cos \omega t - \cos \gamma t + H(t - t_0)[\cos \omega(t - t_0) + \cos \gamma t]) \, dk d\ell, \\ \eta_l(x, y, t) &= \frac{1}{(2\pi)^2} \iint_{\mathbb{R}^2} \frac{\widehat{\zeta}(k, \ell) e^{i(kx + \ell y)}}{\cosh(mh)} \left(\frac{\sin \omega t - H(t - t_0) \sin \omega(t - t_0)}{\omega t_0} \right) dk d\ell. \end{aligned}$$

1.1.6 Velocity field

In some applications it is important to know not only the free-surface elevation but also the velocity field in the fluid domain. One of the goals of this work is to provide an initial condition for tsunami propagation codes. For the time being, tsunami modelers take initial seabed deformations and translate them directly to the free surface in order to obtain the initial condition $\eta(x, y, 0)$. Since a priori there is no information on the flow velocities,

they take a zero velocity field as initial condition for the velocity: $\nabla\phi(x, y, z, 0) = 0$. The present computations show that it is indeed a very good approximation if the generation time is short.

In equation (1.24), we obtained the Fourier transform of the velocity potential $\phi(x, y, z, t)$:

$$\bar{\phi}(k, \ell, z, s) = -\frac{gs\widehat{\zeta}(k, \ell)\mathbf{T}(s)}{\cosh(mh)(s^2 + \omega^2)} \left(\cosh(mz) - \frac{s^2}{gm} \sinh(mz) \right). \quad (1.28)$$

Let us evaluate the velocity field at an arbitrary level $z = \beta h$ with $-1 \leq \beta \leq 0$. In the linear approximation the value $\beta = 0$ corresponds to the free surface while $\beta = -1$ corresponds to the bottom. Next we introduce some notation. The horizontal velocities are denoted by \mathbf{u} . The horizontal gradient ($\partial/\partial x, \partial/\partial y$) is denoted by ∇_h . The vertical velocity component is simply w . The Fourier transform parameters are denoted $\mathbf{k} = (k, \ell)$.

Taking the Fourier and Laplace transforms of

$$\mathbf{u}(x, y, t) = \nabla_h \phi(x, y, z, t)|_{z=\beta h}$$

yields

$$\begin{aligned} \bar{\mathbf{u}}(k, \ell, s) &= -i\bar{\phi}(k, \ell, \beta h, s)\mathbf{k} \\ &= i\frac{gs\widehat{\zeta}(k, \ell)\mathbf{T}(s)}{\cosh(mh)(s^2 + \omega^2)} \left(\cosh(\beta mh) - \frac{s^2}{gm} \sinh(\beta mh) \right) \mathbf{k}. \end{aligned}$$

Inverting the Fourier and Laplace transforms gives the general formula for the horizontal velocities:

$$\begin{aligned} \mathbf{u}(x, y, t) &= \frac{ig}{4\pi^2} \iint_{\mathbb{R}^2} \frac{\mathbf{k}\widehat{\zeta}(k, \ell) \cosh(m\beta h) e^{i(kx+\ell y)}}{\cosh(mh)} \frac{1}{2\pi i} \int_{\mu-i\infty}^{\mu+i\infty} \frac{s\mathbf{T}(s)e^{st}}{s^2 + \omega^2} ds d\mathbf{k} \\ &\quad - \frac{i}{4\pi^2} \iint_{\mathbb{R}^2} \frac{\mathbf{k}\widehat{\zeta}(k, \ell) \sinh(m\beta h) e^{i(kx+\ell y)}}{m \cosh(mh)} \frac{1}{2\pi i} \int_{\mu-i\infty}^{\mu+i\infty} \frac{s^3\mathbf{T}(s)e^{st}}{s^2 + \omega^2} ds d\mathbf{k}. \end{aligned}$$

After a few computations, one finds the formulas for the time dependencies T_i , T_e and T_l . For simplicity we only give the velocities along the free surface ($\beta = 0$):

$$\begin{aligned} \mathbf{u}_i(x, y, t) &= \frac{ig}{4\pi^2} \iint_{\mathbb{R}^2} \frac{\mathbf{k}\widehat{\zeta}(k, \ell) e^{i(kx+\ell y)}}{\cosh(mh)} \frac{\sin \omega t}{\omega} d\mathbf{k}, \\ \mathbf{u}_e(x, y, t) &= \frac{ig\alpha}{4\pi^2} \iint_{\mathbb{R}^2} \frac{\mathbf{k}\widehat{\zeta}(k, \ell) e^{i(kx+\ell y)}}{(\alpha^2 + \omega^2) \cosh(mh)} \left(e^{-\alpha t} - \cos \omega t + \frac{\alpha}{\omega} \sin \omega t \right) d\mathbf{k}, \\ \mathbf{u}_l(x, y, t) &= \frac{ig}{4t_0\pi^2} \iint_{\mathbb{R}^2} \frac{\mathbf{k}\widehat{\zeta}(k, \ell) e^{i(kx+\ell y)}}{\omega^2 \cosh(mh)} \\ &\quad (1 - \cos \omega t - H(t - t_0)[1 - \cos \omega(t - t_0)]) d\mathbf{k}. \end{aligned}$$

Next we determine the vertical component of the velocity $w(x, y, z, t)$. It is easy to obtain the Fourier–Laplace transform $\bar{w}(k, \ell, z, s)$ by differentiating (1.28):

$$\bar{w}(k, \ell, z, s) = \frac{\partial \bar{\phi}}{\partial z} = \frac{sg\widehat{\zeta}(k, \ell)\mathbf{T}(s)}{\cosh(mh)(s^2 + \omega^2)} \left(\frac{s^2}{g} \cosh(mz) - m \sinh(mz) \right).$$

Inverting this transform yields

$$\begin{aligned} w(x, y, z, t) &= \frac{1}{4\pi^2} \iint_{\mathbb{R}^2} \frac{\cosh(mz)\widehat{\zeta}(k, \ell)}{\cosh(mh)} e^{i(kx+\ell y)} \frac{1}{2\pi i} \int_{\mu-i\infty}^{\mu+i\infty} \frac{s^3 \mathbf{T}(s) e^{st}}{s^2 + \omega^2} ds d\mathbf{k} \\ &\quad - \frac{g}{4\pi^2} \iint_{\mathbb{R}^2} \frac{m \sinh(mz)\widehat{\zeta}(k, \ell)}{\cosh(mh)} e^{i(kx+\ell y)} \frac{1}{2\pi i} \int_{\mu-i\infty}^{\mu+i\infty} \frac{s \mathbf{T}(s) e^{st}}{s^2 + \omega^2} ds d\mathbf{k}, \end{aligned}$$

for $-h < z \leq 0$. One can easily obtain the expression of the vertical velocity at a given vertical level by substituting $z = \beta h$ in the expression for w .

The easiest way to compute the vertical velocity w along the free surface is to use the boundary condition (1.14). Indeed, the expression for w can be simply derived by differentiating the known formula for $\eta_{i,e,c,l}(x, y, t)$. Note that formally the derivative gives the distributions $\delta(t)$ and $\delta(t - t_0)$ under the integral sign. It is a consequence of the idealized time behaviour (such as the instantaneous scenario) and it is a disadvantage of the Laplace transform method. In order to avoid these distributions we can consider the solutions only for $t > 0$ and $t \neq t_0$. From a practical point of view there is no restriction since for any $\varepsilon > 0$ we can set $t = \varepsilon$ or $t = t_0 + \varepsilon$. For small values of ε this will give a very good approximation of the solution behaviour at these ‘‘critical’’ instants of time. Under this assumption we give the distribution-free expressions for the vertical velocity along the free surface:

$$\begin{aligned} w_i(x, y, t) &= -\frac{1}{4\pi^2} \iint_{\mathbb{R}^2} \frac{\widehat{\zeta}(k, \ell) e^{i(kx+\ell y)}}{\cosh(mh)} \omega \sin \omega t d\mathbf{k}, \\ w_e(x, y, t) &= \frac{\alpha^3}{4\pi^2} \iint_{\mathbb{R}^2} \frac{\widehat{\zeta}(k, \ell) e^{i(kx+\ell y)}}{(\alpha^2 + \omega^2) \cosh(mh)} \left(e^{-\alpha t} + \frac{\omega^2}{\alpha^2} \cos \omega t - \frac{\omega}{\alpha} \sin \omega t \right) d\mathbf{k}, \\ w_c(x, y, t) &= -\frac{\gamma^2}{4\pi^2} \iint_{\mathbb{R}^2} \frac{\widehat{\zeta}(k, \ell) e^{i(kx+\ell y)}}{2(\gamma^2 - \omega^2) \cosh(mh)} (\omega \sin \omega t - \gamma \sin \gamma t \\ &\quad + H(t - t_0) [\omega \sin \omega(t - t_0) + \gamma \sin \gamma t]) d\mathbf{k}, \\ w_l(x, y, t) &= \frac{1}{4t_0\pi^2} \iint_{\mathbb{R}^2} \frac{\widehat{\zeta}(k, \ell) e^{i(kx+\ell y)}}{\cosh(mh)} [\cos \omega t - H(t - t_0) \cos \omega(t - t_0)] d\mathbf{k}. \end{aligned}$$

1.1.6.1 Pressure on the bottom

Since tsunameters have one component that measures the pressure at the bottom (bottom pressure recorder or simply BPR [GBM⁺05]), it is interesting to provide as well the expression $p_b(x, y, t)$ for the pressure at the bottom. The pressure $p(x, y, z, t)$ can be obtained from Bernoulli's equation, which was written explicitly for the free surface in equation (1.11), but is valid everywhere in the fluid:

$$\frac{\partial \phi}{\partial t} + \frac{1}{2} |\nabla \phi|^2 + gz + \frac{p}{\rho} = 0. \quad (1.29)$$

After linearization, equation (1.29) becomes

$$\frac{\partial \phi}{\partial t} + gz + \frac{p}{\rho} = 0. \quad (1.30)$$

Along the bottom, it reduces to

$$\frac{\partial \phi}{\partial t} + g(-h + \zeta) + \frac{p_b}{\rho} = 0, \quad z = -h. \quad (1.31)$$

The time-derivative of the velocity potential is readily available in Fourier space. Inverting the Fourier and Laplace transforms and evaluating the resulting expression at $z = -h$ gives for the four time scenarios, respectively,

$$\begin{aligned} \frac{\partial \phi_i}{\partial t} &= -\frac{g}{(2\pi)^2} \iint_{\mathbb{R}^2} \frac{\widehat{\zeta}(k, \ell) e^{i(kx + \ell y)}}{\cosh^2(mh)} \cos \omega t \, d\mathbf{k}, \\ \frac{\partial \phi_e}{\partial t} &= \frac{g\alpha^2}{(2\pi)^2} \iint_{\mathbb{R}^2} \frac{\widehat{\zeta}(k, \ell) e^{i(kx + \ell y)}}{\alpha^2 + \omega^2} \left(e^{-\alpha t} - \cos \omega t - \frac{\omega}{\alpha} \sin \omega t \right) d\mathbf{k} + \frac{\alpha^4}{(2\pi)^2} \\ &\quad \iint_{\mathbb{R}^2} \frac{\widehat{\zeta}(k, \ell) \tanh(mh) e^{i(kx + \ell y)}}{m(\alpha^2 + \omega^2)} \left(e^{-\alpha t} + \left(\frac{\omega}{\alpha}\right)^2 \cos \omega t + \left(\frac{\omega}{\alpha}\right)^3 \sin \omega t \right) d\mathbf{k}, \\ \frac{\partial \phi_l}{\partial t} &= -\frac{g}{t_0(2\pi)^2} \iint_{\mathbb{R}^2} \frac{\widehat{\zeta}(k, \ell) e^{i(kx + \ell y)}}{\omega \cosh^2(mh)} [\sin \omega t - H(t - t_0) \sin \omega(t - t_0)] d\mathbf{k}. \end{aligned}$$

The bottom pressure deviation from the hydrostatic pressure is then given by

$$p_b(x, y, t) = -\rho \left. \frac{\partial \phi}{\partial t} \right|_{z=-h} - \rho g \zeta.$$

Plots of the bottom pressure will be given in Section 1.1.8.

1.1.7 Asymptotic analysis of integral solutions

In this subsection, we apply the method of stationary phase in order to estimate the far-field behaviour of the solutions. There is a lot of literature on this topic (see for example [Erd56, Mur92, PL71, BH86, ES94]). This method is a classical method in asymptotic analysis. To our knowledge, the stationary phase method was first used by Kelvin [Kel87] in the context of linear water-wave theory.

The motivation to obtain asymptotic formulas for integral solutions was mainly due to numerical difficulties to calculate the solutions for large values of x and y . From equation (1.25), it is clear that the integrand is highly oscillatory. In order to be able to resolve these oscillations, several discretization points are needed per period. This becomes extremely expensive as $r = \sqrt{x^2 + y^2} \rightarrow \infty$. The numerical method used in the present study is based on a Filon-type quadrature formula [Fil28] and has been adapted to double integrals with $\exp[i(kx + \ell y)]$ oscillations. The idea of this method consists in interpolating only the amplitude of the integrand at discretization points by some kind of polynomial or spline and then performing exact integration for the oscillating part of the integrand. This method seems to be quite efficient.

Let us first obtain an asymptotic representation for integral solutions of the general form

$$\eta(x, y, t) = \frac{1}{4\pi^2} \iint_{\mathbb{R}^2} \frac{\widehat{\zeta}(k, \ell) e^{i(kx + \ell y)}}{\cosh(mh)} T(m, t) dk d\ell, \quad m = \sqrt{k^2 + \ell^2}. \quad (1.32)$$

Comparing with equation (1.27) shows that $T(m, t)$ is in fact

$$T(m, t) = \frac{1}{2\pi i} \int_{\mu - i\infty}^{\mu + i\infty} \frac{s^2 \mathbf{T}(s)}{s^2 + \omega^2} e^{st} ds.$$

For example, we showed above that for an instantaneous seabed deformation $T(m, t) = \cos \omega t$, where $\omega^2 = gm \tanh mh$. For the time being, we do not specify the time behaviour $\mathbf{T}(s)$.

In equation (1.32), we switch to polar coordinates m and $\psi = \arctan(\ell/k)$:

$$\begin{aligned} \eta(x, y, t) &= \frac{1}{4\pi^2} \int_0^\infty \int_0^{2\pi} \frac{\widehat{\zeta}(m, \psi) e^{imr \cos(\varphi - \psi)}}{\cosh(mh)} T(m, t) m d\psi dm \\ &= \frac{1}{4\pi^2} \int_0^\infty \frac{m T(m, t)}{\cosh(mh)} dm \int_0^{2\pi} \widehat{\zeta}(m, \psi) e^{imr \cos(\varphi - \psi)} d\psi, \end{aligned}$$

where (r, φ) are the polar coordinates of (x, y) . In the last expression, the phase function is $\Phi = mr \cos(\varphi - \psi)$. Stationary phase points satisfy the condition $\partial\Phi/\partial\psi = 0$, which

yields two phases: $\psi_1 = \varphi$ and $\psi_2 = \varphi + \pi$. An approximation to equation (1.32) is then obtained by applying the method of stationary phase to the integral over ψ :

$$\eta(r, \phi, t) \simeq \frac{1}{\sqrt{8\pi^3 r}} \int_0^\infty \frac{\sqrt{m} T(m, t)}{\cosh(mh)} \left(\widehat{\zeta}(m, \varphi) e^{i(\frac{\pi}{4} - mr)} + \widehat{\zeta}(m, \varphi + \pi) e^{i(mr - \frac{\pi}{4})} \right) dm.$$

This expression cannot be simplified if we do not make any further hypotheses on the function $T(m, t)$.

Since we are looking for the far field solution behaviour, the details of wave formation are not important. Thus we will assume that the initial seabed deformation is instantaneous:

$$T(m, t) = \cos \omega t = \frac{e^{i\omega t} + e^{-i\omega t}}{2}.$$

Inserting this particular function $T(m, t)$ in equation (1.32) yields

$$\eta(r, \varphi, t) = \frac{1}{8\pi^2} (I_1 + I_2),$$

where

$$I_1 = \int_0^\infty \frac{m \widehat{\zeta}(m, \psi)}{\cosh(mh)} \int_0^{2\pi} e^{i(\omega t + mr \cos(\varphi - \psi))} d\psi dm,$$

$$I_2 = \int_0^\infty \frac{m \widehat{\zeta}(m, \psi)}{\cosh(mh)} \int_0^{2\pi} e^{i(-\omega t + mr \cos(\varphi - \psi))} d\psi dm.$$

The stationary phase function in these integrals is

$$\Phi(m, \psi) = mr \cos(\varphi - \psi) \pm \omega t, \quad \omega^2(m) = gm \tanh mh.$$

The points of stationary phase are then obtained from the conditions

$$\frac{\partial \Phi}{\partial \psi} = 0, \quad \frac{\partial \Phi}{\partial m} = 0.$$

The first equation gives two points, $\psi_1 = \varphi$ and $\psi_2 = \varphi + \pi$, as before. The second condition yields

$$\frac{r}{t} \cos(\varphi - \psi_{1,2}) = \mp \frac{d\omega}{dm}. \quad (1.33)$$

Since $d\omega/dm$ decreases from \sqrt{gh} to 0 as m goes from 0 to ∞ (see Figure 1.10), this equation has a unique solution for m if $|r/t| \leq \sqrt{gh}$. This unique solution will be denoted by m^* .

For $|r| > t\sqrt{gh}$, there is no stationary phase. It means physically that the wave has not yet reached this region. So we can approximately set $I_1 \approx 0$ and $I_2 \approx 0$. From the positivity of the function $d\omega/dm$ one can deduce that $\psi_1 = \varphi$ is a stationary phase point only for the integral I_2 . Similarly, $\psi_2 = \varphi + \pi$ is a stationary point only for the integral I_1 .

Let us obtain an asymptotic formula for the first integral:

$$\begin{aligned}
I_1 &\approx \int_0^\infty \frac{m}{\cosh(mh)} \left(\sqrt{\frac{2\pi}{mr}} \widehat{\zeta}(m, \varphi + \pi) e^{i(\omega t - mr)} e^{i\frac{\pi}{4}} \right) dm \\
&= \sqrt{\frac{2\pi}{r}} e^{i\frac{\pi}{4}} \int_0^\infty \frac{\widehat{\zeta}(m, \varphi + \pi)}{\cosh(mh)} \sqrt{m} e^{i(\omega t - mr)} dm \\
&\approx \sqrt{\frac{2\pi}{r}} e^{i\frac{\pi}{4}} \left(\sqrt{\frac{2\pi m^*}{|\omega''(m^*)| t}} \frac{\widehat{\zeta}(m^*, \varphi + \pi)}{\cosh(m^*h)} e^{i(\omega(m^*)t - m^*r)} e^{-i\frac{\pi}{4}} \right) \\
&= \frac{2\pi}{t} \sqrt{\frac{m^*}{-\omega''\omega'}} \frac{\widehat{\zeta}(m^*, \varphi + \pi)}{\cosh(m^*h)} e^{i(\omega(m^*)t - m^*r)}.
\end{aligned}$$

In this estimate we have used equation (1.33) evaluated at the stationary phase point (m^*, ψ_2) :

$$r = t \left. \frac{d\omega}{dm} \right|_{m=m^*}. \quad (1.34)$$

Similarly one can obtain an estimate for the integral I_2 :

$$I_2 \approx \frac{2\pi}{t} \sqrt{\frac{m^*}{-\omega''\omega'}} \frac{\widehat{\zeta}(m^*, \varphi)}{\cosh(m^*h)} e^{-i(\omega(m^*)t - m^*r)}.$$

Asymptotic values have been obtained for the integrals. As is easily observed from the expressions for I_1 and I_2 , the wave train decays as $1/t$, or $1/r$, which is equivalent since r and t are connected by relation (1.34).

1.1.8 Numerical results

A lot of numerical computations based on the analytical formulas obtained in the previous sections have been performed. Because of the lack of information about the real dynamical characteristics of tsunami sources, we cannot really conclude which time dependence gives the best description of tsunami generation. At this stage it is still very difficult or even impossible.

Numerical experiments showed that the largest wave amplitudes with the time dependence $T_c(t)$ were obtained for relatively small values of the characteristic time t_0 . The exponential dependence has shown higher amplitudes for relatively longer characteristic

Parameter	Value
Young modulus, E , GPa	9.5
Poisson ratio, ν	0.27
Fault depth, d , km	20
Dip angle, δ , $^\circ$	13
Strike angle, θ , $^\circ$	90
Normal angle, ϕ , $^\circ$	0
Fault length, L , km	60
Fault width, W , km	40
Burger's vector length, $ \mathbf{D} $, m	15
Water depth, h , km	4
Acceleration due to gravity, g , m/s^2	9.8
Wave number, k , $1/m$	10^{-4}
Angular frequency, ω , Hz	10^{-2}

Table 1.4: Physical parameters used in the numerical computations

times. The instantaneous scenario T_i gives at the free surface the initial seabed deformation with a slightly lower amplitude (the factor that we obtained was typically about $0.8 \sim 0.94$). The water has a high-pass filter effect on the initial solid boundary deformation. The linear time dependence $T_i(t)$ showed a linear growth of wave amplitude from 0 to also $\approx 0.9\zeta_0$, where $\zeta_0 = \max_{(x,y) \in \mathbb{R}^2} |\zeta(x,y)|$.

In this section we provide several plots (Figure 1.12) of the free-surface deformation. For illustration purposes, we have chosen the instantaneous seabed deformation since it is the most widely used. The values of the parameters used in the computations are given in Table 1.4. We also give plots of the velocity components on the free surface a few seconds (physical) after the instantaneous deformation (Figure 1.13). Finally, plots of the bottom dynamic pressure are given in Figure 1.14.

From Figure 1.13 it is clear that the velocity field is really negligible in the beginning of wave formation. Numerical computations showed that this situation does not change if one takes other time-dependences.

The main focus of the present section is the generation of waves by a moving bottom. The asymptotic behaviour of various sets of initial data propagating in a fluid of uniform depth has been studied in detail by Hammack and Segur [HS74, HS78]. In particular, they showed that the behaviours for an initial elevation wave and for an initial depression wave are different.

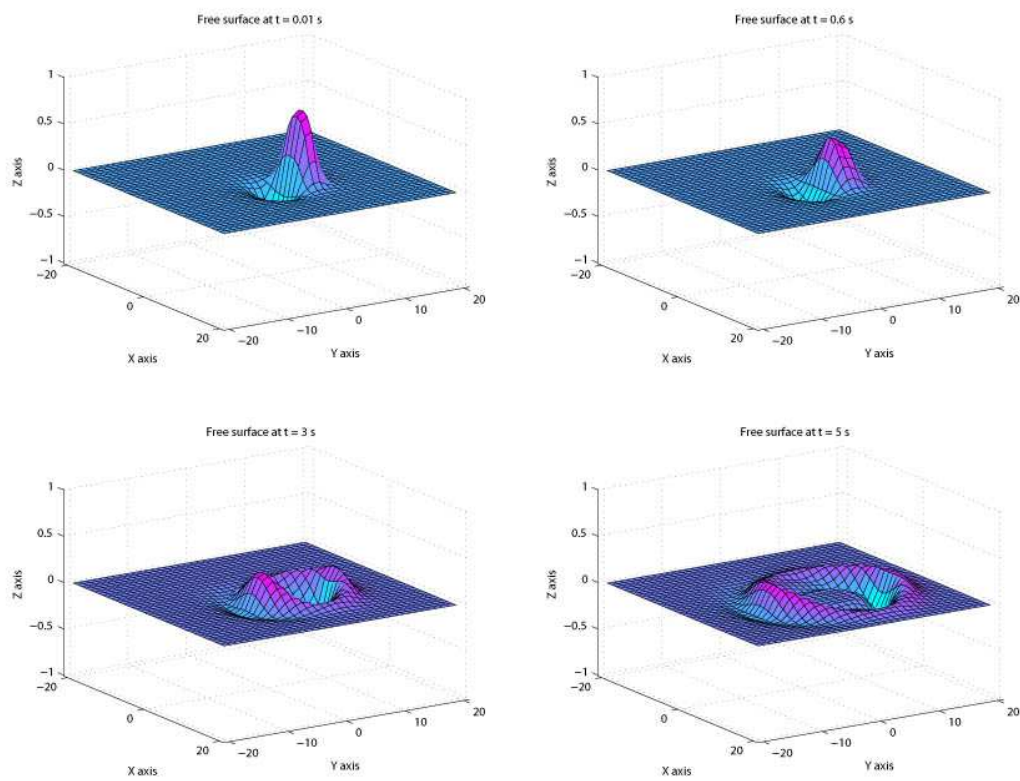


Figure 1.12: Free-surface elevation at $t = 0.01, 0.6, 3, 5$ in dimensionless time. In physical time it corresponds to one second, one minute, five minutes and eight minutes and a half after the initial seabed deformation.

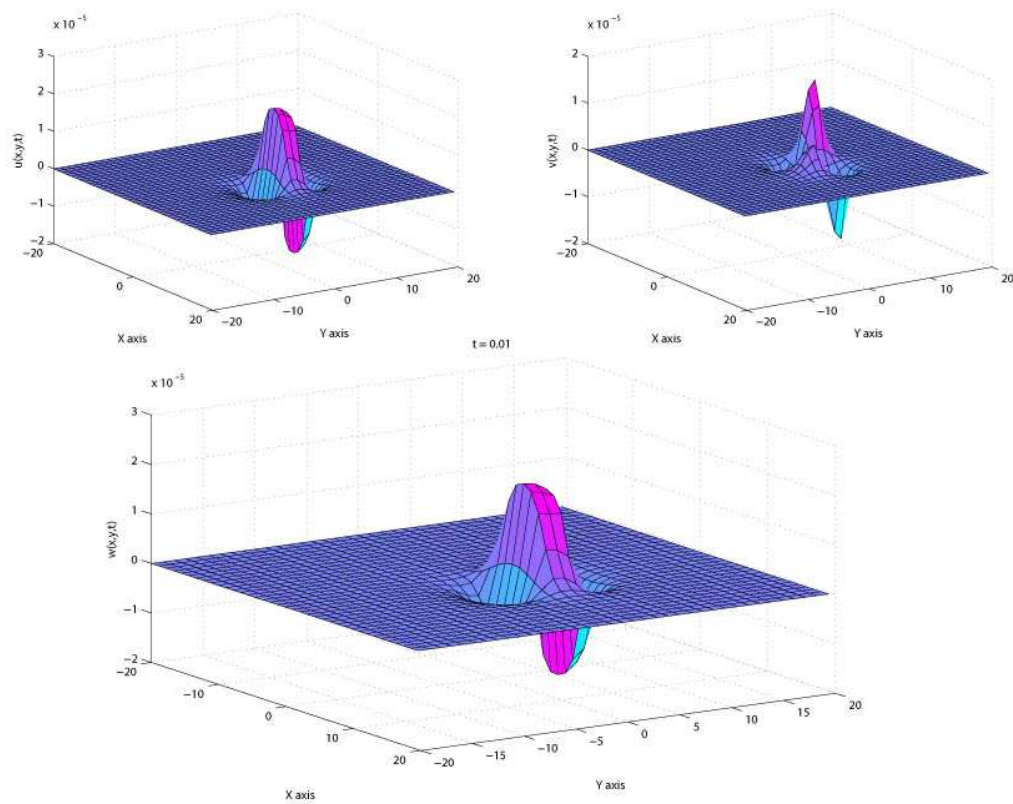


Figure 1.13: Components u , v and w of the velocity field computed along the free surface at $t = 0.01$, that is one second after the initial seabed deformation.

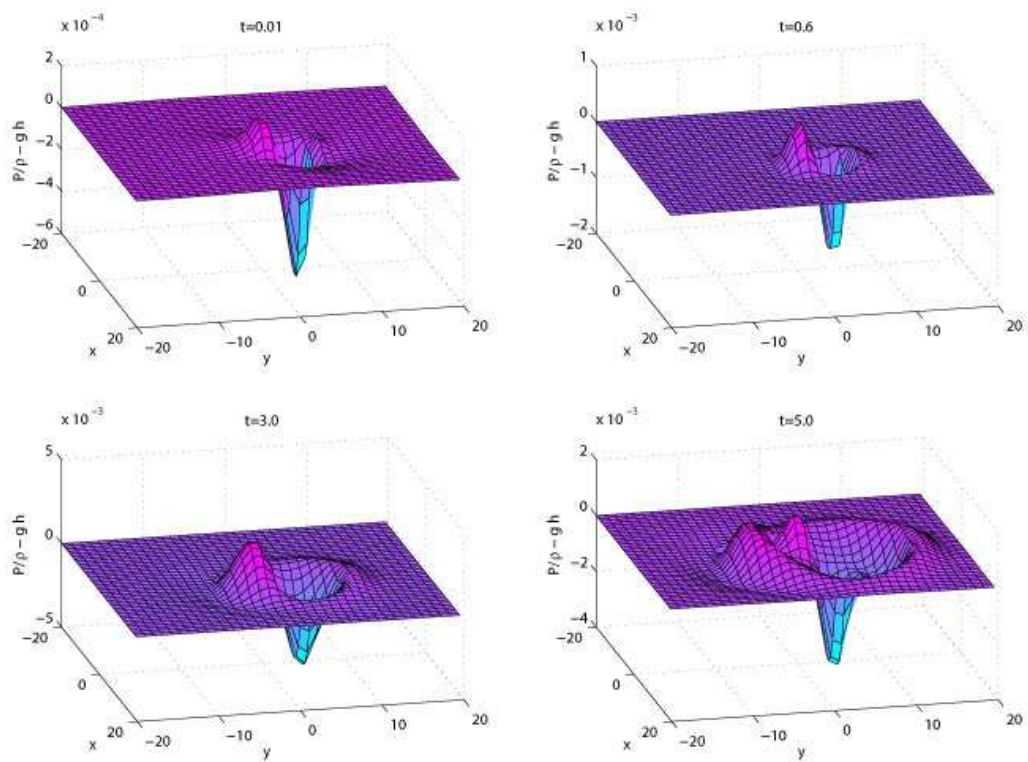


Figure 1.14: Bottom pressure at $t = 0.01, 0.6, 3, 5$ in dimensionless time. In physical time it corresponds to one second, one minute, five minutes and eight minutes and a half after the initial seabed deformation.

1.2 Comparison between three-dimensional linear and non-linear tsunami generation models

Tsunami wave modeling is a challenging task. In particular, it is essential to understand the first minutes of a tsunami, its propagation and finally the resulting inundation and impact on structures. The focus of the present work is on the generation process. There are different natural phenomena that can lead to a tsunami. For example, one can mention submarine mass failures, slides, volcanic eruptions, falls of asteroids, etc. We refer to the recent review on tsunami science [SB06] for a complete bibliography on the topic. The present work focuses on tsunami generation by earthquakes.

Two steps in modeling are necessary for an accurate description of tsunami generation: a model for the earthquake fed by the various seismic parameters, and a model for the formation of surface gravity waves resulting from the deformation of the seafloor. In the absence of sophisticated source models, one often uses analytical solutions based on dislocation theory in an elastic half-space for the seafloor displacement [Oka85]. For the resulting water motion, the standard practice is to transfer the inferred seafloor displacement to the free surface of the ocean. In this study, we will call this approach the *passive generation* approach.¹ This approach leads to a well-posed initial value problem with zero velocity. An open question for tsunami forecasting modelers is the validity of neglecting the initial velocity. In a recent note, Dutykh et al. [DDK06] used linear theory to show that indeed differences may exist between the standard passive generation and the *active generation* that takes into account the dynamics of seafloor displacement. The transient wave generation due to the coupling between the seafloor motion and the free surface has been considered by a few authors only. One of the reasons is that it is commonly assumed that the source details are not important.² Ben-Menahem and Rosenman [BMR72] calculated the two-dimensional radiation pattern from a moving source (linear theory). Tuck and Hwang [Tuc74] solved the linear long-wave equation in the presence of a moving bottom and a uniformly sloping beach. Hammack [Ham73] generated waves experimentally by raising or lowering a box at one end of a channel. According to Synolakis and Bernard [SB06], Houston and Garcia [HG74] were the first to use more geophysically real-

¹In the pioneering paper [Kaj63], Kajiura analyzed the applicability of the passive approach using Green's functions. In the tsunami literature, this approach is sometimes called the piston model of tsunami generation.

²As pointed out by Geist et al. [GTS06], the 2004 Indian Ocean tsunami shed some doubts about this belief. The measurements from land based stations that use the Global Positioning System to track ground movements revealed that the fault continued to slip after it stopped releasing seismic energy. Even though this slip was relatively slow, it contributed to the tsunami and may explain the surprising tsunami heights.

istic initial conditions. For obvious reasons, the quantitative differences in the distribution of seafloor displacement due to underwater earthquakes compared with more conventional earthquakes are still poorly known. Villeneuve and Savage [VS93] derived model equations which combine the linear effect of frequency dispersion and the nonlinear effect of amplitude dispersion, and included the effects of a moving bed. Todorovska and Trifunac [TT01] considered the generation of tsunamis by a slowly spreading uplift of the seafloor.

In this work, we mostly follow the standard passive generation approach. Several tsunami generation models and numerical methods suited for these models are presented and compared. The focus of our work is on modelling the fluid motion. It is assumed that the seabed deformation satisfies all the necessary hypotheses required to apply Okada's solution. The main objective is to confirm or infirm the lack of importance of nonlinear effects and/or frequency dispersion in tsunami generation. This result may have implications in terms of computational cost. The goal is to optimize the ratio between the complexity of the model and the accuracy of the results. Government agencies need to compute accurately tsunami propagation in real time in order to know where to evacuate people. Therefore any saving in computational time is crucial (see for example the code MOST used by the National Oceanic and Atmospheric Administration in the US [TS98] or the code TUNAMI developed by the Disaster Control Research Center in Japan). Liu and Liggett [LL83] already performed comparisons between linear and nonlinear water waves but their study was restricted to simple bottom deformations, namely the generation of transient waves by an upthrust of a rectangular block, and the nonlinear computations were restricted to two-dimensional flows. Bona et al. [BPS81] assessed how well a model equation with weak nonlinearity and dispersion describes the propagation of surface water waves generated at one end of a long channel. In their experiments, they found that the inclusion of a dissipative term was more important than the inclusion of nonlinearity, although the inclusion of nonlinearity was undoubtedly beneficial in describing the observations. The importance of dispersive effects in tsunami propagation is not directly addressed in the present study. Indeed these effects cannot be measured without taking into account the duration (or distance) of tsunami propagation [Tuc79].

1.2.1 Physical problem description

In the whole chapter, the vertical coordinate is denoted by z , while the two horizontal coordinates are denoted by x and y , respectively. The sea bottom deformation following an underwater earthquake is a complex phenomenon. This is why, for theoretical or experimental studies, researchers have often used simplified bottom motions such as the vertical motion of a box. In order to determine the deformations of the sea bottom due to an earthquake, we use the analytical solution obtained for a dislocation in an elastic

<i>parameter</i>	<i>value</i>
Dip angle δ	13°
Fault depth d_f , km	3
Fault length L , km	6
Fault width W , km	4
Magnitude of Burger's vector $ \mathbf{D} $, m	1
Young's modulus E , GPa	9.5
Poisson ratio ν	0.23

Table 1.5: Typical parameter set for the source used to model the seafloor deformation due to an earthquake in the present study. The dip angle, Young's modulus and Poisson ratio correspond roughly to those of the 2004 Sumatra event. The fault depth, length and width, as well as the magnitude of Burger's vector, have been reduced for computation purposes.

half-space [Oka85]. This solution, which at present time is used by the majority of tsunami wave modelers to produce an initial condition for tsunami propagation simulations, provides an explicit expression of the bottom surface deformation that depends on a dozen of source parameters such as the dip angle δ , fault depth d_f , fault dimensions (length and width), Burger's vector \mathbf{D} , Young's modulus, Poisson ratio, etc. Some of these parameters are shown in Figure 1.3. More details can be found in [DD07c] for example.

A value of 90° for the dip angle corresponds to a vertical fault. Varying the fault slip $|\mathbf{D}|$ does not change the co-seismic deformation pattern, only its magnitude. The values of the parameters used in the present study are given in Table 1.5. A typical dip-slip solution is shown in Figure 1.15 (the angle ϕ is equal to 0, while the rake angle θ is equal to $\pi/2$).

Let $z = \zeta(x, y, t)$ denote the deformation of the sea bottom. Hammack and Segur [HS74] suggested that there are two main kinds of behaviour for the generated waves depending on whether the net volume V of the initial bottom surface deformation

$$V = \int_{\mathbb{R}^2} \zeta(x, y, 0) dx dy$$

is positive or not.³ A positive V is achieved for example for a “reverse fault”, i.e. when the dip angle δ satisfies $0 \leq \delta \leq \pi/2$ or $-\pi \leq \delta \leq -\pi/2$, as shown in Figure 1.16. A negative V is achieved for a “normal fault”, i.e. when the dip angle δ satisfies $\pi/2 \leq \delta \leq \pi$ or $-\pi/2 \leq \delta \leq 0$.

The conclusions of [HS74] are based on the Korteweg–de Vries (KdV) equation and were

³However it should be noted that the analysis of [HS74] is restricted to one-dimensional uni-directional waves. We assume here that their conclusions can be extended to two-dimensional bi-directional waves.

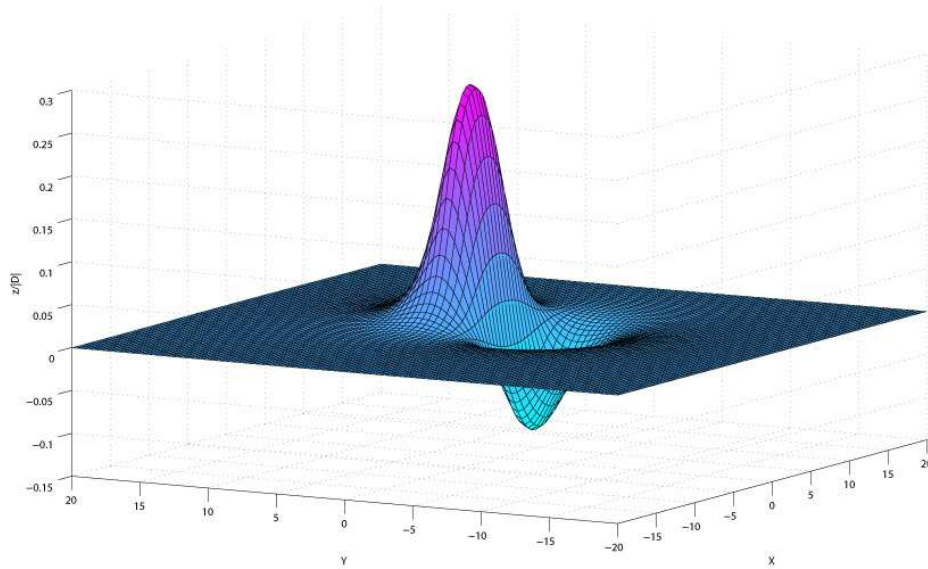


Figure 1.15: Typical seafloor deformation due to dip-slip faulting. The parameters are those of Table 1.5. The distances along the horizontal axes x and y are expressed in kilometers.

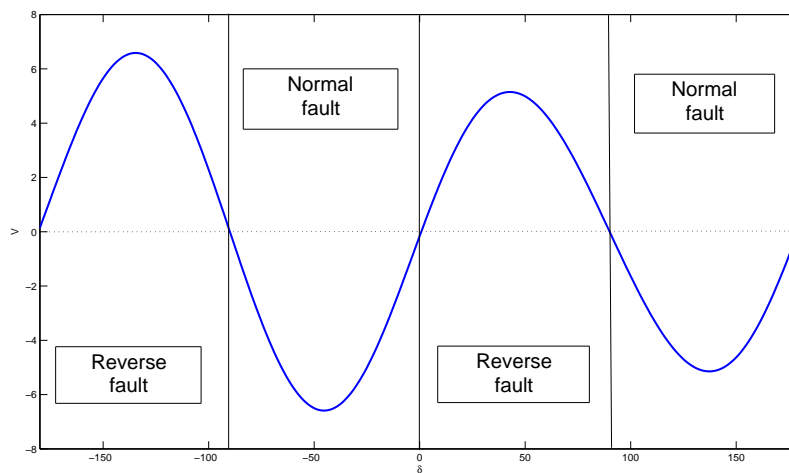


Figure 1.16: Initial net volume V (in km^3) of the seafloor displacement as a function of the dip angle δ (in $^\circ$). All the other parameters, which are given in Table 1.5, are kept constant.

in part confirmed by their experiments. If V is positive, waves of stable form (solitons) evolve and are followed by a dispersive train of oscillatory waves, regardless of the exact structure of $\zeta(x, y, 0)$. If V is negative, and if the initial data is non-positive everywhere, no solitons evolve. But, if V is negative and there is a region of elevation in the initial data (which corresponds to a typical Okada solution for a normal fault), solitons can evolve and we have checked this last result using the FNPF equations (see Figure 1.17). In this study, we focus on the case where V is positive with a dip angle δ equal to 13° , according to the seismic data of the 26 December 2004 Sumatra-Andaman event (see for example [LKA⁺05]). However, the sea bottom deformation often has an N -shape, with subsidence on one side of the fault and uplift on the other side as shown in Figure 1.15. In that case, one may expect the positive V behaviour on one side and the negative V behaviour on the other side. Recall that the experiments of Hammack and Segur [HS74] were performed in the presence of a vertical wall next to the moving bottom and their analysis was based on the uni-directional KdV wave equation.

We now consider the fluid domain. A sketch is shown in Figure 1.9. The fluid domain Ω is bounded above by the free surface and below by the rigid ocean floor. It is unbounded in the horizontal x - and y - directions. So, one can write

$$\Omega = \mathbb{R}^2 \times [-h(x, y) + \zeta(x, y, t), \eta(x, y, t)].$$

Before the earthquake the fluid is assumed to be at rest, thus the free surface and the solid boundary are defined by $z = 0$ and $z = -h(x, y)$, respectively. For simplicity $h(x, y)$ is assumed to be a constant. Of course, in real situations, this is never the case but for our purpose the bottom bathymetry is not important. Starting at time $t = 0$, the solid boundary moves in a prescribed manner which is given by

$$z = -h + \zeta(x, y, t), \quad t \geq 0.$$

The deformation of the sea bottom is assumed to have all the necessary properties needed to compute its Fourier transform in x, y and its Laplace transform in t . The resulting deformation of the free surface $z = \eta(x, y, t)$ is to be found as part of the solution. It is also assumed that the fluid is incompressible and the flow irrotational. The latter implies the existence of a velocity potential $\phi(x, y, z, t)$ which completely describes the flow. By definition of ϕ the fluid velocity vector can be expressed as $\mathbf{q} = \nabla\phi$. Thus, the continuity equation becomes

$$\nabla \cdot \mathbf{q} = \Delta\phi = 0, \quad (x, y, z) \in \Omega. \quad (1.35)$$

The potential $\phi(x, y, z, t)$ must satisfy the following kinematic boundary conditions on the

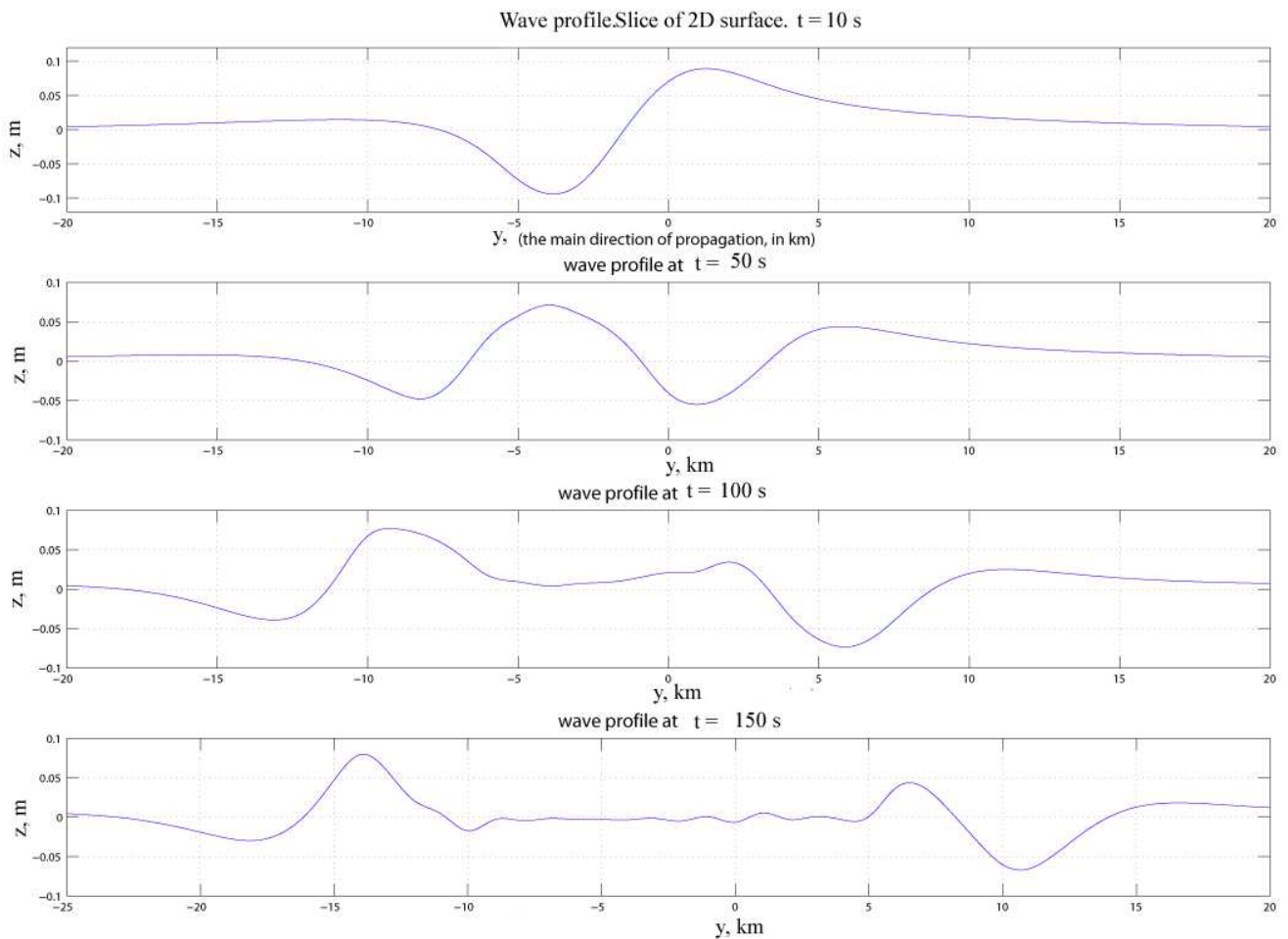


Figure 1.17: Wave profiles at different times for the case of a normal fault ($\delta = 167^\circ$). The seafloor deformation occurs instantaneously at $t = 0$. The water depth $h(x, y)$ is assumed to be constant.

free surface and the solid boundary, respectively:

$$\begin{aligned}\frac{\partial\phi}{\partial z} &= \frac{\partial\eta}{\partial t} + \frac{\partial\phi}{\partial x}\frac{\partial\eta}{\partial x} + \frac{\partial\phi}{\partial y}\frac{\partial\eta}{\partial y}, & z = \eta(x, y, t), \\ \frac{\partial\phi}{\partial z} &= \frac{\partial\zeta}{\partial t} + \frac{\partial\phi}{\partial x}\frac{\partial\zeta}{\partial x} + \frac{\partial\phi}{\partial y}\frac{\partial\zeta}{\partial y}, & z = -h + \zeta(x, y, t).\end{aligned}$$

Further assuming the flow to be inviscid and neglecting surface tension effects, one can write the dynamic condition to be satisfied on the free surface as

$$\frac{\partial\phi}{\partial t} + \frac{1}{2}|\nabla\phi|^2 + g\eta = 0, \quad z = \eta(x, y, t), \quad (1.36)$$

where g is the acceleration due to gravity. The atmospheric pressure has been chosen as reference pressure.

The equations are more transparent when written in dimensionless variables. However the choice of the reference lengths and speeds is subtle. Different choices lead to different models. Let the new independent variables be

$$\tilde{x} = x/\lambda, \quad \tilde{y} = y/\lambda, \quad \tilde{z} = z/d, \quad \tilde{t} = c_0 t/\lambda,$$

where λ is the horizontal scale of the motion and d a typical water depth. The speed c_0 is the long wave speed based on the depth d ($c_0 = \sqrt{gd}$). Let the new dependent variables be

$$\tilde{\eta} = \frac{\eta}{a}, \quad \tilde{\zeta} = \frac{\zeta}{a}, \quad \tilde{\phi} = \frac{c_0}{ag\lambda}\phi,$$

where a is a characteristic wave amplitude.

In dimensionless form, and after dropping the tildes, the equations become

$$\frac{\partial^2\phi}{\partial z^2} + \mu^2 \left(\frac{\partial^2\phi}{\partial x^2} + \frac{\partial^2\phi}{\partial y^2} \right) = 0, \quad (x, y, z) \in \Omega, \quad (1.37)$$

$$\frac{\partial\phi}{\partial z} = \mu^2 \frac{\partial\eta}{\partial t} + \varepsilon\mu^2 \left(\frac{\partial\phi}{\partial x}\frac{\partial\eta}{\partial x} + \frac{\partial\phi}{\partial y}\frac{\partial\eta}{\partial y} \right), \quad z = \varepsilon\eta(x, y, t), \quad (1.38)$$

$$\frac{\partial\phi}{\partial z} = \mu^2 \frac{\partial\zeta}{\partial t} + \varepsilon\mu^2 \left(\frac{\partial\phi}{\partial x}\frac{\partial\zeta}{\partial x} + \frac{\partial\phi}{\partial y}\frac{\partial\zeta}{\partial y} \right), \quad z = -\frac{h}{d} + \varepsilon\zeta(x, y, t), \quad (1.39)$$

$$\mu^2 \frac{\partial\phi}{\partial t} + \frac{1}{2}\varepsilon \left(\mu^2 \left(\frac{\partial\phi}{\partial x} \right)^2 + \mu^2 \left(\frac{\partial\phi}{\partial y} \right)^2 + \left(\frac{\partial\phi}{\partial z} \right)^2 \right) + \mu^2\eta = 0, \quad z = \varepsilon\eta(x, y, t), \quad (1.40)$$

where two dimensionless numbers have been introduced:

$$\varepsilon = a/d, \quad \mu = d/\lambda. \quad (1.41)$$

For the propagation of tsunamis, both numbers ε and μ are small. Indeed the satellite altimetry observations of the 2004 Boxing Day tsunami waves obtained by two satellites that passed over the Indian Ocean a couple of hours after the rupture process occurred gave an amplitude a of roughly 60 cm in the open ocean. The typical wavelength estimated from the width of the segments that experienced slip is between 160 and 240 km [LKA⁺05]. The water depth ranges from 4 km towards the west of the rupture to 1 km towards the east. Therefore average values for ε and μ in the open ocean are $\varepsilon \approx 2 \times 10^{-4}$ and $\mu \approx 2 \times 10^{-2}$. A more precise range for these two dimensionless numbers is

$$1.5 \times 10^{-4} < \varepsilon < 6 \times 10^{-4}, \quad 4 \times 10^{-3} < \mu < 2.5 \times 10^{-2}. \quad (1.42)$$

The water-wave problem, either in the form of an initial value problem (IVP) or in the form of a boundary value problem (BVP), is difficult to solve because of the nonlinearities in the boundary conditions and the unknown computational domain.

1.2.2 Linear theory

First we perform the linearization of the above equations and boundary conditions. It is equivalent to taking the limit of (1.37)–(1.40) as $\varepsilon \rightarrow 0$. The linearized problem can also be obtained by expanding the unknown functions as power series of the small parameter ε . Collecting terms of the lowest order in ε yields the linear approximation. For the sake of convenience, we now switch back to the physical variables. The linearized problem in dimensional variables reads

$$\Delta\phi = 0, \quad (x, y, z) \in \mathbb{R}^2 \times [-h, 0], \quad (1.43)$$

$$\frac{\partial\phi}{\partial z} = \frac{\partial\eta}{\partial t}, \quad z = 0, \quad (1.44)$$

$$\frac{\partial\phi}{\partial z} = \frac{\partial\zeta}{\partial t}, \quad z = -h, \quad (1.45)$$

$$\frac{\partial\phi}{\partial t} + g\eta = 0, \quad z = 0. \quad (1.46)$$

The bottom motion appears in equation (1.45). Combining equations (1.44) and (1.46) yields the single free-surface condition

$$\frac{\partial^2\phi}{\partial t^2} + g\frac{\partial\phi}{\partial z} = 0, \quad z = 0. \quad (1.47)$$

Most studies of tsunami generation assume that the initial free-surface deformation is equal to the vertical displacement of the ocean bottom and take a zero velocity field as initial condition. The details of wave motion are completely neglected during the time

that the source operates. While tsunami modelers often justify this assumption by the fact that the earthquake rupture occurs very rapidly, there are some specific cases where the time scale and/or the horizontal extent of the bottom deformation may become an important factor. This was emphasized for example by Todorovska and Trifunac [TT01] and Todorovska et al. [THT02], who considered the generation of tsunamis by a slowly spreading uplift of the seafloor in order to explain some observations related to past tsunamis. However they did not use realistic source models.

Our claim is that it is important to make a distinction between two mechanisms of generation: an active mechanism in which the bottom moves according to a given time law and a passive mechanism in which the seafloor deformation is simply translated to the free surface. Recently Dutykh et al. [DDK06] showed that even in the case of an instantaneous seafloor deformation, there may be differences between these two generation processes.

1.2.3 Active generation

This case was extensively studied in Section 1.1. So, we do not repeat the computations here and give only final expressions (on the free surface and for $t > 0$) which correspond to instantaneous bottom motion:

$$\eta(x, y, t) = \frac{1}{(2\pi)^2} \iint_{\mathbb{R}^2} \frac{\widehat{\zeta}_0(k, \ell) e^{i(kx + \ell y)}}{\cosh(mh)} \cos \omega t \, dk d\ell, \quad (1.48)$$

$$\mathbf{u}(x, y, t; 0) = \frac{ig}{4\pi^2} \iint_{\mathbb{R}^2} \frac{\mathbf{k} \widehat{\zeta}_0(k, \ell) e^{i(kx + \ell y)}}{\cosh(mh)} \frac{\sin \omega t}{\omega} d\mathbf{k}, \quad (1.49)$$

$$w(x, y, t; 0) = -\frac{1}{4\pi^2} \iint_{\mathbb{R}^2} \frac{\widehat{\zeta}_0(k, \ell) e^{i(kx + \ell y)}}{\cosh(mh)} \omega \sin \omega t \, d\mathbf{k}. \quad (1.50)$$

1.2.4 Passive generation

In this case equation (1.45) becomes

$$\frac{\partial \phi}{\partial z} = 0, \quad z = -h, \quad (1.51)$$

and the initial condition for η now reads

$$\eta(x, y, 0) = \zeta_0(x, y),$$

where $\zeta_0(x, y)$ is the seafloor deformation. Initial velocities are assumed to be zero.

Again we apply the Fourier transform in the horizontal coordinates (x, y) . The Laplace transform is not applied since there is no substantial dynamics in the problem. Equations (1.43), (1.51) and (1.47) become

$$\frac{d^2 \widehat{\phi}}{dz^2} - (k^2 + \ell^2) \widehat{\phi} = 0, \quad (1.52)$$

$$\frac{d\widehat{\phi}}{dz}(k, \ell, -h, t) = 0, \quad (1.53)$$

$$\frac{\partial^2 \widehat{\phi}}{\partial t^2}(k, \ell, 0, t) + g \frac{\partial \widehat{\phi}}{\partial z}(k, \ell, 0, t) = 0. \quad (1.54)$$

A general solution to Laplace's equation (1.52) is again given by

$$\widehat{\phi}(k, \ell, z, t) = A(k, \ell, t) \cosh(mz) + B(k, \ell, t) \sinh(mz), \quad (1.55)$$

where $m = \sqrt{k^2 + \ell^2}$. The relationship between the functions $A(k, \ell, t)$ and $B(k, \ell, t)$ can be easily found from the boundary condition (1.53):

$$B(k, \ell, t) = A(k, \ell, t) \tanh(mh). \quad (1.56)$$

From equation (1.54) and the initial conditions one finds

$$A(k, \ell, t) = -\frac{g}{\omega} \widehat{\zeta}_0(k, \ell) \sin \omega t. \quad (1.57)$$

Substituting the expressions for the functions A and B in (1.55) yields

$$\widehat{\phi}(k, \ell, z, t) = -\frac{g}{\omega} \widehat{\zeta}_0(k, \ell) \sin \omega t \left(\cosh(mz) + \tanh(mh) \sinh(mz) \right). \quad (1.58)$$

From (1.46), the free-surface elevation becomes

$$\widehat{\eta}(k, \ell, t) = \widehat{\zeta}_0(k, \ell) \cos \omega t.$$

Inverting the Fourier transform provides the general integral solution

$$\eta(x, y, t) = \frac{1}{(2\pi)^2} \iint_{\mathbb{R}^2} \widehat{\zeta}_0(k, \ell) \cos \omega t e^{i(kx + \ell y)} dk d\ell. \quad (1.59)$$

Let us now evaluate the velocity field in the fluid domain. Equation (1.58) gives the Fourier transform of the velocity potential $\phi(x, y, z, t)$. Taking the Fourier transform of

$$\mathbf{u}(x, y, t; \beta) = \nabla_h \phi(x, y, z, t)|_{z=\beta h}$$

yields

$$\begin{aligned}\widehat{\mathbf{u}}(k, \ell, t; \beta) &= -i\widehat{\phi}(k, \ell, \beta h, t)\mathbf{k} \\ &= i\frac{g}{\omega}\widehat{\zeta}_0(k, \ell)\sin\omega t\left(\cosh(\beta mh) + \tanh(mh)\sinh(\beta mh)\right)\mathbf{k}.\end{aligned}$$

Inverting the Fourier transform gives the general formula for the horizontal velocities

$$\mathbf{u}(x, y, t; \beta) = \frac{ig}{4\pi^2} \iint_{\mathbb{R}^2} \mathbf{k}\widehat{\zeta}_0(k, \ell) \frac{\sin\omega t}{\omega} \left(\cosh(\beta mh) + \tanh(mh)\sinh(\beta mh)\right) e^{i(kx+\ell y)} d\mathbf{k}.$$

Along the free surface $\beta = 0$, the horizontal velocity vector becomes

$$\mathbf{u}(x, y, t; 0) = \frac{ig}{4\pi^2} \iint_{\mathbb{R}^2} \mathbf{k}\widehat{\zeta}_0(k, \ell) \frac{\sin\omega t}{\omega} e^{i(kx+\ell y)} d\mathbf{k}. \quad (1.60)$$

Next we determine the vertical component of the velocity $w(x, y, t; \beta)$ at a given vertical level $z = \beta h$. It is easy to obtain the Fourier transform $\widehat{w}(k, \ell, t; \beta)$ by differentiating (1.58):

$$\widehat{w}(k, \ell, t; \beta) = \left. \frac{\partial \widehat{\phi}}{\partial z} \right|_{z=\beta h} = -mg \frac{\sin\omega t}{\omega} \widehat{\zeta}_0(k, \ell) \left(\sinh(\beta mh) + \tanh(mh)\cosh(\beta mh)\right).$$

Inverting this transform yields

$$w(x, y, t; \beta) = -\frac{g}{4\pi^2} \iint_{\mathbb{R}^2} \frac{m\sin\omega t}{\omega} \widehat{\zeta}_0(k, \ell) \left(\sinh(\beta mh) + \tanh(mh)\cosh(\beta mh)\right) e^{i(kx+\ell y)} d\mathbf{k}$$

for $-1 \leq \beta \leq 0$. Using the dispersion relation, one can write the vertical component of the velocity along the free surface ($\beta = 0$) as

$$w(x, y, t; 0) = -\frac{1}{4\pi^2} \iint_{\mathbb{R}^2} \omega \sin\omega t \widehat{\zeta}_0(k, \ell) e^{i(kx+\ell y)} d\mathbf{k}. \quad (1.61)$$

All the formulas obtained in this section are valid only if the integrals converge.

Again, one can compute the bottom pressure. At $z = -h$, one has

$$\left. \frac{\partial \phi}{\partial t} \right|_{z=-h} = -\frac{g}{(2\pi)^2} \iint_{\mathbb{R}^2} \frac{\widehat{\zeta}_0(k, \ell) e^{i(kx+\ell y)}}{\cosh(mh)} \cos\omega t d\mathbf{k}.$$

The bottom pressure deviation from the hydrostatic pressure is then given by

$$p_b(x, y, t) = -\rho \left. \frac{\partial \phi}{\partial t} \right|_{z=-h} - \rho g \zeta.$$

Again, away from the deformed seabed, p_b reduces to $-\rho\phi_t|_{z=-h}$. The only difference between p_b and $\rho g\eta$ is the presence of an additional $\cosh(mh)$ term in the denominator of p_b .

The main differences between passive and active generation processes are that (i) the wave amplitudes and velocities obtained with the instantly moving bottom are lower than those generated by initial translation of the bottom motion and that (ii) the water column plays the role of a low-pass filter (compare equations (1.48)–(1.50) with equations (1.59)–(1.61)). High frequencies are attenuated in the moving bottom solution. Ward [War01], who studied landslide tsunamis, also commented on the $1/\cosh(mh)$ term, which low-pass filters the source spectrum. So the filter favors long waves. In the discussion section, we will come back to the differences between passive generation and active generation.

1.2.4.1 Numerical method for the linear problem

All the expressions derived from linear theory are explicit but they must be computed numerically. It is not a trivial task because of the oscillatory behaviour of the integrand functions. All integrals were computed with Filon type numerical integration formulas [Fil28], which explicitly take into account this oscillatory behaviour. Numerical results will be shown in Section 1.2.9.

1.2.5 Nonlinear shallow water equations

Synolakis and Bernard [SB06] introduced a clear distinction between the various shallow-water models. At the lowest order of approximation, one obtains the linear shallow water wave equation. The next level of approximation provides the nondispersive nonlinear shallow water equations (NSW). In the next level, dispersive terms are added and the resulting equations constitute the Boussinesq equations. Since there are many different ways to go to this level of approximation, there are a lot of different types of Boussinesq equations. The NSW equations are the most commonly used equations for tsunami propagation (see in particular the code MOST developed by the National Oceanic and Atmospheric Administration in the US [TS98] or the code TUNAMI developed by the Disaster Control Research Center in Japan). They are also used for generation and runup/inundation. For wave runup, the effects of bottom friction become important and must be included in the codes. Our analysis will focus on the NSW equations. For simplicity, we assume below that h is constant. Therefore one can take h as reference depth, so that the seafloor is given by $z = -1 + \varepsilon\zeta$.

1.2.6 Mathematical model

In this subsection, partial derivatives are denoted by subscripts. When μ^2 is a small parameter, the water is considered to be shallow. For the shallow water theory, one formally expands the potential ϕ in powers of μ^2 :

$$\phi = \phi_0 + \mu^2 \phi_1 + \mu^4 \phi_2 + \dots .$$

This expansion is substituted into the governing equation and the boundary conditions. The lowest-order term in Laplace's equation is

$$\phi_{0zz} = 0.$$

The boundary conditions imply that $\phi_0 = \phi_0(x, y, t)$. Thus the vertical velocity component is zero and the horizontal velocity components are independent of the vertical coordinate z at lowest order. Let us introduce the notation $u := \phi_{0x}(x, y, t)$ and $v := \phi_{0y}(x, y, t)$. Solving Laplace's equation and taking into account the bottom kinematic condition yield the following expressions for ϕ_1 and ϕ_2 :

$$\begin{aligned} \phi_1(x, y, z, t) &= -\frac{1}{2}Z^2(u_x + v_y) + z[\zeta_t + \varepsilon(u\zeta_x + v\zeta_y)], \\ \phi_2(x, y, z, t) &= \frac{1}{24}Z^4(\Delta u_x + \Delta v_y) + \varepsilon\left(\varepsilon\frac{z^2}{2}|\nabla\zeta|^2 - \frac{1}{6}Z^3\Delta\zeta\right)(u_x + v_y) \\ &\quad - \frac{\varepsilon}{3}Z^3\nabla\zeta \cdot \nabla(u_x + v_y) - \frac{z^3}{6}(\Delta\zeta_t + \varepsilon\Delta(u\zeta_x + v\zeta_y)) + \\ &\quad z(-1 + \varepsilon\zeta)[\varepsilon\nabla\zeta \cdot \nabla(\zeta_t + \varepsilon(u\zeta_x + v\zeta_y)) - \varepsilon^2|\nabla\zeta|^2(u_x + v_y) - \\ &\quad \frac{1}{2}(-1 + \varepsilon\zeta)(\Delta\zeta_t + \varepsilon\Delta(u\zeta_x + v\zeta_y))] , \end{aligned}$$

where

$$Z = 1 + z - \varepsilon\zeta.$$

The next step consists in retaining terms of requested order in the free-surface boundary conditions. Powers of ε will appear when expanding in Taylor series the free-surface conditions around $z = 0$. For example, if one keeps terms of order $\varepsilon\mu^2$ and μ^4 in the dynamic boundary condition (1.40) and in the kinematic boundary condition (1.38), one obtains

$$\mu^2\phi_{0t} - \frac{1}{2}\mu^4(u_{tx} + v_{ty}) + \mu^2\eta + \frac{1}{2}\varepsilon\mu^2(u^2 + v^2) = 0, \quad (1.62)$$

$$\begin{aligned} \mu^2[\eta_t + \varepsilon(u\eta_x + v\eta_y) + (1 + \varepsilon(\eta - \zeta))(u_x + v_y) - \zeta_t - \varepsilon(u\zeta_x + v\zeta_y)] = \\ \frac{1}{6}\mu^4(\Delta u_x + \Delta v_y). \quad (1.63) \end{aligned}$$

Differentiating (1.62) first with respect to x and then with respect to y gives a set of two equations:

$$u_t + \varepsilon(uu_x + vv_x) + \eta_x - \frac{1}{2}\mu^2(u_{txx} + v_{txy}) = 0, \quad (1.64)$$

$$v_t + \varepsilon(uu_y + vv_y) + \eta_y - \frac{1}{2}\mu^2(u_{txy} + v_{tyy}) = 0. \quad (1.65)$$

The kinematic condition (1.63) becomes

$$(\eta - \zeta)_t + [u(1 + \varepsilon(\eta - \zeta))]_x + [v(1 + \varepsilon(\eta - \zeta))]_y = \frac{1}{6}\mu^2(\Delta u_x + \Delta v_y). \quad (1.66)$$

Equations (1.64), (1.65) and (1.66) contain in fact various shallow-water models. The so-called fundamental NSW equations which contain no dispersive effects are obtained by neglecting the terms of order μ^2 :

$$u_t + \varepsilon(uu_x + vv_x) + \eta_x = 0, \quad (1.67)$$

$$v_t + \varepsilon(uv_x + vv_y) + \eta_y = 0, \quad (1.68)$$

$$\eta_t + [u(1 + \varepsilon(\eta - \zeta))]_x + [v(1 + \varepsilon(\eta - \zeta))]_y = \zeta_t. \quad (1.69)$$

Going back to a bathymetry $h^*(x, y, t)$ equal to $1 - \varepsilon\zeta(x, y, t)$ and using the fact that (u, v) is the horizontal gradient of ϕ_0 , one can rewrite the system of NSW equations as

$$u_t + \frac{\varepsilon}{2}(u^2 + v^2)_x + \eta_x = 0, \quad (1.70)$$

$$v_t + \frac{\varepsilon}{2}(u^2 + v^2)_y + \eta_y = 0, \quad (1.71)$$

$$\eta_t + [u(h^* + \varepsilon\eta)]_x + [v(h^* + \varepsilon\eta)]_y = -\frac{1}{\varepsilon}h_t^*. \quad (1.72)$$

The system of equations (1.70)–(1.72) has been used for example by Titov and Synolakis [TS98] for the numerical computation of tidal wave run-up. Note that this model does not include any bottom friction terms.

The NSW equations with dispersion (1.64)–(1.66), also known as the Boussinesq equations, can be written in the following form:

$$u_t + \frac{\varepsilon}{2}(u^2 + v^2)_x + \eta_x - \frac{1}{2}\mu^2\Delta u_t = 0, \quad (1.73)$$

$$v_t + \frac{\varepsilon}{2}(u^2 + v^2)_y + \eta_y - \frac{1}{2}\mu^2\Delta v_t = 0, \quad (1.74)$$

$$\eta_t + [u(h^* + \varepsilon\eta)]_x + [v(h^* + \varepsilon\eta)]_y - \frac{1}{6}\mu^2(\Delta u_x + \Delta v_y) = -\frac{1}{\varepsilon}h_t^*. \quad (1.75)$$

Kulikov et al. [KML05] have argued that the satellite altimetry observations of the Indian Ocean tsunami show some dispersive effects. However the steepness is so small that the

origin of these effects is questionable. Guesmia et al. [GHM98] compared Boussinesq and shallow-water models and came to the conclusion that the effects of frequency dispersion are minor. As pointed out in [KS06], dispersive effects are necessary only when examining steep gravity waves, which are not encountered in the context of tsunami hydrodynamics in deep water. However they can be encountered in experiments such as those of Hammack [Ham73] because the parameter μ is much bigger.

1.2.7 Numerical method

In order to solve the NSW equations, a finite-volume approach is used. For example LeVeque [LeV98] used a high-order finite volume scheme to solve a system of NSW equations. Here the flux scheme we use is the characteristic flux scheme, which was introduced by Ghidaglia et al. [GKC96]. This numerical method satisfies the conservative properties at the discrete level. The detailed description of this scheme is given in Appendix A.

1.2.8 Numerical method for the full equations

The fully nonlinear potential flow (FNPF) equations (1.37)–(1.40) are solved by using a numerical model based on the Boundary Element Method (BEM). An accurate code was developed by Grilli et al. [GGD01]. It uses a high-order three-dimensional boundary element method combined with mixed Eulerian–Lagrangian time updating, based on second-order explicit Taylor expansions with adaptive time steps. The efficiency of the code was recently greatly improved by introducing a more efficient spatial solver, based on the fast multipole algorithm [FD06]. By replacing every matrix–vector product of the iterative solver and avoiding the building of the influence matrix, this algorithm reduces the computing complexity from $O(N^2)$ to nearly $O(N)$ up to logarithms, where N is the number of nodes on the boundary.

By using Green’s second identity, Laplace’s equation (1.35) is transformed into the boundary integral equation

$$\alpha(\mathbf{x}_l)\phi(\mathbf{x}_l) = \int_{\Gamma} \left(\frac{\partial\phi}{\partial n}(\mathbf{x})G(\mathbf{x}, \mathbf{x}_l) - \phi(\mathbf{x})\frac{\partial G}{\partial n}(\mathbf{x}, \mathbf{x}_l) \right) d\Gamma, \quad (1.76)$$

where G is the three-dimensional free space Green’s function. The notation $\partial G/\partial n$ means the normal derivative, that is $\partial G/\partial n = \nabla G \cdot \mathbf{n}$, with \mathbf{n} the unit outward normal vector. The vectors $\mathbf{x} = (x, y, z)$ and $\mathbf{x}_l = (x_l, y_l, z_l)$ are position vectors for points on the boundary, and $\alpha(\mathbf{x}_l) = \theta_l/(4\pi)$ is a geometric coefficient, with θ_l the exterior solid angle made by the boundary at point \mathbf{x}_l . The boundary Γ is divided into various parts with different boundary conditions. On the free surface, one rewrites the nonlinear kinematic

and dynamic boundary conditions in a mixed Eulerian-Lagrangian form,

$$\frac{D\mathbf{R}}{Dt} = \nabla\phi, \quad (1.77)$$

$$\frac{D\phi}{Dt} = -gz + \frac{1}{2}\nabla\phi \cdot \nabla\phi, \quad (1.78)$$

with \mathbf{R} the position vector of a free-surface fluid particle. The material derivative is defined as

$$\frac{D}{Dt} = \frac{\partial}{\partial t} + \mathbf{q} \cdot \nabla. \quad (1.79)$$

For time integration, second-order explicit Taylor series expansions are used to find the new position and the potential on the free surface at time $t + \Delta t$. This time stepping scheme presents the advantage of being explicit, and the use of spatial derivatives along the free surface provides a better stability of the computed solution.

The integral equations are solved by BEM. The boundary is discretized into N collocation nodes and M high-order elements are used to interpolate between these nodes. Within each element, the boundary geometry and the field variables are discretized using polynomial shape functions. The integrals on the boundary are converted into a sum on the elements, each one being calculated on the reference element. The matrices are built with the numerical computation of the integrals on the reference element. The linear systems resulting from the two boundary integral equations (one for the pair $(\phi, \partial\phi/\partial n)$ and one for the pair $(\partial\phi/\partial t, \partial^2\phi/\partial t\partial n)$) are full and non symmetric. Assembling the matrix as well as performing the integrations accurately are time consuming tasks. They are done only once at each time step, since the same matrix is used for both systems. Solving the linear system is another time consuming task. Even with the GMRES algorithm with preconditioning, the computational complexity is $O(N^2)$, which is the same as the complexity of the assembling phase. The introduction of the fast multipole algorithm reduces considerably the complexity of the problem. The matrix is no longer built. Far away nodes are placed in groups, so less time is spent in numerical integrations and memory requirements are reduced. The hierarchical structure involved in the algorithm gives automatically the distance criteria for adaptive integrations.

Grilli et al. [GVW02] used the earlier version of the code to study tsunami generation by underwater landslides. They included the bottom motion due to the landslide. For the comparisons shown below, we only used the passive approach: we did not include the dynamics of the bottom motion.

1.2.9 Comparisons and discussion

The passive generation approach is followed for the numerical comparisons between the three models: (i) linear equations, (ii) NSW equations and (iii) fully nonlinear equations.

As shown in Section 1.2.2 (one can have a look at [DDK06]), this generation process gives the largest transient-wave amplitudes for a given permanent deformation of the seafloor. Therefore it is in some sense a worst case scenario.

The small dimensionless numbers ε and μ^2 introduced in (1.41) represent the magnitude of the nonlinear terms and dispersive terms in the governing equations, respectively. Hence, the relative importance of the nonlinear and the dispersive effects is given by the parameter

$$S = \frac{\text{nonlinear terms}}{\text{dispersive terms}} = \frac{\varepsilon}{\mu^2} = \frac{a\lambda^2}{d^3}, \quad (1.80)$$

which is called the Stokes (or Ursell) number [Urs53].⁴ An important assumption in the derivation of the Boussinesq system (1.73)–(1.75) is that the Ursell number is $O(1)$. Here, the symbol $O(\cdot)$ is used informally in the way that is common in the construction and formal analysis of model equations for physical phenomena. We are concerned with the limits $\varepsilon \rightarrow 0$ and $\mu \rightarrow 0$. Thus, $S = O(1)$ means that, as $\varepsilon \rightarrow 0$ and $\mu \rightarrow 0$, S takes values that are neither very large nor very small. We emphasize here that the Ursell number does not convey any information by itself about the separate negligibility of nonlinear and frequency dispersion effects. Another important aspect of models is the time scale of their validity. In the NSW equations, terms of order $O(\varepsilon^2)$ and $O(\mu^2)$ have been neglected. Therefore one expects these terms to make an order-one relative contribution on a time scale of order $\min(\varepsilon^{-2}, \mu^{-2})$.

All the figures shown below are two-dimensional plots for convenience but we recall that all computations for the three models are three-dimensional. Figure 1.18 shows profiles of the free-surface elevation along the main direction of propagation (y -axis) of transient waves generated by a permanent seafloor deformation corresponding to the parameters given in Table 1.5. This deformation, which has been plotted in Figure 1.15, has been translated to the free surface. The water depth is 100 m. The small dimensionless numbers are roughly $\varepsilon = 5 \times 10^{-4}$ and $\mu = 10^{-2}$, with a corresponding Ursell number equal to 5. One can see that the front system splits in two and propagates in both directions, with a leading wave of depression to the left and a leading wave of elevation to the right, in qualitative agreement with the satellite and tide gauge measurements of the 2004 Sumatra event. When tsunamis are generated along subduction zones, they usually split in two; one moves quickly inland while the second heads toward the open ocean. The three models are

⁴One finds sometimes in the literature a subtle difference between the Stokes and Ursell numbers. Both involve a wave amplitude multiplied by the square of a wavelength divided by the cube of a water depth. The Stokes number is defined specifically for the excitation of a closed basin while the Ursell number is used in a more general context to describe the evolution of a long wave system. Therefore only the characteristic length is different. For the Stokes number the length is the usual wavelength λ related to the frequency ω by $\lambda \approx 2\pi\sqrt{gd}/\omega$. In the Ursell number, the length refers to the local wave shape independent of the exciting conditions.

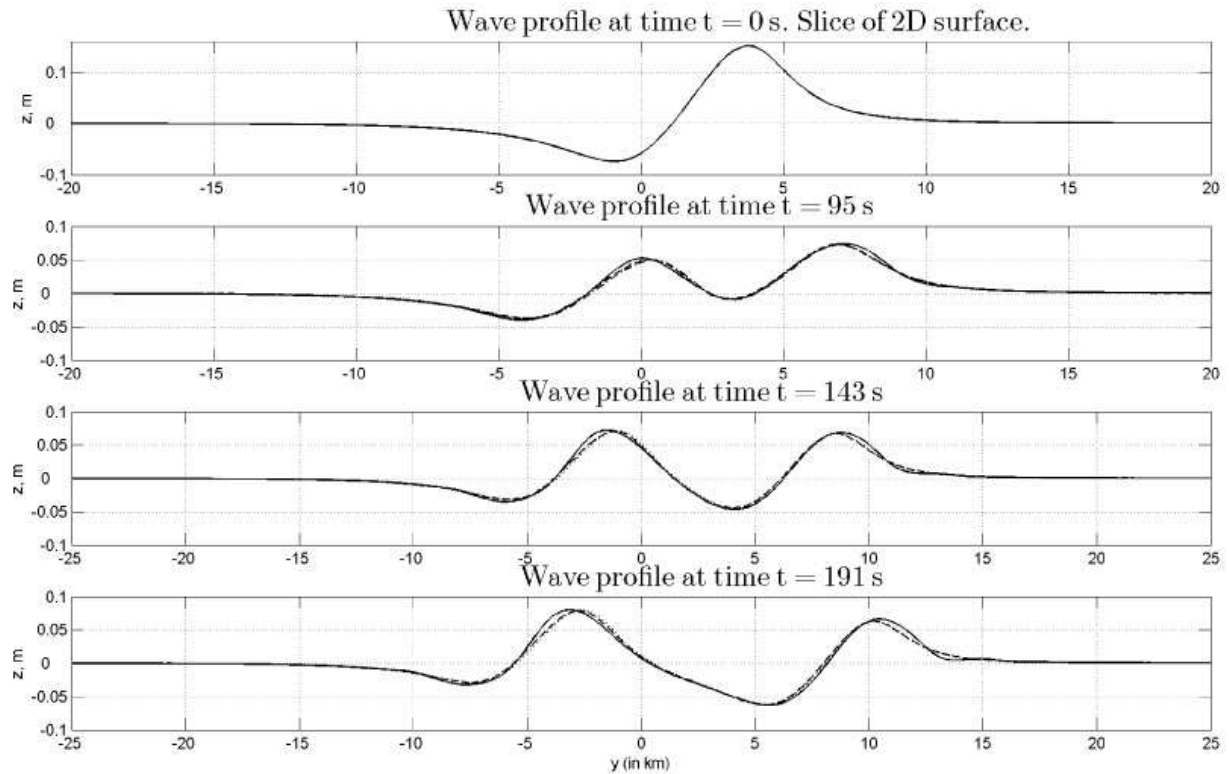


Figure 1.18: Comparisons of the free-surface elevation at $x = 0$ resulting from the integration of the linear equations (\cdots), NSW equations ($---$) and nonlinear equations ($-$) at different times of the propagation of transient waves generated by an earthquake ($t = 0$ s, $t = 95$ s, $t = 143$ s, $t = 191$ s). The parameters for the earthquake are those given in Table 1.5. The water depth is $h = 100$ m. One has the following estimates: $\varepsilon = 5 \times 10^{-4}$, $\mu^2 = 10^{-4}$ and consequently $S = 5$.

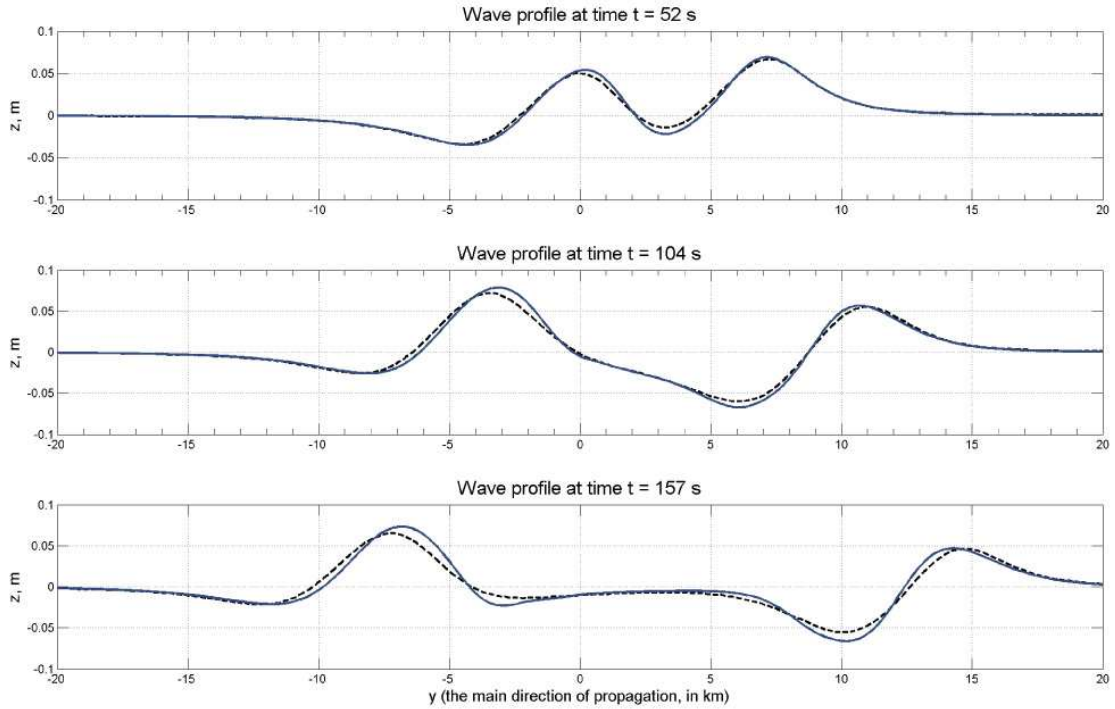


Figure 1.19: Comparisons of the free-surface elevation at $x = 0$ resulting from the integration of the linear equations (\cdots), NSW equations ($---$) and nonlinear equations ($-$) at different times of the propagation of transient waves generated by an earthquake ($t = 52$ s, $t = 104$ s, $t = 157$ s). The parameters for the earthquake are those given in Table 1.5. The water depth is $h = 500$ m. One has the following estimates: $\varepsilon = 10^{-4}$, $\mu^2 = 2.5 \times 10^{-3}$ and consequently $S = 0.04$.

almost undistinguishable at all times: the waves propagate with the same speed and the same profile. Nonlinear effects and dispersive effects are clearly negligible during the first moments of transient waves generated by a moving bottom, at least for these particular choices of ε and μ .

Let us now decrease the Ursell number by increasing the water depth. Figure 1.19 illustrates the evolution of transient water waves computed with the three models for the same parameters as those of Figure 1.18, except for the water depth now equal to 500 m. The small dimensionless numbers are roughly $\varepsilon = 10^{-4}$ and $\mu = 5 \times 10^{-2}$, with a corresponding Ursell number equal to 0.04. The linear and nonlinear profiles cannot be distinguished within graphical accuracy. Only the NSW profile is slightly different.

Let us introduce several sensors (tide gauges) at selected locations which are representative of the initial deformation of the free surface (see Figure 1.20). One can study the evolution of the surface elevation during the generation time at each gauge. Figure 1.21

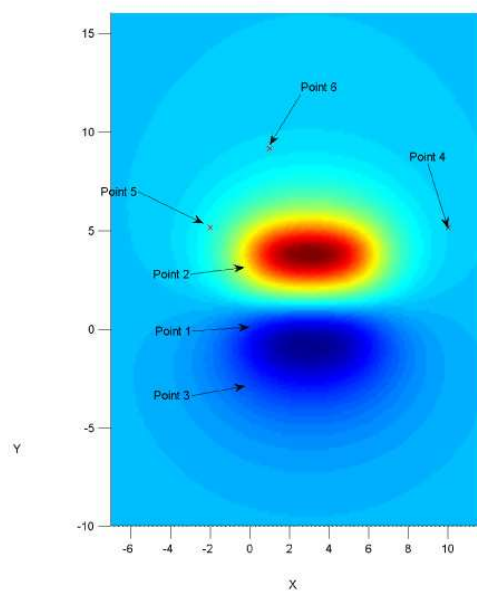


Figure 1.20: Top view of the initial free surface deformation showing the location of six selected gauges, with the following coordinates (in km): (1) 0,0 ; (2) 0,3 ; (3) 0,-3 ; (4) 10,5; (5) -2,5 ; (6) 1,10. The lower oval area represents the initial subsidence while the upper oval area represents the initial uplift.

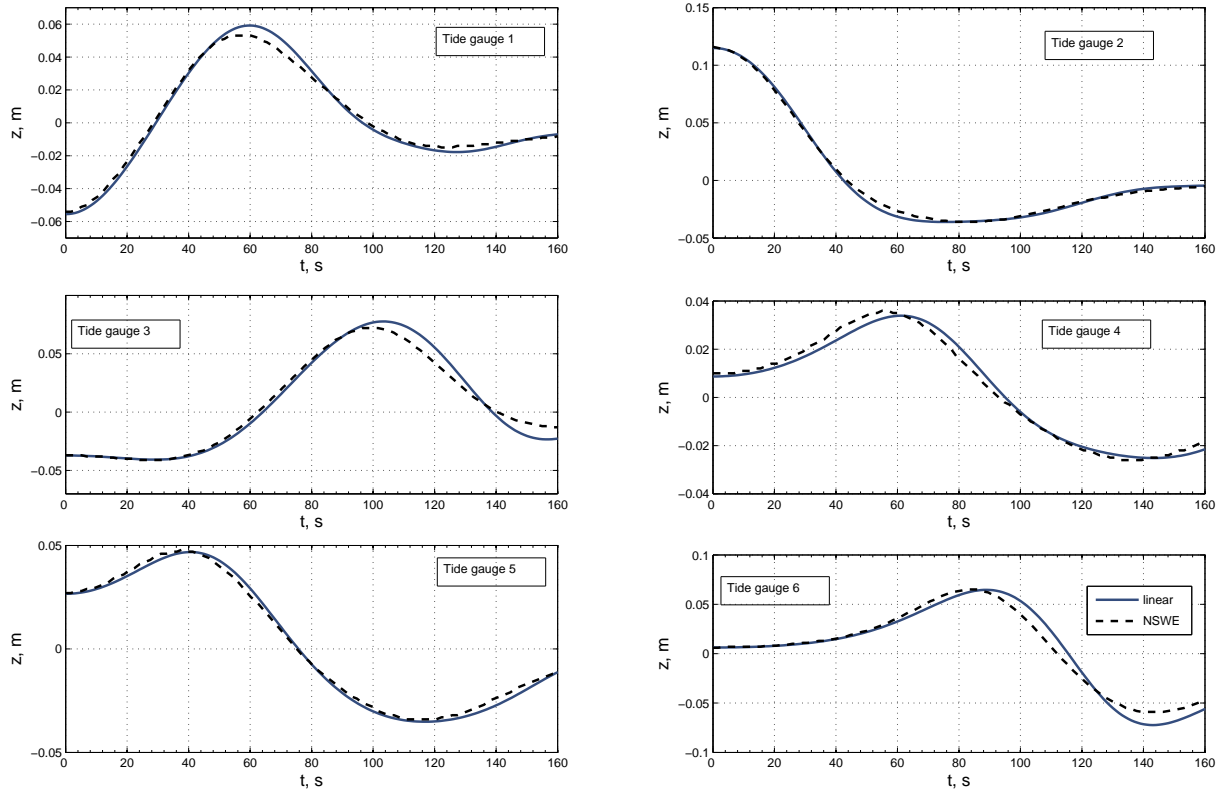


Figure 1.21: Transient waves generated by an underwater earthquake. Comparisons of the free-surface elevation as a function of time at the selected gauges shown in Figure 1.20: —, linear model ; -- nonlinear shallow water model. The time t is expressed in seconds. The physical parameters are those of Figure 1.19. Since the fully nonlinear results cannot be distinguished from the linear ones, they are not shown.

shows free-surface elevations corresponding to the linear and nonlinear shallow water models. They are plotted on the same graph for comparison purposes. Again there is a slight difference between the linear and the NSW models, but dispersion effects are still small.

Let us decrease the Ursell number even further by increasing the water depth. Figures 1.22 and 1.23 illustrate the evolution of transient water waves computed with the three models for the same parameters as those of Figure 1.18, except for the water depth now equal to 1 km. The small dimensionless numbers are roughly $\varepsilon = 5 \times 10^{-5}$ and $\mu = 0.1$, with a corresponding Ursell number equal to 0.005. On one hand, linear and fully nonlinear models are essentially undistinguishable at all times: the waves propagate with the same speed and the same profile. Nonlinear effects are clearly negligible during the first moments of transient waves generated by a moving bottom, at least in this context. On the

other hand, the numerical solution obtained with the NSW model gives slightly different results. Waves computed with this model do not propagate with the same speed and have different amplitudes compared to those obtained with the linear and fully nonlinear models. Dispersive effects come into the picture essentially because the waves are shorter compared to the water depth. As shown in the previous examples, dispersive effects do not play a role for long enough waves.

Figure 1.24 shows the transient waves at the gauges selected in Figure 1.20. One can see that the elevations obtained with the linear and fully nonlinear models are very close within graphical accuracy. On the contrary, the nonlinear shallow water model leads to a higher speed and the difference is obvious for the points away from the generation zone.

These results show that one cannot neglect the dispersive effects any longer. The NSW equations, which contain no dispersive effects, lead to different speed and amplitudes. Moreover, the oscillatory behaviour just behind the two front waves is no longer present. This oscillatory behaviour has been observed for the water waves computed with the linear and fully nonlinear models and is due to the presence of frequency dispersion. So, one should replace the NSW equations with Boussinesq models which combine the two fundamental effects of nonlinearity and dispersion. Wei et al. [WKS95] provided comparisons for two-dimensional waves resulting from the integration of a Boussinesq model and the two-dimensional version of the FNPF model described above. In fact they used a fully nonlinear variant of the Boussinesq model, which predicts wave heights, phase speeds and particle kinematics more accurately than the standard weakly nonlinear approximation first derived by Peregrine [Per67] and improved by Nwogu's modified Boussinesq model [Nwo93]. We refer to the review [Kir03] on Boussinesq models and their applications for a complete description of modern Boussinesq theory.

From a physical point of view, we emphasize that the wavelength of the tsunami waves is directly related to the mechanism of generation and to the dimensions of the source event. And so is the dimensionless number μ which determines the importance of the dispersive effects. In general it will remain small.

Adapting the discussion by Bona et al. [BCL05], one can expect the solutions to the long wave models to be good approximations of the solutions to the full water-wave equations on a time scale of the order $\min(\varepsilon^{-1}, \mu^{-2})$ and also the neglected effects to make an order-one relative contribution on a time scale of order $\min(\varepsilon^{-2}, \mu^{-4}, \varepsilon^{-1}\mu^{-2})$. Even though we have not computed precisely the constant in front of these estimates, the results shown in this study are in agreement with these estimates. Considering the 2004 Boxing Day tsunami, it is clear that dispersive and nonlinear effects did not have sufficient time to develop during the first hours due to the extreme smallness of ε and μ^2 , except of course when the tsunami waves approached the coast.

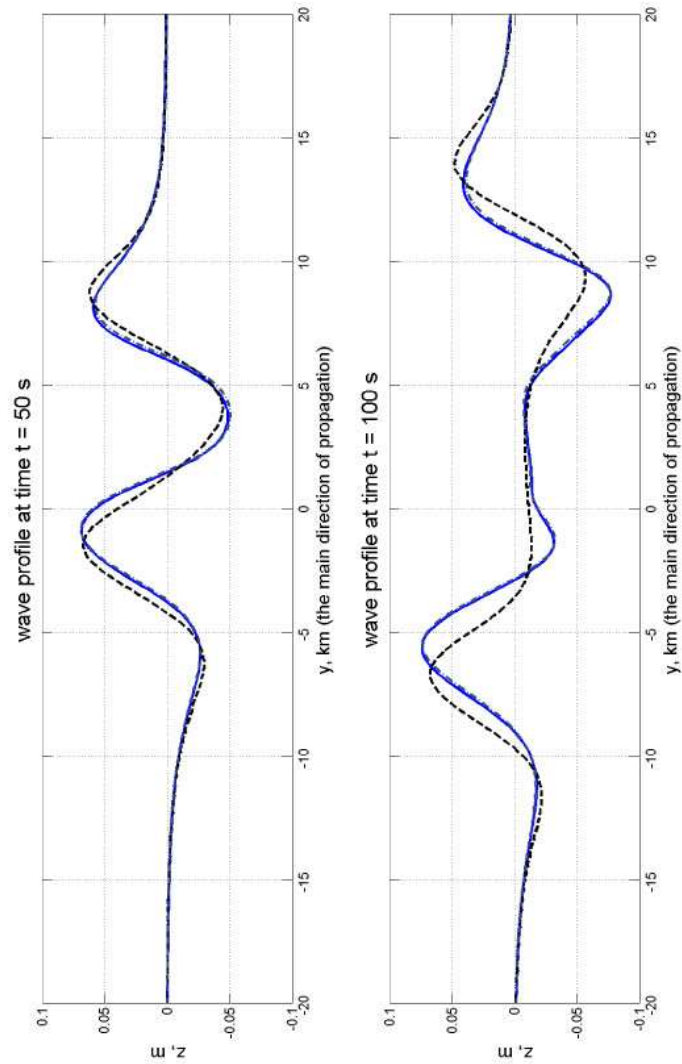


Figure 1.22: Comparisons of the free-surface elevation at $x = 0$ resulting from the integration of the linear equations ($- \cdot -$), NSW equations ($--$) and FNPF equations ($-$) at different times of the propagation of transient waves generated by an earthquake ($t = 50$ s, $t = 100$ s). The parameters for the earthquake are those given in Table 1.5. The water depth is 1 km. One has the following estimates: $\varepsilon = 5 \times 10^{-5}$, $\mu^2 = 10^{-2}$ and consequently $S = 0.005$.

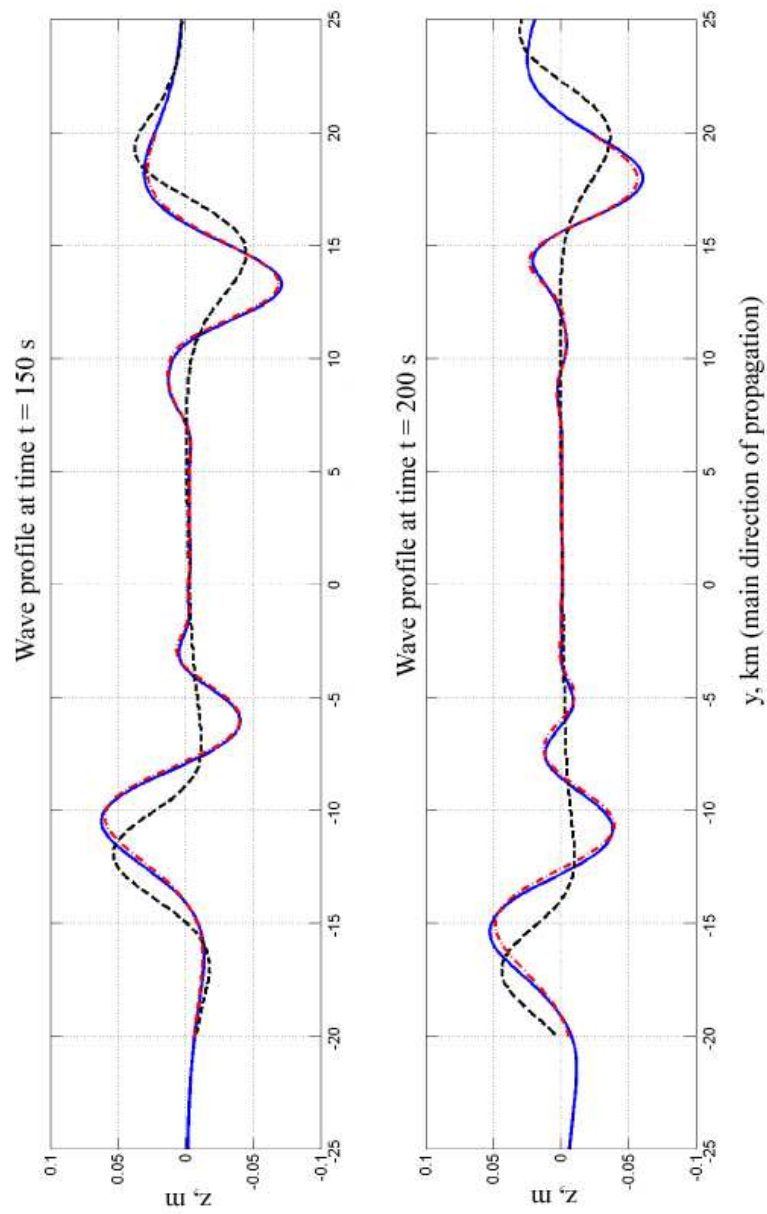


Figure 1.23: Same as Figure 1.22 for later times ($t = 150$ s, $t = 200$ s).

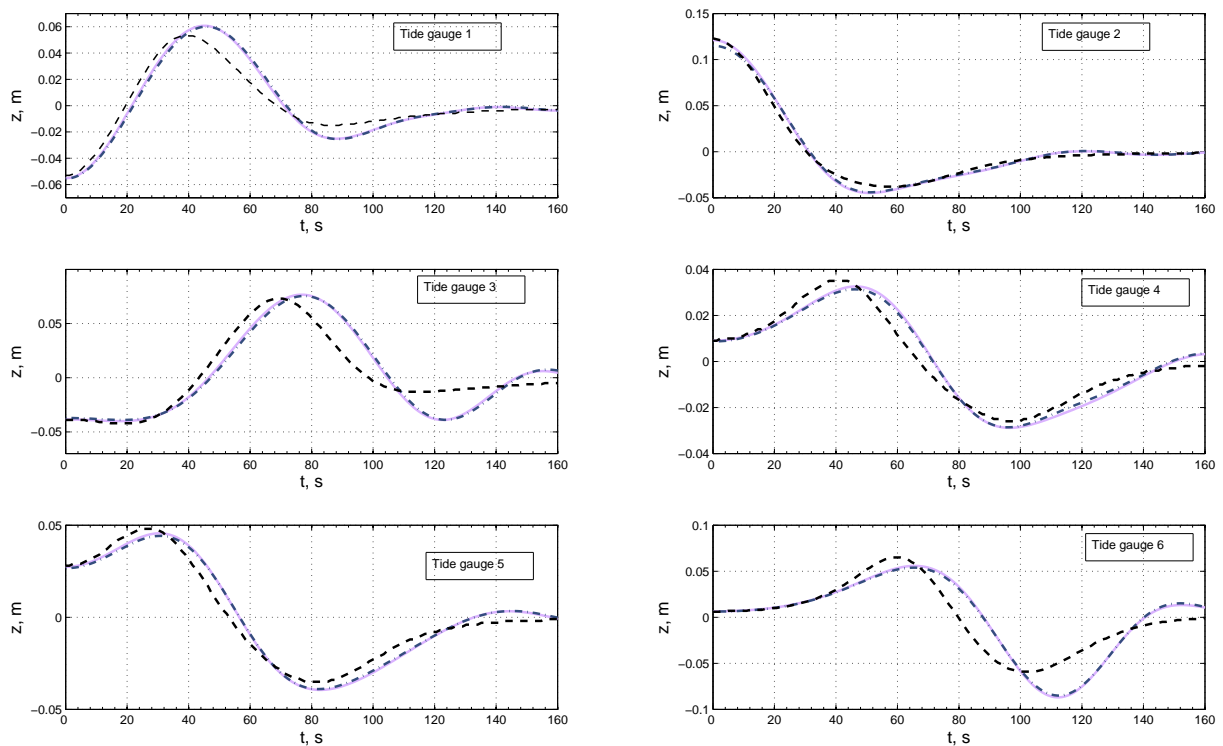


Figure 1.24: Transient waves generated by an underwater earthquake. The physical parameters are those of Figures 1.22 and 1.23. Comparisons of the free-surface elevation as a function of time at the selected gauges shown in Figure 1.20: —, linear model ; -- nonlinear shallow water model. The time t is expressed in seconds. The FNPF results cannot be distinguished from the linear results.

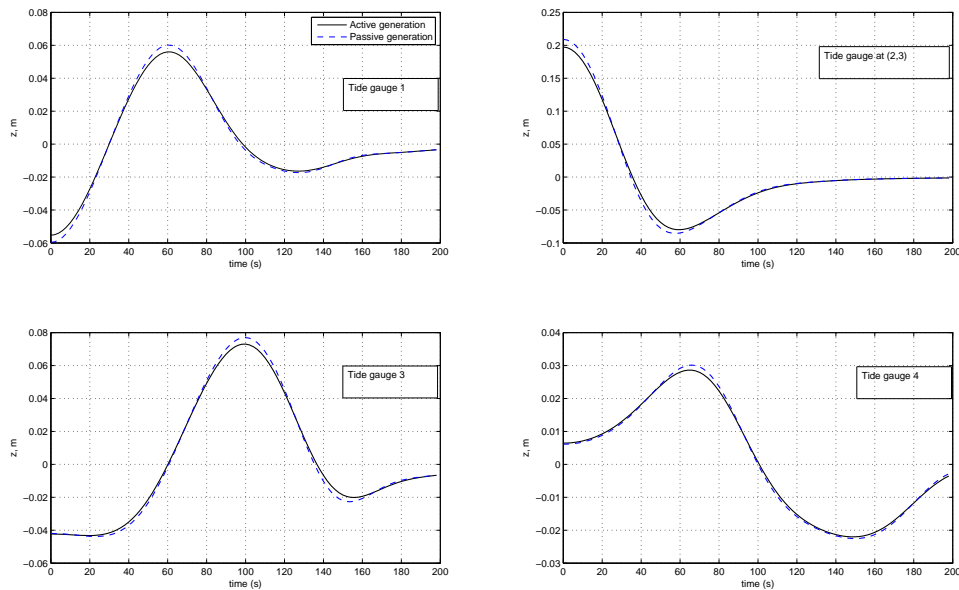


Figure 1.25: Transient waves generated by an underwater earthquake. The computations are based on linear wave theory. Comparisons of the free-surface elevation as a function of time at selected gauges for active and passive generation processes. The time t is expressed in seconds. The physical parameters are those of Figure 1.19. In particular, the water depth is $h = 500$ m.

Let us conclude this section with a discussion on the generation methods, which extends the results given in [DDK06]⁵. We show the major differences between the classical passive approach and the active approach of wave generation by a moving bottom. Recall that the classical approach consists in translating the sea bed deformation to the free surface and letting it propagate. Results are presented for waves computed with the linear model.

Figure 1.25 shows the waves measured at several artificial gauges. The parameters are those of Table 1.5, and the water depth is $h = 500$ m. The solid line represents the solution with an instantaneous bottom deformation while the dashed line represents the passive wave generation scenario. Both scenarios give roughly the same wave profiles. Let us now consider a slightly different set of parameters: the only difference is the water depth which is now $h = 1$ km. As shown in Figure 1.26, the two generation models differ. The passive mechanism gives higher wave amplitudes.

Let us quantify this difference by considering the relative difference between the two

⁵In Figures 1 and 2 of [DDK06], a mistake was introduced in the time scale. All times must be multiplied by a factor $\sqrt{1000}$.

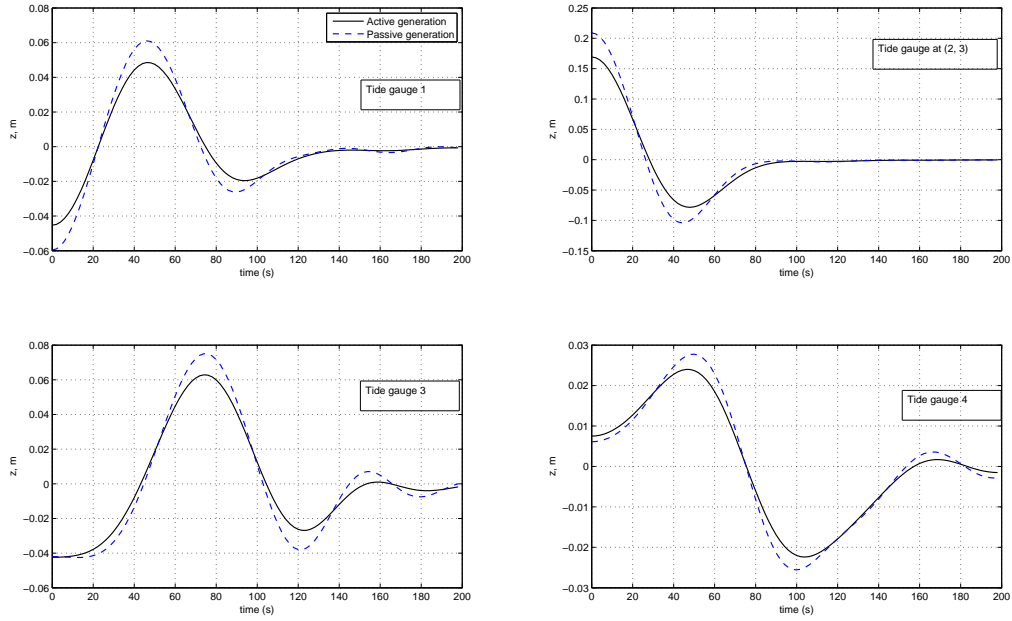


Figure 1.26: Same as Figure 1.25, except for the water depth, which is equal to 1 km.

mechanisms defined by

$$r(x, y, t) = \frac{|\eta_{\text{active}}(x, y, t) - \eta_{\text{passive}}(x, y, t)|}{\|\eta_{\text{active}}\|_{\infty}}.$$

Intuitively this quantity represents the deviation of the passive solution from the active one with a moving bottom in units of the maximum amplitude of $\eta_{\text{active}}(x, y, t)$.

Results are presented on Figures (1.27) and (1.28). The differences can be easily explained by looking at the analytical formulas (1.48) and (1.59) of Section 1.2.2. These differences, which can be crucial for accurate tsunami modelling, are twofold.

First of all, the wave amplitudes obtained with the instantly moving bottom are lower than those generated by the passive approach (this statement follows from the inequality $\cosh mh \geq 1$). The numerical experiments show that this difference is about 6% in the first case and 20% in the second case.

The second feature is more subtle. The water column has an effect of a low-pass filter. In other words, if the initial deformation contains high frequencies, they will be attenuated in the moving bottom solution because of the presence of the hyperbolic cosine $\cosh(mh)$ in the denominator which grows exponentially with m . Incidentally, in the framework of the NSW equations, there is no difference between the passive and the active approach for an instantaneous seabed deformation [Tuc79, Tuc74].

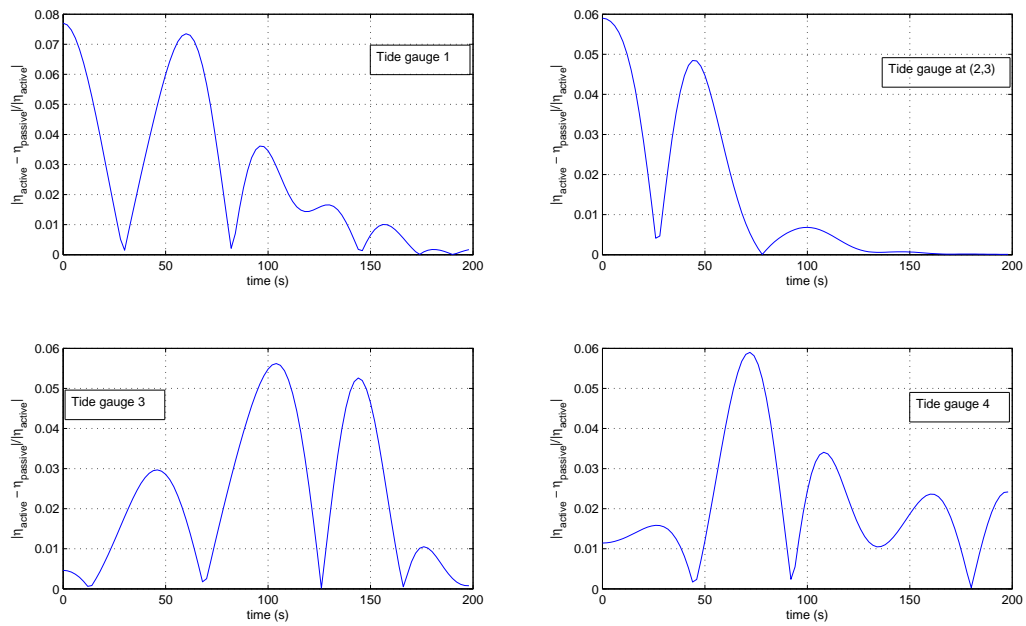


Figure 1.27: Relative difference between the two solutions shown in Figure 1.25. The time t is expressed in seconds.

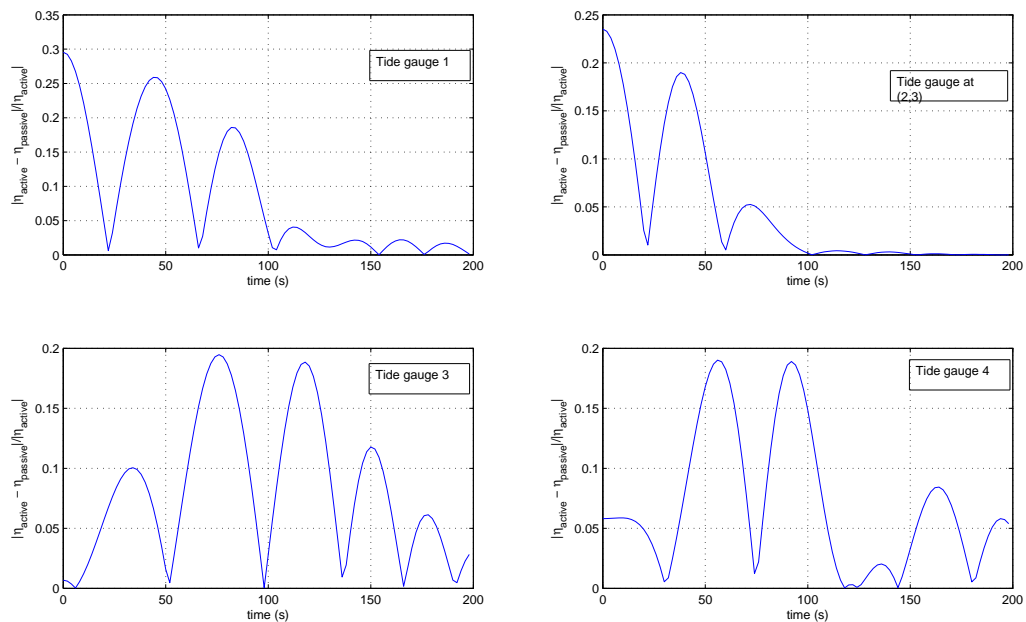


Figure 1.28: Relative difference between the two solutions shown in Figure 1.26.

If we prescribe a more realistic bottom motion as in [DD07c] for example, the results will depend on the characteristic time of the seabed deformation. When the characteristic time of the bottom motion decreases, the linearized solution tends to the instantaneous wave generation scenario. So, in the framework of linear water wave equations, one cannot exceed the passive generation amplitude with an active process. However, during slow events, Todorovska and Trifunac [TT01] have shown that amplification of one order of magnitude may occur when the sea floor uplift spreads with velocity similar to the long wave tsunami velocity.

1.2.10 Conclusions

Comparisons between linear and nonlinear models for tsunami generation by an underwater earthquake have been presented. There are two main conclusions that are of great importance for modelling the first instants of a tsunami and for providing an efficient initial condition to propagation models. To begin with, a very good agreement is observed from the superposition of plots of wave profiles computed with the linear and fully nonlinear models. Secondly, the nonlinear shallow water model was not sufficient to model some of the waves generated by a moving bottom because of the presence of frequency dispersion. However classical tsunami waves are much longer, compared to the water depth, than the waves considered in the present work, so that the NSW model is also sufficient to describe tsunami generation by a moving bottom. Comparisons between the NSW equations and the FNPF equations for modeling tsunami run-up are left for future work. Another aspect which deserves attention is the consideration of Earth rotation and the derivation of Boussinesq models in spherical coordinates.

1.3 Tsunami generation by dynamic displacement of sea bed due to dip-slip faulting

1.3.1 Introduction

The accuracy of the computation of the whole life of a tsunami, from generation to inundation, obviously depends on the construction of the initial condition. Moreover, the error made on the initial condition cannot be corrected by the numerical method used to propagate the tsunami. This is why the process of tsunami generation must be modelled as accurately as possible. Even though the constraint of being able to predict tsunami arrival time, height and location as fast as possible must definitely be taken into account (in other words, a trade-off must be found between the precision and the speed of computation of

the initial condition), we believe that so far the scientific community has not paid enough attention to the crucial subject of tsunami generation.

After the pioneer work of Kajiura [Kaj70] it has become a common practice in the tsunami community to translate the static sea bed deformation generated by an underwater earthquake onto the free surface and let it propagate. We will refer to this method as *passive approach*. The validity of this technique was already discussed in [OTM01, DDK06]. Three-dimensional analytical expressions derived from Volterra's formula applied to the general study of dislocations [MS71, Oka85] are used to construct the static initial deformation. Similar analytical expressions for two-dimensional problems were also derived by Freund & Barnett [FB76], who used the theory of analytic functions of a complex variable. Obviously, the popularity of these analytic solutions can be explained by their relatively simple explicit form. Thus, their computation is easy and inexpensive. A nice feature of the solution of Freund & Barnett is that nonuniform slip distributions can be easily considered. In particular, slip distributions which remove the singular behavior of the internal stresses at the ends of the slip zone can be dealt with, simply by imposing the so-called smooth closure condition on the slip: the slip is zero at the ends.

When simplifying hypotheses such as homogeneity or isotropy are removed, analytical solutions are no longer available and the governing equations must be solved numerically. Static deformations caused by slip along a fault have been extensively simulated by Mastlark [Mas03], who used several dislocation models based on the finite-element method (FEM) to estimate the importance of different physical hypotheses. Anisotropy and heterogeneity turned out to be the most important factors in this type of modelling. Megna et al. [MBS05] also used the FEM to compare numerical results with analytical solutions. However neither in [Mas03] nor in [MBS05] were the dynamical aspects and the coupling with hydrodynamics considered. Moreover the consequences for the resulting tsunami waves were not pointed out.

When one uses as initial condition a static seismic source together with the translation of the sea bed deformation onto the free surface, one neglects the rupture velocity and the rise time. Several studies have already been performed to understand wave formation due to different prescribed bottom motions, either by introducing some type of rise time, or by introducing some type of rupture velocity. For example, Todorovska & Trifunac [TT01] studied the generation of waves by a slowly spreading uplift of the bottom. The studies of Hammack [Ham73] and Dutykh & Dias [DD07c] take into account the rise time. Hammack [Ham73] generated waves experimentally by raising or lowering a box at one end of a channel, and considered various laws for the rise or the fall of the box. In their review paper, Dutykh & Dias [DD07c] generated waves theoretically by multiplying the static deformations caused by slip along a fault by various time laws: instantaneous,

exponential, trigonometric, linear. Haskell [Has69] was one of the first to take into account the rupture velocity. In fact he considered both rise time and rupture velocity. Let us consider the source shown in Figure 1.29. The two horizontal coordinates x and y , and the vertical coordinate z are denoted by $\vec{x} = (x, y, z)$.

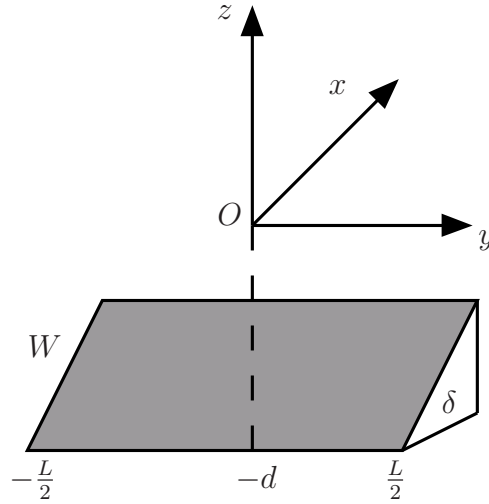


Figure 1.29: Geometry of the source model. The fault has width W , length L , depth d and dip angle δ .

Let $\vec{b}(\vec{x}, t)$ denote the fault displacement function and $\vec{b}_0(\vec{x})$ the final displacement. The following form for $\vec{b}(\vec{x}, t)$ was considered by Haskell:

$$\vec{b}(\vec{x}, t) = \begin{cases} 0 & t - \zeta/V < 0 \\ (\vec{b}_0/T)(t - \zeta/V) & 0 < t - \zeta/V < T \\ \vec{b}_0 & t - \zeta/V > T \end{cases} \quad (1.81)$$

where T is the rise time and V the rupture velocity. The coordinate ζ is a coordinate along the fault. Equation (1.81) implies that at $t = 0$ a fracture front is established instantaneously over a width W of the y -axis at depth d . The front propagates unilaterally at constant velocity V over a length $L \cos \delta$ of the x -axis. At any fixed point on the fault plane the relative displacement increases at constant velocity from 0 at $t = \zeta/V$ to a constant final value \vec{b}_0 at $t = T + \zeta/V$. More recently, Okumura & Kawata [OK07] used Haskell's approach to investigate the effects of rise time and rupture velocity on tsunami generation. They considered two cases of sea bottom motion: (i) with only rise time and (ii) with both rise time and rupture velocity. They found that the effects of rupture velocity are much smaller than those of rise time when the rise time is assumed to be long (over 10 min). Ohmachi et al. [OTM01] also considered rise time and rupture velocity but unfortunately

the dynamics is not clearly explained in their paper. Apparently they did not solve the elastodynamic equations with the second-order time derivative (see next section). Another interesting attempt to understand dynamical effects is that of Madariaga [Mad03]. He considers a dip-slip dislocation propagating in a half-space. He solves the elastodynamic equations by using the double Laplace transform. The solution is elegant but it is relatively complex. Unfortunately Madariaga does not provide any plots of the deformation of the free surface and does not consider the coupling with the water layer. The present study can be considered as an attempt to understand the coupling between seismic faulting and hydrodynamics by integrating numerically the time-dependent elasticity equations as well as the time-dependent fluid equations. The authors have already addressed the problem of tsunami generation in [DDK06, DD07c]. The main feature of the present study is the use of a more realistic earthquake source model.

The work is organised as follows. In Section 1.3.2 we briefly describe the mathematical models, both for solid and fluid motions, which are used in the present study. Section 1.3.3 contains details on the numerical methods used to solve the governing equations. The numerical method for the solid motion is validated in Section 1.3.4. The last Section 1.3.5, provides a comparison between the traditional approach to tsunami generation (in which the static sea bed deformation is translated onto the free surface) and the more realistic approach of dynamic generation (in which the wavetrain is generated by the motion of the bottom). We reveal numerically that the dynamical aspects of tsunami generation can for example lead to a leading depression wave when one expects a leading elevation wave.

1.3.2 Mathematical models

Even though the numerical results shown in this study are for two-dimensional configurations, the modeling is performed for three-dimensional problems. The horizontal coordinates are denoted by x and y , while the vertical coordinate is denoted by z . The displacements are denoted by u_x, u_y and u_z . We use different origins along the vertical axis for the solid and fluid motions. In the earth domain, $z = 0$ denotes the sea bed at rest (assumed to be flat). In the fluid domain, $z = 0$ denotes the sea surface at rest.

1.3.2.1 Dynamic fault model

We assume that the fault is inside a geological viscous medium. Earth's crust is assumed to be a viscoelastic material of density ρ . We choose the Kelvin-Voigt viscosity model [Qui97] which consists in using complex elastic coefficients (with negative imaginary parts in order to dissipate wave energy). For isotropic media it means that the Lamé coefficients

have a nonpositive imaginary part:

$$\lambda^* = \lambda_r - i\lambda_i, \quad \mu^* = \mu_r - i\mu_i,$$

where $\lambda_r, \mu_r > 0$ and $\lambda_i, \mu_i \geq 0$. The classical elasticity equations are obtained by choosing $\lambda_i \equiv 0$ and $\mu_i \equiv 0$. Notice that on the time-scales relevant to our problem, elasticity is sufficient and the assumption of a Kelvin-Voigt viscous material is unnecessary. But we keep it for the sake of completeness.

Let c_P and c_S be the classical velocities for the propagation of P and S waves in a medium of density ρ :

$$c_P = \sqrt{\frac{\lambda_r + 2\mu_r}{\rho}}, \quad c_S = \sqrt{\frac{\mu_r}{\rho}}.$$

Complex Lamé coefficients yield complex velocities for wave propagation,

$$c_P^* = c_P \sqrt{1 + \frac{i}{Q_P}}, \quad c_S^* = c_S \sqrt{1 + \frac{i}{Q_S}},$$

where the coefficients Q_P and Q_S are defined as follows:

$$Q_P = -\frac{\lambda_r + 2\mu_r}{\lambda_i + 2\mu_i}, \quad Q_S = -\frac{\mu_r}{\mu_i}.$$

The factors Q_P and Q_S measure the viscosity of the geological medium. In this study we restrict our attention to the weakly viscous case. Mathematically it means that $1/Q_P \ll 1$ and $1/Q_S \ll 1$.

Let $\underline{\underline{\sigma}}$ represent the stress tensor. The displacement field $\vec{u}(x, y, z, t) = (u_x, u_y, u_z)$ satisfies the classical elastodynamic equations from continuum mechanics:

$$\nabla \cdot \underline{\underline{\sigma}} = \rho \frac{\partial^2 \vec{u}}{\partial t^2}. \quad (1.82)$$

It is common in seismology to assume that the stress tensor $\underline{\underline{\sigma}}$ is determined by Hooke's law through the strain tensor $\varepsilon = \frac{1}{2}(\nabla \vec{u} + \nabla^t \vec{u})$. Therefore

$$\underline{\underline{\sigma}} = \lambda^*(\nabla \cdot \vec{u})\mathbb{I} + 2\mu^*\varepsilon. \quad (1.83)$$

Thus, we come to the following linear viscoelastodynamic problem⁶:

$$\nabla \cdot (\lambda^*(\nabla \cdot \vec{u})\mathbb{I} + \mu^*(\nabla \vec{u} + \nabla^t \vec{u})) = \rho \frac{\partial^2 \vec{u}}{\partial t^2}. \quad (1.84)$$

⁶We use the prefix ‘visco-’ due to the presence of the imaginary part in the Lamé coefficients, which is responsible for small wave damping.

Recall that the mechanical characteristics ρ , λ^* and μ^* can possibly depend on the spatial coordinates (x, y, z) . However we will assume that they are constant in the numerical applications.

The fault is modeled as a dislocation inside a viscoelastic material. This type of model is widely used for the interpretation of seismic motion. A dislocation is considered as a surface (in three-dimensional problems) or a line (in two-dimensional problems) in a continuous medium where the displacement field is discontinuous. The displacement vector is increased by the amount of the Burgers vector \vec{b} along any contour C enclosing the dislocation surface (or line), i.e.

$$\oint_C d\vec{u} = \vec{b}. \quad (1.85)$$

We let a dislocation run at speed V along a fault inclined at an angle δ with respect to the horizontal. Rupture starts at position $x = 0$ and $z = -d$ (it is supposed to be infinitely long in the transverse y -direction) and propagates with constant rupture speed V for a finite time L/V in the direction δ stopping at a distance L . Let ζ be a coordinate along the dislocation line. On the fault located in the interval $0 < \zeta < L$ slip is assumed to be constant. The rise time is assumed to be 0.

1.3.2.2 Fluid layer model

Since the main purpose is to model tsunami generation processes and since tsunamis are long waves, it is natural to choose the nonlinear shallow water equations (NSWE) as hydrodynamic model. These equations are widely used in tsunami modelling, especially in codes for operational use [TS98, SB06]. The validity of the NSWE model and the question of the importance of dispersive effects have already been addressed by the authors in the previous Section (one can have a look at our publication [KDD07]).

Let η denote the free-surface elevation with respect to the still water level $z = 0$, $\vec{v} = (v_x, v_y)$ the horizontal velocity vector, g the acceleration due to gravity and $z = -h(x, y, t)$ the bathymetry. The NSWE in dimensional form read

$$\begin{aligned} \frac{\partial \eta}{\partial t} + \nabla \cdot ((h + \eta)\vec{v}) &= -\frac{\partial h}{\partial t}, \\ \frac{\partial \vec{v}}{\partial t} + \frac{1}{2}\nabla|\vec{v}|^2 + g\nabla\eta &= 0. \end{aligned}$$

The effect of the moving bottom appears in the source term $-\partial h/\partial t$ in the first equation.

The unknowns η and \vec{v} are functions of time and of the horizontal coordinates x and y . Since the NSWE are essentially obtained from depth-averaging the Euler equations, the dependence on the vertical coordinate z disappears from the equations.

The coupling between the earth and fluid models is made through the function $h(x, y, t)$ which describes the moving sea bottom bathymetry.

1.3.3 Numerical methods

In the present study we made two natural choices. The solid mechanics equations of the model are solved using the FEM with fully implicit time integration, while for the hydrodynamic part we take advantage of the hyperbolic structure of the governing equations and use a solver based on the finite-volume (FV) scheme (see for example [BQ06, KDD07]).

1.3.3.1 Discretization of the viscoelastodynamic equations

In order to apply the FEM one first rewrites the governing equation (1.84) in variational form. The time-derivative operator is discretized through a classical second-order finite-difference scheme. The method we use is fully implicit and has the advantage of being free of any Courant-Friedrichs-Lewy-type condition. In such problems implicit schemes become advantageous since the velocity of propagation of seismic waves is of the order of 3 to 4 km/s. We apply the $\mathbb{P}2$ finite-element discretization procedure. For the numerical computations, the freely available code FreeFem++ [HPHO] is used.

Let us say a few words about the boundary conditions and the treatment of the dislocation in the program. Concerning the boundary conditions, we assume that the sea bed is a free surface, that is $\underline{\underline{\sigma}} \cdot \vec{n} = \vec{0}$ at $z = 0$. The other boundaries are assumed to be fixed or, in other words, Dirichlet type boundary conditions $\vec{u} = \vec{0}$ are applied. The authors are aware of the reflective properties of this type of boundary conditions. In order to avoid the reflection of seismic waves along the boundaries during the simulation time, we take a computational domain which is sufficiently large. This approach is not computationally expensive since we use adaptive mesh algorithms [HPHO] and in the regions far away from the fault, element sizes are considerably bigger than in the fault vicinity.

Next we discuss the implementation of the dislocation surface. Across the fault, the displacement field is discontinuous and satisfies the following relation:

$$\vec{u}^+(\vec{x}, t) - \vec{u}^-(\vec{x}, t) = \vec{b}(\vec{x}, t), \quad (1.86)$$

where the signs \pm denote the upper and lower boundary of the dislocation surface, respectively. The propagation of Burger's vector along the fault is given by

$$\vec{b}(\vec{x}, t) = \vec{b}_0 H(t - \zeta/V), \quad (1.87)$$

where V is the rupture velocity, H the Heaviside unit step function and ζ a coordinate along the dislocation line.

Remark 1 *Due to the presence of huge hydrostatic pressures in the crust, the two sides of the fault cannot detach physically. In any case this situation does not occur in nature. Mathematically it means that the vector \vec{b} is tangent to the dislocation surface at each point.*

1.3.3.2 Finite-volume scheme

In this study we adopt the characteristic flux (CF) approach proposed in [GKC96, GKC01] and described in details in Appendix A. This approach is a particular scheme of FV methods. There are other schemes that have been proposed for the NSWE (see [BQ06] for example).

We chose this method for the following reasons. First of all, the CF scheme is easy to implement. Then it is not based on the solution to the Riemann problem and consequently we do not impose a one-dimensional wave structure which is no longer relevant in two dimensions. It is a multidimensional scheme and we do not need to split operators in order to treat separately each dimension. And finally, the characteristic flux is more versatile than Roe's scheme in the sense that it does not rely on an algebraic property of the flux.

In this section we consider an application of the characteristic fluxes scheme to NSWE. In this case one can explicitly find eigenvalues, as well as left and right eigenvectors. This property together with the use of an approximate Riemann solver makes all the computations very efficient.

Let $\vec{v} = (v_x, v_y)$. The flux of the NSWE system is given by

$$\mathbf{F}(\mathbf{V}) = \begin{pmatrix} (h + \eta)v_x & (h + \eta)v_y \\ \frac{1}{2}|\vec{v}|^2 + g\eta & 0 \\ 0 & \frac{1}{2}|\vec{v}|^2 + g\eta \end{pmatrix}, \quad (1.88)$$

where $\mathbf{V} = (\eta, u, v)$ is the vector of conservative variables⁷. The flux $\mathbf{F}(\mathbf{V})$ projected on the normal \mathbf{n} becomes

$$\mathbf{F} \cdot \mathbf{n} = \begin{pmatrix} (h + \eta)(\vec{v} \cdot \mathbf{n}) \\ (\frac{1}{2}|\vec{v}|^2 + g\eta)\mathbf{n} \end{pmatrix}.$$

It follows that the Jacobian matrix is given by

$$\mathbb{A}_n := \frac{\partial(\mathbf{F}(\mathbf{V}) \cdot \mathbf{n})}{\partial \mathbf{V}} = \begin{pmatrix} \vec{v} \cdot \mathbf{n} & (h + \eta)\mathbf{n} \\ g\mathbf{n} & \vec{v} \otimes \mathbf{n} \end{pmatrix}. \quad (1.89)$$

It has three distinct eigenvalues

$$\lambda_{1,3} = \vec{v} \cdot \mathbf{n} \pm c_s, \quad \lambda_2 = 0,$$

⁷In the present study the physical variables coincide with the conservative ones.

where $c_s = \sqrt{g(h + \eta)}$ is the velocity of long gravity waves.

The right eigenvectors constitute the columns of the matrix R :

$$R = \begin{pmatrix} -c_s & (c_s^2/g)\vec{v} \cdot \mathbf{t} & c_s \\ gn_x & n_y c_s^2 - v_y(\vec{v} \cdot \mathbf{n}) & gn_x \\ gn_y & -n_x c_s^2 + v_x(\vec{v} \cdot \mathbf{n}) & gn_y \end{pmatrix}, \quad (1.90)$$

where \mathbf{t} is the tangent vector. The matrix of left eigenvectors can also be computed analytically through R^{-1} .

Using these expressions it is straightforward to compute the sign matrix defined as

$$\text{sign}(\mathbb{A}_n) := R \text{sign}(\Lambda) R^{-1},$$

and the numerical scheme is thus completely defined.

1.3.4 Validation of the numerical method

In this section we consider an analytic solution to the line dislocation problem in the static case. Use is made of the well-known result described for example by Freund & Barnett [FB76] or Okada [Oka85]. In order to simplify the expressions, we only consider the two-dimensional case (in other words, the fault is infinite in the y -direction). In fact the most appropriate expression is that given by equation (24) in [Mad03]. We checked that it is in full agreement with the limit of Okada's solution as the width becomes infinite. The sketch of the domain is given in Figure 1.29. The fault has infinite width ($W \rightarrow \infty$). Its length is L , its depth d and its dip angle δ .

In the present work we only give the vertical displacement component u_z along the free surface, since it plays the most important role in tsunami formation. It can be expressed as the difference between two contributions, that from a first dislocation located at the beginning of the fault and that from a second dislocation located at the end of the fault. Let $d_L = d - L \sin \delta$. One has

$$u_z = |\vec{b}_0| \left[U_z \left(\frac{x}{d}, \delta \right) - U_z \left(\frac{x - L \cos \delta}{d_L}, \delta \right) \right], \quad (1.91)$$

where

$$U_z \left(\frac{x}{d}, \delta \right) = \frac{1}{\pi} \left[\sin \delta \arctan \frac{x}{d} - \frac{d(d \cos \delta - x \sin \delta)}{x^2 + d^2} \right]. \quad (1.92)$$

For the validation of our numerical method we chose the most violent fault which corresponds to the dip angle $\delta = \pi/2$. The values of the other parameters are given in Table 1.6. This problem was solved by FEM after neglecting the dynamic terms. The results of the comparison with solution (1.92) are given in Figure 1.30. Good qualitative

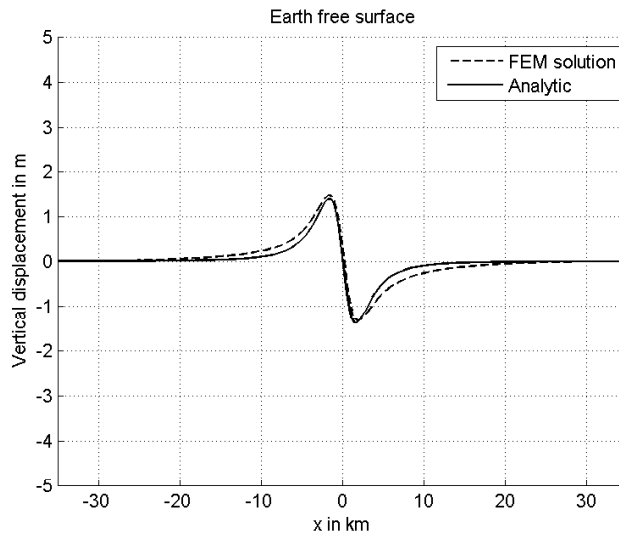


Figure 1.30: Comparison between analytical and numerical solutions for a static two-dimensional fault with a dip angle equal to $\pi/2$.

and quantitative agreement can be seen. Megna et al. [MBS05], who also considered static displacement due to uniform slip across a normal fault, compared the two-dimensional FEM results with the analytical solution in the case of a normal fault. In their conclusion, they state that it is for the vertical component of the surface displacement that the discrepancies are the largest.

1.3.5 Results of the simulation

In this section, we use the set of physical parameters given in Table 1.6. The static sea bed deformation obtained with the analytical solution is depicted in Figure 1.31. Note that the only difference between Figures 1.30 and 1.31 is the value of the dip angle.

In order to illustrate the numerical computations we chose several test cases of active/passive tsunami generation. The passive generation approach was introduced in [Kaj70]. It consists in translating the static sea bed deformation onto the free surface and letting it propagate under gravity. On the other hand, the active approach uses the bottom motion for wave generation. We proceed by computing the first eight or fifteen seconds of the earthquake dynamics. Then the bottom configuration is assumed to remain frozen during the rest of the simulation. Concerning the dynamical aspects of rupture propagation, we consider the Heaviside-type approach (1.87) where the dislocation propagates along the fault with rupture velocity V . One could use instead a dislocation for which Burger's vector \vec{b}_0 is also space-dependent. But the main goal of the present study

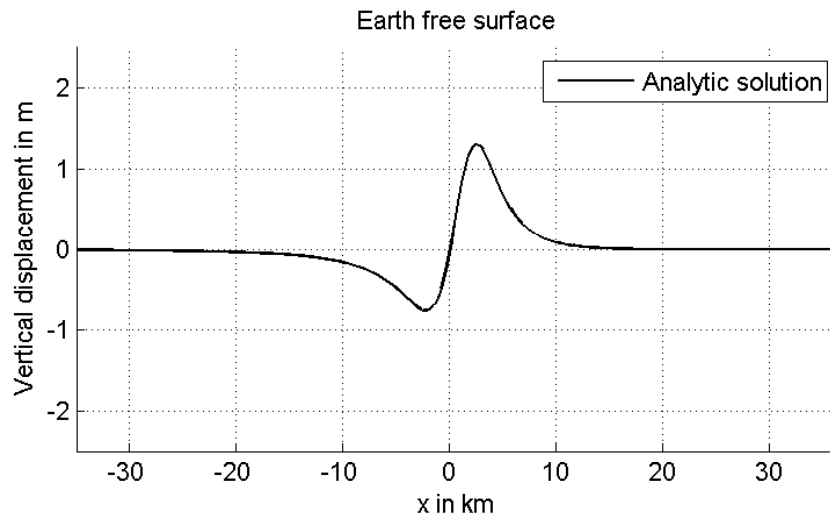


Figure 1.31: Static deformation due to the dislocation corresponding to the parameters given in Table 1.6.

Parameter	Value
Young modulus, E , GPa	9.5
Poisson ratio, ν	0.27
Damping coefficient, λ_i	500
Damping coefficient, μ_i	200
Fault depth, d , km	4
Fault length, L , km	2
Dip angle, δ , $^\circ$	13
Burger's vector length, $ \vec{b}_0 $, m	10
Water depth (uniform), h_0 , m	400
Acceleration due to gravity, g , m/s^2	9.8

Table 1.6: Typical physical parameters used in the numerical computations. The water depth as well as the spatial extent in the main direction of propagation were chosen so that dispersive effects can be neglected.

is to make an attempt to include the dynamic displacement of the sea bed. In the dynamical approach, we consider three cases: the limiting case where the rupture velocity V is infinite, a fast event with $V = 2.5$ km/s and a slower event with $V = 1$ km/s.

We show below the differences between the passive and the dynamic approaches. This question has already been addressed by the authors [DDK06] in the framework of the linearized potential flow equations and of a simplified model for bottom deformation.

In the first comparison we use a strong coupling between the dynamic displacement of the sea bed and the fluid layer equations and compare it with the passive approach, in which the static solution shown in Figure 1.31 is translated onto the free surface as initial condition. The rupture velocity V is assumed to be infinite. Moreover the earthquake dynamics is computed during the first eight seconds. The free surface at the beginning of the tsunami generation process is shown on Figure 1.32. Further steps of this process are given in Figures 1.33-1.34. The reader may have the impression that the passive solution does not evolve. In fact, the explanation lies in the presence of two different time scales in this problem. The fast time scale is provided by the earthquake (P - and S -waves) and the slow one by water gravity waves. Since the active generation solution is directly coupled to the bottom dynamics, it evolves with the fast time scale. It is interesting to compare Figures 1.33 and 1.34. One can see that the active approach gives at the beginning an amplitude which is almost twice larger but the amplitudes become comparable a few seconds later.

The free-surface elevations are computed until the wave enters the purely propagation stage. This corresponds to Figure 1.35. One notices that the resulting wave amplitude and velocity are almost the same. Of course the waveform is different. One can see as well that the location of the elevation wave is the same, while the depression wave is slightly shifted. It can be explained by the larger extent of the dynamic solution. Thus, we can conclude from this first comparison that if one is only interested in tsunami travel time or even in rough inundation zone estimation, the passive approach can be used.

The second comparison focuses on the influence of the rupture velocity at two separate times (Figures 1.36 and 1.37). The differences between the fast and the relatively slow rupture velocities are small.

The most interesting comparison is the third one, which focuses on the duration of the earthquake. Recall that our somewhat artificial definition of earthquake duration is the time at which we stop the bottom motion. After that time, the sea bottom remains frozen. Figure 1.38 shows the effect of a longer earthquake. One sees that the shapes of the wave train obtained with the dynamic analysis look more complicated than that obtained by the passive analysis. In particular, the distinction between leading elevation wave and leading depression wave is not as clear when using the dynamical analysis. It could be an

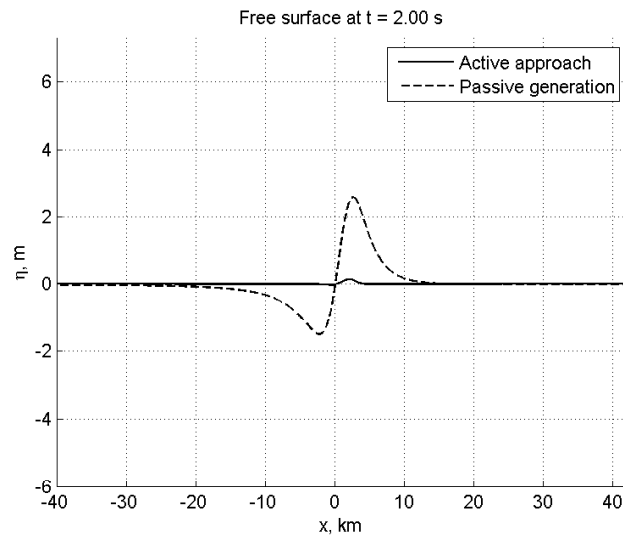


Figure 1.32: Water free surface at the beginning of the earthquake ($t = 2$ s) according to two approaches of tsunami generation: passive versus active (with infinite rupture velocity).

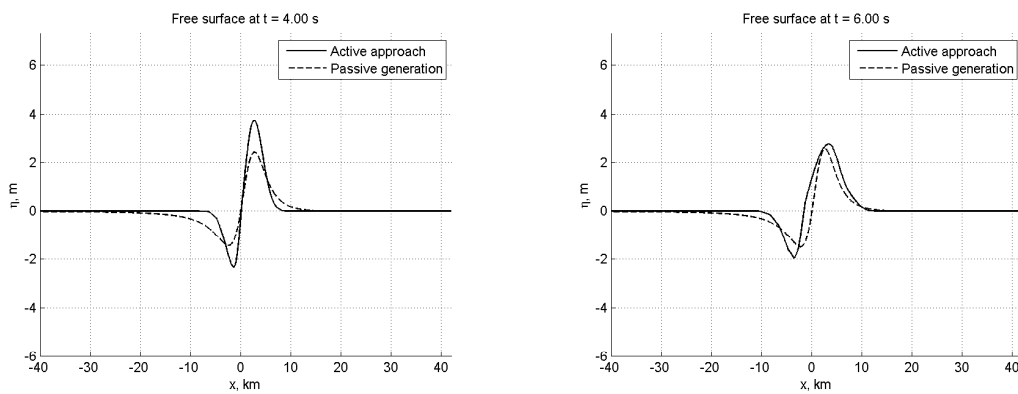


Figure 1.33: Same as Figure 1.32 for times $t = 4$ s and $t = 6$ s.

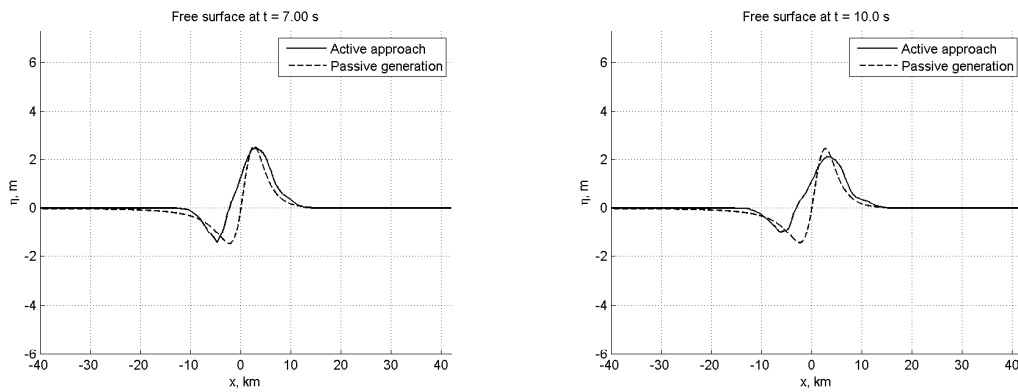


Figure 1.34: Same as Figure 1.32 for times $t = 7\text{s}$ and $t = 10\text{s}$.

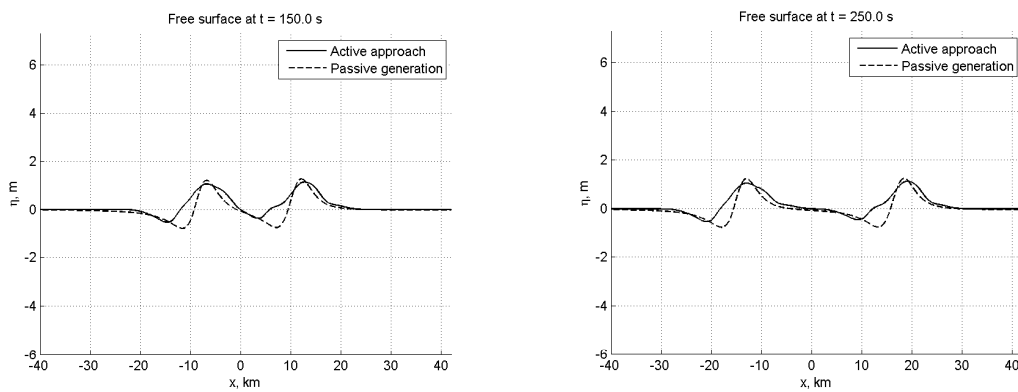


Figure 1.35: Same as Figure 1.32 for times $t = 150\text{s}$ and $t = 250\text{s}$. The wave is leaving the generation zone (left plot) and starting to propagate (right plot).

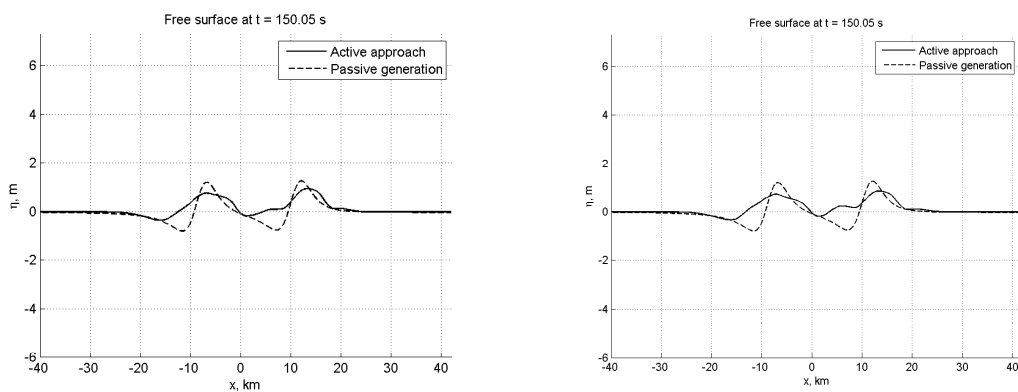


Figure 1.36: Same as Figure 1.35 (left plot) for two rupture velocities: $V = 1\text{ km/s}$ (left) and $V = 2.5\text{ km/s}$ (right).

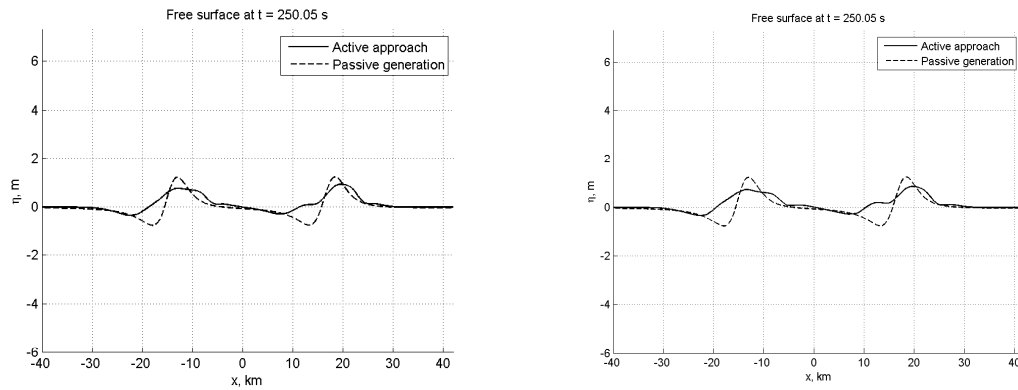


Figure 1.37: Same as Figure 1.36 at time $t = 250$ s.

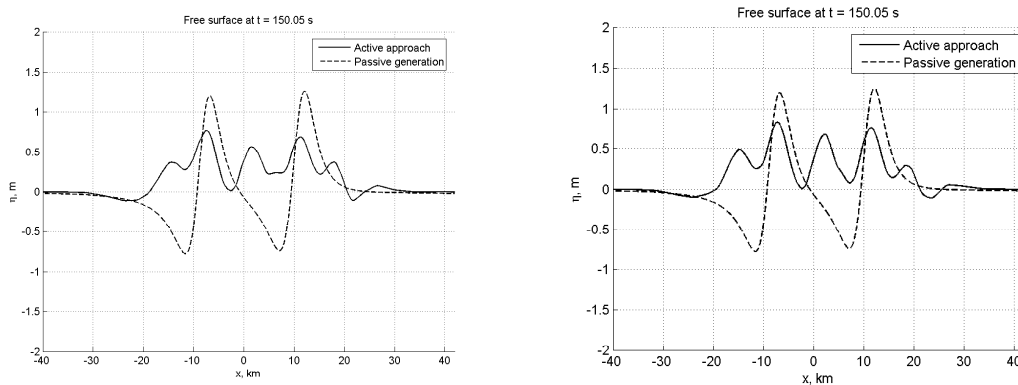


Figure 1.38: Water free surface at $t = 150$ s for a longer earthquake. The rupture motion stops after 15s. The left plot compares the infinite rupture velocity solution with the passive approach. The right plot compares the case of a slow rupture ($V = 1$ km/s) with the passive case.

explanation for the discrepancies between modeled and recorded time series of water levels at various locations along the California coast for the 1960 Chilean tsunami [BUST06].

1.3.6 Conclusions

An approach to model the dynamical character of sea bed deformations during an underwater earthquake was presented. The governing elastodynamic equations were solved by a finite-element method. The principal novelty of the present study is the coupling of the resulting displacement field with the hydrodynamic model.

Two methods for tsunami generation have been compared: static versus dynamic. The computational results speak by themselves. One can say that the dynamic approach leads to higher water levels in the near-fault area. These significant differences only occur during

the first instants of the surface deformation and level off later on. However it was also observed that the shape of the wave train can be altered by dynamical effects. Consequently the distinction between leading elevation wave and leading depression wave may not be as clear as anticipated. Of course the present method is computationally more expensive but there is an overall gain in accuracy. Not surprisingly more accurate tsunami computations require finer initial conditions such as those obtained by the active generation methodology used in the present study.

In future work we intend to extend this modeling to three space dimensions since it is evident that the two-dimensional computations presented here have little interest beyond academics.

Chapter 2

Dissipative Boussinesq equations

*We are usually convinced more easily by reasons we have found ourselves
than by those which have occurred to others.*

Blaise Pascal (1623 – 1662)

Contents

2.1	Introduction	82
2.2	Derivation of the Boussinesq equations	85
2.2.1	Asymptotic expansion	89
2.3	Analysis of the linear dispersion relations	93
2.3.1	Linearized potential flow equations	93
2.3.2	Dissipative Boussinesq equations	95
2.3.3	Discussion	99
2.4	Alternative version of the Boussinesq equations	99
2.4.1	Derivation of the equations	100
2.5	Improvement of the linear dispersion relations	104
2.6	Regularization of Boussinesq equations	105
2.7	Bottom friction	107
2.8	Spectral Fourier method	108
2.8.1	Validation of the numerical method	110
2.9	Numerical results	113
2.9.1	Construction of the initial condition	113
2.9.2	Comparison between the dissipative models	115

2.10 Conclusions	119
-----------------------------------	------------

2.1 Introduction

Boussinesq equations are widely used in coastal and ocean engineering. One example among others is tsunami wave modelling. These equations can also be used to model tidal oscillations. Of course, these types of wave motion are perfectly described by the Navier-Stokes equations, but currently it is impossible to solve fully three-dimensional (3D) models in any significant domain. Thus, approximate models such as the Boussinesq equations must be used.

The years 1871 and 1872 were particularly important in the development of the Boussinesq equations. It is in 1871 that Valentin Joseph Boussinesq received the Poncelet prize from the Academy of Sciences for his work. In the Volumes 72 and 73 of the “Comptes Rendus Hebdomadaires des Séances de l’Académie des Sciences”, which cover respectively the six-month periods January–June 1871 and July–December 1871, there are several contributions of Boussinesq. On June 19, 1871, Boussinesq presents the now famous note on the solitary wave entitled “Théorie de l’intumescence liquide appelée onde solitaire ou de translation, se propageant dans un canal rectangulaire” (**72**, pp. 755–759), which will be extended later in the note entitled “Théorie générale des mouvements qui sont propagés dans un canal rectangulaire horizontal” (**73**, pp. 256–260). Saint-Venant presents a couple of notes of Boussinesq entitled “Sur le mouvement permanent varié de l’eau dans les tuyaux de conduite et dans les canaux découverts” (**73**, pp. 34–38 and pp. 101–105). Saint-Venant himself publishes a couple of notes entitled “Théorie du mouvement non permanent des eaux, avec application aux crues des rivières et à l’introduction des marées dans leur lit” (**73**, pp. 147–154 and pp. 237–240). All these notes deal with shallow-water theory. On November 13, 1871, Boussinesq submits a paper entitled “Théorie des ondes et des remous qui se propagent le long d’un canal rectangulaire horizontal, en communiquant au liquide contenu dans ce canal des vitesses sensiblement pareilles de la surface au fond”, which will be published in 1872 in the *Journal de Mathématiques Pures et Appliquées* (**17**, pp. 55–108).

Articles [Bou71a, Bou72] included dispersive effects for the first time in the Saint-Venant equations [dSV71]. One should mention that Boussinesq’s derivation was restricted to 1+1 dimensions (x and t) and a horizontal bottom. Boussinesq equations contain more physics than the Saint-Venant equations but at the same time they are more complicated from the mathematical and numerical points of views. These equations possess a hyperbolic structure (the same as in the nonlinear shallow-water equations) combined with high-order derivatives to model wave dispersion. There have been a lot of further developments of

these equations like in [Per67, Nwo93, WKGS95, MS98].

Let us outline the physical assumptions. The Boussinesq equations are intended to describe the irrotational motion of an incompressible homogeneous inviscid fluid in the long wave limit. The goal of this type of modelling is to reduce 3D problems to two-dimensional (2D) ones. This is done by assuming a polynomial (usually linear) vertical distribution of the flow field, while taking into account non-hydrostatic effects. This is the principal physical difference with the nonlinear shallow-water (NSW) equations.

There are a lot of forms of the Boussinesq equations. This diversity is due to different possibilities in the choice of the velocity variable. In most cases one chooses the velocity at an arbitrary water level or the depth-averaged velocity vector. The resulting model performance is highly sensitive to linear dispersion properties. The right choice of the velocity variable can significantly improve the propagation of moderately long waves. A good review is given by [Kir03]. There is another technique used by [BCS02]. Formally, one can transform higher-order terms by invoking lower-order asymptotic relations. It provides an elegant way to improve the properties of the linear dispersion relation and it gives a quite general mathematical framework to study these systems.

The main purpose of this work is to include dissipative effects in the Boussinesq equations. It is well-known that the effect of viscosity on free oscillatory waves on deep water was studied by [Lam32]. What is less known is that Boussinesq himself studied this effect as well. Boussinesq wrote three related papers in 1895 in the “Comptes Rendus Hebdomadaires des Séances de l’Académie des Sciences”: (i) “Sur l’extinction graduelle de la houle de mer aux grandes distances de son lieu de production : formation des équations du problème” (120, pp. 1381-1386), (ii) “Lois de l’extinction de la houle en haute mer” (121, pp. 15-20), (iii) “Sur la manière dont se régularise au loin, en s’y réduisant à une houle simple, toute agitation confuse mais périodique des flots” (121, pp. 85-88). It should be pointed out that the famous treatise on hydrodynamics by Lamb has six editions. The paragraphs on wave damping are not present in the first edition (1879) while they are present in the third edition (1906). The authors did not have access to the second edition (1895), so it is possible that Boussinesq and Lamb published similar results at the same time. Indeed Lamb derived the decay rate of the linear wave amplitude in two different ways: in paragraph 348 of the sixth edition by a dissipation calculation (this is also what [Bou95] did) and in paragraph 349 by a direct calculation based on the linearized Navier-Stokes equations. Let α denote the wave amplitude, ν the kinematic viscosity of the fluid and k the wavenumber of the decaying wave. Boussinesq (see Eq. (12) in [Bou95]) and Lamb both showed that

$$\frac{d\alpha}{dt} = -2\nu k^2 \alpha(t). \quad (2.1)$$

Equation (2.1) leads to the classical law for viscous decay of waves of amplitude α , namely

$\alpha \sim \exp(-2\nu k^2 t)$ (see Eq. (13) in [Bou95] after a few calculations).

In the present study, we use two different models for dissipation and derive corresponding systems of long-wave equations. There are several methods to derive the Boussinesq equations but the resulting equations are not the same. So one expects the solutions to be different. We will investigate numerically whether corresponding solutions remain close or not.

One may ask why dissipation is needed in Boussinesq equations. First of all, real world liquids are viscous. This physical effect is “translated” in the language of partial differential equations by dissipative terms (e.g. the Laplacian in the Navier-Stokes equations). So, it is natural to have analogous terms in the long wave limit. In other words, a non-dissipative model means that there is no energy loss, which is not pertinent from a physical point of view, since any flow is accompanied by energy dissipation.

Let us mention an earlier numerical and experimental study by [BPS81]. They pointed out the importance of dissipative effects for accurate long wave modelling. In the “Résumé” section one can read

[...] it was found that the inclusion of a dissipative term was much more important than the inclusion of the nonlinear term, although the inclusion of the nonlinear term was undoubtedly beneficial in describing the observations [...].

The complexity of the mathematical equations due to the inclusion of this term is negligible compared to the benefit of a better physical description.

Let us consider the incompressible Navier-Stokes (N-S) equations for a Newtonian fluid:

$$\begin{aligned}\nabla \cdot \vec{u}^* &= 0, \\ \frac{\partial \vec{u}^*}{\partial t^*} + \vec{u}^* \cdot \nabla \vec{u}^* &= -\frac{\nabla p^*}{\rho} + \nu \Delta \vec{u}^* + \frac{\mathbb{F}^*}{\rho},\end{aligned}$$

where $\vec{u}^*(x, y, z, t) = (u^*, v^*, w^*)(x^*, y^*, z^*, t^*)$ is the fluid velocity vector, p^* the pressure, \mathbb{F}^* the body force vector, ρ the constant fluid density and ν the kinematic viscosity.

Switching to dimensionless variables by introducing a characteristic velocity U , a characteristic length L and a characteristic pressure ρU^2 , neglecting body forces¹ in this discussion, the N-S equations become

$$\begin{aligned}\nabla \cdot \vec{u} &= 0, \\ \frac{\partial \vec{u}}{\partial t} + \vec{u} \cdot \nabla \vec{u} &= -\nabla p + \frac{1}{Re} \Delta \vec{u},\end{aligned}$$

¹The presence or absence of body forces is not important for discussing viscous effects.

where Re is the well-known dimensionless parameter known as the Reynolds number and defined as

$$Re = \frac{F_{inertia}}{F_{viscous}} = \frac{UL}{\nu}.$$

From a physical point of view the Reynolds number is a measure of the relative importance of inertial forces compared to viscous effects. For typical tsunami propagation applications the characteristic particle velocity U is about 5 cm/s and the characteristic wave amplitude, which we use here as characteristic length scale, is about 1 m. The kinematic viscosity ν depends on the temperature but its order of magnitude for water is 10^{-6} m²/s. Considering that as the tsunami approaches the coast both the particle velocity and the wave amplitude increase, one can write that the corresponding Reynolds number is of the order of 10^5 or 10^6 . This simple estimate clearly shows that the flow is turbulent (as many other flows in nature).

It is a common practice in fluid dynamics (addition of an “eddy viscosity” into the governing equations for Large Eddy Simulations) to ignore the small-scale vortices when one is only interested in large-scale motion. It can significantly simplify computational and modelling aspects. So the inclusion of dissipation can be viewed as the simplest way to take into account the turbulence.

There are several authors [Tuc74, LH92, SVBM02, SKP96, DDZ07, RFF91] who included dissipation due to viscosity in potential flow solutions and there are also authors [KCKD00, Zel91, HH70] who already included in Boussinesq models ad-hoc dissipative terms into momentum conservation equations in order to model wave breaking. Modelling this effect is not the primary goal of the present work, since the flow is no longer irrotational after wave breaking. Strictly speaking the Boussinesq equations can no longer be valid at this stage. Nevertheless scientists and engineers continue to use these equations even to model the run-up on the beach. In our approach a suitable choice of the eddy viscosity, which is a function of both space and time, can model wave breaking at least as well as in the articles cited above.

2.2 Derivation of the Boussinesq equations

In order to derive the Boussinesq equations, we begin with the full water-wave problem. A Cartesian coordinate system (x', y', z') is used, with the x' - and y' -axis along the still water level and the z' - axis pointing vertically upwards. Let Ω_t be the fluid domain in \mathbb{R}^3 which is occupied by an inviscid and incompressible fluid. The subscript t underlines the fact that the domain varies with time and is not known a priori. The domain Ω_t is bounded below by the seabed $z' = -h'(x', y', t')$ and above by the free surface $z' = \eta'(x', y', t')$. In this section we choose the domain Ω_t to be unbounded in the horizontal directions in order

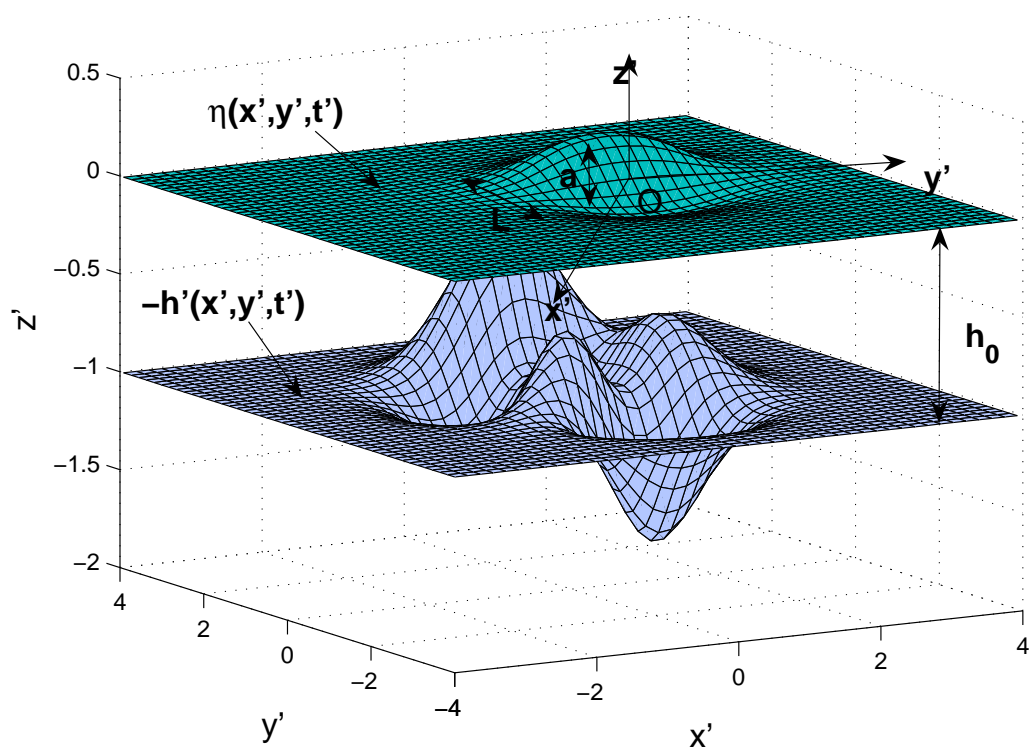


Figure 2.1: Sketch of the fluid domain

to avoid the discussion on lateral boundary conditions. The reason is twofold. First of all, the choice of the boundary value problem (BVP) (e.g. generating and/or absorbing boundary, wall, run-up on a beach) depends on the application under consideration and secondly, the question of the well-posedness of the BVP for the Boussinesq equations is essentially open. Primes stand for dimensional variables. A typical sketch of the domain Ω_t is given in Figure 2.1. If the flow is assumed to be irrotational one can introduce the velocity potential ϕ' defined by

$$\vec{u}' = \nabla' \phi', \quad \nabla' := \left(\frac{\partial}{\partial x'}, \frac{\partial}{\partial y'}, \frac{\partial}{\partial z'} \right)^T,$$

where \vec{u}' denotes the velocity field. Then we write down the following system of equations for potential flow theory in the presence of a free surface:

$$\begin{aligned} \Delta' \phi' &= 0, & (x', y', z') \in \Omega_t &= \mathbb{R}^2 \times [-h', \eta'], \\ \phi'_{z'} &= \eta'_{t'} + \nabla' \phi' \cdot \nabla' \eta', & z' &= \eta', \\ \phi'_{t'} + \frac{1}{2} |\nabla' \phi'|^2 + g\eta' &= 0, & z' &= \eta', \\ \phi'_{z'} + h'_{t'} + \nabla' \phi' \cdot \nabla' h' &= 0, & z' &= -h', \end{aligned} \tag{2.2}$$

where g denotes the acceleration due to gravity (surface tension effects are usually neglected for long-wave applications). It has been assumed implicitly that the free surface is a graph and that the pressure is constant on the free surface (no forcing). Moreover we assume that the total water depth remains positive, i.e. $\eta' + h' > 0$ (there is no dry zone).

As written, this system of equations does not contain any dissipation. Thus, we complete the free-surface dynamic boundary condition (2.2) by adding a dissipative term to account for the viscous effects²:

$$\phi'_{t'} + \frac{1}{2} |\nabla' \phi'|^2 + g\eta' + D'_{\phi'} = 0, \quad z' = \eta'.$$

In this work we investigate two models for the dissipative term $D'_{\phi'}$. For simplicity, one can choose a constant dissipation model (referred hereafter as Model I) which is often used (e.g. [JT^{PS}96]):

$$\text{Model I:} \quad D'_{\phi'} := \delta_1 \phi'. \tag{2.3}$$

There is a more physically realistic dissipation model which is obtained upon balancing of normal stress on the free surface (e.g. [RFF91, ZV97, DDZ07]):

$$\text{Model II:} \quad D'_{\phi'} := \delta_2 \phi'_{z'z'}. \tag{2.4}$$

²[DDZ07] pointed out that a viscous correction should also be added to the kinematic boundary condition if one takes into account the vortical component of the velocity. This correction will be added in future work.

The derivation of Boussinesq equations is more transparent when one works with scaled variables. Let us introduce the following independent and dependent non-dimensional variables:

$$x = \frac{x'}{\ell}, \quad y = \frac{y'}{\ell}, \quad z = \frac{z'}{h_0}, \quad t = \frac{\sqrt{gh_0}}{\ell} t',$$

$$h = \frac{h'}{h_0}, \quad \eta = \frac{\eta'}{a_0}, \quad \phi = \frac{\sqrt{gh_0}}{ga_0\ell} \phi',$$

where h_0 , ℓ and a_0 denote a characteristic water depth, wavelength and wave amplitude, respectively.

After this change of variables, the set of equations becomes

$$\mu^2(\phi_{xx} + \phi_{yy}) + \phi_{zz} = 0, \quad (x, y, z) \in \Omega_t, \quad (2.5)$$

$$\phi_z = \mu^2 \eta_t + \varepsilon \mu^2 \nabla \phi \cdot \nabla \eta, \quad z = \varepsilon \eta, \quad (2.6)$$

$$\mu^2 \phi_t + \frac{1}{2} \varepsilon \mu^2 |\nabla \phi|^2 + \frac{1}{2} \varepsilon \phi_z^2 + \mu^2 \eta + \varepsilon D_\phi = 0, \quad z = \varepsilon \eta \quad (2.7)$$

$$\phi_z + \frac{\mu^2}{\varepsilon} h_t + \varepsilon \mu^2 \nabla \phi \cdot \nabla h = 0, \quad z = -h, \quad (2.8)$$

where ε and μ are the classical nonlinearity and frequency dispersion parameters defined by

$$\varepsilon := \frac{a_0}{h_0}, \quad \mu := \frac{h_0}{\ell}. \quad (2.9)$$

In these equations and hereafter the symbol ∇ denotes the horizontal gradient:

$$\nabla := \left(\frac{\partial}{\partial x}, \frac{\partial}{\partial y} \right)^T.$$

The dissipative term D_ϕ is given by the chosen model (2.3) or (2.4):

$$\text{Model I: } D_\phi = \frac{1}{R_1} \phi, \quad \text{Model II: } D_\phi = \frac{1}{R_2} \phi_{zz},$$

where the following dimensionless numbers have been introduced:

$$R_1 := \frac{1}{\delta_1} \left(\frac{ga_0\ell}{h_0^2 \sqrt{gh_0}} \right), \quad R_2 := \frac{1}{\delta_2} \left(\frac{ga_0\ell}{\sqrt{gh_0}} \right).$$

From this dimensional analysis, one can conclude that the dimension of the coefficient δ_1 is $[s^{-1}]$ and that of δ_2 is $[m^2 s^{-1}]$. Thus, it is natural to call the first coefficient viscous frequency (since it has the dimensions of a frequency) and the second one kinematic viscosity (by analogy with the N-S equations).

<i>parameter</i>	<i>value</i>
Acceleration due to gravity g , m/s ²	10
Amplitude a_0 , m	1
Wave length ℓ , km	100
Water depth h_0 , km	4
Kinematic viscosity δ , m ² /s	10^{-6}

Table 2.1: Typical values of characteristic parameters in tsunami applications

It is interesting to estimate R_2 , since we know how to relate the value of δ_2 to the kinematic viscosity of water. Typical parameters which are used in tsunami wave modelling are given in Table 2.1. For these parameters $R_2 = 5 \times 10^9$ and $\mu^2 = 1.6 \times 10^{-3}$. The ratio between inertial forces and viscous forces is $\frac{1}{2}\varepsilon\mu^2|\nabla\phi|^2/\varepsilon|D_\phi|$. Its order of magnitude is μ^2R_2 , that is 8×10^6 . It clearly shows that the flow is turbulent and eddy-viscosity type approaches should be used. It means that, at zeroth-order approximation, the main effect of turbulence is energy dissipation. Thus, one needs to increase the importance of viscous terms in the governing equations in order to account for turbulent dissipation.

As an example, we refer one more time to the work by [BPS81]. They modeled long wave propagation by using a modified dissipative Korteweg–de Vries equation:

$$\eta_t + \eta_x + \frac{3}{2}\eta\eta_x - \mu\eta_{xx} - \frac{1}{6}\eta_{xxt} = 0. \quad (2.10)$$

In numerical computations the authors took the coefficient $\mu = 0.014$. This value gave good agreement with laboratory data.

From now on, we will use the notation $\nu_i := 1/R_i$. This will allow us to unify the physical origin of the numbers R_i with the eddy-viscosity approach. In other words, for the sake of convenience, we will “forget” about the origin of these coefficients, because their values can be given by other physical considerations.

2.2.1 Asymptotic expansion

Consider a formal asymptotic expansion of the velocity potential ϕ in powers of the small parameter μ^2 :

$$\phi = \phi_0 + \mu^2\phi_1 + \mu^4\phi_2 + \dots \quad (2.11)$$

Then substitute this expansion into the continuity equation (2.5) and the boundary conditions. After substitution, the Laplace equation becomes

$$\mu^2(\nabla^2\phi_0 + \mu^2\nabla^2\phi_1 + \mu^4\nabla^2\phi_2 + \dots) + \phi_{0zz} + \mu^2\phi_{1zz} + \mu^4\phi_{2zz} + \dots = 0.$$

Collecting the same order terms yields the following equations in the domain Ω_t :

$$\mu^0 : \quad \phi_{0zz} = 0, \quad (2.12)$$

$$\mu^2 : \quad \phi_{1zz} + \nabla^2 \phi_0 = 0, \quad (2.13)$$

$$\mu^4 : \quad \phi_{2zz} + \nabla^2 \phi_1 = 0. \quad (2.14)$$

Performing the same computation for the bottom boundary condition yields the following relations at $z = -h$:

$$\mu^0 : \quad \phi_{0z} = 0, \quad (2.15)$$

$$\mu^2 : \quad \phi_{1z} + \frac{1}{\varepsilon} h_t + \nabla \phi_0 \cdot \nabla h = 0, \quad (2.16)$$

$$\mu^4 : \quad \phi_{2z} + \nabla \phi_1 \cdot \nabla h = 0. \quad (2.17)$$

From equation (2.12) and the boundary condition (2.15) one immediately concludes that

$$\phi_0 = \phi_0(x, y, t).$$

Let us define the horizontal velocity vector

$$\vec{u}(x, y, t) := \nabla \phi_0, \quad \vec{u} = (u, v)^T.$$

The expansion of Laplace equation in powers of μ^2 gives recurrence relations between ϕ_0, ϕ_1, ϕ_2 , etc. Using (2.13) one can express ϕ_1 in terms of the derivatives of ϕ_0 :

$$\phi_{1zz} = -\nabla \cdot \vec{u}.$$

Integrating once with respect to z yields

$$\phi_{1z} = -z \nabla \cdot \vec{u} + C_1(x, y, t).$$

The unknown function $C_1(x, y, t)$ can be found by using condition (2.16):

$$\phi_{1z} = -(z + h) \nabla \cdot \vec{u} - \frac{1}{\varepsilon} h_t - \vec{u} \cdot \nabla h,$$

and integrating one more time with respect to z gives the expression for ϕ_1 :

$$\phi_1 = -\frac{1}{2}(z + h)^2 \nabla \cdot \vec{u} - z \left(\frac{1}{\varepsilon} h_t + \vec{u} \cdot \nabla h \right). \quad (2.18)$$

Now we will determine ϕ_2 . For this purpose we use equation (2.14):

$$\begin{aligned} \phi_{2zz} = & \frac{1}{2}(z + h)^2 \nabla^2 (\nabla \cdot \vec{u}) + ((h + z) \nabla^2 h + |\nabla h|^2) \nabla \cdot \vec{u} + \\ & + 2(h + z) \nabla h \cdot \nabla (\nabla \cdot \vec{u}) + z \left(\frac{1}{\varepsilon} \nabla^2 h_t + \nabla^2 (\vec{u} \cdot \nabla h) \right). \end{aligned} \quad (2.19)$$

Integrating twice with respect to z and using the bottom boundary condition (2.17) yields the following expression for ϕ_2 :

$$\begin{aligned} \phi_2 = & \frac{1}{24}(h+z)^4 \nabla^2(\nabla \cdot \vec{u}) + \left(\frac{1}{6}(z+h)^3 \nabla^2 h + \frac{1}{2}z^2 |\nabla h|^2 \right) \nabla \cdot \vec{u} \\ & + \frac{1}{3}(z+h)^3 \nabla h \cdot \nabla(\nabla \cdot \vec{u}) + \frac{z^3}{6} \left(\frac{1}{\varepsilon} \nabla^2 h_t + \nabla^2(\vec{u} \cdot \nabla h) \right) \\ & - zh \left(\frac{h}{2} \nabla^2 \left(\frac{1}{\varepsilon} h_t + \vec{u} \cdot \nabla h \right) + \nabla h \cdot \nabla \left(\frac{1}{\varepsilon} h_t + \vec{u} \cdot \nabla h \right) - |\nabla h|^2 \nabla \cdot \vec{u} \right). \end{aligned} \quad (2.20)$$

Remark 2 *In these equations one finds the term $(1/\varepsilon)h_t$ due to the moving bathymetry. We would like to emphasize that this term is $O(1)$, since in problems of wave generation by a moving bottom the bathymetry $h(x, y, t)$ has the following special form in dimensionless variables:*

$$h(x, y, t) := h_0(x, y) - \varepsilon \zeta(x, y, t), \quad (2.21)$$

where $h_0(x, y)$ is the static seabed and $\zeta(x, y, t)$ is the dynamic component due to a seismic event or a landslide (see for example [DD07c] for a practical algorithm constructing $\zeta(x, y, t)$ in the absence of a dynamic source model). The amplitude of the bottom motion has to be of the same order of magnitude as the resulting waves, since we assume the fluid to be inviscid and incompressible. Thus $(1/\varepsilon)h_t = -\zeta_t = O(1)$.

In the present study we restrict our attention to dispersion terms up to order $O(\mu^2)$. We will also assume that the Ursell-Stokes number [Urs53] is $O(1)$:

$$S := \frac{\varepsilon}{\mu^2} = O(1).$$

This assumption implies that terms of order $O(\varepsilon^2)$ and $O(\varepsilon\mu^2)$ must be neglected, since

$$\varepsilon^2 = S^2 \mu^4 = O(\mu^4), \quad \varepsilon\mu^2 = S\mu^4 = O(\mu^4).$$

Of course, it is possible to obtain high-order Boussinesq equations. We decided not to take this research direction. For high-order asymptotic expansions we refer to [WKGS95, MS98]. Recently, [Ben06] performed a comparative study between fully-nonlinear equations [WKGS95] and Boussinesq equations with optimized dispersion relation [Nwo93]. No substantial difference was revealed.

Now, we are ready to derive dissipative Boussinesq equations in their simplest form. First of all, we substitute the asymptotic expansion (2.11) into the kinematic free-surface boundary condition (2.6):

$$\phi_{0z} + \mu^2 \phi_{1z} + \mu^4 \phi_{2z} = \mu^2 \eta_t + \varepsilon \mu^2 \nabla \phi_0 \cdot \nabla \eta + O(\varepsilon^2 + \varepsilon \mu^4 + \mu^6), \quad z = \varepsilon \eta. \quad (2.22)$$

The first term on the left hand side is equal to zero because of Eq. (2.15).

Using expressions (2.18) and (2.20) one can evaluate ϕ_{1z} and ϕ_{2z} on the free surface:

$$\phi_{1z}|_{z=\varepsilon\eta} = -(h + \varepsilon\eta)\nabla \cdot \vec{u} - \frac{1}{\varepsilon}h_t - \vec{u} \cdot \nabla h,$$

$$\begin{aligned} \phi_{2z}|_{z=\varepsilon\eta} = & \frac{h^3}{6}\nabla^2(\nabla \cdot \vec{u}) + h^2\nabla h \cdot \nabla(\nabla \cdot \vec{u}) + h\left(\frac{h}{2}\nabla^2 h + |\nabla h|^2\right)\nabla \cdot \vec{u} \\ & - \frac{h^2}{2}\frac{1}{\varepsilon}\nabla^2 h_t - h\frac{1}{\varepsilon}\nabla h_t \cdot \nabla h + O(\varepsilon). \end{aligned}$$

Substituting these expressions into (2.22) and retaining only terms of order $O(\varepsilon + \mu^2)$ yields the free-surface elevation equation:

$$\begin{aligned} \eta_t + \nabla \cdot ((h + \varepsilon\eta)\vec{u}) = & -\left(1 + \frac{\mu^2}{2}h^2\nabla^2 + \mu^2 h \nabla h \cdot \nabla\right)\frac{1}{\varepsilon}h_t + \mu^2\frac{h^3}{6}\nabla^2(\nabla \cdot \vec{u}) \\ & + \mu^2 h \left(h\nabla h \cdot \nabla(\nabla \cdot \vec{u}) + \left(\frac{h}{2}\nabla^2 h + |\nabla h|^2\right)\nabla \cdot \vec{u}\right). \end{aligned}$$

The equation for the evolution of the velocity field is derived similarly from the dynamic boundary condition (2.7). This derivation will depend on the selected dissipation model. For both models one has to evaluate ϕ_1 , ϕ_{1t} and ϕ_{1zz} along the free surface $z = \varepsilon\eta$ and then substitute the expressions into the asymptotic form of (2.7):

$$\mu^2\phi_{0t} + \mu^4\phi_{1t} + \frac{1}{2}\varepsilon\mu^2|\nabla\phi_0|^2 + \mu^2\eta + \varepsilon\nu_2\mu^2\phi_{1zz} = O(\varepsilon^2 + \varepsilon\mu^4 + \mu^6),$$

where, as an example, dissipative terms are given according to the second model. After performing all these operations one can write down the following equations:

$$\text{Model I: } \phi_{0t} + \frac{\varepsilon}{2}\vec{u}^2 + \eta + \nu_1\frac{\varepsilon}{\mu^2}\phi_0 - \frac{\nu_1\varepsilon}{2}h^2\nabla \cdot \vec{u} - \frac{\mu^2}{2}h^2\nabla \cdot \vec{u}_t = 0,$$

$$\text{Model II: } \phi_{0t} + \frac{\varepsilon}{2}\vec{u}^2 + \eta - \nu_2\varepsilon\nabla \cdot \vec{u} - \frac{\mu^2}{2}h^2\nabla \cdot \vec{u}_t = 0.$$

The last step consists in differentiating the above equations with respect to the horizontal coordinates in order to obtain equations for the evolution of the velocity. We also perform some minor transformations using the fact that the vector \vec{u} is a gradient by definition, so we have the obvious relation

$$\frac{\partial u}{\partial y} = \frac{\partial v}{\partial x}.$$

The resulting Boussinesq equations for the first and second dissipation models, respectively, are given below:

$$\eta_t + \nabla \cdot ((h + \varepsilon\eta)\vec{u}) = -\left(1 + \frac{\mu^2}{2}h^2\nabla^2 + \mu^2 h \nabla h \cdot \nabla\right)\frac{1}{\varepsilon}h_t + \mu^2\frac{h^3}{6}\nabla^2(\nabla \cdot \vec{u})$$

$$+ \mu^2 h \left(h \nabla h \cdot \nabla (\nabla \cdot \vec{u}) + \left(\frac{h}{2} \nabla^2 h + |\nabla h|^2 \right) \nabla \cdot \vec{u} \right), \quad (2.23)$$

$$\text{Model I: } \vec{u}_t + \frac{1}{2} \varepsilon \nabla \vec{u}^2 + \nabla \eta + \nu_1 S \vec{u} = \frac{1}{2} \varepsilon \nu_1 \nabla (h^2 \nabla \cdot \vec{u}) + \frac{1}{2} \mu^2 \nabla (h^2 \nabla \cdot \vec{u}_t), \quad (2.24)$$

$$\text{Model II: } \vec{u}_t + \frac{1}{2} \varepsilon \nabla \vec{u}^2 + \nabla \eta = \varepsilon \nu_2 \nabla^2 \vec{u} + \frac{1}{2} \mu^2 \nabla (h^2 \nabla \cdot \vec{u}_t). \quad (2.25)$$

2.3 Analysis of the linear dispersion relations

For simplicity, we will consider in this section only 2D problems. The generalization to 3D problems is straightforward and does not change the analysis.

2.3.1 Linearization of the full potential flow equations with dissipation

First we write down the linearization of the full potential flow equations in dimensional form, after dropping the primes:

$$\Delta \phi = 0, \quad (x, z) \in \mathbb{R} \times [-h, 0], \quad (2.26)$$

$$\phi_z = \eta_t, \quad z = 0, \quad (2.27)$$

$$\phi_t + g\eta + D_\phi = 0, \quad z = 0, \quad (2.28)$$

$$\phi_z = 0, \quad z = -h. \quad (2.29)$$

Remark 3 *In this section the water layer is assumed to be of uniform depth, so $h = \text{const}$.*

As above the term D_ϕ depends on the selected dissipation model and is equal to $\delta_1 \phi$ or $\delta_2 \phi_{zz}$. The next step consists in choosing a special form of solutions:

$$\phi(x, z, t) = \varphi_0 e^{i(kx - \omega t)} \varphi(z), \quad \eta(x, t) = \eta_0 e^{i(kx - \omega t)}, \quad (2.30)$$

where φ_0 and η_0 are constants. Substituting this form of solutions into equations (2.26), (2.27) and (2.29) yields the following boundary value problem for an ordinary differential equation:

$$\varphi''(z) - k^2 \varphi(z) = 0, \quad z \in [-h, 0],$$

$$\varphi'(0) = \frac{\eta_0}{\varphi_0} (-i\omega), \quad \varphi'(-h) = 0.$$

Straightforward computations give the solution to this problem:

$$\varphi(z) = -i \frac{\eta_0}{\varphi_0} \left(\frac{e^{k(2h+z)} + e^{-kz}}{e^{2kh} - 1} \right) \frac{\omega}{k}.$$

The dispersion relation can be thought as a necessary condition for solutions of the form (2.30) to exist. The problem is that ω and k cannot be arbitrary. We obtain the required relation $\omega = \omega(k)$, which is called the dispersion relation, after substituting this solution into (2.28).

When the dissipative term is chosen according to model I (2.3), $D_\phi = \delta_1 \phi$ and the dispersion relation is given implicitly by

$$\omega^2 + i\delta_1 \omega - gk \tanh(kh) = 0,$$

or in explicit form by

$$\omega = \pm \sqrt{gk \tanh(kh) - \frac{\delta_1^2}{4}} - \frac{i\delta_1}{2}. \quad (2.31)$$

For the second dissipation model (2.4) one obtains the following relation:

$$\omega^2 + i\delta_2 \omega k^2 - gk \tanh(kh) = 0.$$

One can easily solve this quadratic equation for ω as a function of k :

$$\omega = \pm \sqrt{gk \tanh(kh) - \left(\frac{\delta_2 k^2}{2}\right)^2} - \frac{i\delta_2}{2} k^2. \quad (2.32)$$

If $\delta_{1,2} \equiv 0$ one easily recognizes the dispersion relation of the classical water-wave problem:

$$\omega = \pm \sqrt{gk \tanh(kh)}. \quad (2.33)$$

Remark 4 *It is important to have the property $\text{Im} \omega(k) \leq 0, \forall k$ in order to avoid the exponential growth of certain wavelengths, since*

$$e^{i(kx - \omega(k)t)} = e^{\text{Im} \omega(k)t} \cdot e^{i(kx - \text{Re} \omega(k)t)}.$$

For our analysis it is more interesting to look at the phase speed which is defined as

$$c_p(k) := \frac{\omega(k)}{k}.$$

The phase velocity is directly connected to the speed of wave propagation and is extremely important for accurate tsunami modelling since tsunami arrival time obviously depends on the propagation speed. The expressions for the phase velocity are obtained from the corresponding dispersion relations (2.31) and (2.32):

$$c_p^{(1)}(k) = \pm \sqrt{gh \frac{\tanh(kh)}{kh} - \left(\frac{\delta_1}{2k}\right)^2} - \frac{i\delta_1}{2k}, \quad (2.34)$$

$$c_p^{(2)}(k) = \pm \sqrt{gh \frac{\tanh(kh)}{kh} - \left(\frac{\delta_2 k}{2}\right)^2} - \frac{i\delta_2}{2} k. \quad (2.35)$$

It can be shown that in order to keep the phase velocity unchanged by the addition of dissipation, similar dissipative terms must be included in both the kinematic and the dynamic boundary conditions [DDZ07].

2.3.2 Dissipative Boussinesq equations

The analysis of the dispersion relation is even more straightforward for Boussinesq equations. In order to be coherent with the previous subsection, we switch to dimensional variables. As usual we begin with the (1 + 1)D linearized equations:

$$\eta_t + hu_x = \frac{h^3}{6}u_{xxx},$$

$$\text{Model I: } u_t + g\eta_x + \delta_1 u = \frac{1}{2}\delta_1 h^2 u_{xx} + \frac{1}{2}h^2 u_{xxt},$$

$$\text{Model II: } u_t + g\eta_x = \delta_2 u_{xx} + \frac{1}{2}h^2 u_{xxt}.$$

Now we substitute a special ansatz in these equations:

$$\eta = \eta_0 e^{i(kx - \omega t)}, \quad u = u_0 e^{i(kx - \omega t)},$$

where η_0 and u_0 are constants. In the case of the first model, one obtains the following homogeneous system of linear equations:

$$\begin{aligned} (-i\omega)\eta_0 + ikh \left(1 + \frac{1}{6}(kh)^2\right) u_0 &= 0, \\ gik\eta_0 + \left(-i\omega + \delta_1 + \frac{\delta_1}{2}(kh)^2 - \frac{i\omega}{2}(kh)^2\right) u_0 &= 0. \end{aligned}$$

This system admits nontrivial solutions if its determinant is equal to zero. It gives the required dispersion relation:

$$\omega^2 + i\omega\delta_1 - ghk^2 \left(\frac{1 + \frac{1}{6}(kh)^2}{1 + \frac{1}{2}(kh)^2}\right) = 0.$$

A similar relation is found for the second model:

$$\omega^2 + \frac{i\omega\delta_2}{1 + \frac{1}{2}(kh)^2} k^2 - ghk^2 \left(\frac{1 + \frac{1}{6}(kh)^2}{1 + \frac{1}{2}(kh)^2}\right) = 0.$$

The corresponding phase velocities are given by

$$c_{pb}^{(1)} = \sqrt{gh \left(\frac{1 + \frac{1}{6}(kh)^2}{1 + \frac{1}{2}(kh)^2}\right) - \left(\frac{\delta_1}{2k}\right)^2} - \frac{i\delta_1}{2k}, \quad (2.36)$$

$$c_{pb}^{(2)} = \sqrt{gh \left(\frac{1 + \frac{1}{6}(kh)^2}{1 + \frac{1}{2}(kh)^2}\right) - \left(\frac{\delta_2 k}{2 + (kh)^2}\right)^2} - \frac{i\delta_2 k}{2 + (kh)^2}. \quad (2.37)$$

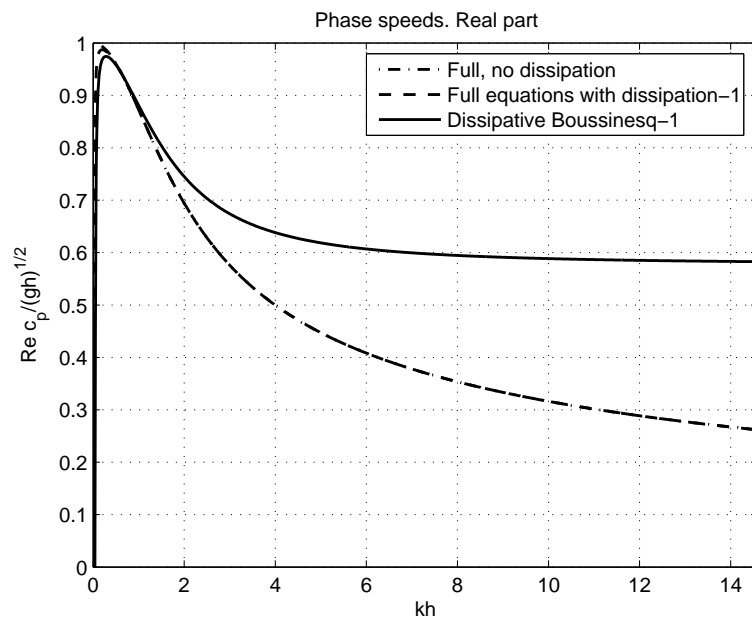


Figure 2.2: Dissipation model I. Real part of the phase velocity.

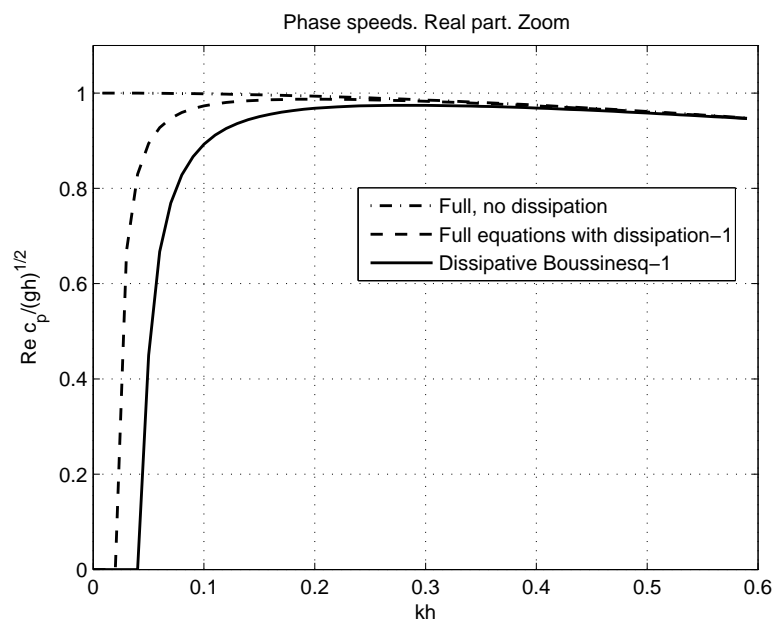


Figure 2.3: Dissipation model I. Same as Figure 2.2 with a zoom on long waves.

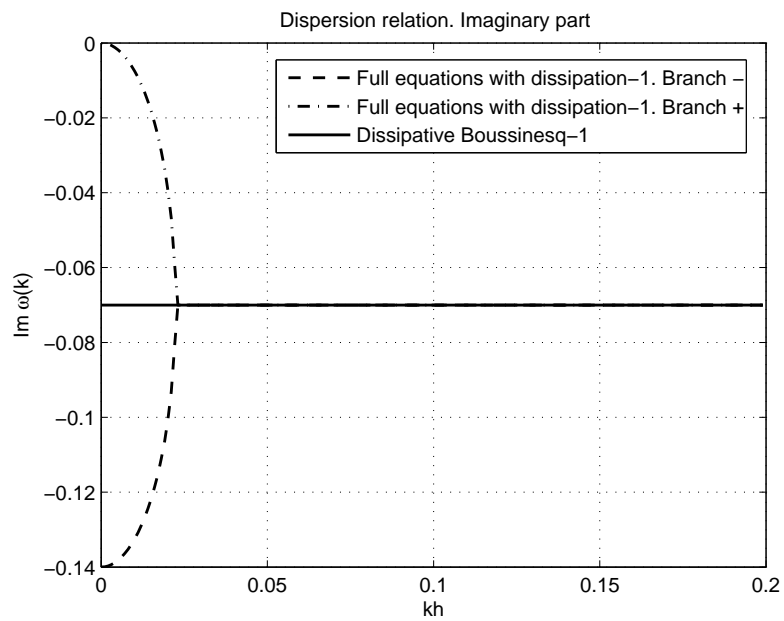


Figure 2.4: Dissipation model I. Imaginary part of the frequency.

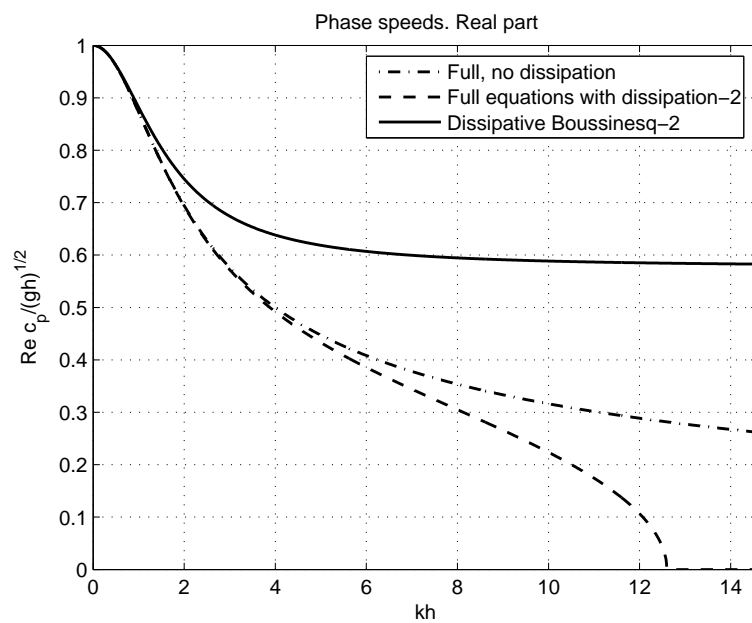


Figure 2.5: Dissipation model II. Real part of the phase velocity.

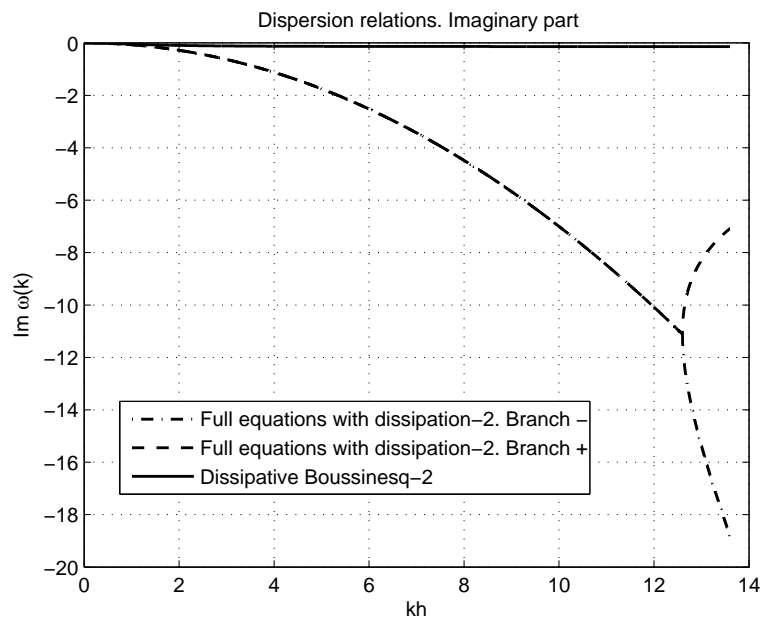


Figure 2.6: Dissipation model II. Imaginary part of the frequency.

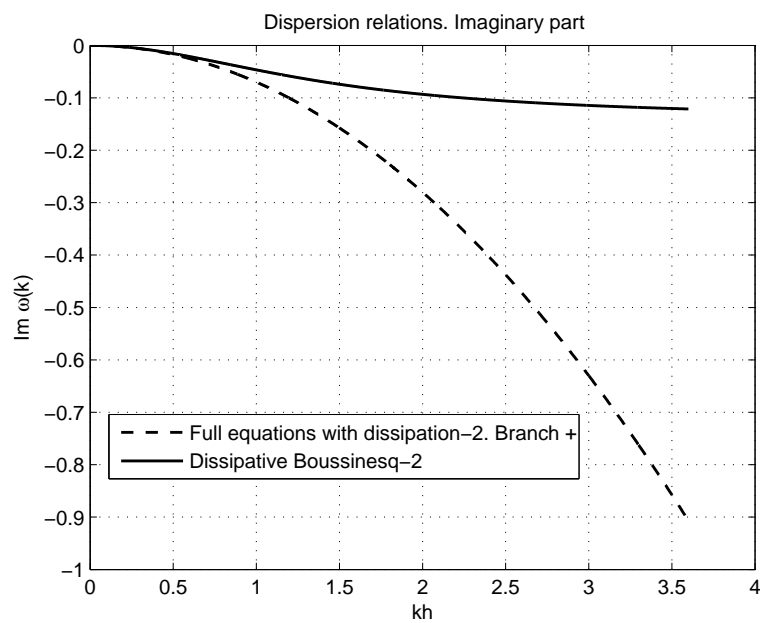


Figure 2.7: Dissipation model II. Same as Figure 2.6 with a zoom on long waves.

2.3.3 Discussion

Let us now provide a discussion on the dispersion relations. The real and imaginary parts of the phase velocities (2.34) – (2.37) for the full and long wave linearized equations are shown graphically on Figures 2.2 – 2.7. In this example the parameters are given by $\delta_1 = 0.14, \delta_2 = 0.14$. Together with the dissipative models we also plotted for comparison the well-known phase velocity corresponding to the full conservative (linearized) water-wave problem:

$$c_p(k) = \sqrt{gh \frac{\tanh(kh)}{kh}}.$$

First of all, one can see that dissipation is very selective, as is often the case in physics. Clearly, the first dissipation model prefers very long waves, while the second model dissipates essentially short waves. Moreover one can see from the expressions (2.34), (2.36) that the phase velocity has a $1/k$ singular behaviour in the vicinity of $kh = 0$ (in the long wave limit). Furthermore, it can be clearly seen in Figure 2.3 that very long linear waves are not advected in the first dissipation model, since the real part of their phase velocity is identically equal to zero.

That is why we suggest to make use of the second model in applications involving very long waves such as tsunamis.

On the other hand we would like to point out that the second model admits a critical wavenumber k_c such that the phase velocity (2.35) becomes purely imaginary with negative imaginary part. From a physical point of view it means that the waves shorter than k_c are not advected, but only dissipated. When one switches to the Boussinesq approximation, this property disappears for physically realistic values of the parameters g, h and δ_2 (see Table 2.1).

Let us clarify this situation. The qualitative behaviour of the phase velocity $c_{pb}^{(2)}$ (see equation (2.37)) depends on the roots of the following polynomial equation:

$$(kh)^4 + \left(8 - \frac{3\delta_2^2}{gh^3}\right) (kh)^2 + 12 = 0.$$

This equation does not have real roots since $\frac{3\delta_2^2}{gh^3} \ll 1$.

2.4 Alternative version of the Boussinesq equations

In this section we give an alternative derivation of Boussinesq equations. We use another classical method for deriving Boussinesq-type equations [Whi99, Ben74, Per72], which provides slightly different governing equations. Namely, the hyperbolic structure is the

same, but the dispersive terms differ. In numerical simulations we suggest to use this system of equations.

The derivation follows closely the paper by [MS98]. The main differences are that we neglect the terms of order $O(\mu^4)$, take into account a moving bathymetry and, of course, dissipative effects which are modelled this time according to model II (2.4) because, in our opinion, this model is more appropriate for long wave applications. Anyhow, the derivation process can be performed in a similar fashion for model I (2.3).

2.4.1 Derivation of the equations

The starting point is the same: equations (2.5), (2.6), (2.7) and (2.8). This time the procedure begins with representing the velocity potential $\phi(x, y, z, t)$ as a formal expansion in powers of z rather than of μ^2 :

$$\phi(x, y, z, t) = \sum_{n=0}^{\infty} z^n \phi_n(x, y, t). \quad (2.38)$$

We would like to emphasize that this expansion is only formal and no convergence result is needed. In other words, it is just convenient to use this notation in asymptotic expansions but in practice, seldom more than four terms are used. It is not necessary to justify the convergence of the sum with three or four terms.

When we substitute the expansion (2.38) into Laplace equation (2.5), we have an infinite polynomial in z . Requiring that ϕ formally satisfies Laplace equation implies that the coefficients of each power of z vanish (since the right-hand side is identically zero). This leads to the classical recurrence relation

$$\phi_{n+2}(x, y, t) = -\frac{\mu^2}{(n+1)(n+2)} \nabla^2 \phi_n(x, y, t), \quad n = 0, 1, 2, \dots$$

Using this relation one can eliminate all but two unknown functions in (2.38):

$$\phi(x, y, z, t) = \sum_{n=0}^{\infty} (-1)^n \mu^{2n} \left(\frac{z^{2n}}{(2n)!} \nabla^{2n} \phi_0 + \frac{z^{2n+1}}{(2n+1)!} \nabla^{2n} \phi_1 \right).$$

The following notation is introduced:

$$\vec{u}_0 := \vec{u}(x, y, 0, t), \quad w_0 := \frac{1}{\mu^2} w(x, y, 0, t).$$

It is straightforward to find the relations between \vec{u}_0 , w_0 and ϕ_0 , ϕ_1 if one remembers that $(\vec{u}, w) = (\nabla, \frac{\partial}{\partial z})\phi$:

$$\vec{u}_0 = \nabla \phi_0, \quad w_0 = \frac{1}{\mu^2} \phi_1.$$

Using the definition of the velocity potential ϕ one can express the velocity field in terms of \vec{u}_0 , w_0 :

$$\vec{u} = \sum_{n=0}^{\infty} (-1)^n \left(\frac{z^{2n}}{(2n)!} \mu^{2n} \nabla (\nabla^{2n-2} (\nabla \cdot \vec{u}_0)) + \frac{z^{2n+1}}{(2n+1)!} \mu^{2n+2} \nabla (\nabla^{2n} w_0) \right),$$

$$w = \sum_{n=0}^{\infty} (-1)^n \left(-\frac{z^{2n+1}}{(2n+1)!} \mu^{2n+2} \nabla^{2n} (\nabla \cdot \vec{u}_0) + \frac{z^{2n}}{(2n)!} \mu^{2n+2} \nabla^{2n} w_0 \right).$$

These formulas are exact but not practical. In the present work we neglect the terms of order $O(\mu^4)$ and higher. In this asymptotic framework the above formulas become much simpler:

$$\phi = \phi_0 + z\phi_1 - \frac{\mu^2 z^2}{2} \left(\nabla^2 \phi_0 + \frac{z}{3} \nabla^2 \phi_1 \right) + O(\mu^4), \quad (2.39)$$

$$\vec{u} = \vec{u}_0 + z\mu^2 \nabla w_0 - \frac{\mu^2 z^2}{2} \nabla (\nabla \cdot \vec{u}_0) + O(\mu^4), \quad (2.40)$$

$$w = \mu^2 w_0 - z\mu^2 \nabla \cdot \vec{u}_0 + O(\mu^4). \quad (2.41)$$

In order to establish the relation between w_0 and \vec{u}_0 one uses the bottom kinematic boundary condition (2.8), which has the following form after substituting the asymptotic expansions (2.39), (2.40), (2.41) in it:

$$\begin{aligned} h_t + \varepsilon \nabla h \cdot \left(\vec{u}_0 - h\mu^2 \nabla w_0 - \frac{\mu^2 h^2}{2} \nabla (\nabla \cdot \vec{u}_0) \right) \\ + \varepsilon \left(w_0 - \frac{h^3}{6} \mu^2 \nabla^2 (\nabla \cdot \vec{u}_0) - \frac{\mu^2 h^2}{2} \nabla^2 w_0 \right) + O(\mu^4) = 0. \end{aligned} \quad (2.42)$$

In order to obtain the expression of w_0 in terms of \vec{u}_0 one introduces one more expansion:

$$w_0(x, y, t) = w_0^{(0)}(x, y, t) + \mu^2 w_0^{(1)}(x, y, t) + \dots \quad (2.43)$$

We insert this expansion into the asymptotic bottom boundary condition (2.42). This leads to the following explicit expressions for $w_0^{(0)}$ and $w_0^{(1)}$:

$$w_0^{(0)} = -\frac{1}{\varepsilon} h_t - \nabla \cdot (h\vec{u}_0),$$

$$\begin{aligned} w_0^{(1)} = \frac{h^2}{2} \left(\nabla h \cdot \nabla (\nabla \cdot \vec{u}_0) + \frac{h}{3} \nabla^2 (\nabla \cdot \vec{u}_0) \right) \\ - h \left(\nabla h \cdot \frac{1}{\varepsilon} \nabla h_t + \nabla h \cdot \nabla (\nabla \cdot (h\vec{u}_0)) + \frac{h}{2} \left(\frac{1}{\varepsilon} \nabla^2 h_t + \nabla^2 (\nabla \cdot (h\vec{u}_0)) \right) \right). \end{aligned}$$

Substituting these expansions into (2.43) and performing some simplifications yields the required relation between \vec{u}_0 and w_0 :

$$w_0 = -\frac{1}{\varepsilon}h_t - \nabla \cdot (h\vec{u}_0) - \mu^2 \nabla \cdot \left(\frac{h^2}{2\varepsilon} \nabla h_t + \frac{h^2}{2} \nabla (\nabla \cdot (h\vec{u}_0)) - \frac{h^3}{6} \nabla (\nabla \cdot \vec{u}_0) \right) + O(\mu^4). \quad (2.44)$$

Now one can eliminate the vertical velocity w_0 since one has its expression (2.44) in terms of \vec{u}_0 . Equations (2.40)-(2.41) become

$$\vec{u} = \vec{u}_0 - z \frac{\mu^2}{\varepsilon} \nabla h_t - \mu^2 \left(z \nabla (\nabla \cdot (h\vec{u}_0)) + \frac{z^2}{2} \nabla (\nabla \cdot \vec{u}_0) \right) + O(\mu^4), \quad (2.45)$$

$$w = -\frac{\mu^2}{\varepsilon} h_t - \mu^2 \left(\nabla \cdot (h\vec{u}_0) + z \nabla \cdot \vec{u}_0 \right) + O(\mu^4). \quad (2.46)$$

In this work we apply a trick due to [Nwo93]. Namely, we introduce a new velocity variable \mathbf{u}_α defined at an arbitrary water level $z_\alpha = -\alpha h$. Technically this change of variables is done as follows. First we evaluate (2.45) at $z = z_\alpha$, which gives the connection between \vec{u}_0 and \mathbf{u}_α :

$$\mathbf{u}_\alpha = \vec{u}_0 - z_\alpha \frac{\mu^2}{\varepsilon} \nabla h_t - \mu^2 \left(z_\alpha \nabla (\nabla \cdot (h\vec{u}_0)) + \frac{z_\alpha^2}{2} \nabla (\nabla \cdot \vec{u}_0) \right) + O(\mu^4).$$

Using the standard techniques of inversion one can rewrite the last expression as an asymptotic formula for \vec{u}_0 in terms of \mathbf{u}_α :

$$\vec{u}_0 = \mathbf{u}_\alpha + z_\alpha \frac{\mu^2}{\varepsilon} h_t + \mu^2 \left(z_\alpha \nabla (\nabla \cdot (h\mathbf{u}_\alpha)) + \frac{z_\alpha^2}{2} \nabla (\nabla \cdot \mathbf{u}_\alpha) \right) + O(\mu^4). \quad (2.47)$$

Remark 5 *Behind this change of variables there is one subtlety which is generally hushed up in the literature. In fact, the wave motion is assumed to be irrotational since we use the potential flow formulation (2.5), (2.6), (2.7), (2.8) of the water-wave problem. By construction $\text{rot}(\vec{u}, w) = \mathcal{O}$ when \vec{u} and w are computed according to (2.45), (2.46) or, in other words, in terms of the variable \vec{u}_0 . When one turns to the velocity variable \mathbf{u}_α defined at an arbitrary level, one can improve the linear dispersion relation and this is important for wave modelling. But on the other hand, one loses the property that the flow is irrotational. That is to say, a direct computation shows that $\text{rot}(\vec{u}, w) \neq \mathcal{O}$ when \vec{u} and w are expressed in terms of the variable \mathbf{u}_α . The purpose of this remark is simply to inform the reader about the price to be paid while improving the dispersion relation properties. It seems that this point is not clearly mentioned in the literature on this topic.*

Let us now derive the Boussinesq equations. There are two different methods to obtain the free-surface elevation equation. The first method consists in integrating the continuity equation (2.5) over the depth and then use the kinematic free-surface and bottom boundary conditions. The second way is more straightforward. It consists in using directly the kinematic free-surface boundary condition (2.6):

$$\eta_t + \varepsilon \nabla \phi \cdot \nabla \eta - \frac{1}{\mu^2} \phi_z = 0.$$

Then one can substitute (2.39) into (2.6) and perform several simplifications. Neglecting all terms of order $O(\varepsilon^2 + \varepsilon\mu^2 + \mu^4)$ yields the following equation³:

$$\begin{aligned} \eta_t + \nabla \cdot ((h + \varepsilon\eta)\vec{u}_0) + \frac{\mu^2}{2} \nabla \cdot \left(h^2 \nabla (\nabla \cdot (h\vec{u}_0)) - \frac{h^3}{3} \nabla (\nabla \cdot \vec{u}_0) \right) = \\ = \zeta_t + \frac{\mu^2}{2} \nabla \cdot (h^2 \nabla \zeta_t). \end{aligned}$$

Recall that $\zeta(x, y, t)$ is defined according to (2.21). When the bathymetry is static, $\zeta \equiv 0$. We prefer to introduce this function in order to eliminate the division by ε in the source terms since this division can give the impression that stiff source terms are present in our problem, which is not the case.

In order to be able to optimize the dispersion relation properties, we switch to the variable \mathbf{u}_α . Technically it is done by using the relation (2.47) between \vec{u}_0 and \mathbf{u}_α . The result is given below:

$$\begin{aligned} \eta_t + \nabla \cdot ((h + \varepsilon\eta)\mathbf{u}_\alpha) + \mu^2 \nabla \cdot \left(h(z_\alpha + \frac{h}{2}) \nabla (\nabla \cdot (h\mathbf{u}_\alpha)) + \frac{h}{2} (z_\alpha^2 - \frac{h^2}{3}) \nabla (\nabla \cdot \mathbf{u}_\alpha) \right) = \\ = \zeta_t + \mu^2 \nabla \cdot \left(h(z_\alpha + \frac{h}{2}) \nabla \zeta_t \right). \quad (2.48) \end{aligned}$$

As above, the equation for the horizontal velocity field is derived from the dynamic free-surface boundary condition (2.7). It is done exactly as in section 2.2 and we do not insist on this point:

$$\vec{u}_{0t} + \frac{\varepsilon}{2} \nabla |\vec{u}_0|^2 + \nabla \eta - \varepsilon \delta \nabla^2 \vec{u}_0 = \mathcal{O}.$$

Switching to the variable \mathbf{u}_α yields the following governing equation:

$$\begin{aligned} \mathbf{u}_{\alpha t} + \frac{\varepsilon}{2} \nabla |\mathbf{u}_\alpha|^2 + \nabla \eta + \mu^2 \left(z_\alpha \nabla (\nabla \cdot (h\mathbf{u}_\alpha)) + \frac{z_\alpha^2}{2} \nabla (\nabla \cdot \mathbf{u}_\alpha) \right)_t = \\ = \varepsilon \delta \Delta \mathbf{u}_\alpha + \mu^2 (z_\alpha \nabla \zeta_t)_t. \quad (2.49) \end{aligned}$$

³We already discussed this point on page 91. In this section we also assume that the Stokes-Ursell number S is of order $O(1)$.

In several numerical methods it can be advantageous to rewrite the system (2.48), (2.49) in vector form:

$$\mathbf{U}_t + \mu^2 \mathcal{L}(\mathbf{U})_t + \nabla \cdot \mathbb{F}(\mathbf{U}) + \mu^2 \nabla \cdot \mathbf{P}(\mathbf{U}) = \mathbf{S}(x, y, t) + \varepsilon \delta \nabla \cdot (\mathbf{D} \nabla \mathbf{U}),$$

where

$$\begin{aligned} \mathbf{U} &:= \begin{pmatrix} \eta \\ u_\alpha \\ v_\alpha \end{pmatrix}, & \nabla \cdot \mathbb{F} &:= \frac{\partial F}{\partial x} + \frac{\partial G}{\partial y}, \\ F &:= \begin{pmatrix} (h + \varepsilon \eta) u_\alpha \\ \frac{\varepsilon}{2} |\mathbf{u}_\alpha|^2 + \eta \\ 0 \end{pmatrix}, & G &:= \begin{pmatrix} (h + \varepsilon \eta) v_\alpha \\ 0 \\ \frac{\varepsilon}{2} |\mathbf{u}_\alpha|^2 + \eta \end{pmatrix}, \\ \mathcal{L} &:= \begin{pmatrix} 0 \\ z_\alpha \nabla (\nabla \cdot (h \mathbf{u}_\alpha)) + \frac{z_\alpha^2}{2} \nabla (\nabla \cdot \mathbf{u}_\alpha) \end{pmatrix}, \\ \mathbf{P} &:= \begin{pmatrix} h(z_\alpha + \frac{h}{2}) \nabla (\nabla \cdot (h \mathbf{u}_\alpha)) + \frac{h}{2} (z_\alpha^2 - \frac{h^2}{3}) \nabla (\nabla \cdot \mathbf{u}_\alpha) \\ \mathcal{O} \end{pmatrix}, \\ \mathbf{S} &:= \begin{pmatrix} \zeta_t + \mu^2 \nabla \cdot (h(z_\alpha + \frac{h}{2}) \nabla \zeta_t) \\ \mu^2 (z_\alpha \nabla \zeta_t)_t \end{pmatrix}, \\ \mathbf{D} &:= \begin{pmatrix} 0 & 0 & 0 \\ 0 & 1 & 0 \\ 0 & 0 & 1 \end{pmatrix}. \end{aligned}$$

2.5 Improvement of the linear dispersion relations

As said above, the idea of using one free parameter $\alpha \in [0, 1]$ to optimize the linear dispersion relation properties appears to have been proposed first by [Nwo93].

The idea of manipulating the dispersion relation was well-known before 1993. See for example [Mur89, MMS91]. But these authors started with a desired dispersion relation and artificially added extra terms to the momentum equation in order to produce the desired characteristics. We prefer to follow the ideas of [Nwo93].

Remark 6 *When one plays with the dispersion relation it is important to remember that the resulting problem must be well-posed, at least linearly. We refer to [BCS02] as a general reference on this topic. Usually Boussinesq-type models with good dispersion characteristics are linearly well-posed as well.*

In order to look for an optimal value of α we will drop dissipative terms. Indeed we want to concentrate our attention on the propagation properties which are more important.

The choice for the parameter α depends on the optimization criterion. In the present work we choose α by comparing the coefficients in the Taylor expansions of the phase velocity in the vicinity of $kh = 0$, which corresponds to the long-wave limit. Another possibility is to match the dispersion relation of the full linearized equations (2.33) in the least square sense. One can also use Padé approximants [Wit84] since rational functions have better approximation properties than polynomials.

We briefly describe the procedure. First of all one has to obtain the phase velocity of the linearized, non-viscous, Boussinesq equations (2.48)-(2.49). The result is

$$\frac{c_b^2(k)}{gh} = \frac{1 - \left(\frac{\alpha^2}{2} - \alpha + \frac{1}{3}\right)(kh)^2}{1 - \alpha\left(\frac{\alpha}{2} - 1\right)(kh)^2} = 1 - \frac{1}{3}(kh)^2 + \frac{\alpha(2 - \alpha)}{6}(kh)^4 + O((kh)^6). \quad (2.50)$$

On the other hand one can write down the phase velocity of the full linearized equations (2.33):

$$\frac{c^2(k)}{gh} = \frac{\tanh(kh)}{kh} = 1 - \frac{1}{3}(kh)^2 + \frac{2}{15}(kh)^4 + O((kh)^6). \quad (2.51)$$

If one insists on the dispersion relation (2.50) to be exact up to order $O((kh)^4)$ one immediately obtains an equation for α_{opt} :

$$\frac{\alpha_{opt}(2 - \alpha_{opt})}{6} = \frac{2}{15} \Rightarrow \alpha_{opt} = 1 - \frac{\sqrt{5}}{5} \approx 0.55.$$

We suggest using this value of α in numerical computations.

2.6 Regularization of Boussinesq equations

In this section we are going to modify further just obtained Boussinesq equations (2.48), (2.49). For simplicity we assume the bottom to be static $h = h(x, y)$ and we drop out viscous terms. This operation will allow us to obtain very « gentle » system of equations from the numerical point of view. The influence of this modification on dispersion relation properties will be discussed below.

The main idea behind is very simple. It was already extensively exploited in [BCS02] and other publications. We are going to use lower order asymptotic relations in order to « play » with dispersive terms. Namely, from (2.48), (2.49) one can deduce two following relations:

$$\begin{aligned} \eta_t &= -\nabla \cdot (h\vec{u}) + \mathcal{O}(\varepsilon + \mu^2), \\ \vec{u}_t &= -\nabla\eta + \mathcal{O}(\varepsilon + \mu^2). \end{aligned} \quad (2.52)$$

In the present work we will only use the relation (2.52). With its help we can modify the first dispersive term in the equation (2.48):

$$\mu^2 \nabla \cdot \left(h \left(z_\alpha + \frac{h}{2} \right) \nabla (\nabla \cdot (h \mathbf{u}_\alpha)) \right) = -\mu^2 \nabla \cdot \left(h \left(z_\alpha + \frac{h}{2} \right) \nabla \eta \right)_t + \mathcal{O}(\varepsilon \mu^2 + \mu^4).$$

Thus, the regularized system of equations reads:

$$\eta_t + \nabla \cdot ((h + \varepsilon \eta) \mathbf{u}_\alpha) - \mu^2 \nabla \cdot \left(h \left(z_\alpha + \frac{h}{2} \right) \nabla \eta \right)_t + \mu^2 \nabla \cdot \left(\frac{h}{2} \left(z_\alpha^2 - \frac{h^2}{3} \right) \nabla (\nabla \cdot \mathbf{u}_\alpha) \right) = 0, \quad (2.53)$$

$$\mathbf{u}_{\alpha t} + \frac{\varepsilon}{2} \nabla |\mathbf{u}_\alpha|^2 + \nabla \eta + \mu^2 \left(z_\alpha \nabla (\nabla \cdot (h \mathbf{u}_\alpha)) + \frac{z_\alpha^2}{2} \nabla (\nabla \cdot \mathbf{u}_\alpha) \right)_t = \vec{0}. \quad (2.54)$$

Just obtained system of equations has the same relation with classical Boussinesq equations [Per67] as KdV equation $u_t + u_x + uu_x + u_{xxx} = 0$ is related to BBM model [BBM72] $u_t + u_x + uu_x - u_{xxt} = 0$. The main purpose of this little modification is to decrease the order of dispersive operator which can be stiff from the numerical point of view:

$$(1 - \partial_{xx})u_t + u_x + uu_x = 0 \rightarrow u_t + (1 - \partial_{xx})^{-1}(u_x + uu_x) = 0.$$

In practice, it can drastically change the CFL condition from $\Delta t = \mathcal{O}(\Delta x^2)$ for KdV (see [Tre00] for example) to $\Delta t = \mathcal{O}(\Delta x)$ for BBM equation (or even unconditionally stable schemes if one considers an equivalent integral representation of solutions [BPS81, BPS85]).

We have to say that this operation does not change the formal order of approximation. Moreover, the experiments show that the regularized equations (such as BBM) completed by dissipative terms seem to be excellent in description of long water waves [BPS81].

The dispersion relation of just obtained equations (2.53), (2.54) is the following:

$$\begin{aligned} \frac{c_r^2(k)}{gh} &:= \frac{1 + \frac{1}{2}(\frac{1}{3} - \alpha^2)}{\left(1 + (\frac{1}{2} - \alpha)(kh)^2\right) \left(1 + \alpha(1 - \frac{\alpha}{2})(kh)^2\right)} = \\ &= 1 - \frac{1}{3}(kh)^2 - \left(\frac{1}{2}\alpha^3 - \frac{13}{12}\alpha^2 + \frac{1}{2}\alpha - \frac{1}{6}\right)(kh)^4 + \mathcal{O}((kh)^6) \end{aligned} \quad (2.55)$$

Here again we can choose the parameter α so that the dispersion relation (2.55) be exact up to terms of order $\mathcal{O}((kh)^4)$. In this way we get the following equation for α :

$$\frac{1}{2}\alpha^3 - \frac{13}{12}\alpha^2 + \frac{1}{2}\alpha - \frac{1}{30} = 0.$$

This equation has only one root which has physical sense and lead to linearly well-posed problem $\alpha_{opt} := 0.0800$ (let us recall that $\alpha = 0$ corresponds to the free surface and $\alpha = 1$ to the bottom level). We suggest to use this value in numerical simulations. In Figure 2.8 we plot dispersion relations (2.50), (2.51) and (2.55) with optimal values of α .

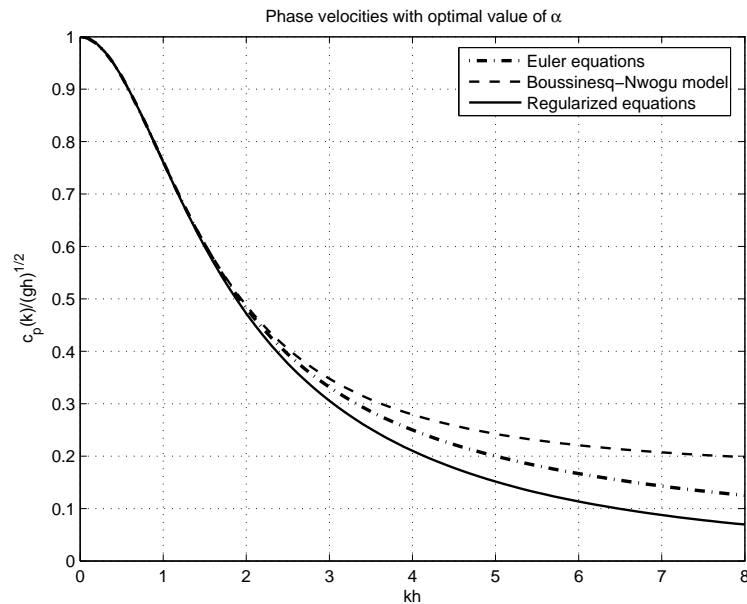


Figure 2.8: Dispersion relations of complete water wave problem, Nwogu version of Boussinesq equations and its regularized version

2.7 Bottom friction

In this section, one switches back to dimensional variables. It is a common practice in hydraulics engineering to take into account the effect of bottom friction or bottom rugosity. In the Boussinesq and nonlinear shallow water equations there is also a possibility to include some kind of empirical terms to model these physical effects. From the mathematical and especially numerical viewpoints these terms do not add any complexity, since they have the form of source terms that do not involve differential operators. So it is highly recommended to introduce these source terms in numerical models.

There is no unique bottom friction law. Most frequently, Chézy and Darcy-Weisbach laws are used. Both laws have similar structures. We give here these models in dimensional form. The following terms have to be added to the source terms of Boussinesq equations when one wants to include bottom friction modelling.

- Chézy law:

$$\mathbf{S}_f = -C_f g \frac{\vec{u} |\vec{u}|}{h + \eta},$$

where C_f is the Chézy coefficient.

- Darcy-Weisbach law:

$$\mathbf{S}_f = -\frac{\lambda \vec{u} |\vec{u}|}{8(h + \eta)},$$

where λ is the so-called resistance value. This parameter is determined according to the simplified form of the Colebrook-White relation:

$$\frac{1}{\sqrt{\lambda}} = -2.03 \log \left(\frac{k_s}{14.84(h + \eta)} \right).$$

Here k_s denotes the friction parameter, which depends on the composition of the bottom. Typically k_s can vary from 1mm for concrete to 300mm for bottom with dense vegetation.

- Manning-Strickler law:

$$\mathbf{S}_f = -k^2 g \frac{\vec{u} |\vec{u}|}{(h + \eta)^{\frac{4}{3}}},$$

where k is the Manning roughness coefficient.

Remark 7 *In chapter 4 we develop an alternative approach to bottom friction modelling. Our analysis is based on formal asymptotic expansion of Navier-Stokes equations in fluid and in the bottom boundary layer. The resulting viscous-potential formulation contains local and nonlocal dissipative terms. Then we derive corresponding long wave equations which take the following form in the absence of dispersive terms:*

$$\eta_t + \nabla \cdot ((h + \eta)\vec{u}) = 2\nu \Delta \eta + \sqrt{\frac{\nu}{\pi}} \int_0^t \frac{\nabla \cdot \vec{u}}{\sqrt{t - \tau}} d\tau,$$

$$\vec{u}_t + \frac{1}{2} \nabla |\vec{u}|^2 + g \nabla \eta = 2\nu \Delta \vec{u}.$$

The principal difference with just presented « engineer's » approach consists in at least formal justification of the governing equations.

2.8 Spectral Fourier method

In this study we adopted a well-known and widely used spectral Fourier method. The main idea consists in discretizing the spatial derivatives using Fourier transforms. The effectiveness of this method is explained by two main reasons. First, the differentiation operation in Fourier transform space is extremely simple due to the following property of Fourier transforms: $\overline{f'} = ik\overline{f}$. Secondly, there are very powerful tools for the fast and accurate computation of discrete Fourier transforms (DFT). So, spatial derivatives are computed with the following algorithm:

- 1: $\bar{f} \leftarrow \text{fft}(f)$
- 2: $\bar{v} \leftarrow ik\bar{f}$
- 3: $f' \leftarrow \text{ifft}(\bar{v})$

where k is the wavenumber.

This approach, which is extremely efficient, has the drawbacks of almost all spectral methods. The first drawback consists in imposing periodic boundary conditions since we use DFT. The second drawback is that we can only handle simple geometries, namely, Cartesian products of 1D intervals. For the purpose of academic research, this type of method is appropriate.

Let us now consider the discretization of the dissipative Boussinesq equations. We show in detail how the discretization is performed on equations (2.23), (2.25). The other systems are discretized in the same way. We chose equations (2.23), (2.25) in order to avoid cumbersome expressions and make the description as clear as possible.

Let us apply the Fourier transform to both sides of equations (2.23), (2.25):

$$\begin{aligned} \bar{\eta}_t = & -i\mathbf{k} \cdot \overline{(h + \varepsilon\eta)\vec{u}} - \frac{1}{\varepsilon}\bar{h}_t - \frac{\mu^2}{2\varepsilon}\overline{h^2\nabla^2 h_t} - \frac{\mu^2}{\varepsilon}\overline{h\nabla h \cdot \nabla h_t} + \frac{\mu^2}{6}\overline{h^3\nabla^2\nabla \cdot \vec{u}} \\ & + \frac{\mu^2}{2}\overline{h^2\nabla^2 h\nabla \cdot \vec{u}} + \mu^2\overline{h|\nabla h|^2\nabla \cdot \vec{u}} + \mu^2\overline{h^2\nabla h \cdot \nabla(\nabla \cdot \vec{u})}, \end{aligned} \quad (2.56)$$

$$\bar{\vec{u}}_t + \frac{1}{2}\varepsilon i\mathbf{k}\overline{|\vec{u}|^2} + i\mathbf{k}\bar{\eta} + \varepsilon\nu_2|\mathbf{k}|^2\bar{\vec{u}} - \frac{1}{2}\mu^2 i\mathbf{k}\overline{h^2\nabla \cdot \vec{u}_t} = 0, \quad (2.57)$$

where $\mathbf{k} = (k_x, k_y)$ denotes the Fourier transform parameters.

Equations (2.56) and (2.57) constitute a system of ordinary differential equations to be integrated numerically. In the present study we use the classical explicit fourth-order Runge-Kutta method.

$$\begin{aligned} k_1 &= \Delta t f(t_n, y_n), \\ k_2 &= \Delta t f\left(t_n + \frac{\Delta t}{2}, y_n + \frac{1}{2}k_1\right), \\ k_3 &= \Delta t f\left(t_n + \frac{\Delta t}{2}, y_n + \frac{1}{2}k_2\right), \\ k_4 &= \Delta t f(t_n + \Delta t, y_n + k_3), \\ y_{n+1} &= y_n + \frac{1}{6}k_1 + \frac{1}{3}k_2 + \frac{1}{3}k_3 + \frac{1}{6}k_4 + O(\Delta t^6). \end{aligned}$$

Remark 8 A lot of researchers who integrated numerically the KdV equation noticed that the stability criterion has the form

$$\Delta t = \frac{\lambda}{N^2},$$

where λ is the Courant-Friedrichs-Lewy (CFL) number and N the number of points of discretization. In order to increase the time integration step Δt they solved exactly the linear part of the partial differential equation since the linear term is the one involving high frequencies and constraining the stability. This method, which is usually called the integrating factor method, allows an increase of the CFL number up to a factor ten, but it cannot fix the dependence on $1/N^2$.

We do not have this difficulty because we use regularized dispersive terms. The regularization effect can be seen from equation (2.57). The same idea was exploited by [BPS81], who used the modified KdV equation (2.10).

Let us briefly explain how we treat the non-linear terms. Since the time integration scheme is explicit, one can easily handle nonlinearities. For example the term $\overline{(h + \varepsilon\eta)}\bar{u}$ is computed as follows:

$$\overline{(h + \varepsilon\eta)}\bar{u} = \text{fft} \left((h + \varepsilon \text{Re ifft}(\bar{\eta})) \cdot \text{Re ifft}(\bar{u}) \right).$$

The other nonlinear terms are computed in the same way.

2.8.1 Validation of the numerical method

One way to validate a numerical scheme is to compare the numerical results with analytical solutions. Unfortunately, the authors did not succeed in deriving analytical solutions to the (1 + 1)D dissipative Boussinesq equations over a flat bottom. But for validation purposes, one can neglect the viscous term. With this simplification several solitary wave solutions can be obtained. We follow closely the work of [Che98]. In (1 + 1)D in the presence of a flat bottom, the Boussinesq system without dissipation becomes

$$\eta_t + u_x + \varepsilon(u\eta)_x - \frac{\mu^2}{6}u_{xxx} = 0, \quad (2.58)$$

$$u_t + \eta_x + \varepsilon uu_x - \frac{\mu^2}{2}u_{xxt} = 0. \quad (2.59)$$

We look for solitary-wave solutions travelling to the left in the form

$$\eta(x, t) = \eta(\xi) = \eta(x_0 + x + ct), \quad u(x, t) = B\eta(\xi),$$

where we introduced the new variable $\xi = x_0 + x + ct$ and B, c, x_0 are constants. From the physical point of view this change of variables is nothing else than Galilean transformation. In other words we choose a new frame of reference which moves with the same celerity as the solitary wave. Since c is constant (there is no acceleration), the observer moving with the wave will see a steady picture.

In the following primes denote derivation with respect to ξ . Substituting this special form into the governing equations (2.58)-(2.59) gives

$$c\eta' + u' + \varepsilon(u\eta)' - \frac{\mu^2}{6}u''' = 0,$$

$$cu' + \eta' + \varepsilon uu' - c\frac{\mu^2}{2}u''' = 0.$$

One can decrease the order of derivatives by integrating once:

$$c\eta + u + \varepsilon u\eta - \frac{\mu^2}{6}u'' = 0,$$

$$cu + \eta + \frac{\varepsilon}{2}u^2 - c\frac{\mu^2}{2}u'' = 0.$$

The solution is integrable on \mathbb{R} and there are no integration constants, since a priori the solution behaviour at infinity is known: the solitary wave is exponentially small at large distances from the crest. Mathematically it can be expressed as

$$\lim_{\xi \rightarrow \pm\infty} \eta(x, t) = \lim_{\xi \rightarrow \pm\infty} u(x, t) = 0.$$

Now we use the relation $u(\xi) = B\eta(\xi)$ to eliminate the variable u from the system:

$$(c + B)\eta - B\frac{\mu^2}{6}\eta'' = -\varepsilon B\eta^2, \quad (2.60)$$

$$(1 + cB)\eta - cB\frac{\mu^2}{2}\eta'' = -\frac{\varepsilon}{2}B^2\eta^2. \quad (2.61)$$

In order to have non-trivial solutions both equations must be compatible. Compatibility conditions are obtained by comparing the coefficients of corresponding terms in equations (2.60)-(2.61):

$$\begin{aligned} \frac{1}{2}B^2 - \frac{1}{2}Bc &= 1, \\ \frac{1}{6}B^2 - Bc &= 0. \end{aligned}$$

These relations can be thought as a system of linear equations with respect to B^2 and Bc . The unique solution of those equations is

$$B^2 = \frac{12}{5}, \quad c = \frac{B}{6}.$$

Choosing $B > 0$ so that $c > 0$ leads to

$$B = \frac{6}{\sqrt{15}}, \quad c = \frac{1}{\sqrt{15}}.$$

These constants determine the amplitude and the propagation speed of the solitary wave. In order to find the shape of the wave, one differentiates once equation (2.61):

$$7\eta' - \mu^2\eta''' = -12\varepsilon\eta\eta'. \quad (2.62)$$

The solution to this equation is well-known (see for example [New77, Che98]):

Lemma 1 *Let α, β be real constants; the equation*

$$\alpha\eta'(\xi) - \beta\eta'''(\xi) = \eta(\xi)\eta'(\xi)$$

has a solitary-wave solution if $\alpha\beta > 0$. Moreover, the solitary-wave solution is

$$\eta(\xi) = 3\alpha \operatorname{sech}^2 \left(\frac{1}{2} \sqrt{\frac{\alpha}{\beta}} (\xi + \xi_0) \right)$$

where ξ_0 is an arbitrary constant.

Applying this lemma to equation (2.62) yields the following solution:

$$\begin{aligned} \eta(x, t) &= -\frac{7}{4\varepsilon} \operatorname{sech}^2 \left(\frac{\sqrt{7}}{2\mu} (x + ct + x_0) \right), \\ u(x, t) &= -\frac{7\sqrt{15}}{10\varepsilon} \operatorname{sech}^2 \left(\frac{\sqrt{7}}{2\mu} (x + ct + x_0) \right). \end{aligned} \quad (2.63)$$

Note that this exact solitary wave solution is not physical. Indeed the velocity is negative whereas one expects it to be positive for a depression wave propagating to the left. In any case, the goal here is to validate the numerical computations by comparing with an exact solution. The methodology is simple. We choose a solitary wave as initial condition and let it propagate during a certain time T with the spectral method. At the end of the computations one computes the L_∞ norm of the difference between the analytical solution (2.63) and the numerical one $\tilde{\eta}(x, T)$:

$$\epsilon_N := \max_{1 \leq i \leq N} |\eta(x_i, T) - \tilde{\eta}(x_i, T)|,$$

where $\{x_i\}_{1 \leq i \leq N}$ are the discretization points.

Figure 2.9 shows the graph of ϵ_N as a function of N . This result shows an excellent performance of this spectral method with an exponential convergence rate. In general, the error ϵ_N is bounded below by the maximum between the error due to the time integration algorithm and floating point arithmetic precision.

The exponential convergence rate to the exact solution is one of the features of spectral methods. It explains the success of these methods in several domains such as direct numerical simulation (DNS) of turbulence. One of the main drawbacks of spectral methods consists in the difficulties in handling complex geometries and various types of boundary conditions.

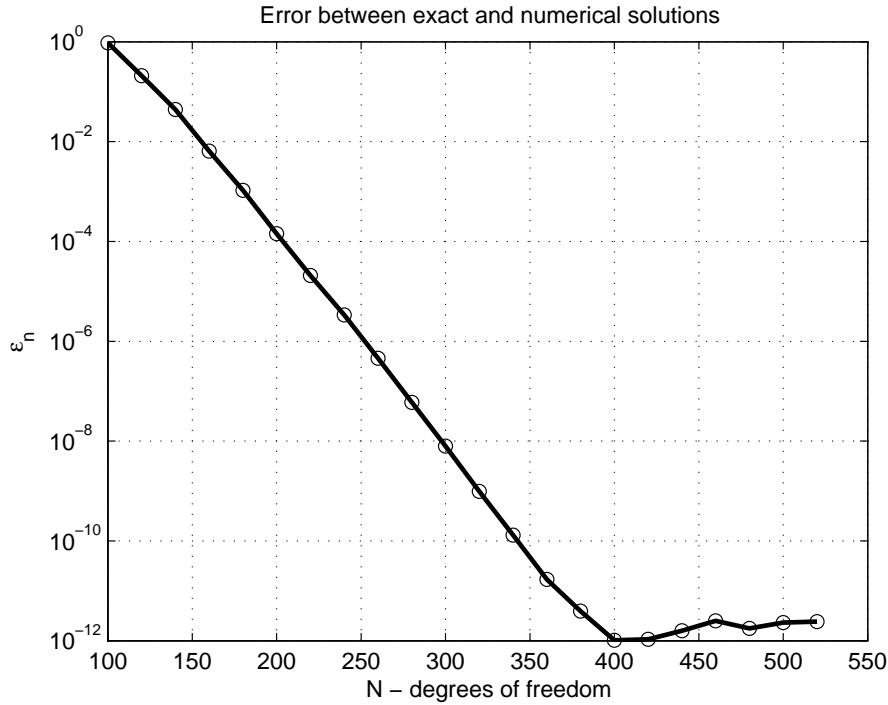


Figure 2.9: Error on the numerical computation of a solitary wave solution. Here $T = 1$.

2.9 Numerical results

In this section we perform comparisons between the two dissipation models (2.24) and (2.25). Even though the computations we show deal with a 1D wave propagating in the negative x -direction, they have been performed with the 2D version of the code. The bathymetry $z = -h(x, y)$ is chosen to be a regularized step function which is translated in the y -direction. A typical function $h(x, y)$ is given by

$$h(x) = \begin{cases} h_l, & x \leq x_0, \\ h_l + \frac{1}{2}(h_r - h_l) \left(1 + \sin\left(\frac{\pi}{\Delta x}(x - x_0 - \frac{1}{2}\Delta x)\right)\right), & x_0 < x < x_0 + \Delta x, \\ h_r, & x \geq x_0 + \Delta x. \end{cases} \quad (2.64)$$

This test case is interesting from a practical point of view since it clearly illustrates the phenomena of long wave reflection by bottom topography. The parameters used in this computation are given in Table 2.2. All values are given in nondimensional form.

2.9.1 Construction of the initial condition

We propagate on the free surface a so-called approximate soliton. Its classical construction is as follows. We begin with the non-dissipative Boussinesq equations on a flat

<i>parameter</i>	h_l	h_r	x_0	Δx	ε	μ	ν_1, ν_2
<i>value</i>	0.5	1.0	-0.5	0.3	0.005	0.06	0.14

Table 2.2: Typical values of the parameters used in the numerical computations

bottom:

$$\begin{aligned} \eta_t + ((1 + \varepsilon\eta)u)_x - \frac{\mu^2}{6}u_{xxx} &= 0, \\ u_t + \eta_x + \frac{\varepsilon}{2}(u^2)_x - \frac{\mu^2}{2}u_{xxt} &= 0, \end{aligned} \quad (2.65)$$

and look for u in the following form:

$$u = -\eta + \varepsilon P + \mu^2 Q + O(\varepsilon^2 + \varepsilon\mu^2 + \mu^4). \quad (2.66)$$

It is precisely at this step that one makes an approximation. One substitutes this asymptotic expansion into the governing equations and retains only the terms of order $O(\varepsilon + \mu^2)$:

$$\begin{aligned} \eta_t - \eta_x + \varepsilon P_x + \mu^2 Q_x - 2\varepsilon\eta\eta_x + \frac{\mu^2}{6}\eta_{xxx} &= O(\varepsilon^2 + \varepsilon\mu^2 + \mu^4), \\ -\eta_t + \eta_x + \varepsilon P_t + \mu^2 Q_t + \varepsilon\eta\eta_x + \frac{\mu^2}{2}\eta_{xxt} &= O(\varepsilon^2 + \varepsilon\mu^2 + \mu^4). \end{aligned} \quad (2.67)$$

Add these two equations and set the coefficients of ε and μ^2 equal to 0:

$$\varepsilon : \quad P_x + P_t - \eta\eta_x = 0, \quad (2.68)$$

$$\mu^2 : \quad Q_x + Q_t + \frac{1}{6}\eta_{xxx} + \frac{1}{2}\eta_{xxt} = 0. \quad (2.69)$$

Since the water depth is $h = 1 + \varepsilon\eta = 1 + O(\varepsilon)$, the approximate solitary wave should travel to the left with a celerity $c = 1 + O(\varepsilon)$ and depend on the variable $x + ct = x + t + O(\varepsilon)$. Consequently one has the following relations:

$$\frac{\partial f}{\partial t} = \frac{\partial f}{\partial x} + O(\varepsilon + \mu^2), \quad f \in \{\eta, P, Q\}.$$

Replacing time derivatives by spatial ones in (2.68)-(2.69) yields

$$P_x = \frac{1}{2}\eta\eta_x, \quad Q_x = -\frac{1}{3}\eta_{xxx}.$$

By integration (using the fact that solitary waves tend to zero at infinity), one obtains

$$P = \frac{1}{4}\eta^2, \quad Q = -\frac{1}{3}\eta_{xx} \quad (2.70)$$

and the relation (2.66) connecting η and u becomes

$$u = -\eta + \frac{\varepsilon}{4}\eta^2 - \frac{\mu^2}{3}\eta_{xx} + \dots \quad (2.71)$$

Substituting this expression for u into (2.67) yields a classical KdV equation for η :

$$\eta_t - \left(1 + \frac{3}{2}\varepsilon\eta\right)\eta_x - \frac{\mu^2}{6}\eta_{xxx} = 0, \quad (2.72)$$

which admits solitary wave solutions of the form $\eta = \eta(x + ct)$:

$$\eta(x, t) = \frac{2(c-1)}{\varepsilon} \operatorname{sech}^2 \left(\frac{1}{2\mu} \sqrt{6(c-1)}(x + ct) \right),$$

where $c > 1$. The velocity u is obtained from (2.71) by simple substitution. This approximate soliton is used in the numerical computations.

2.9.2 Comparison between the dissipative models

The snapshot of the function $\eta(x, y, t_0)$ (divided by 10 for clarity's sake) during and just after reflection by the step is given on Figure 2.10.

Then we compare the two sets of equations (2.23), (2.24) and (2.23), (2.25). To do so we look at the section of the free surface at $y = 0$ along the propagation direction.

Figure 2.11 shows that even at the beginning of the computations the two models give slightly different results. The amplitude of the pulse obtained with model I is smaller. It can be explained by the presence of the term $\nu_1 S \vec{u}$ which is bigger in magnitude than $\varepsilon \nu_2 \nabla^2 \vec{u}$. Within graphical accuracy, there is almost no difference between the conservative case and model II.

In Figure 2.12 one can see that differences between the two solitons continue to grow. In particular we see an important drawback of the dissipation model I: just after the wave crest the free surface has some kind of residual deformation which is clearly non-physical. Our numerical experiments show that the amplitude of this residue depends almost linearly on the parameter ν_1 . We could hardly predict this effect directly from the equations without numerical experiments.

We would like to point out several soliton transformations in Figure 2.13 due to the interaction with bathymetry. First of all, since the depth decreases, the wave amplitude grows. Quantitatively speaking, the wave amplitude before the interaction is equal exactly to 8 (without including dissipation) and over the step it becomes roughly 9.4. On the other hand the soliton becomes less symmetric which is also expected. Because of periodic numerical boundary conditions we also observe the residue of the free-surface deformation coming through the left boundary.

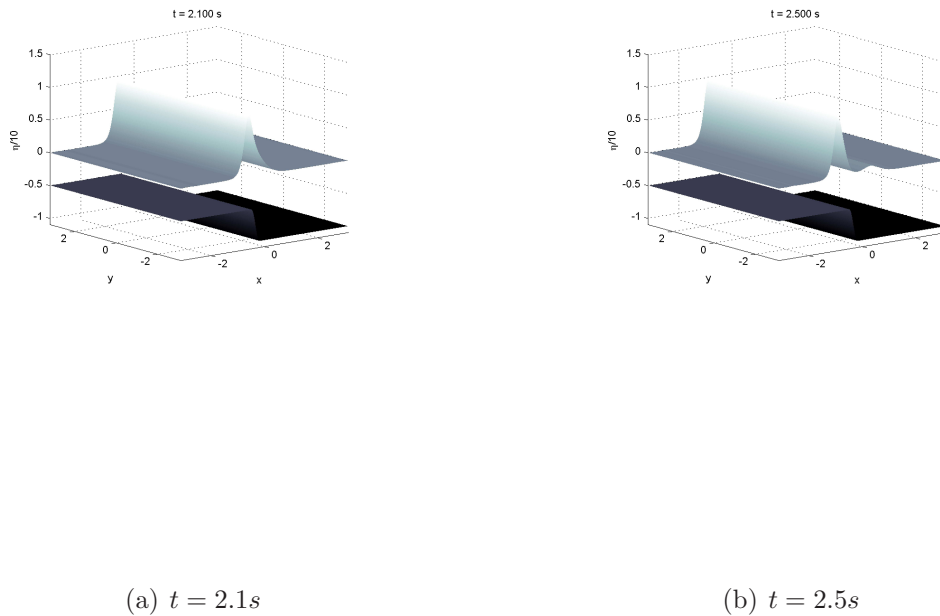


Figure 2.10: Interaction between a left-running solitary wave and a step.

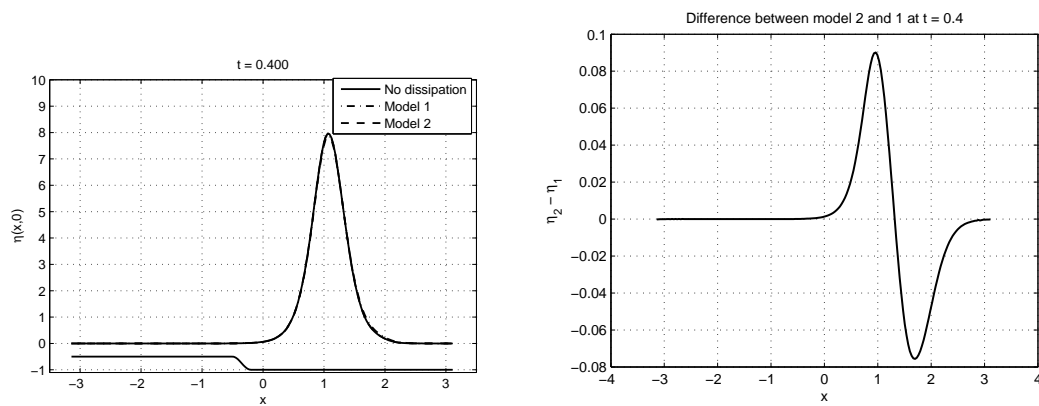


Figure 2.11: Free-surface snapshot before the interaction with the step: (left) the curves corresponding to the three models are almost superimposed; (right) difference between model II and model I.

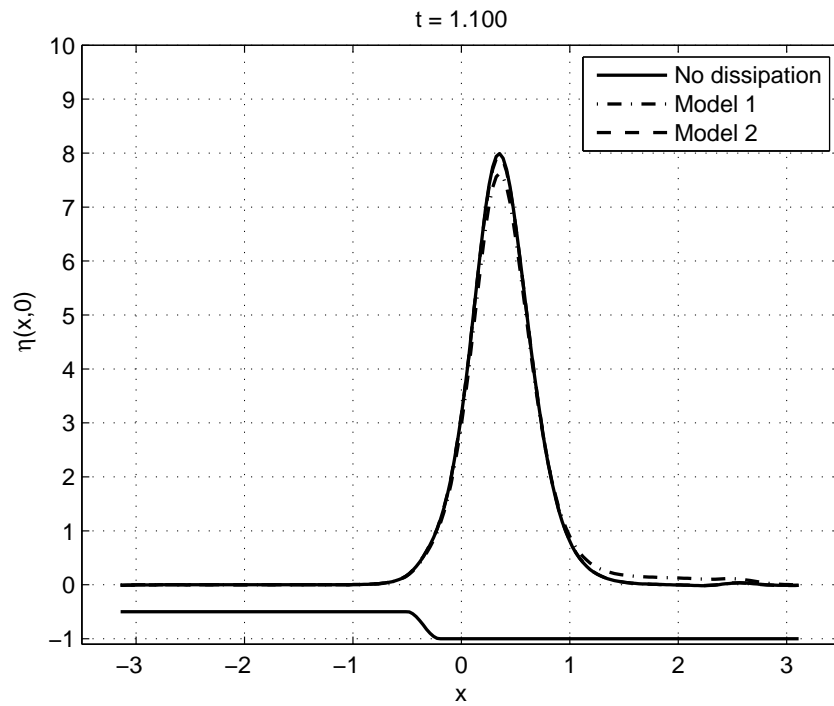


Figure 2.12: Free surface just before the interaction with the step

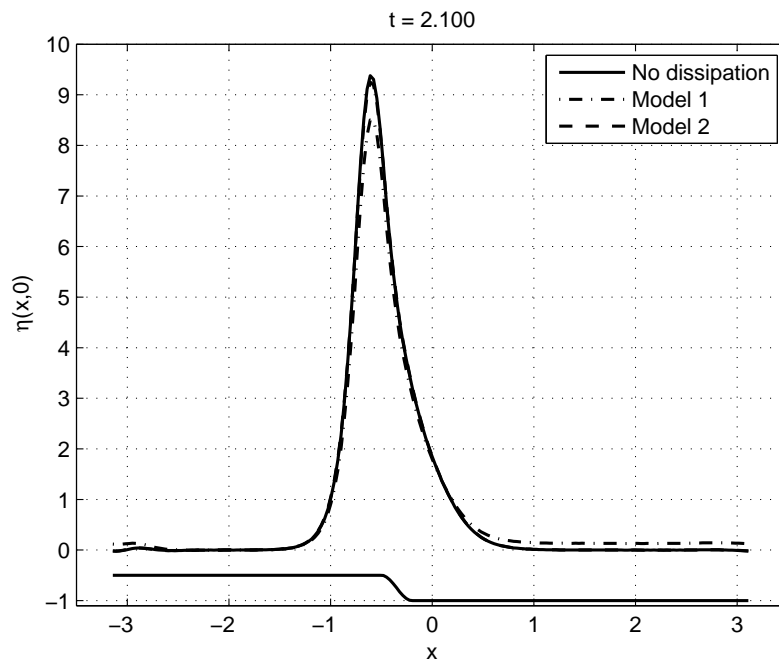


Figure 2.13: Beginning of the solitary wave deformation under the change in bathymetry

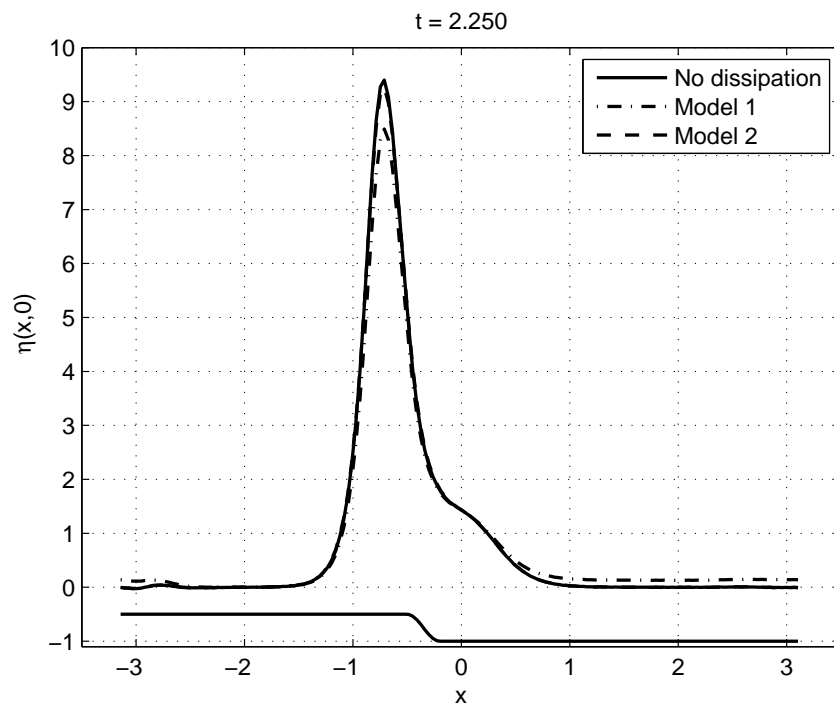


Figure 2.14: Initiation of the reflected wave separation

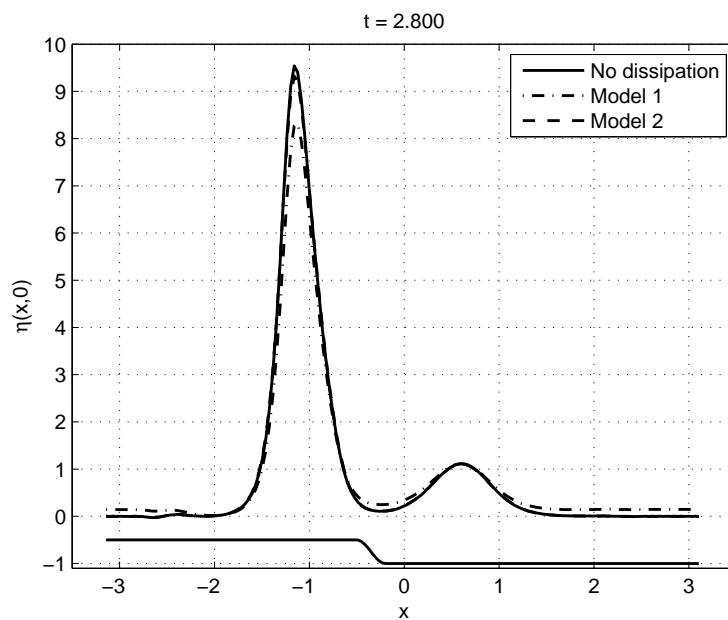


Figure 2.15: Separation of the reflected wave

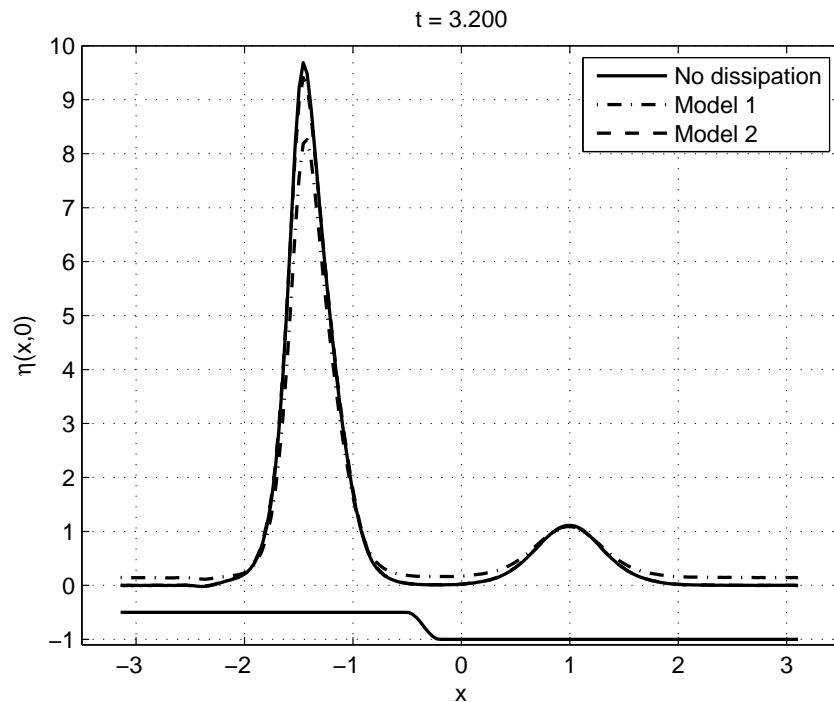


Figure 2.16: Two separate waves moving in opposite directions

Figures 2.14, 2.15 and 2.16 show the process of wave reflection from the step at the bottom. The reflected wave clearly moves in the opposite direction.

2.10 Conclusions

Comparisons have been made between two dissipation models. Model II, in which the decay is proportional to the second derivative of the velocity, appears to be better. At this stage we cannot show comparisons with laboratory experiments in order to demonstrate the performance of model II. Nevertheless, there is an indirect evidence. We refer one more time to the theoretical as well as experimental work of [BPS81]. In order to model wave trains, they added to the Korteweg–de Vries equation an ad-hoc dissipative term in the form of the Laplacian (but in 1D). This term coincides with the results of our derivation if we model dissipation in the equations according to the second model. Their work shows excellent agreement between experiments and numerical solutions to dissipative KdV equation. Moreover our dissipative Boussinesq equations are in the same relationship with the classical Boussinesq equations [Per67] as Euler and Navier-Stokes equations. This is a second argument towards the physical pertinency of the results obtained with model

II.

Chapter 3

Two phase approach to free surface compressible flows

I think that there is a moral to this story, namely that it is more important to have beauty in one's equations than to have them fit experiment. [...] It seems that if one is working from the point of view of getting beauty in one's equations, and if one has really a sound insight, one is on a sure line of progress. If there is not complete agreement between the results of one's work and experiment, one should not allow oneself to be too discouraged, because the discrepancy may well be due to minor features that are not properly taken into account and that will get cleared up with further development of the theory.

Paul Adrien Maurice Dirac (1902 – 1984)

Contents

3.1	Introduction	122
3.2	Mathematical model	125
3.2.1	Sound speed in the mixture	126
3.2.2	Equation of state	127
3.3	Formal limit in barotropic case	129
3.4	Finite volume scheme on unstructured meshes	131
3.4.1	Sign matrix computation	136
3.4.2	Second order scheme	137
3.4.3	TVD and MUSCL schemes	138
3.4.4	Diffusive fluxes computation	144
3.4.5	Solution interpolation to mesh nodes	146

3.4.6	Time stepping methods	148
3.4.7	Boundary conditions treatment	151
3.5	Numerical results	153
3.5.1	Convergence test	154
3.5.2	Falling water column	157
3.5.3	Water drop test case	157
3.6	Conclusions	162

3.1 Introduction

Two-phase or even multiphase flows are very common in nature. They occur in a system containing gas and liquid¹ with a meniscus separating the two phases. Probably, the most important applications of two-phase flow are in large-scale power systems. The design of power stations requires a detailed understanding of two-phase flow heat-transfer and pressure drop behaviour, which is significantly different from the single-phase case. Even more critically, nuclear reactors use water to remove heat from the reactor core using two-phase flow. Another important application of two-phase flows is pump cavitation. Two-phase flows in nature include many interesting examples such as clouds, groundwater flow, bubbles, rain, waves on the sea, foam, fountains and gas/oil slicks.

Several features make two-phase flow an interesting and challenging branch of fluid mechanics. First of all, surface tension complicates considerably all dynamical problems. In the present study we do not take into account this effect since in our applications it is unimportant. Then, in the case of air and water at standard temperature and pressure, the density of the two phases differs by a factor of about 1000. Similar differences are typical of water liquid/water vapor densities and can make the computation very stiff. The sound speed changes dramatically for materials undergoing phase change, and can be orders of magnitude different (see Figure 3.2). This introduces strong compressible effects into the problem. Finally, the phase changes are not instantaneous, and the liquid vapor system will not necessarily be in phase equilibrium.

In the present chapter we are going to present a mathematical model which is issued from two-phase flows fluid mechanics. Namely, we are going to use the homogeneous model (with equal velocity, pressure and temperature for both phases). Basically, our contribution consists in suggesting to use this model for the numerical simulation of free-surface aerated flows in various containers. The most important applications are issued from petroleum

¹They can occur even in a system containing two different liquids as well.



Figure 3.1: Example of homogeneous water/air mixture just after the wave breaking. This image is taken from [BOPB07].

industry and simulation of wave impacts onto a wall or breakwater. Figure 3.1 shows an image of a broken wave. It gives an example of homogeneous water/air mixture and shows the physical situation which we aim to model.

Accurate predictions of wave loading are crucial to the design of coastal structures. When a wave breaks directly onto a vertical or inclined wall, impact pressures can be extremely large in comparison to the pressures exerted by nonbreaking waves. Despite all this, many engineers disregard wave impact loading in the belief that the duration of the impulse is too short for the structure to respond. Presently, the loading due to breaking waves is difficult to predict and is poorly understood in general. We refer to [Per03] as general excellent review of water-wave impact problem.

Interesting experimental results are obtained in [BOPB07]. The authors report that even for series of supposedly regular waves, there is great variability in the violence of the impacts. The greatest impact pressures are highly localized in space and time. They are produced when the front of the breaker is almost parallel to the wall at the instant of impact. If the wave overturns as it hits the wall, it can trap an air pocket. The compressibility of the trapped or entrained air will affect the dynamics and is often thought to reduce the maximum pressure due to a cushioning effect. However, an air pocket will

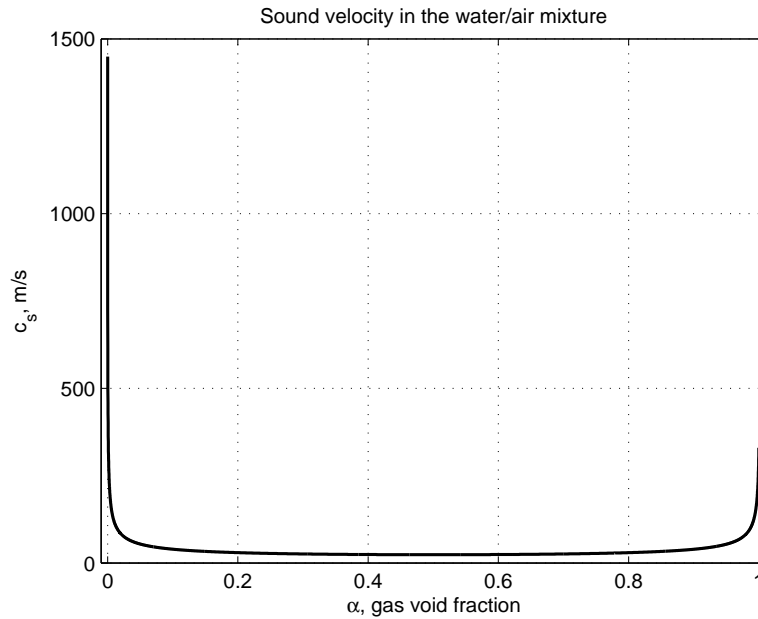


Figure 3.2: Sound speed c_s in the water/air mixture at normal conditions. It is plotted as a function of gas void fraction α .

also tend to distribute the impact pressures more widely so that the overall force on the wall may not be reduced.

Wave impacts are classified as low-aeration when the measurements indicate that the water adjacent to the wall contains relatively little air (typically a voids ratio $< 5\%$). On the other hand, an impact is called a high-aeration impact if it contains a higher level of entrained air, sometimes accompanied by clear evidence of entrapment. Bullock et al. [BOPB07] showed that low-aeration impacts have temporally and spatially localised pressure spike of short rise time and duration (≈ 80 to 200 ms) while in high-aeration situation the rise time, fall time and duration are longer (≈ 100 to 400 ms) and the pressure spike is less localised.

Even when the pressures during a high-aeration impact are lower, the fact that the impact is generally less spatially localised than a low-aeration impact reduces the chance of the resultant force being lower. When this is combined with the longer duration, the impulse associated with the impact may well be higher. It suggests that the greater persistence of air in seawater waves may not help to protect structures from impact damage as is often assumed.

3.2 Mathematical model

We would like to begin this section by explaining our choice of a compressible model for the liquid phase. If the liquid is pure (water, for example), the importance of its compressibility is questionable². In the present work we aim to model the mixtures of gas and liquid which typically occur in oil containers and broken waves (see Figure 3.1). In order to show the importance of compressibility effects, we depict on Figure 3.2 the dependence of sound velocity in the mixture of water and air as a function of gas volume fraction at normal conditions. The reader can see that the sound velocity drops down very quickly (to about $50\frac{m}{s}$) when we add a small quantity of air and the Mach number is not so small anymore. Recall that according to [BOPB07] low-aerated impacts contain about 5% of air, thus dropping down significantly the sound speed.

In this section we present the equations which govern the motion of two phase mixtures in a computational domain Ω . First of all, we need to introduce the notation which will be used throughout this chapter. We use superscripts \pm to denote any quantity which is related to liquid and gas respectively. For example, α^+ and α^- denote the volume fraction of liquid and gas and obviously satisfy the condition $\alpha^+ + \alpha^- = 1$. Then, we have the following classical quantities: ρ^\pm , \vec{u} , p , e , E , \vec{g} which denote the density of each phase, the velocity field vector, the pressure, the internal and total energy and the acceleration due to gravity correspondingly.

Conservation of mass (one equation for each phase), momentum and energy lead to the four following equations:

$$(\alpha^\pm \rho^\pm)_t + \nabla \cdot (\alpha^\pm \rho^\pm \vec{u}) = 0, \quad (3.1)$$

$$(\rho \vec{u})_t + \nabla \cdot (\rho \vec{u} \otimes \vec{u} + p \mathbb{I}) = \rho \vec{g}, \quad (3.2)$$

$$(\rho E)_t + \nabla \cdot (\rho H \vec{u}) = \rho \vec{g} \cdot \vec{u}, \quad (3.3)$$

where $\rho := \alpha^+ \rho^+ + \alpha^- \rho^-$ (the total density), $H := E + \frac{p}{\rho}$ (the specific enthalpy), $E = e + \frac{1}{2} |\vec{u}|^2$ (the total energy). This system can be seen as the single energy and infinite drag limit of the more conventional six equations model [Ish75].

The above system contains five unknowns $\alpha^\pm \rho^\pm$, \vec{u} , p and E and only four governing equations (3.1) - (3.3). In order to close the system, we need to provide the so-called equation of state (EOS) $p = p^\pm(\rho^\pm, e)$. The construction of the EOS will be discussed below (see Section 3.2.2).

It is possible to rewrite these equations as a system of balance laws

$$\frac{\partial \mathbf{w}}{\partial t} + \nabla \cdot \mathcal{F}(\mathbf{w}) = \mathcal{S}(\mathbf{w}),$$

²More precisely, if the problem under consideration does not require explicitly the compressibility (like in acoustics, for example), this effect can usually be neglected since it complicates considerably the study.

where the conservative variables in the 2D case are defined as follows:

$$\mathbf{w} = (w_i)_{i=1}^5 := (\alpha^+ \rho^+, \alpha^- \rho^-, \rho u, \rho v, \rho E). \quad (3.4)$$

The flux projection on the normal direction $\vec{n} = (n_1, n_2)$ can be expressed in physical and conservative variables

$$\begin{aligned} \mathcal{F} \cdot \vec{n} &= (\alpha^+ \rho^+ u_n, \alpha^- \rho^- u_n, \rho u u_n + p n_1, \rho v u_n + p n_2, \rho H u_n) = \\ & \left(w_1 \frac{w_3 n_1 + w_4 n_2}{w_1 + w_2}, w_2 \frac{w_3 n_1 + w_4 n_2}{w_1 + w_2}, w_3 \frac{w_3 n_1 + w_4 n_2}{w_1 + w_2} + p n_1, \right. \\ & \left. w_4 \frac{w_3 n_1 + w_4 n_2}{w_1 + w_2} + p n_2, (w_5 + p) \frac{w_3 n_1 + w_4 n_2}{w_1 + w_2} \right) \end{aligned} \quad (3.5)$$

where $u_n := \vec{u} \cdot \vec{n} = u n_1 + v n_2$ is the velocity projection on the normal direction \vec{n} . The jacobian matrix $\mathbb{A}_n(\mathbf{w}) := \frac{\partial(\mathcal{F} \cdot \vec{n})(\mathbf{w})}{\partial \mathbf{w}}$ can be easily computed. Its expression in the physical variables is

$$\mathbb{A}_n = \begin{pmatrix} u_n c^- & -u_n c^+ & c^+ n_1 & c^+ n_2 & 0 \\ -u_n c^- & u_n c^+ & c^- n_1 & c^- n_2 & 0 \\ -u u_n + \frac{\partial p}{\partial w_1} n_1 & -u u_n + \frac{\partial p}{\partial w_2} n_1 & u_n + u n_1 + \frac{\partial p}{\partial w_3} n_1 & u n_2 + \frac{\partial p}{\partial w_4} n_1 & \frac{\partial p}{\partial w_5} n_1 \\ -v u_n + \frac{\partial p}{\partial w_1} n_2 & -v u_n + \frac{\partial p}{\partial w_2} n_2 & v n_1 + \frac{\partial p}{\partial w_3} n_2 & u_n + v n_2 + \frac{\partial p}{\partial w_4} n_2 & \frac{\partial p}{\partial w_5} n_2 \\ u_n \left(\frac{\partial p}{\partial w_1} - H \right) & u_n \left(\frac{\partial p}{\partial w_2} - H \right) & u_n \frac{\partial p}{\partial w_3} + H n_1 & u_n \frac{\partial p}{\partial w_4} + H n_2 & u_n \left(1 + \frac{\partial p}{\partial w_5} \right) \end{pmatrix}$$

This matrix has three distinct eigenvalues:

$$\lambda_1 = u_n - c_s, \quad \lambda_{2,3,4} = u_n, \quad \lambda_5 = u_n + c_s,$$

where c_s is defined in the next section. One can conclude that the system (3.1) – (3.3) is hyperbolic. This hyperbolicity represents the major advantage of this model. The computation of the eigenvectors is trickier but can still be performed analytically. We do not give here the final expressions since they are cumbersome.

3.2.1 Sound speed in the mixture

In [Ghi08] it is shown by direct computation of the eigenvalues of the Jacobian $\mathbb{A}_n(\mathbf{w})$ that the square of the sound speed in the mixture is given by

$$c_s^2 := \frac{\rho^+ \rho^- (c_s^+)^2 (c_s^-)^2}{\rho (\alpha^+ \rho^- (c_s^-)^2 + \alpha^- \rho^+ (c_s^+)^2)},$$

where c_s^\pm are the sound velocities in each phase. In the present setting they are defined by formulas (3.8).

3.2.2 Equation of state

In the present work we assume that the light fluid is described by an ideal gas type law

$$p^- = (\gamma - 1)\rho^- e^-, \quad e^- = c_v^- T^-, \quad (3.6)$$

while the heavy fluid is modeled by Tate's law³ [GZI⁺79, HA71]

$$p^+ + \pi_0 = (\mathcal{N} - 1)\rho^+ e^+, \quad e^+ = c_v^+ T^+ + \frac{\pi_0}{\mathcal{N}\rho^+}, \quad (3.7)$$

where the quantities γ , c_v^\pm , \mathcal{N} , π_0 are constants. For example, pure water is well described when we take $\mathcal{N} = 7$ and $\pi_0 = 2.1 \times 10^9 Pa$.

Remark 9 *In practice, the constants c_v^\pm can be calculated after simple algebraic manipulations of equations (3.6), (3.7) and matching with experimental values at normal conditions:*

$$c_v^- \equiv \frac{p_0}{(\gamma - 1)\rho_0^- T_0},$$

$$c_v^+ \equiv \frac{\mathcal{N}p_0 + \pi_0}{(\mathcal{N} - 1)\mathcal{N}\rho_0^+ T_0}.$$

For example, for an air/water mixture under normal conditions we have the values given in Table 3.1.

The sound velocities in each phase are given by the following formulas:

$$(c_s^-)^2 = \frac{\gamma p^-}{\rho^-}, \quad (c_s^+)^2 = \frac{\mathcal{N}p^+ + \pi_0}{\rho^+}. \quad (3.8)$$

In order to construct an equation of state for the mixture, we make the additional assumption that the two phases are in thermodynamic equilibrium:

$$p^+ = p^-, \quad T^+ = T^-. \quad (3.9)$$

Below values of the common pressure and common temperature will be denoted by p and T respectively.

Now, let us construct a system of nonlinear equations which will help us obtain the pressure in the mixture. To do this, we first introduce the following notation for the mass fractions of each phase in the mixture

$$c^\pm := \frac{\alpha^\pm \rho^\pm}{\rho}.$$

³In the literature Tate's law is sometimes called the stiffened gas law.

<i>parameter</i>	<i>value</i>
p_0	10^5 Pa
ρ_0^+	10^3 kg/m^3
ρ_0^-	1.29 kg/m^3
T_0	300 K
γ	1.4
\mathcal{N}	7
π_0	$2.1 \times 10^9 \text{ Pa}$
c_v^+	$166.72 \frac{\text{J}}{\text{kg}\cdot\text{K}}$
c_v^-	$646.0 \frac{\text{J}}{\text{kg}\cdot\text{K}}$
g	100 m/s^2

Table 3.1: Values of the parameters for an air/water mixture under normal conditions. We would like to comment on the rather high value of the acceleration due to gravity. Obviously, it does not correspond to any physical situation. Nevertheless, we choose this value in order to accelerate all dynamic processes in our test cases.

We would like to reduce the number of unknowns. To do this, we express the internal energies e^\pm of each phase as a function of the other thermodynamic variables and constants. Let us write the two following relations:

$$c^+e^+ + c^-e^- = e, \quad T^+(\rho^+, e^+) = T^-(\rho^-, e^-).$$

After substituting the expressions (3.6), (3.7) for T^\pm , our system becomes

$$\begin{aligned} c^+e^+ + c^-e^- &= e, \\ \frac{e^+}{c_v^+} - \frac{e^-}{c_v^-} &= \frac{\pi_0}{\mathcal{N}c_v^+\rho^+}. \end{aligned}$$

This linear system can be easily solved to give us the expressions for e^\pm

$$e^+ = \frac{1}{\mathcal{D}} \left(\frac{e}{c_v^-} + \frac{\pi_0 c^-}{\mathcal{N}c_v^+\rho^+} \right), \quad (3.10)$$

$$e^- = \frac{1}{\mathcal{D}c_v^+} \left(e - \frac{\pi_0 c^+}{\mathcal{N}\rho^+} \right), \quad (3.11)$$

where $\mathcal{D} := \frac{c^+}{c_v^-} + \frac{c^-}{c_v^+}$.

Let us analyse the obtained results. From (3.9) we have an additional relation

$$p \equiv p^+(\rho^+, e^+) = p^-(\rho^-, e^-).$$

It means that the pressure p is completely determined if we know (ρ^+, e^+) or (ρ^-, e^-) . Since internal energies e^\pm are expressed in terms of (α^\pm, ρ^\pm) by expressions (3.10), (3.11), it is sufficient to determine these four quantities (α^\pm, ρ^\pm) . It is done by solving the following system of nonlinear equations:

$$\begin{aligned} (\mathcal{N} - 1)\rho^+ \left(\frac{e}{c_v^-} + \frac{\pi_0 c^-}{\mathcal{N} c_v^+ \rho^+} \right) - (\gamma - 1) \frac{\rho^-}{c_v^+} \left(e - \frac{\pi_0 c^+}{\mathcal{N} \rho^+} \right) &= \mathcal{D}\pi_0, \\ \alpha^+ + \alpha^- &= 1, \\ \alpha^+ \rho^+ &= w_1, \\ \alpha^- \rho^- &= w_2. \end{aligned}$$

The last two equations can be easily eliminated to reduce the system to two equations

$$\begin{aligned} (\mathcal{N} - 1)\rho^+ \left(\frac{e}{c_v^-} + \frac{\pi_0 c^-}{\mathcal{N} c_v^+ \rho^+} \right) - (\gamma - 1) \frac{\rho^-}{c_v^+} \left(e - \frac{\pi_0 c^+}{\mathcal{N} \rho^+} \right) &= \mathcal{D}\pi_0, \\ \frac{w_1}{\rho^+} + \frac{w_2}{\rho^-} &= 1. \end{aligned}$$

Finally, using the second equation, one can express ρ^- in terms of ρ^+ and the conservative variables $w_{1,2}$ as

$$\rho^- = \frac{\rho^+ w_2}{\rho^+ - w_1}.$$

This expression is then substituted in the pressure equality condition to give the following single equation with respect to ρ^+ :

$$\begin{aligned} (\mathcal{N} - 1) \frac{e}{c_v^-} \rho^+ (\rho^+ - w_1) + \frac{(\mathcal{N} - 1) \pi_0 c^-}{\mathcal{N} c_v^+} (\rho^+ - w_1) \\ - (\gamma - 1) \frac{e}{c_v^+} \rho^+ w_2 + (\gamma - 1) \frac{\pi_0 c^+}{\mathcal{N} c_v^+} w_2 = \mathcal{D}\pi_0 (\rho^+ - w_1). \end{aligned}$$

This equation can be solved analytically (we do not give here the solution's expression since it is cumbersome) or by a Newton-type numerical method. Once ρ^+ is determined, we can find e^+ from (3.10) and, finally, the pressure

$$p = (\mathcal{N} - 1) \rho^+ e^+ - \pi_0.$$

3.3 Formal limit in barotropic case

The propagation of waves at the interface between a heavy compressible fluid of density ρ^+ and a light compressible fluid of density ρ^- is investigated. The superscript $+$ is used to

denote the heavy fluid while the superscript $-$ is used to denote the light fluid. A typical geometry is shown in Figure 3.3.

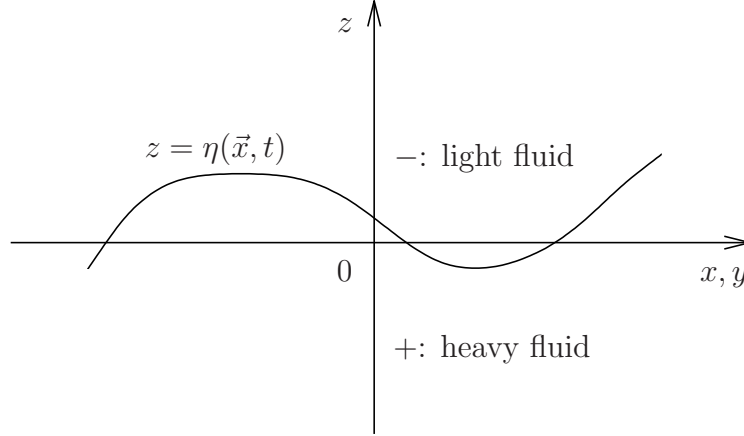


Figure 3.3: Sketch of the flow.

The governing equations are

$$(\alpha^\pm \rho^\pm)_t + \nabla \cdot (\alpha^\pm \rho^\pm \vec{u}) = 0, \quad (3.12)$$

$$(\rho \vec{u})_t + \nabla \cdot (\rho \vec{u} \otimes \vec{u}) + \nabla p = \rho \vec{g}, \quad (3.13)$$

where $\vec{u} = (u, v, w)$ is the common velocity, α^\pm are the volume fractions of each fluid, ρ^\pm the densities of each fluid, with the relations $\alpha^+ + \alpha^- = 1$, $\rho := \alpha^+ \rho^+ + \alpha^- \rho^-$ and the equation of state reads:

$$p \equiv p^+(\rho^+) = p^-(\rho^-). \quad (3.14)$$

The speeds of sound are given by

$$(c_s^\pm)^2 = \frac{\partial p}{\partial \rho^\pm}.$$

Let

$$\gamma^\pm = \frac{\rho^\pm (c_s^\pm)^2}{p}, \quad \bar{\gamma} = \alpha^+ \gamma^- + \alpha^- \gamma^+.$$

Let also

$$\delta^\pm \gamma = \gamma^\pm - \bar{\gamma}.$$

Then one can show that

$$\alpha_t^\pm + (\vec{u} \cdot \nabla) \alpha^\pm + \alpha^+ \alpha^- \frac{\delta^\pm \gamma}{\bar{\gamma}} \nabla \cdot \vec{u} = 0, \quad (3.15)$$

$$p_t + (\vec{u} \cdot \nabla)p + p \frac{\gamma^+ \gamma^-}{\bar{\gamma}} \nabla \cdot \vec{u} = 0. \quad (3.16)$$

Consider the case where α^- is either 0 or 1. More precisely let

$$\alpha^- := H(z - \eta(\vec{x}, t)), \quad (3.17)$$

where H is the Heaviside step function. Physically this substitution means that we consider two pure phases separated by an interface. It follows that

$$\alpha^+ \alpha^- = 0.$$

Substituting the expression (3.17) into the equation (3.15) for α^- gives

$$\eta_t + (u, v) \cdot \nabla_x \eta = w.$$

Equations (3.12) and (3.13) become

$$\begin{aligned} \rho_t + (\vec{u} \cdot \nabla)\rho + \rho \nabla \cdot \vec{u} &= 0, \\ \vec{u}_t + (\vec{u} \cdot \nabla)\vec{u} + \frac{\nabla p}{\rho} &= \vec{g}. \end{aligned}$$

This system of equations is nothing else than the system of a discontinuous two-fluid system with an interface at $z = \eta(\vec{x}, t)$.

This simple computation shows an interesting property of our model. For the important special case of barotropic equations, we can show that our model automatically degenerates into a discontinuous two-fluid system where two pure phases are separated by an interface.

3.4 Finite volume scheme on unstructured meshes

Finite volume methods are a class of discretization schemes that have proven highly successful in solving numerically of a wide class of conservation law systems. These systems often come from compressible fluid dynamics. In electromagnetism, for example, Discontinuous Galerkin methods have proven to be more efficient [CLS04]. When compared to other discretization methods such as finite elements or finite differences, the primary interests of finite volume methods are robustness, applicability on very general unstructured meshes, and the intrinsic local conservation properties. Hence, with this type of discretization, we conserve “exactly” the mass, momentum and total energy⁴.

In order to solve numerically the system of balance laws (3.1) – (3.3) we rewrite the governing equations in the following form

$$\frac{\partial \mathbf{w}}{\partial t} + \nabla \cdot \mathcal{F}(\mathbf{w}) = \nabla \cdot (\mathcal{D} \nabla \mathbf{w}) + \mathcal{S}(\mathbf{w}), \quad (3.18)$$

⁴This statement is true in the absence of source terms and appropriate boundary conditions.

where $\mathbf{w}(x, t) : \mathbb{R}^d \times \mathbb{R}^+ \mapsto \mathbb{R}^m$ is the vector of conservative variables (in the present study $d = 2$ or 3 and $m = 5$), $\mathcal{F}(\mathbf{w})$ is the advective flux function, \mathcal{D} the diffusion matrix and $\mathcal{S}(\mathbf{w})$ the source term. We must say that the governing equations (3.1) – (3.3) considered in this chapter do not possess viscous terms. However, we prefer to include in the discussion their discretization since it can be useful for Navier-Stokes or viscous Saint-Venant and Boussinesq equations [DD07a]. The system (3.18) should be provided with initial condition

$$\mathbf{w}(x, 0) = \mathbf{w}_0(x) \quad (3.19)$$

and appropriate boundary conditions.

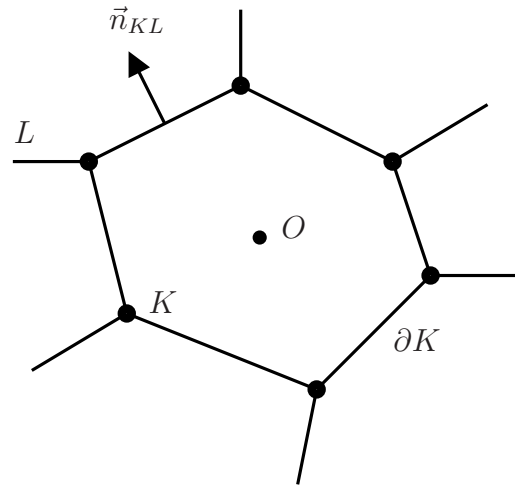


Figure 3.4: An example of control volume K with barycenter O . The normal pointing from K to L is denoted by \vec{n}_{KL} .

The computational domain $\Omega \subset \mathbb{R}^d$ is triangulated into a set of non overlapping control volumes that completely cover the domain. Let \mathcal{T} denote a tessellation of the domain Ω with control volume K such that

$$\cup_{K \in \mathcal{T}} \bar{K} = \bar{\Omega}, \quad \bar{K} := K \cup \partial K.$$

For two distinct control volumes K and L in \mathcal{T} , the intersection is either an edge (2D) or face (3D) with oriented normal \vec{n}_{KL} or else a set of measure at most $d - 2$ (in 2D it is just a vertex, in 3D it can also be a segment, for example). We need to introduce the following notation for the neighbourhood of K

$$\mathcal{N}(K) := \{L \in \mathcal{T} : \text{area}(K \cap L) \neq 0\},$$

a set of all control volumes L which share a face (or an edge in 2D) with the given volume K . In this chapter, we denote by $\text{vol}(\cdot)$ and $\text{area}(\cdot)$ the d and $d - 1$ dimensional measures⁵ respectively.

The choice of control volume tessellation is flexible in the finite volume method. In the present study we retained a so-called cell-centered approach (see Figure 3.5), which means that degrees of freedom are associated to cell barycenters. There exists an alternative vertex-centered method [BJ89, BO04] (see Figure 3.6) which necessitates the construction of dual mesh even for first-order schemes. In the *cell-centered* finite volume scheme, the triangles themselves serve as control volumes with solution unknowns attributed to triangles barycenters. In the *vertex-centered* finite volume scheme, control volumes are formed as a geometric dual to the triangle complex and solution unknowns stored on vertex basis.

Remark 10 *Except for the construction of dual mesh in vertex-centered approach, these two methods are almost equivalent in the interior of the computational domain Ω . However, the boundary conditions treatment is different and it is harder (or less natural in author's opinion) when data is stored at vertices. This is one more reason why we retained the cell centers to store the solution's information.*

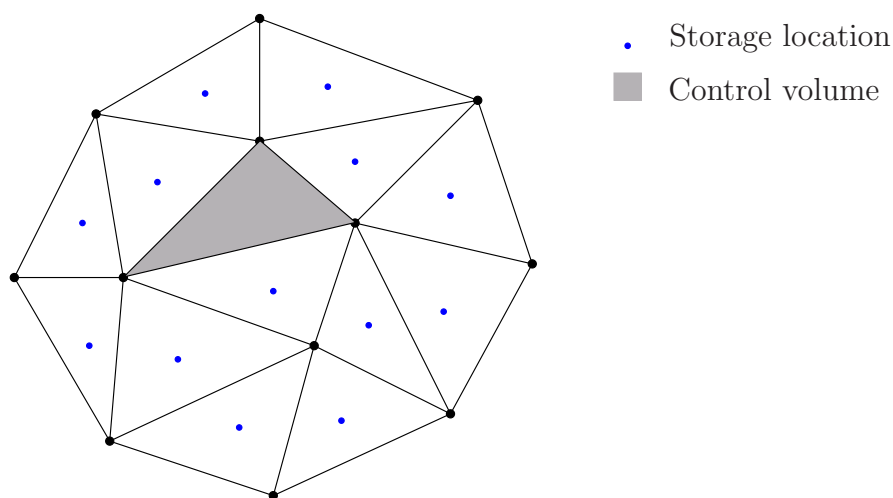


Figure 3.5: Illustration for cell-centered finite volume method

The first steps in Finite Volume (FV) methods are classical. We start by integrating equation (3.18) on the control volume K (see Figure 3.4 for illustration) and we apply Gauss-Ostrogradsky theorem for advective and diffusive fluxes. Then, in each control

⁵In other words, in 3D the notation $\text{area}(\cdot)$ and $\text{vol}(\cdot)$ are very natural and mean area and volume respectively, while in 2D they refer to the area and the length.

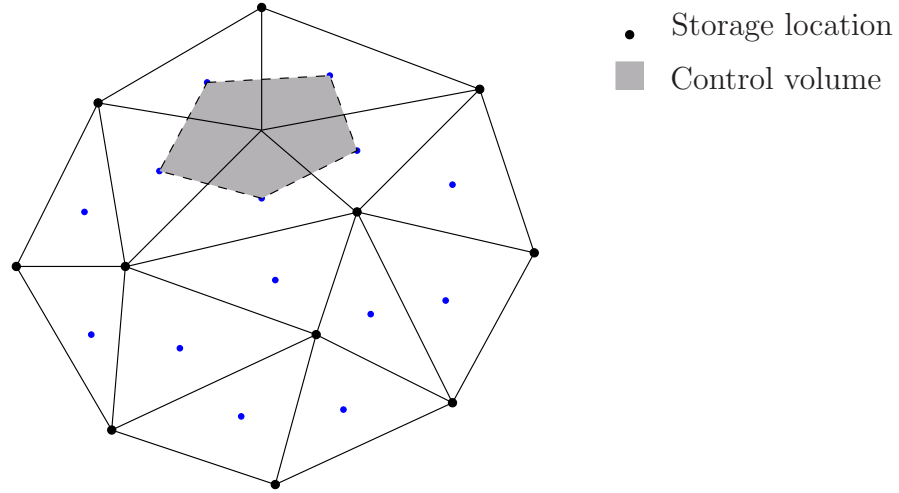


Figure 3.6: Illustration for vertex-centered finite volume method

volume, an integral conservation law statement is imposed:

$$\frac{d}{dt} \int_K \mathbf{w} \, d\Omega + \int_{\partial K} \mathcal{F}(\mathbf{w}) \cdot \vec{n}_{KL} \, d\sigma = \int_{\partial K} (\mathcal{D}\nabla\mathbf{w}) \cdot \vec{n}_{KL} \, d\sigma + \int_K \mathcal{S}(\mathbf{w}) \, d\Omega. \quad (3.20)$$

Physically an integral conservation law asserts that the rate of change of the total amount of a substance (for example: mass, momentum, total energy, etc) with density \mathbf{w} in a fixed control volume K is balanced by the flux \mathcal{F} , diffusion \mathcal{D} of the substance through the boundary ∂K and the production of this quantity \mathcal{S} inside the control volume.

The next step consists in introducing the so-called control volume cell average for each $K \in \mathcal{T}$

$$\mathbf{w}_K(t) := \frac{1}{\text{vol}(K)} \int_K \mathbf{w}(\vec{x}, t) \, d\Omega.$$

After the averaging step, the finite volume method can be interpreted as producing a system of evolution equations for cell averages, since

$$\frac{d}{dt} \int_K \mathbf{w}(\vec{x}, t) \, d\Omega = \text{vol}(K) \frac{d\mathbf{w}_K}{dt}.$$

Godunov was the first [God59] who pursued and applied these ideas to the discretization of the gas dynamics equations.

However, the averaging process implies piecewise constant solution representation in each control volume with value equal to the cell average. The use of such representation renders the numerical solution multivalued at control volume interfaces. Thereby the calculation of the fluxes $\int_{\partial K} (\mathcal{F}(\mathbf{w}) \cdot \vec{n}_{KL}) \, d\sigma$ at these interfaces is ambiguous. Next fundamental aspect of finite volume methods is the idea of substituting the true flux at interfaces by a

numerical flux function

$$(\mathcal{F}(\mathbf{w}) \cdot \vec{n})|_{\partial K \cap \partial L} \longleftarrow \Phi(\mathbf{w}_K, \mathbf{w}_L; \vec{n}_{KL}) : \mathbb{R}^m \times \mathbb{R}^m \mapsto \mathbb{R}^m ,$$

a Lipschitz continuous function of the two interface states \mathbf{w}_K and \mathbf{w}_L . The heart of the matter in finite volume method consists in the choice of the numerical flux function Φ . In general this function is calculated as an exact or even better approximate local solution of the Riemann problem posed at these interfaces. In the present study we decided to choose the numerical flux function according to VFFC scheme extensively described in Appendix A.

The numerical flux is assumed to satisfy the properties:

Conservation. This property ensures that fluxes from adjacent control volumes sharing an interface exactly cancel when summed. This is achieved if the numerical flux function satisfies the identity

$$\Phi(\mathbf{w}_K, \mathbf{w}_L; \vec{n}_{KL}) = -\Phi(\mathbf{w}_L, \mathbf{w}_K; \vec{n}_{LK}).$$

Consistency. The consistency is obtained when the numerical flux with identical state arguments (in other words it means that the solution is continuous through an interface) reduces to the true flux of the same state, i.e.

$$\Phi(\mathbf{w}, \mathbf{w}; \vec{n}) = (\mathcal{F} \cdot \vec{n})(\mathbf{w}).$$

After introducing the cell averages \mathbf{w}_K and numerical fluxes into (3.20), the integral conservation law statement becomes

$$\begin{aligned} \frac{d\mathbf{w}_K}{dt} + \sum_{L \in \mathcal{N}(K)} \frac{\text{area}(L \cap K)}{\text{vol}(K)} \Phi(\mathbf{w}_K, \mathbf{w}_L; \vec{n}_{KL}) &= \\ &= \frac{1}{\text{vol}(K)} \sum_{L \in \mathcal{N}(K)} \int_{K \cap L} (\mathcal{D}\nabla \mathbf{w}) \cdot \vec{n}_{KL} d\sigma + \frac{1}{\text{vol}(K)} \int_K \mathcal{S}(\mathbf{w}) d\Omega . \end{aligned}$$

The discretization of diffusive fluxes will be discussed in Section 3.4.4. We denote by \mathcal{S}_K the approximation of the following quantity $\frac{1}{\text{vol}(K)} \int_K \mathcal{S}(\mathbf{w}) d\Omega$. In practice, the source term discretization is discussed in Section A.1.3. Thus, the following system of ordinary differential equations (ODE) is called a semi-discrete finite volume method:

$$\frac{d\mathbf{w}_K}{dt} + \sum_{L \in \mathcal{N}(K)} \frac{\text{area}(L \cap K)}{\text{vol}(K)} (\Phi(\mathbf{w}_K, \mathbf{w}_L; \vec{n}_{KL}) - (\mathcal{D}\nabla \mathbf{w}) \cdot \vec{n}_{KL}) = \mathcal{S}_K, \quad \forall K \in \mathcal{T} . \quad (3.21)$$

The initial condition for this system is given by projecting (3.19) onto the space of piecewise constant functions

$$\mathbf{w}_K(0) = \frac{1}{\text{vol } K} \int_K \mathbf{w}_0(x) d\Omega .$$

This system of ODE should also be discretized. There is a variety of explicit and implicit time integration methods. Let \mathbf{w}_K^n denote a numerical approximation of the cell average solution in the control volume K at time $t^n = n\Delta t$. The simplest time integration method is the forward Euler scheme

$$\frac{d\mathbf{w}_K}{dt} \simeq \frac{\mathbf{w}_K^{n+1} - \mathbf{w}_K^n}{\Delta t} .$$

When applied to (3.21) it produces the fully-discrete finite volume scheme. The time integration approach used in this study is detailed in Section 3.4.6.

3.4.1 Sign matrix computation

In the context of the VFFC scheme (see Appendix A for more details), we need to compute the so-called sign matrix which is defined in the following way

$$U_n := \text{sign}(\mathbb{A}_n) = R \text{sign}(\Lambda)L,$$

where R , L are matrices composed of right and left eigenvectors correspondingly, and $\Lambda = \text{diag}(\lambda_1, \dots, \lambda_m)$ is the diagonal matrix of eigenvalues of the Jacobian.

This definition gives the first “direct” method of sign matrix computation. Since the advection operator is relatively simple, after a few tricks, we can succeed in computing analytically the matrices R and L . For more complicated two-phase models it is almost impossible to perform this computation in closed analytical form. In this case, one has to apply numerical techniques for eigensystem computation. It turns out to be costly and quite approximative. In the present work we use physical information about the model in numerical computations.

There is another way which is less expensive. The main idea is to construct a kind of interpolation polynomial which takes the following values

$$P(u_n \pm c_s) = \text{sign}(u_n \pm c_s), \quad P(u_n) = \text{sign}(u_n).$$

These three conditions allow us to construct a second degree interpolation polynomial. Obviously, when $P(\lambda)$ is evaluated with $\lambda = \mathbb{A}_n$ we obtain the sign matrix U_n as a result. The construction of Lagrange interpolation polynomial $P(\lambda)$ is simple and we give only its

expression

$$P(\lambda) = \left(\frac{\text{sign}(u_n + c_s) - 2 \text{sign}(u_n) + \text{sign}(u_n - c_s)}{2c_s^2} (\lambda - u_n) + \frac{\text{sign}(u_n) - \text{sign}(u_n - c_s)}{c_s} \right) (\lambda - u_n + c_s) + \text{sign}(u_n - c_s).$$

In our research code we have implemented both methods. Our experience shows that the interpolation method is quicker and gives correct results in most test cases. However, when we approach pure phase states, it shows a rather bad numerical behaviour. It can lead to instabilities and diminish overall code robustness. Thus, whenever possible we suggest to use the computation of the Jacobian eigenstructure.

3.4.2 Second order scheme

If we analyze the above scheme, we understand that in fact, we have only one degree of freedom per data storage location. Hence, it seems that we can expect to be first order accurate at most. In the numerical community first order schemes are generally considered to be too inaccurate for most quantitative calculations. Of course, we can always make the mesh spacing extremely small but it cannot be a solution since it makes the scheme inefficient. From the theoretical point of view the situation is even worse since an $\mathcal{O}(h^{\frac{1}{2}})$ L_1 -norm error bound for the monotone and E-flux schemes [Osh84] is known to be sharp [Pet91], although an $\mathcal{O}(h)$ solution error is routinely observed in numerical experiments. On the other hand, Godunov has shown [God59] that all linear schemes that preserve solution monotonicity are at most first order accurate. This rather negative result suggests that a higher order accurate scheme has to be essentially nonlinear in order to attain simultaneously a monotone resolution of discontinuities and high order accuracy in continuous regions.

A significant breakthrough in the generalization of finite volume methods to higher order accuracy is due to N.E. Kolgan [Kol72, Kol75] and van Leer [vL79]. They proposed a kind of post-treatment procedure currently known as solution *reconstruction* or MUSCL⁶ scheme. In the above papers the authors used linear reconstruction (it will be retained in this study as well) but we must say that this method was already extended to quadratic approximations in each cell [BF90].

3.4.2.1 Historical remark

In general, when we read numerical articles which use the MUSCL scheme, the authors often cite the paper by van Leer [vL79]. It is commonly believed in the scientific commu-

⁶MUSCL stands for monotone upstream-centered scheme for conservation laws.

nity that B. van Leer was first to propose the gradient reconstruction and slope limiting ideas. Unfortunately, because of political reasons, the works of N.E. Kolgan [Kol72, Kol75] remained unknown for a long time. We would like to underline the fact that the first publication of Kolgan came out seven years before van Leer's paper. Van Leer seems to be aware of this situation since in his recent review paper [vL06] one can find "A historical injustice" section:

"It has been pointed out to me by Dr. Vladimir Sabelnikov, formerly of TsAGI, the Central Aerodynamical National Laboratory near Moscow, that a scheme closely resembling MUSCL (including limiting) was developed in this laboratory by V. P. Kolgan (1972). Kolgan died young; his work apparently received little notice outside TsAGI."

Thus, it is desirable to correctly attribute this result in future publications.

3.4.3 TVD and MUSCL schemes

There is a property of scalar nonlinear conservation laws, which was probably observed for the first time by Peter Lax [Lax73]:

The total increasing and decreasing variations of a differentiable solution between any pair of characteristics are conserved.

In the presence of shock waves, information is lost and the total variation decreases. For compactly supported or periodic solutions, one can establish the following inequality

$$\int_{-\infty}^{+\infty} |du(x, t_2)| \leq \int_{-\infty}^{+\infty} |du(x, t_1)|, \quad t_2 \geq t_1. \quad (3.22)$$

This motivated Harten [Har83] to introduce the notion of discrete total variation of numerical solution $u_h := \{u_j\}$

$$TV(u_h) := \sum_j |u_{j+1} - u_j|,$$

and the discrete counterpart to (3.22)

$$TV(u_h^{n+1}) \leq TV(u_h^n).$$

If this property is fulfilled we say that a finite volume scheme is total variation diminishing (TVD). The following theorem was proved in [Har83]:

Theorem 1 (i): *Monotone schemes are TVD*

(ii): *TVD schemes are monotonicity preserving, i.e. the number of solution extrema is preserved in time.*

Remark 11 *From the mathematical point of view it would be more correct to say “the total variation non-increasing (TVNI) scheme” but the “wrong” term TVD is generally accepted in the scientific literature.*

In one space dimension the construction of TVD schemes is not a problem anymore. Let us recall that in this study we are rather interested in two space dimensions (or even three in future work). In these cases the situation is considerably more complicated. Even if we consider the simplest case of structured cartesian meshes and apply a 1D TVD scheme on a dimension-by-dimension basis, a result of Goodman and Leveque shows [GV85] that TVD schemes in two or more space dimensions are only first order accurate. Motivated by this negative result, weaker conditions yielding solution monotonicity preservation should be developed.

In this chapter we will describe the construction and practical implementation of a second-order nonlinear scheme on unstructured (possibly highly distorted) meshes. The main idea is to find our solution as a piecewise affine function on each cell. This kind of linear reconstruction operators on simplicial control volumes often exploit the fact that the cell average is also a pointwise value of any valid (conservative) linear reconstruction evaluated at the gravity center of a simplex. This reduces the reconstruction problem to that of gradient estimation given cell averaged data. In this case, we express the reconstruction in the form

$$\mathbf{w}_K(\vec{x}) = \bar{\mathbf{w}}_K + (\nabla \mathbf{w})_K \cdot (\vec{x} - \vec{x}_0), \quad K \in \mathcal{T}, \quad (3.23)$$

where $\bar{\mathbf{w}}_K$ is the cell averaged value given by finite volume method, $(\nabla \mathbf{w})_K$ is the solution gradient estimation (to be determined) on the cell K , $\vec{x} \in K$ and the point \vec{x}_0 is chosen to be the gravity center for the simplex K .

It is very important to note that with this type of representation (3.23) we remain absolutely conservative, i.e.

$$\frac{1}{\text{vol}(K)} \int_K \mathbf{w}_K(\vec{x}) \, d\Omega \equiv \bar{\mathbf{w}}_K$$

due to the choice of the point \vec{x}_0 . This point is crucial for finite volumes because of intrinsic conservative properties of this method.

In next sections we describe briefly two common techniques: Green-Gauss integration and least squares methods for solution gradient estimation on each cell. There are other

available techniques. We can mention here an implicit gradient reconstruction method proposed in [MG96] and reused later in [AMS04], for example. We decided not to implement this approach in our research code since this procedure is computationally expensive⁷.

3.4.3.1 Green-Gauss gradient reconstruction

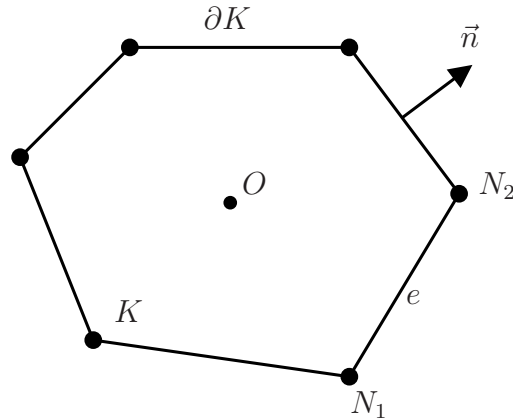


Figure 3.7: Illustration for Green-Gauss gradient reconstruction. Control volume K with barycenter O and exterior normal \vec{n} .

This gradient reconstruction technique can be easily implemented on simplicial meshes. It is based on two very simple ideas: the mean value approximation and Green-Gauss-Ostrogradsky formula.

Consider a control volume K with barycenter O . The exterior normal to an edge $e \in \partial K$ is denoted by \vec{n}_e . This configuration is depicted on Figure 3.7. In order to estimate the solution gradient on K (or in other words, to estimate its value at gravity center O) we make the following mean value approximation

$$(\nabla \mathbf{w})_K = (\nabla \mathbf{w})|_O \cong \frac{1}{\text{vol}(K)} \int_K \nabla \mathbf{w} \, d\Omega,$$

and if we apply Green-Gauss-Ostrogradsky formula

$$(\nabla \mathbf{w})_K \cong \frac{1}{\text{vol}(K)} \int_{\partial K} \mathbf{w} \otimes \vec{n} \, d\sigma = \frac{1}{\text{vol}(K)} \sum_{e \in \partial K} \int_e \mathbf{w} \otimes \vec{n}_e \, d\sigma \cong \sum_{e \in \partial K} \frac{\text{area}(e)}{\text{vol}(K)} \mathbf{w}|_{e/2} \otimes \vec{n}_e,$$

⁷In order to reconstruct the solution gradient we have to solve a linear system of equations. Recall that the gradient is estimated at each time step on each control volume. This factor slows down considerably explicit time discretizations.

where $\mathbf{w}|_{e/2}$ denote the solution value at the face (or edge in 2D) centroid. The face value needed to compute the reconstruction gradient can be obtained from a weighted average of the values at the vertices on the face [HC89]. In 2D it simply becomes

$$\mathbf{w}|_{e/2} = \frac{\mathbf{w}_{N_1} + \mathbf{w}_{N_2}}{2}.$$

This approximation yields the following formula for gradient estimation:

$$(\nabla \mathbf{w})_K \cong \sum_{e \in \partial K} \frac{\text{area}(e)}{\text{vol}(K)} \frac{(\mathbf{w}_{N_1} + \mathbf{w}_{N_2})}{2} \otimes \vec{n}_e.$$

The gradient calculation is exact whenever the numerical solution varies linearly over the support of the reconstruction.

This procedure requires the knowledge of the solution values at the mesh nodes $\{N_i\}$. Recall that a cell centered finite volume scheme provides us with data located at cell gravity centers. Thus, an interpolation technique is needed. We have to say that the quality of Green-Gauss gradient reconstruction greatly depends on the chosen interpolation method. The method retained in this study is explained in Section 3.4.5.

3.4.3.2 Least-squares gradient reconstruction method

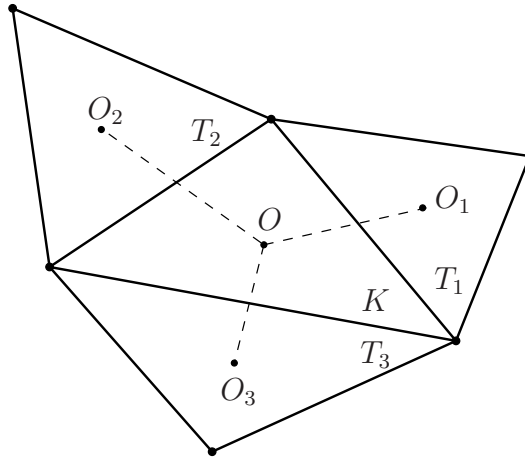


Figure 3.8: Illustration for least-squares gradient reconstruction. We depict a triangle control volume with three adjacent neighbors.

In this section we consider a triangle⁸ control volume K with three adjacent neighbors T_1 , T_2 and T_3 . Their barycenters are denoted by $O(\vec{x}_0)$, $O_1(\vec{x}_1)$, $O_2(\vec{x}_2)$ and $O_3(\vec{x}_3)$

⁸Generalization to other simplicial control volumes is straightforward.

respectively. In the following we denote by \mathbf{w}_i the solution value at gravity centers O_i :

$$\mathbf{w}_i := \mathbf{w}(\vec{x}_i), \quad \mathbf{w}_0 := \mathbf{w}(\vec{x}_0).$$

Our purpose here is to estimate $\nabla \mathbf{w} = (\partial_x \mathbf{w}, \partial_y \mathbf{w})$ on the cell K . Using Taylor formula, we can write down the three following relations:

$$\mathbf{w}_1 - \mathbf{w}_0 = (\nabla \mathbf{w})_K \cdot (\vec{x}_1 - \vec{x}_0) + \mathcal{O}(h^2), \quad (3.24)$$

$$\mathbf{w}_2 - \mathbf{w}_0 = (\nabla \mathbf{w})_K \cdot (\vec{x}_2 - \vec{x}_0) + \mathcal{O}(h^2), \quad (3.25)$$

$$\mathbf{w}_3 - \mathbf{w}_0 = (\nabla \mathbf{w})_K \cdot (\vec{x}_3 - \vec{x}_0) + \mathcal{O}(h^2). \quad (3.26)$$

If we drop higher order terms $\mathcal{O}(h^2)$, these relations can be viewed as a linear system of three equations for two unknowns⁹ $(\partial_x \mathbf{w}, \partial_y \mathbf{w})$. This situation is due to the fact that the number of edges incident to a simplex mesh in \mathbb{R}^d is greater or equal (in this case see Remark 12) to d thereby producing linear constraint equations (3.24) – (3.26) which will be solved analytically here in a least squares sense.

First of all, each constraint (3.24) – (3.26) is multiplied by a weight $\omega_i \in (0, 1)$ which will be chosen below to account for distorted meshes. In matrix form our non-square system becomes

$$\begin{pmatrix} \omega_1 \Delta x_1 & \omega_1 \Delta y_1 \\ \omega_2 \Delta x_2 & \omega_2 \Delta y_2 \\ \omega_3 \Delta x_3 & \omega_3 \Delta y_3 \end{pmatrix} (\nabla \mathbf{w})_K = \begin{pmatrix} \omega_1 (\mathbf{w}_1 - \mathbf{w}_0) \\ \omega_2 (\mathbf{w}_2 - \mathbf{w}_0) \\ \omega_3 (\mathbf{w}_3 - \mathbf{w}_0) \end{pmatrix},$$

where $\Delta x_i = x_i - x_0$, $\Delta y_i = y_i - y_0$. For further developments it is convenient to rewrite our constraints in abstract form

$$[\vec{L}_1, \vec{L}_2] \cdot (\nabla \mathbf{w})_K = \vec{f}. \quad (3.27)$$

We use a normal equation technique in order to solve symbolically this abstract form in a least squares sense. Multiplying on the left both sides of (3.27) by $[\vec{L}_1, \vec{L}_2]^t$ yields

$$G(\nabla \mathbf{w})_K = \vec{b}, \quad G = (l_{ij})_{1 \leq i, j \leq 2} = \begin{pmatrix} (\vec{L}_1 \cdot \vec{L}_1) & (\vec{L}_1 \cdot \vec{L}_2) \\ (\vec{L}_2 \cdot \vec{L}_1) & (\vec{L}_2 \cdot \vec{L}_2) \end{pmatrix} \quad (3.28)$$

where G is the Gram matrix of vectors $\{\vec{L}_1, \vec{L}_2\}$ and $\vec{b} = \begin{pmatrix} (\vec{L}_1 \cdot \vec{f}) \\ (\vec{L}_2 \cdot \vec{f}) \end{pmatrix}$. The so-called normal equation (3.28) is easily solved by Cramer's rule to give the following result

$$(\nabla \mathbf{w})_K = \frac{1}{l_{11}l_{22} - l_{12}^2} \begin{pmatrix} l_{22}(\vec{L}_1 \cdot \vec{f}) - l_{12}(\vec{L}_2 \cdot \vec{f}) \\ l_{11}(\vec{L}_2 \cdot \vec{f}) - l_{12}(\vec{L}_1 \cdot \vec{f}) \end{pmatrix}.$$

⁹This simple estimation is done for scalar case only $\mathbf{w} = (w)$. For more general vector problems the numbers of equations and unknowns have to be changed depending on the dimension of vector \mathbf{w} .

The form of this solution suggests that the least squares linear reconstruction can be efficiently computed without the need for storing a non-square matrix.

Now we have to discuss the choice of weight coefficients $\{\omega_i\}_{i=1}^3$. The basic idea is to attribute bigger weights to cells barycenters closer to the node N under consideration. One of the possible choices consists in taking a harmonic mean of respective distances $r_i = \|\vec{x}_i - \vec{x}_N\|$. This purely metric argument takes the following mathematical form:

$$\omega_i = \frac{\|\vec{x}_i - \vec{x}_N\|^{-k}}{\sum_{j=1}^3 \|\vec{x}_j - \vec{x}_N\|^{-k}},$$

where k in practice is taken to be one or two (in our numerical code we choose $k = 1$).

Remark 12 *When we have a triangle sharing an edge with boundary $\partial\Omega$ (see Figure 3.13 for illustration), the gradient reconstruction procedure becomes even simpler, since the number of constraints is equal to d and linear system (3.24) – (3.26) becomes completely determined:*

$$\begin{aligned} \mathbf{w}_1 - \mathbf{w}_0 &= (\nabla \mathbf{w})_K \cdot (\vec{x}_1 - \vec{x}_0) + \mathcal{O}(h^2), \\ \mathbf{w}_2 - \mathbf{w}_0 &= (\nabla \mathbf{w})_K \cdot (\vec{x}_2 - \vec{x}_0) + \mathcal{O}(h^2), \end{aligned}$$

or in componentwise form it reads

$$\begin{pmatrix} x_1 - x_0 & y_1 - y_0 \\ x_2 - x_0 & y_2 - y_0 \end{pmatrix} (\nabla \mathbf{w})_K = \begin{pmatrix} \mathbf{w}_1 - \mathbf{w}_0 \\ \mathbf{w}_2 - \mathbf{w}_0 \end{pmatrix}.$$

The unique solution to this linear system is given again by Cramer's rule

$$(\nabla \mathbf{w})_K = \frac{\begin{pmatrix} (y_2 - y_0)(\mathbf{w}_1 - \mathbf{w}_0) - (y_1 - y_0)(\mathbf{w}_2 - \mathbf{w}_0) \\ (x_1 - x_0)(\mathbf{w}_2 - \mathbf{w}_0) - (x_2 - x_0)(\mathbf{w}_1 - \mathbf{w}_0) \end{pmatrix}}{(x_1 - x_0)(y_2 - y_0) - (x_2 - x_0)(y_1 - y_0)}.$$

3.4.3.3 Slope limiter

The idea of incorporating limiter functions to obtain non-oscillatory resolution of discontinuities and steep gradients dates back to Boris and Book [BB73]. When the limiter is identically equal to 1, we have the unlimited form of the linear interpolation. In the 1D case one can easily find in the literature about 15 different limiter functions such as CHARM, minmod, superbee, van Albada and many others. On unstructured meshes the situation is quite different. In the present study we decided to retain the Barth-Jespersen limiter proposed in [BJ89]. Here we do not discuss its construction and properties but just give the final formula. We need to introduce the following notation

$$\mathbf{w}_K^{min} := \min_{L \in \mathcal{N}(K)} \mathbf{w}_L, \quad \mathbf{w}_K^{max} := \max_{L \in \mathcal{N}(K)} \mathbf{w}_L.$$

The limited version of (3.23) is given by the following modified reconstruction operator

$$\mathbf{w}_K(\vec{x}) = \bar{\mathbf{w}}_K + \alpha_K (\nabla \mathbf{w})_K \cdot (\vec{x} - \vec{x}_0), \quad K \in \mathcal{T},$$

where it is assumed that $\alpha_K \in [0, 1]$. Obviously, the choice $\alpha_K = 0$ corresponds to the first order scheme while $\alpha_K = 1$ is the unlimited form. Barth and Jespersen [BJ89] propose the following choice of α_K :

$$\alpha_K^{BJ} := \min_{\forall f \in \partial K} \begin{cases} \frac{\mathbf{w}_K^{max} - \bar{\mathbf{w}}_K}{\mathbf{w}_K(\vec{x}_f) - \bar{\mathbf{w}}_K} & \text{if } \mathbf{w}_K(\vec{x}_f) > \mathbf{w}_K^{max}, \\ \frac{\mathbf{w}_K^{min} - \bar{\mathbf{w}}_K}{\mathbf{w}_K(\vec{x}_f) - \bar{\mathbf{w}}_K} & \text{if } \mathbf{w}_K(\vec{x}_f) < \mathbf{w}_K^{min}, \\ 1 & \text{otherwise.} \end{cases}$$

where \vec{x}_f denotes the face f centroid.

Although this limiter function does not fulfill all the requirements of finite volume maximum principle on unstructured meshes [BO04], it can be shown that it yields finite volume schemes possessing a global extremum diminishing property. Also this limiter produces the least amount of slope reduction which can be advantageous for accuracy. Note that in practical implementation little modifications are required to prevent near zero division for almost constant solution data.

3.4.4 Diffusive fluxes computation

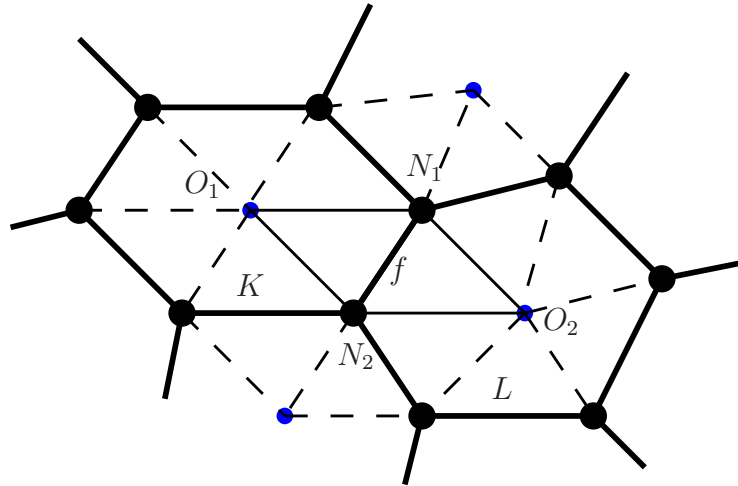


Figure 3.9: Diamond cell constructed around face f .

In this section we briefly describe a method for diffusive fluxes discretization. It was proposed for non-conforming cartesian meshes in [Coi94] and rigorous justification was given later in [CVV99].

When we look at the integral conservation law (3.20) for control volume K , the diffusion term has the following form:

$$\frac{1}{\text{vol}(K)} \sum_{f \in \partial K} \int_f (\mathcal{D} \nabla \mathbf{w}) \cdot \vec{n}_f \, d\sigma,$$

where the integration is performed along all the faces of the cell K . The quantity $(\mathcal{D} \nabla \mathbf{w})$ is called the diffusion flux and should be properly discretized in this section. The diffusion matrix \mathcal{D} is given by physical properties, while \vec{n}_{KL} is determined by mesh geometry. The last integral can be further simplified by applying a second order Gauss quadrature¹⁰:

$$\sum_{f \in \partial K} \frac{\text{area}(f)}{\text{vol}(K)} \mathcal{D} (\nabla \mathbf{w}|_{f/2}) \cdot \vec{n}_f.$$

Thus, in order to compute the diffusive flux, we have just to estimate the solution gradient $\nabla \mathbf{w}$ but this time on the face centroid denoted by $f/2$. In order to express it in terms of cell averages $\{\mathbf{w}_L\}_{L \in \mathcal{T}}$ we apply once again Green-Gauss technique.

We have to start by constructing a dual mesh \mathcal{T}^* . It is composed of diamond cells created around each interior face (diffusive flux computation through a boundary face is another topic which is briefly discussed in Remark 13). Consider two simplicial control volumes K and L with barycenters O_1 and O_2 respectively. These volumes share a common face (or an edge in 2D) f with nodes N_1, N_2, \dots . We denote by f^\diamond the diamond cell associated to the face f . This situation is schematically depicted on Figure 3.9. For the sake of clarity we construct the diamond cell in the 2D case. In the present study we choose f^\diamond as the closed polygon formed by nodes $N_1 O_1 N_2 O_2 N_1$ (see Figure 3.9). Once the diamond cell is defined, we can apply to its boundary the Green-Gauss method (see Section 3.4.3.1):

$$\begin{aligned} (\nabla \mathbf{w}|_{f/2}) &\cong \frac{1}{\text{vol}(f^\diamond)} \int_{f^\diamond} \nabla \mathbf{w} \, d\Omega = \frac{1}{\text{vol}(f^\diamond)} \sum_{\ell \in \partial f^\diamond} \int_{f^\diamond} \mathbf{w} \otimes \vec{n}_\ell \, d\sigma \cong \\ &\sum_{\ell \in \partial f^\diamond} \frac{\text{area}(\ell)}{\text{vol}(f^\diamond)} (\nabla \mathbf{w}|_{f/2}) \otimes \vec{n}_\ell \cong \sum_{\ell \in \partial f^\diamond} \frac{\text{area}(\ell)}{\text{vol}(f^\diamond)} \frac{(\mathbf{w}_{P_1} + \mathbf{w}_{P_2})}{2} \otimes \vec{n}_\ell, \end{aligned}$$

where $\ell \in \{N_1 O_1, O_1 N_2, N_2 O_2, O_2 N_1\}$ and $P_{1,2} \in \{N_1, O_1, N_2, O_2\}$.

Remark 13 *There is a little question omitted in this section. We have not discussed the implementation of boundary conditions for diffusive fluxes. Actually it is rather a complicated topic. We assume that in our physical problems viscosity plays a secondary role. Consider a control volume L having a face ℓ on the boundary $\partial\Omega$. For the time being*

¹⁰In 1D it simply degenerates to a very well known middle point rule $\int_{-1}^1 g(x) \, dx \cong 2g(0)$.

we impose a Neumann type condition on diffusive fluxes. After discretization this condition takes the following form:

$$(\mathcal{D}\nabla\mathbf{w}_\ell) \cdot \vec{n} := (\mathcal{D}\nabla\mathbf{w}_L) \cdot \vec{n}.$$

In other words it means that the gradient on the boundary is replaced by its value on the cell L .

3.4.5 Solution interpolation to mesh nodes

We have seen above that several gradient reconstruction procedures (in particular gradient estimation on the faces) require the knowledge of the solution at mesh nodes (or vertices). This information is not directly given by the finite volume method since we retained the cell-centered approach.

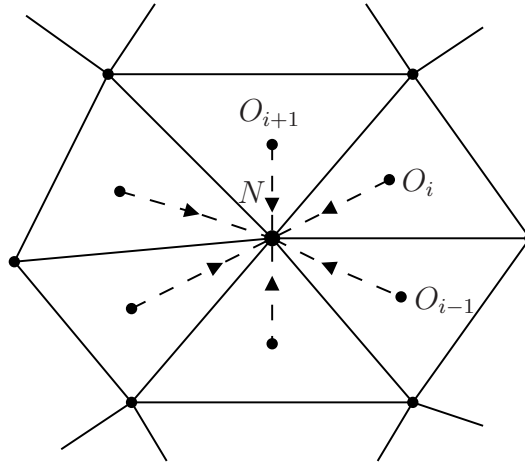


Figure 3.10: Triangles with their barycenters O_i sharing the same vertex N .

Let us consider a node $N(x_n, y_n)$ of the tessellation \mathcal{T} and a control volume K_i with barycenter $O_i(x_i, y_i)$ having this node as a vertex (see Figure 3.10 for illustration). The MUSCL procedure provides us solution gradient on each cell. Thus, using the Taylor formula or, equivalently, representation (3.23) we can estimate the solution value at the node N

$$\mathbf{w}_N = \bar{\mathbf{w}}_{K_i} + (\nabla\mathbf{w})_{K_i} \cdot (\vec{x}_N - \vec{x}_i). \quad (3.29)$$

The problem is that we will have $d(N)$ different values of the solution in the same point depending on the control volume under consideration. Here $d(N)$ is the degree of vertex N in the sense of graph theory. One of the possible ways to overcome this contradiction is the averaging. One interesting technique was proposed in [HC89] and further improved in

[KMC03]. In our turn, we slightly modified this method. The algorithm implemented in our code is briefly described here.

First of all, let us look for the vertex value $\bar{\mathbf{w}}_N$ as a weighted sum of the values \mathbf{w}_{N_i} computed by formula (3.29) from each surrounding cell

$$\bar{\mathbf{w}}_N = \frac{\sum_{i=1}^{d(N)} \omega_i \mathbf{w}_{N_i}}{\sum_{i=1}^{d(N)} \omega_i}.$$

The weighting factors $\{\omega_i\}_{i=1}^{d(N)}$ are made to satisfy the condition of zero pseudo-Laplacian

$$L(x_n) \equiv \sum_{i=1}^{d(N)} \omega_i (x_i - x_n), \quad L(y_n) \equiv \sum_{i=1}^{d(N)} \omega_i (y_i - y_n). \quad (3.30)$$

These conditions have a very simple interpretation. They are imposed so that the method be exact for affine data over the stencil.

As in the original formulation by Holmes and Connell [HC89], the weighting factor ω_i is written as

$$\omega_i = 1 + \Delta\omega_i.$$

The weights $\{\omega_i\}$ are determined by solving an optimization problem in which the cost-function to be minimized is defined as

$$\frac{1}{2} \sum_{i=1}^{d(N)} (r_i \Delta\omega_i)^2 \rightarrow \min \quad (3.31)$$

with two constraints given by (3.30). It should be noted that the cost function is slightly different from the original formulation. The difference lies in the factor of

$$r_i^2 \equiv \|\vec{ON} - \vec{OO}_i\|^2$$

which was introduced in [KMC03]. This modification effectively allows larger values of weight $\Delta\omega_i$ for those cells closer to the node in question.

Employing the method of Lagrange multipliers, the original optimization problem, which was to minimize the cost function given by (3.31) with the constraints (3.30) is equivalent to minimizing the function \mathcal{L} defined by

$$\mathcal{L} = \frac{1}{2} \sum_{i=1}^{d(N)} (r_i \Delta\omega_i)^2 - \lambda \sum_{i=1}^{d(N)} \omega_i (x_i - x_n) - \mu \sum_{i=1}^{d(N)} \omega_i (y_i - y_n) \rightarrow \min$$

which leads to

$$\Delta\omega_i = \frac{\lambda(x_i - x_n) + \mu(y_i - y_n)}{r_i^2}.$$

The two Lagrangian multipliers, λ and μ , are obtained from

$$\lambda = \frac{r_y I_{xy} - r_x I_{yy}}{I_{xx} I_{yy} - I_{xy}^2}, \quad \mu = \frac{r_x I_{xy} - r_y I_{xx}}{I_{xx} I_{yy} - I_{xy}^2},$$

where

$$r_x = \sum_{i=1}^{d(N)} (x_i - x_n), \quad r_y = \sum_{i=1}^{d(N)} (y_i - y_n).$$

$$I_{xx} = \sum_{i=1}^{d(N)} \frac{(x_i - x_n)^2}{r_i^2}, \quad I_{yy} = \sum_{i=1}^{d(N)} \frac{(y_i - y_n)^2}{r_i^2}, \quad I_{xy} = \sum_{i=1}^{d(N)} \frac{(x_i - x_n)(y_i - y_n)}{r_i^2}.$$

The last step consists in renormalizing the weights $\{\omega_i\}_{i=1}^{d(N)}$ to the range $[0, 1]$.

Remark 14 *The above algorithm is not computationally expensive since the weights $\{\omega_i\}_{i=1}^{d(N)}$ depend only on the tessellation \mathcal{T} geometry. It means that they can be computed and stored before the main loop in time and reused during the computations later.*

Remark 15 *Even if we suggest to use the above method (since it gives slightly better results), we would like to give another idea (based on a purely metrics argument) of how to construct the weights $\{\omega_i\}_{i=1}^{d(N)}$. This approach is considerably simpler than optimization problem solving and it was already used in the least squares gradient reconstruction method (see Section 3.4.3.2). In fact, in order to calculate ω_i one can simply take the harmonic mean of distances between the node N under the question and respective cell barycenter O_i (see Figure 3.10):*

$$\omega_i := \frac{||\vec{x}_N - \vec{x}_i||^{-k}}{\sum_{j=1}^{d(N)} ||\vec{x}_N - \vec{x}_j||^{-k}},$$

where k in practice is taken 1 or 2.

We have to say that this choice does not guarantee exact interpolation of globally linear functions.

3.4.6 Time stepping methods

In previous sections we considered the spatial discretization procedure with a finite-volume scheme. It is a common practice in solving time-dependent PDEs to first discretize the spatial variables. This approach is called a method of lines:

$$u_t + \partial_x f(u) = S(u) \xrightarrow{\text{FV}} u_t = \mathcal{L}(u) \quad (3.32)$$

In order to obtain a fully discrete scheme, we have to discretize the time evolution operator. In the present work we decided to retain the so-called Strong Stability-Preserving (SSP)

time discretization methods described in [Shu88, GST01, SR02]. Historically these methods were initially called Total Variation Diminishing (TVD) time discretizations.

The main idea behind SSP methods is to assume that the first order forward Euler method is strongly stable (see the definition below) under a certain norm for our method of lines ODE (3.32). Then, we try to find a higher order scheme. Usually the relevant norm is the total variation¹¹ norm:

$$\text{TV}(u^n) := \sum_j |u_j^n - u_{j-1}^n|$$

and TVD discretizations have the property $\text{TV}(u^{n+1}) \leq \text{TV}(u^n)$.

Remark 16 *Special approaches are needed for hyperbolic PDEs since they contain discontinuous solutions and the usual linear stability analysis is inadequate. Thus a stronger measure of stability is usually required:*

Definition 1 *A sequence $\{u^n\}$ is said to be **strongly stable** in a given norm $\|\cdot\|$ provided that $\|u^{n+1}\| \leq \|u^n\|$ for all $n \geq 0$.*

A general m -stage Runge-Kutta method for (3.32) can be written in the form

$$u^{(0)} = u^n, \tag{3.33}$$

$$u^{(i)} = \sum_{k=0}^{i-1} \left(\alpha_{i,k} u^{(k)} + \Delta t \beta_{i,k} \mathcal{L}(u^{(k)}) \right), \quad \alpha_{i,k} \geq 0, \quad i = 1, \dots, m, \tag{3.34}$$

$$u^{n+1} = u^{(m)}. \tag{3.35}$$

In [SO88] the following result is proved

Theorem 2 *If the forward Euler method is strongly stable under the CFL restriction $\Delta t \leq \Delta t_{FE}$*

$$\|u^n + \Delta t \mathcal{L}(u^n)\| \leq \|u^n\|,$$

then the Runge-Kutta method (3.33) – (3.35) with $\beta_{i,k} \geq 0$ is SSP, $\|u^{n+1}\| \leq \|u^n\|$, provided the following CFL restriction is fulfilled:

$$\Delta t \leq c \Delta t_{FE}, \quad c = \min_{i,k} \frac{\alpha_{i,k}}{\beta_{i,k}}.$$

Here we give a few examples of SSP schemes which are commonly used in applications:

¹¹We have to say that the notion of total variation is used essentially for one-dimensional discrete solutions.

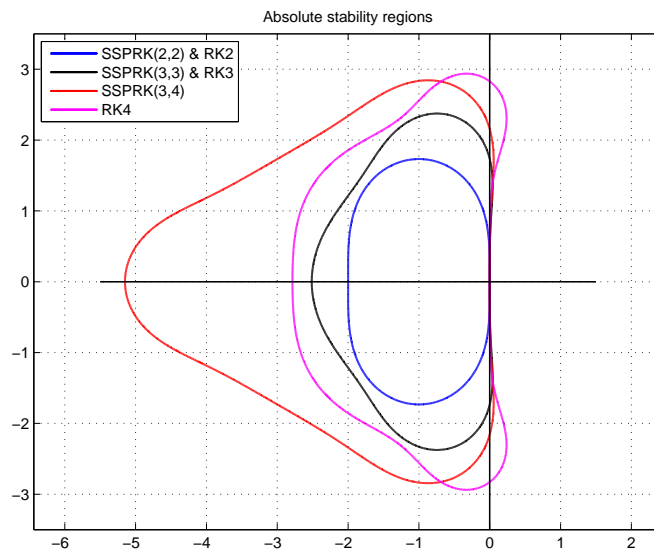


Figure 3.11: Linear absolute stability regions for different time stepping methods

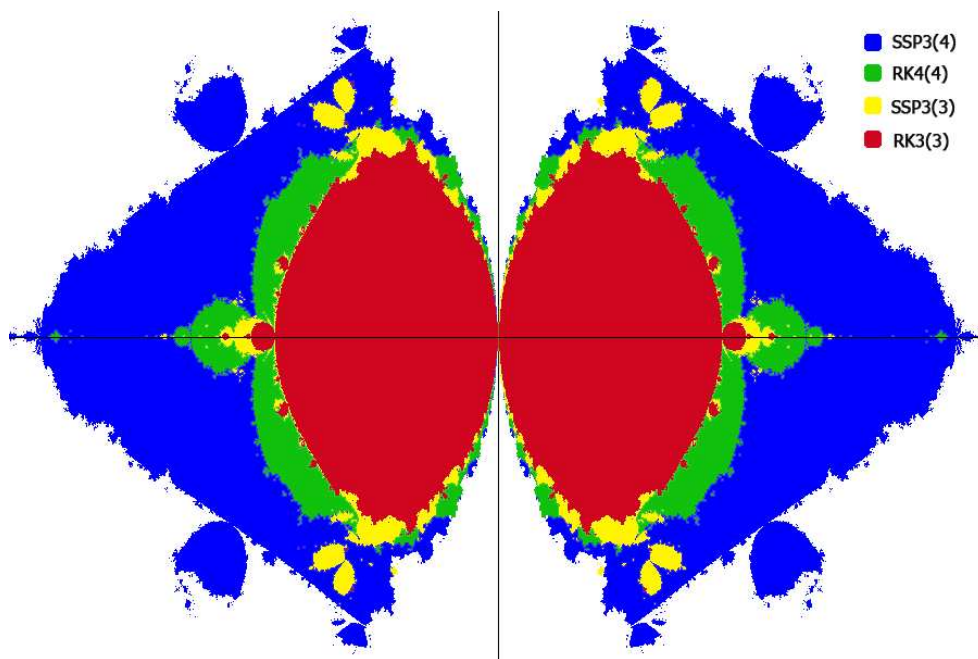


Figure 3.12: Nonlinear absolute stability regions

- Optimal¹² second order two-stage SSP-RK(2,2) scheme with CFL = 1:

$$\begin{aligned} u^{(1)} &= u^{(n)} + \Delta t \mathcal{L}(u^{(n)}), \\ u^{(n+1)} &= \frac{1}{2}u^{(n)} + \frac{1}{2}u^{(1)} + \frac{1}{2}\Delta t \mathcal{L}(u^{(1)}); \end{aligned}$$

- Optimal third order three-stage SSP-RK(3,3) scheme with CFL = 1:

$$\begin{aligned} u^{(1)} &= u^{(n)} + \Delta t \mathcal{L}(u^{(n)}), \\ u^{(2)} &= \frac{3}{4}u^{(n)} + \frac{1}{4}u^{(1)} + \frac{1}{4}\Delta t \mathcal{L}(u^{(1)}), \\ u^{(n+1)} &= \frac{1}{3}u^{(n)} + \frac{2}{3}u^{(2)} + \frac{2}{3}\Delta t \mathcal{L}(u^{(2)}); \end{aligned}$$

- Third order four-stage SSP-RK(3,4) scheme with CFL = 2:

$$\begin{aligned} u^{(1)} &= u^{(n)} + \frac{1}{2}\Delta t \mathcal{L}(u^{(n)}), \\ u^{(2)} &= u^{(1)} + \frac{1}{2}\Delta t \mathcal{L}(u^{(1)}), \\ u^{(3)} &= \frac{2}{3}u^{(n)} + \frac{1}{3}u^{(2)} + \frac{1}{6}\Delta t \mathcal{L}(u^{(n)}), \\ u^{(n+1)} &= u^{(3)} + \frac{1}{2}\Delta t \mathcal{L}(u^{(3)}). \end{aligned}$$

We depicted on Figures 3.11 and 3.12 the linear and nonlinear absolute stability regions of these schemes, and compared them with the classical Runge-Kutta methods respectively. Note that the linear absolute stability region for corresponding RK and SSP-RK schemes is the same. It is a consequence of linearization since these schemes are clearly different for nonlinear problems. That is why we decided to look also at nonlinear absolute stability [CP92].

We tested these different schemes in our numerical code and we decided to adopt SSP-RK(3,4) due to its accuracy and wide stability region. In our opinion this scheme represents a very good trade-off between precision and robustness.

3.4.7 Boundary conditions treatment

In this section we show how to implement the wall boundary condition in the finite volumes framework. The flavor of boundary conditions treatment for hyperbolic systems is given in Section A.2 and we refer to [GP05] for a general discussion.

¹²Optimality in the sense of CFL condition.

From the numerical point of view, we need to employ the boundary conditions when we have a control volume sharing a face (or an edge in 2D) with the computational domain boundary (see Figure 3.13 for illustration). In this situation, the numerical method must be provided by an additional information (such as the value of normal advective or diffusive fluxes on ∂K). Physical conditions completed if necessary by numerical ones allow us to reconstruct the normal flux $\mathcal{F} \cdot \vec{n}$ through the boundary face. Consider the case of a rigid wall boundary

$$\vec{u}(\vec{x}, t) \cdot \vec{n} = 0, \quad \vec{x} \in \partial\Omega, \quad (3.36)$$

and the hyperbolic system (3.1) – (3.3).

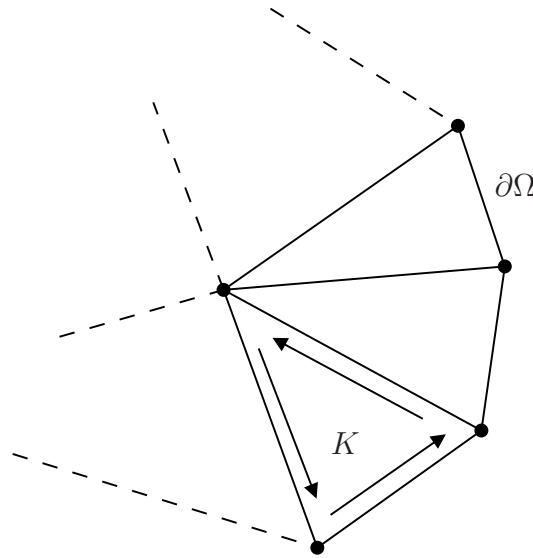


Figure 3.13: Control volume sharing a face with boundary $\partial\Omega$.

The advective flux¹³ through an oriented boundary face with exterior normal \vec{n} is given by (3.5)

$$\mathcal{F} \cdot \vec{n} = (\alpha^+ \rho^+ u_n, \alpha^- \rho^- u_n, \rho u u_n + p n_1, \rho v u_n + p n_2, \rho H u_n), \quad u_n \equiv \vec{u} \cdot \vec{n},$$

and if we take into account physical condition (3.36) it becomes

$$(\mathcal{F} \cdot \vec{n})|_{\vec{x} \in \partial\Omega} = (0, 0, p_b n_1, p_b n_2, 0), \quad p_b := p|_{\vec{x} \in \partial\Omega}$$

The last identity means that we need only to know the pressure value on the wall in order to reconstruct the advective flux $(\mathcal{F} \cdot \vec{n})|_{\vec{x} \in \partial\Omega}$.

¹³A few words about numerical boundary conditions for diffusive fluxes are given in Section 3.4.4

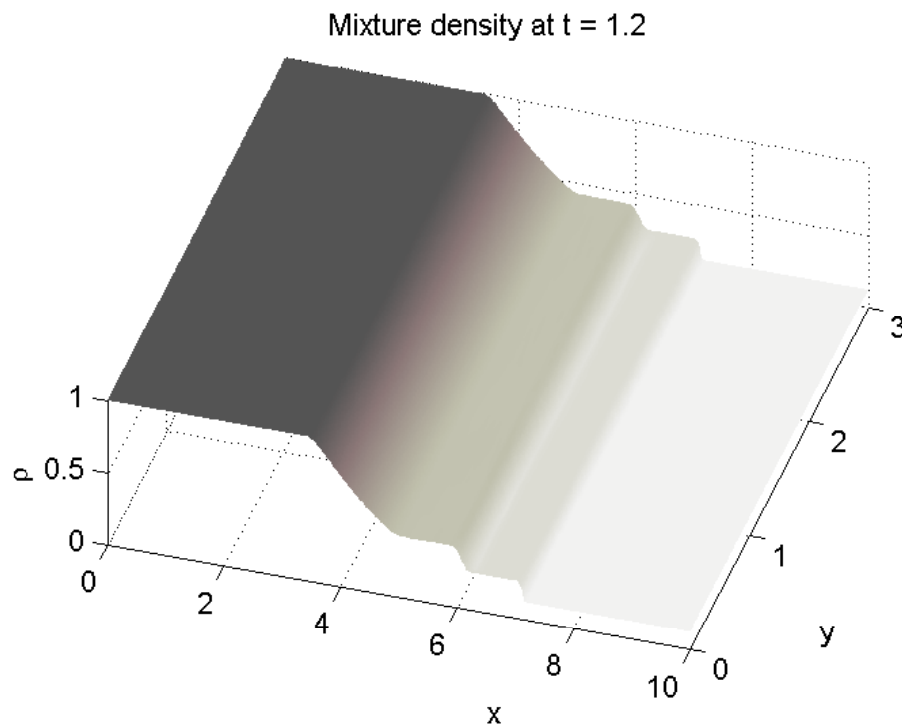


Figure 3.14: Shock tube of Sod. This plot represents the density.

After some straightforward computations (for more details see [GP05]) one establishes the following formula for the boundary pressure

$$p_b = p + \rho u_n c_s,$$

where the right-hand side is evaluated in the boundary cell center.

Remark 17 *The last formula has a very interesting physical interpretation. Actually, the boundary pressure p_b measures the force “exerted” by the wall in order to annihilate completely the normal velocity u_n .*

3.5 Numerical results

In this section we present a few test cases which show our research code performance. In order to reduce the document size, we decided not to put here classical test cases such as the shock tube of Sod [Sod78] etc. . The reader can believe us that our numerical code passed successfully these classical tests (see Figure 3.14).

3.5.1 Convergence test

We begin the presentation of numerical tests by the simplest one – convergence test. We would like to show the accuracy of the MUSCL scheme implementation. To do it, we solve numerically the following scalar linear advection equation

$$\frac{\partial v}{\partial t} + \vec{u}_0 \cdot \nabla v = 0, \quad \vec{u}_0 \in \mathbb{R}^2$$

with smooth¹⁴ initial conditions. Moreover, it has almost compact support in order to reduce the influence of boundary conditions. It is obvious that this equation will just translate the initial form in the direction \vec{u}_0 . So, we have an analytical solution which can be used to quantify the numerical method error. On the other hand, to measure the convergence rate, we constructed a sequence of refined meshes.

On Figure 3.15 we depict the error of numerical method in L_∞ norm as a function of the mesh characteristic size. The slope of these curves represents an approximation to the theoretical convergence rate. On this plot, the blue curve corresponds to the first order upwind scheme while the other two (red and black) correspond to the MUSCL scheme with least-squares (see Section 3.4.3.2) and Green-Gauss (see Section 3.4.3.1) gradient reconstruction procedures respectively. One can see that the blue curve slope is equal approximatively to 0.97 which means first order convergence. The other two curves have almost the same slope equal to 1.90 indicating a second order convergence rate for the MUSCL scheme. We remark that in our implementation of the second-order scheme the least-squares reconstruction seems to give slightly more accurate results than the Green-Gauss procedure.

The next figure represents the measured CPU time in seconds again as a function of the mesh size. Obviously, this kind of data is extremely computer dependent but the qualitative behaviour is the same on all systems. On Figure 3.16 one can see that the “fastest” curve is the blue one (first order upwind scheme). Then we have two almost superimposed (black and red) curves referring to the second-order gradient reconstruction on variables. Here again one can notice that the least-squares method is slightly faster than the Green-Gauss procedure. On this figure we represented one more curve (the highest one) which corresponds to Green-Gauss gradient reconstruction on fluxes (it seems to be very natural in the context of VFFC scheme). Our numerical tests show that this method is quite expensive from the computational point of view and we decided not to retain it.

¹⁴We intentionally choose a smooth initial condition since the discontinuities can decrease the overall accuracy of the scheme.

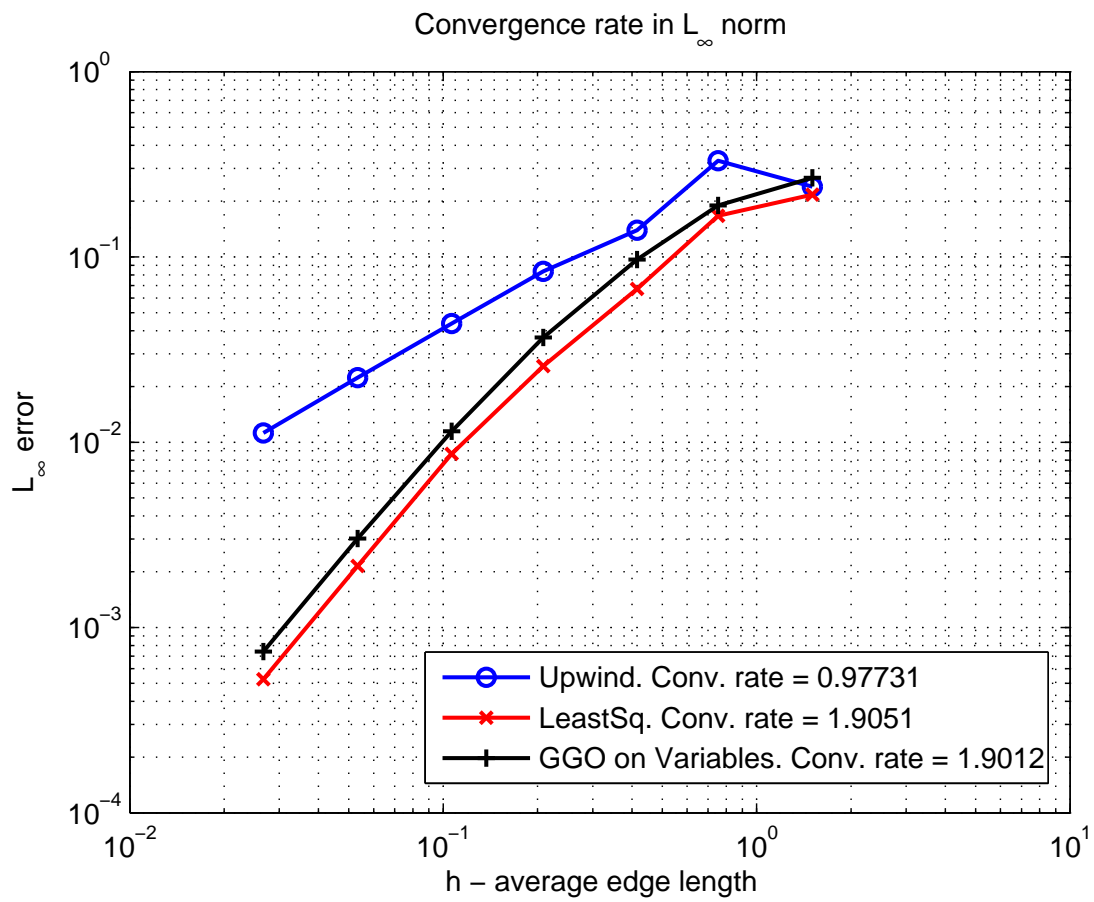


Figure 3.15: Numerical method error in L_∞ norm.

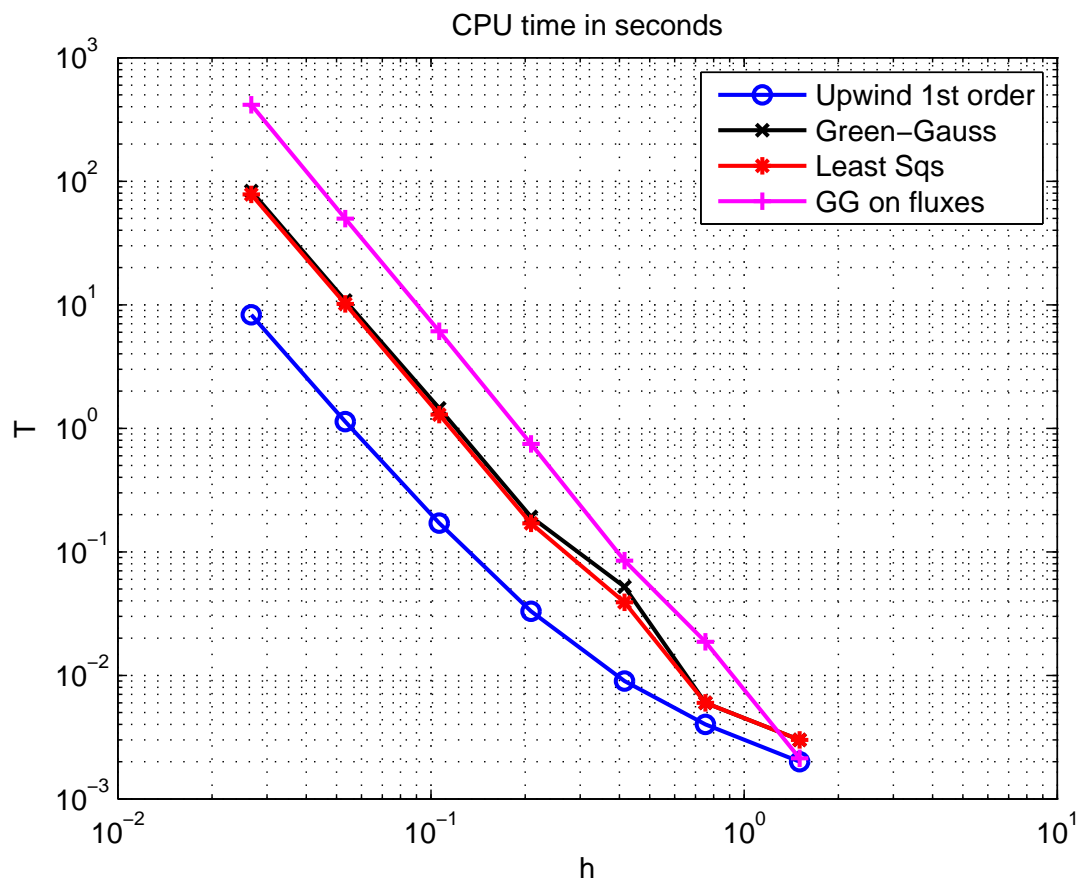


Figure 3.16: CPU time for different finite volume schemes.

3.5.2 Falling water column

The geometry and initial condition for this test case are depicted on Figure 3.17. Initially the velocity field is taken to be zero. The values of the other parameters are given in Table 3.1. The mesh used in this computation contained about 108000 control volumes (in this case it was triangles). The results of this simulation are presented on Figures 3.18 – 3.23.

On the other hand, we depicted on Figure 3.24 the maximal pressure on the right wall as a function of time:

$$t \mapsto \max_{(x,y) \in 1 \times [0,1]} p(x,y,t).$$

We performed another computation when gas was modelled as $\alpha^+ = 0.05$, $\alpha^- = 0.95$ mixture. The pressure is recorded as well and this result is plotted on Figure 3.25. One can see that the peak value is higher and the impact is more localised in time.

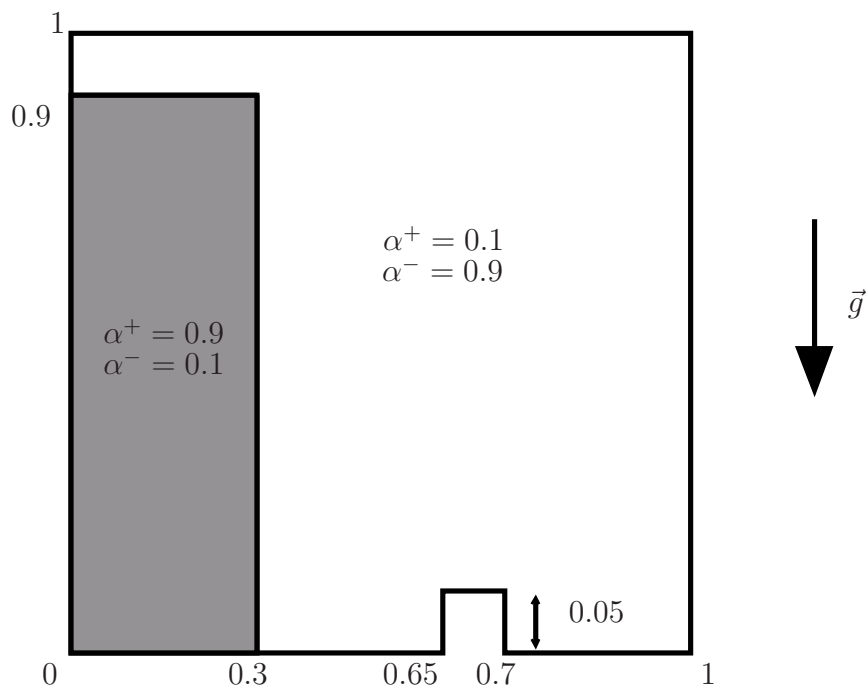


Figure 3.17: Falling water column test case. Geometry and initial condition.

3.5.3 Water drop test case

The geometry and initial condition for this test case are depicted on Figure 3.26. Initially the velocity field is taken to be zero. The values of the other parameters are given

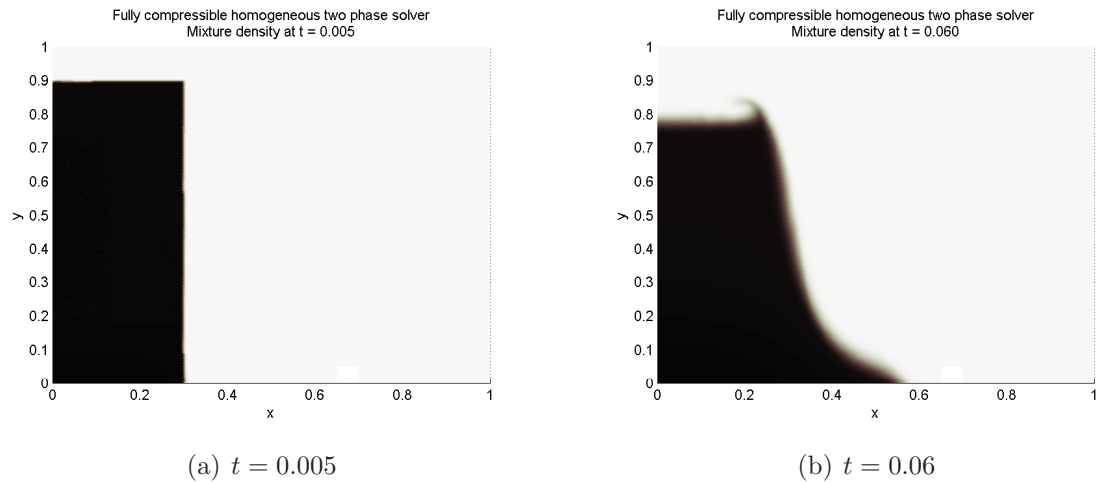


Figure 3.18: Falling water column test case. Initial condition and the beginning of column dropping process.

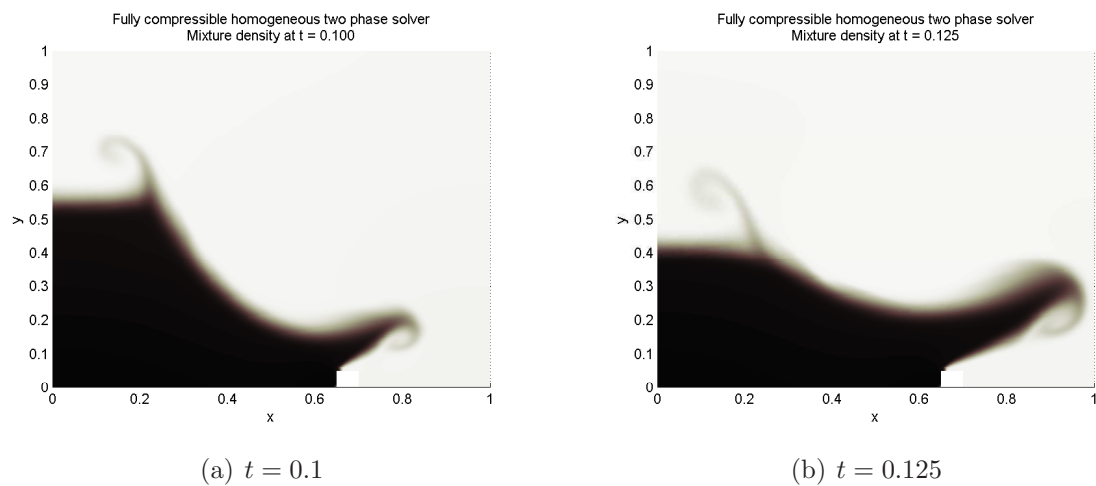


Figure 3.19: Falling water column test case. Splash creation due to the interaction with step.

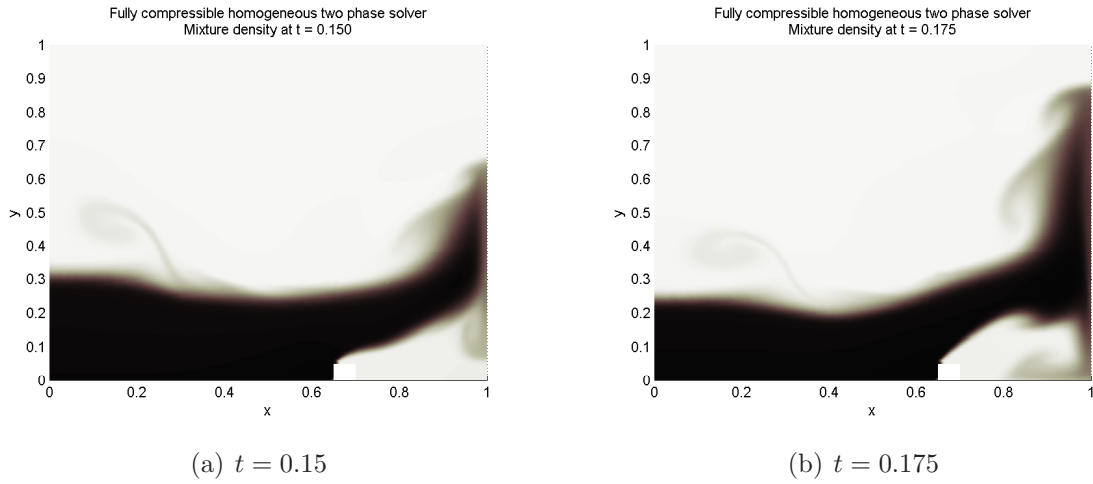


Figure 3.20: Falling water column test case. Water strikes the wall - I.

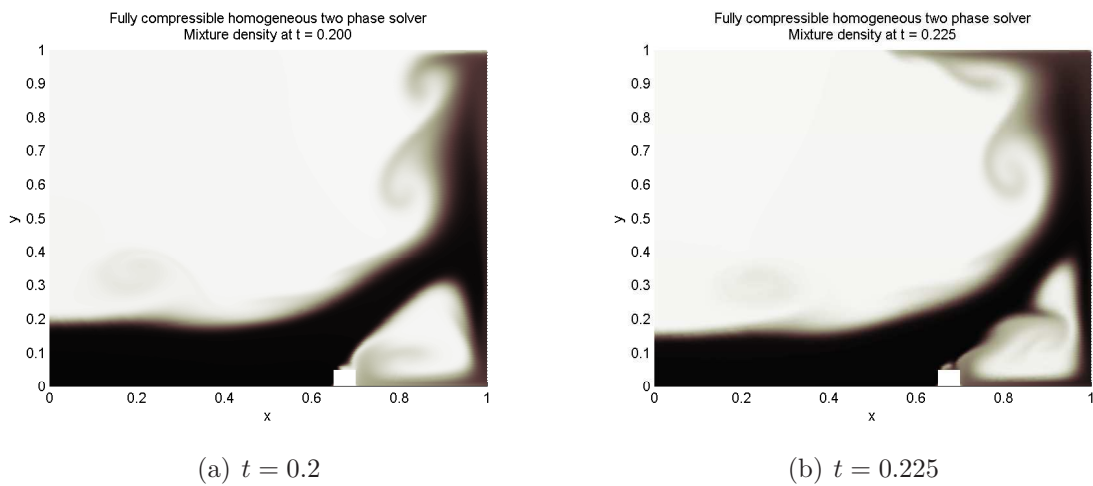


Figure 3.21: Falling water column test case. Water strikes the wall - II.

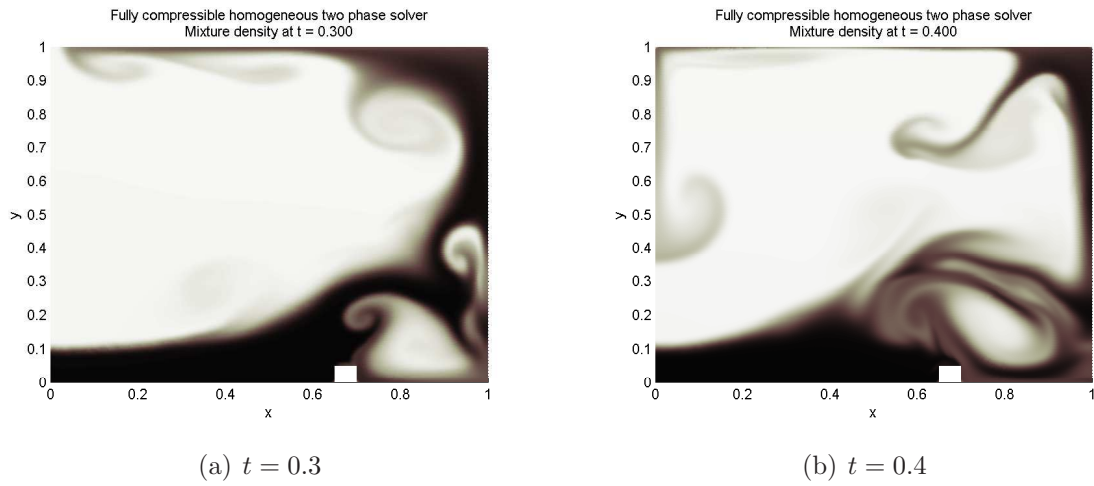


Figure 3.22: Falling water column test case. Splash is climbing the wall.

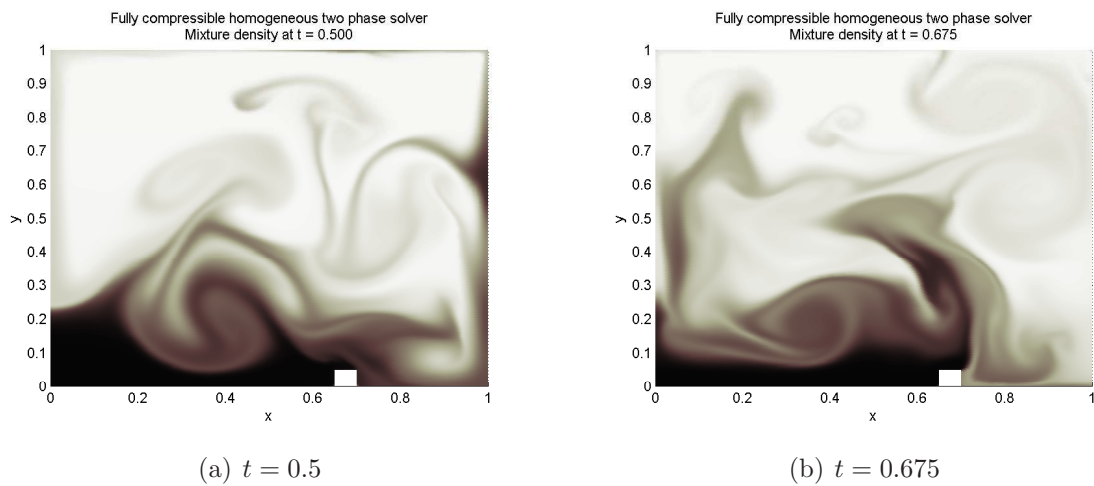


Figure 3.23: Falling water column test case. Turbulent mixing process.

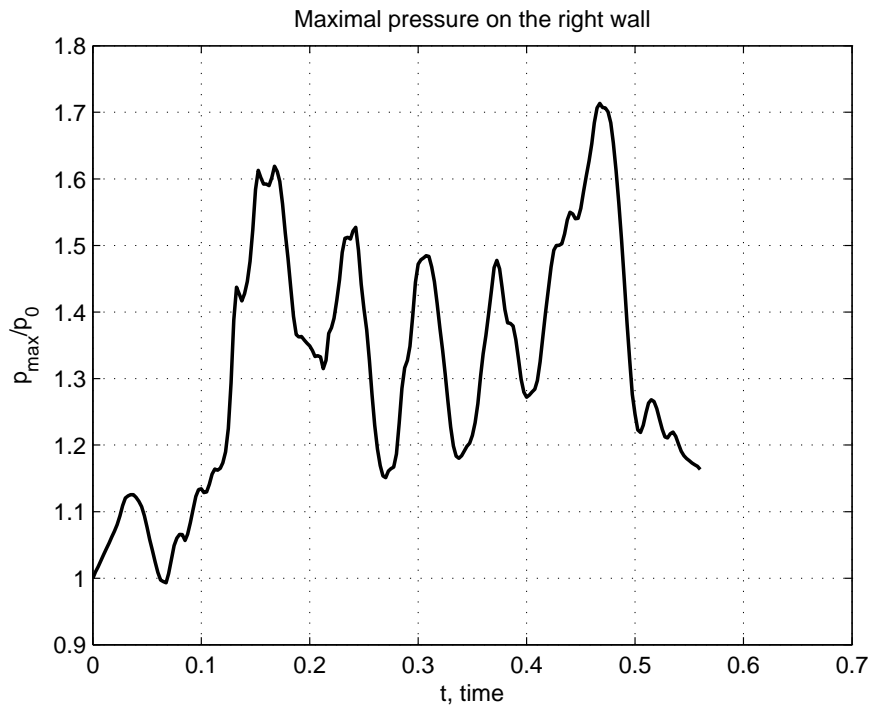


Figure 3.24: Maximal pressure on the right wall. Heavy gas case.

in Table 3.1. The mesh used in this computation contained about 92000 control volumes (in this case it was triangles). The results of this simulation with our code are presented on Figures 3.27 – 3.33. On Figure 3.34 we plot the maximal pressure on the bottom as a function of time:

$$t \longmapsto \max_{(x,y) \in [0,1] \times 0} p(x,y,t).$$

From this figure, it is clear to see that the pressure exerted on the bottom reaches $2.5p_0$ due to the drop impact at $t \approx 0.16$.

Remark 18 *Beginning with Figure 3.32 one can see some asymmetry in the solution. It is not expected since the initial condition, computational domain and forcing term are fully symmetric with respect to the line $x = 0.5$. This discrepancy is explained by the use of unstructured meshes in the computation. The arbitrariness of the orientation of the triangles introduces small perturbations which are sufficient to break the symmetry at the discrete level. At the present time, symmetry preserving schemes on unstructured meshes represent a big challenge in numerical analysis. The author is not aware of any work in this direction.*

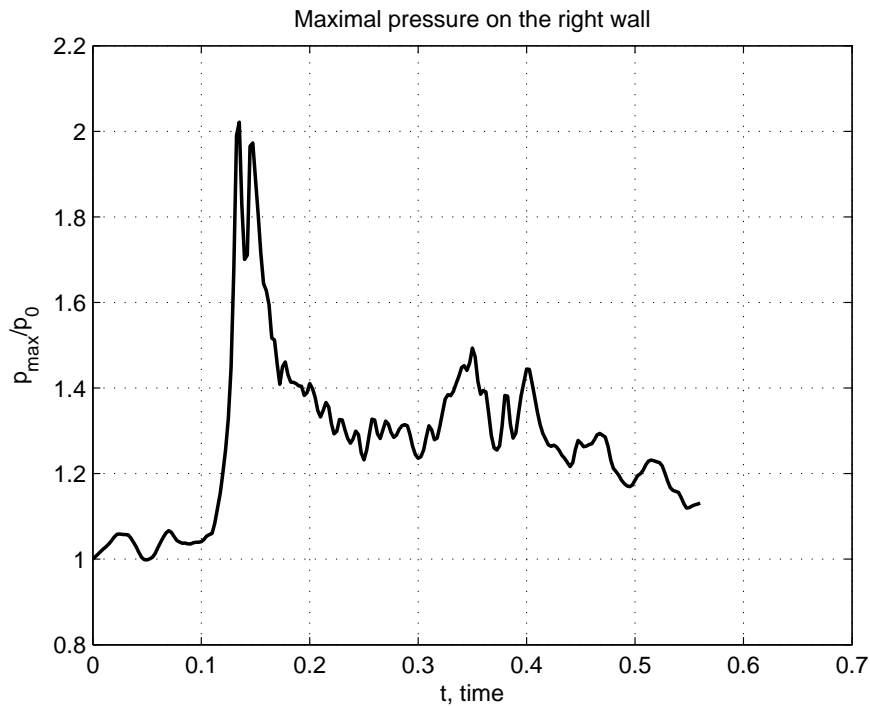


Figure 3.25: Maximal pressure on the right wall as a function of time. Light gas.

3.6 Conclusions

In this chapter we presented a simple mathematical model for simulating water waves impacts. The validation of this approach is the subject of future publications. Namely, we are going to perform qualitative and quantitative comparison with the more general six equations model [Ish75].

On the other hand, we presented a numerical approach for discretizing the governing equations. It is a second order finite volume scheme on unstructured meshes. This method was implemented in our research code. By construction, our code has excellent mass, momentum and total energy conservation properties. Different numerical tests from Section 3.5 validate the numerical method.

In the future we would like to carry out a parametric study with our solver. The influence of aeration, gas properties and other factors on the impact pressures is very important for industrial applications.

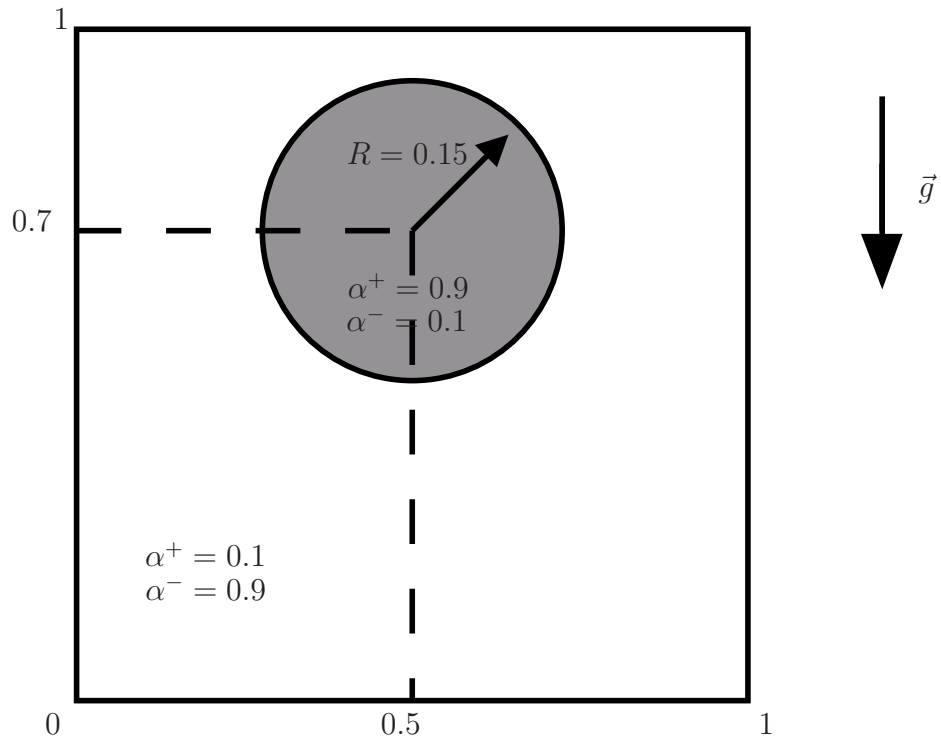


Figure 3.26: Geometry and initial condition for water drop test case.

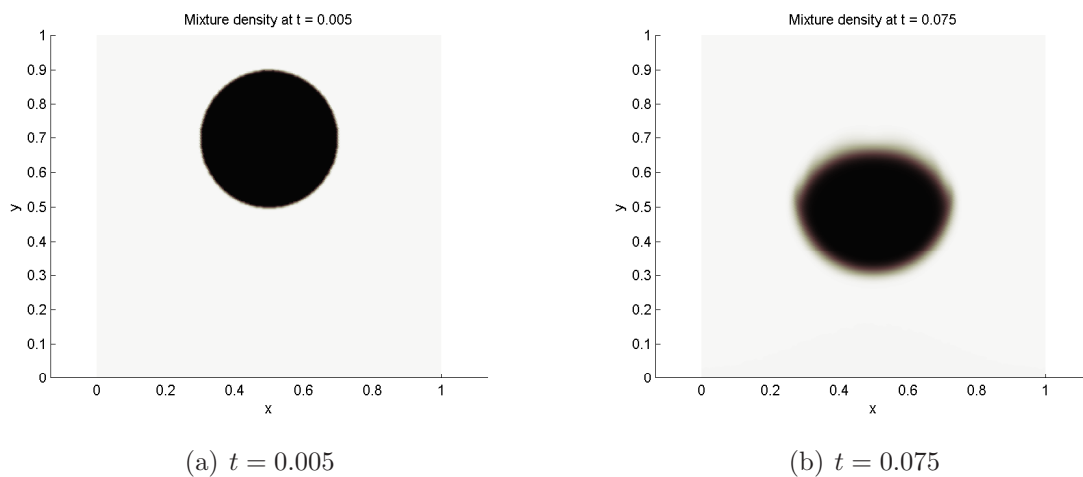


Figure 3.27: Water drop test case. Initial configuration and the beginning of the fall.

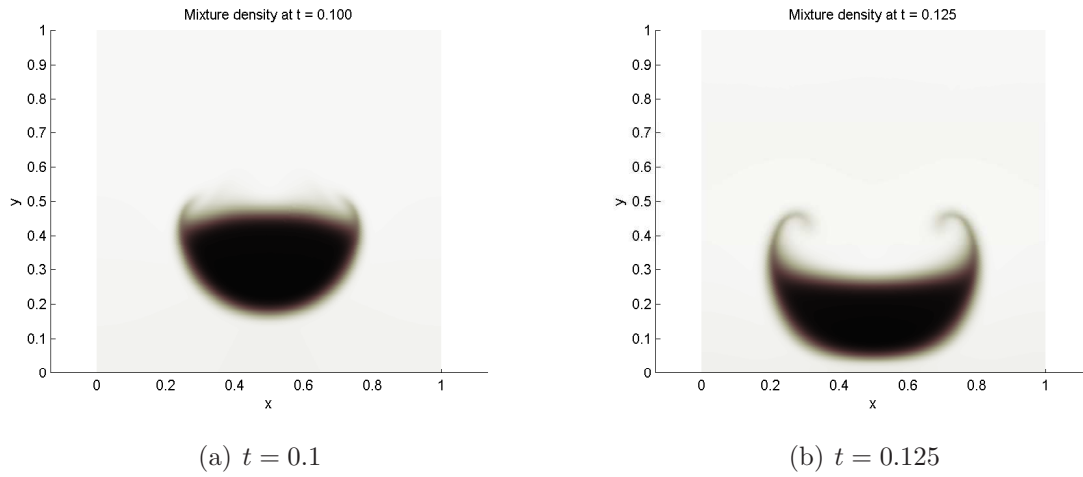


Figure 3.28: Water drop test case. Drop approaching container bottom.

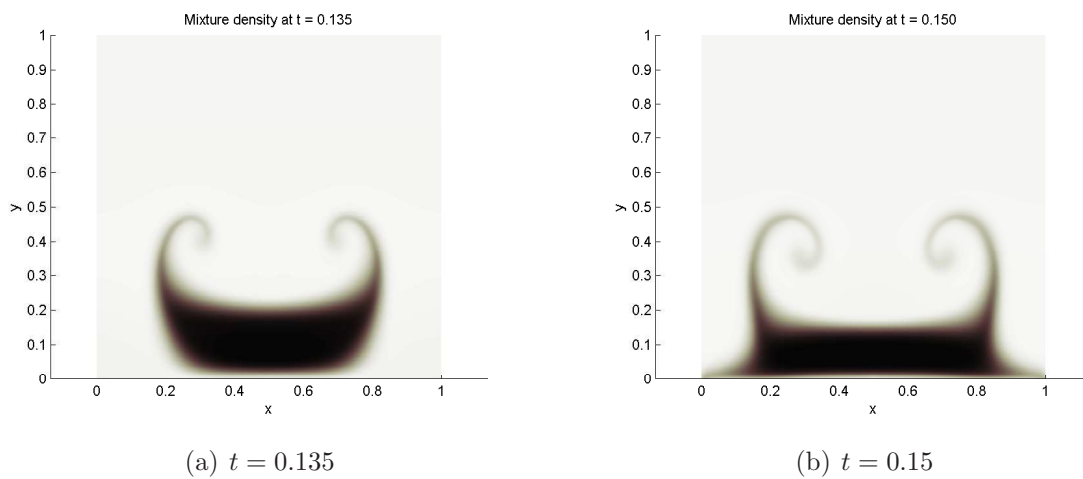


Figure 3.29: Water drop test case. Drop/bottom compressible interaction.

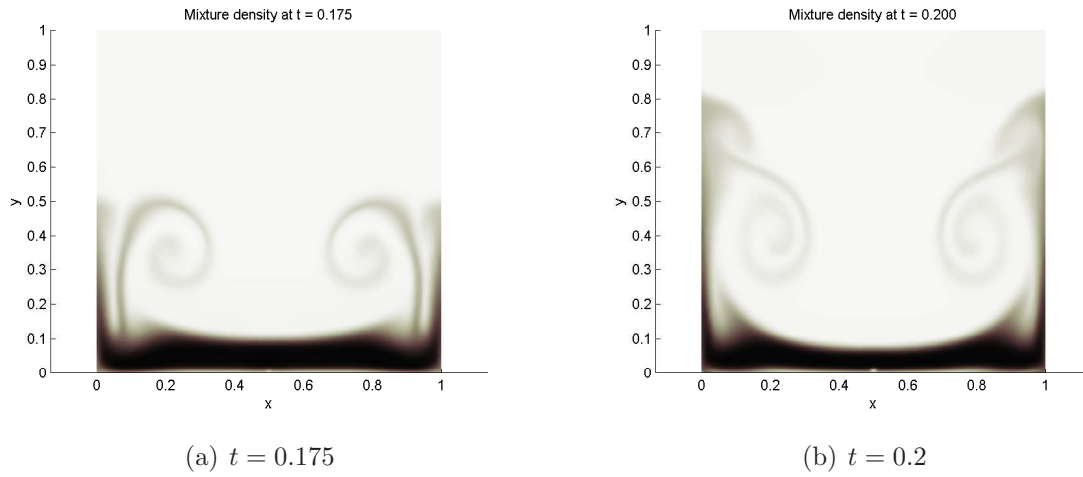


Figure 3.30: Water drop test case. Vertical jets formation.

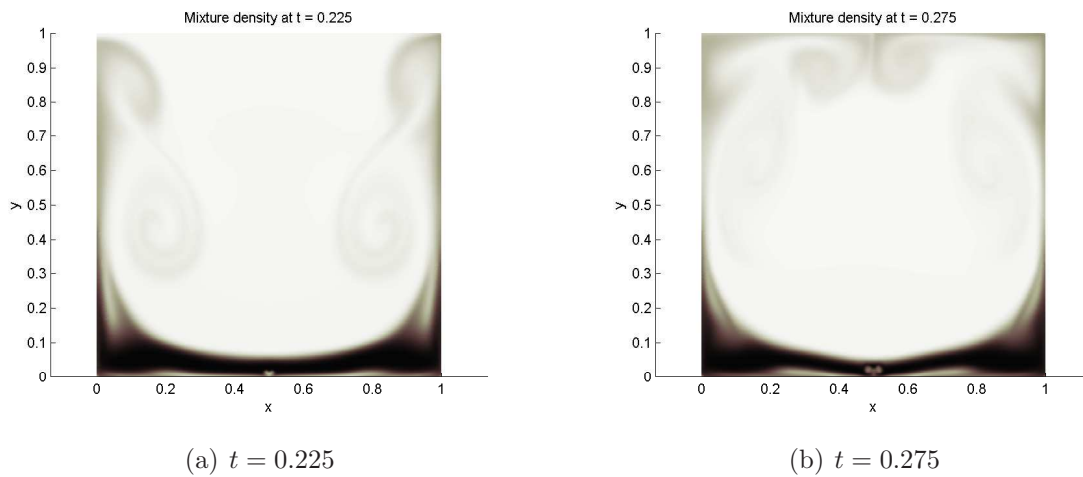


Figure 3.31: Water drop test case. Side jets crossing.

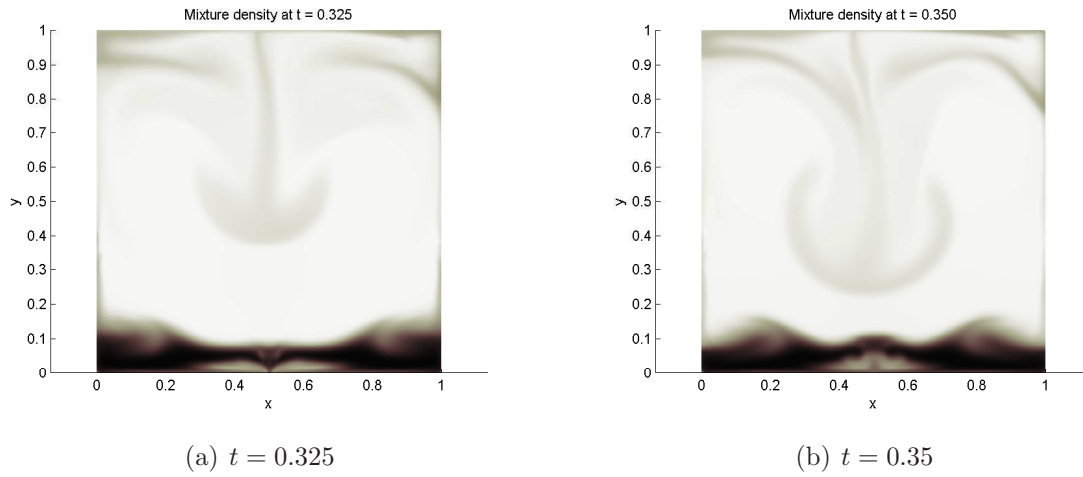


Figure 3.32: Water drop test case. Side jets interflow at the center.

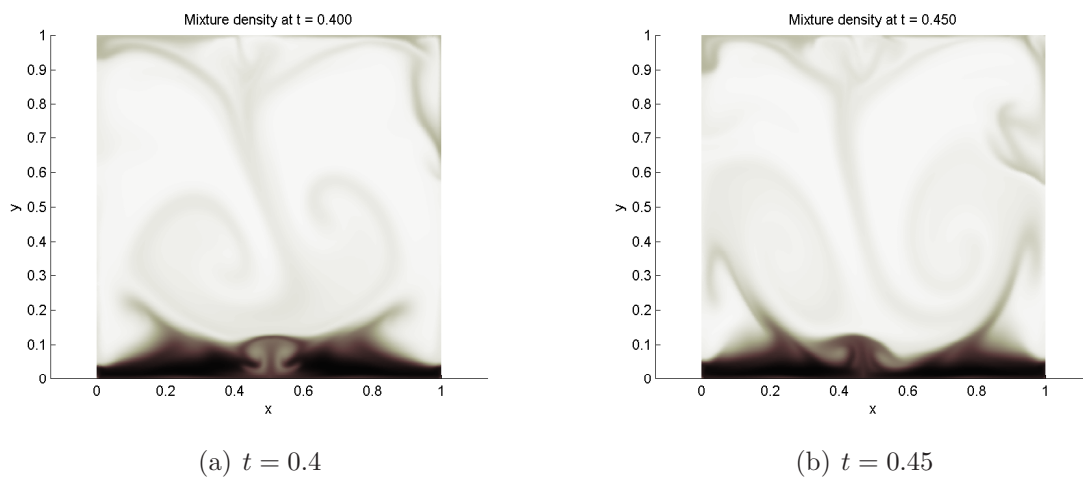


Figure 3.33: Water drop test case. Central jet reflection from the bottom.

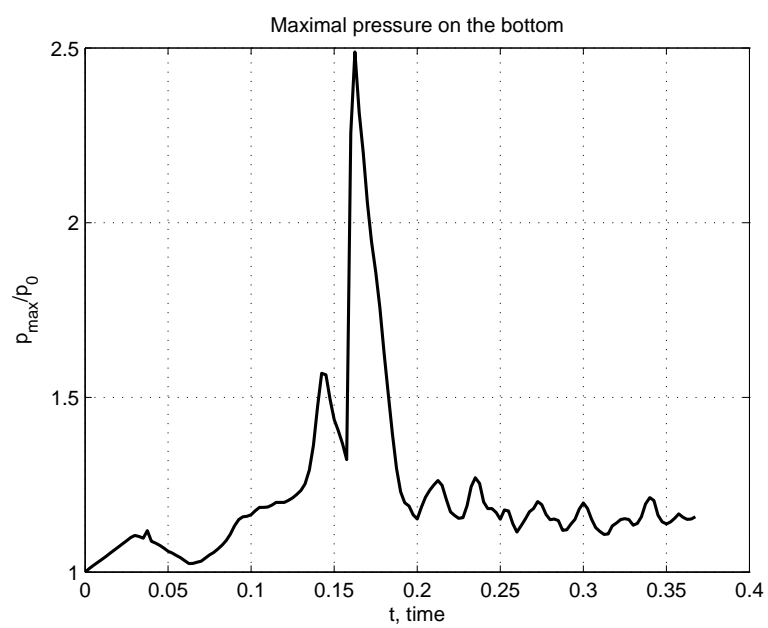


Figure 3.34: Water drop test case. Maximal bottom pressure as a function of time.

Chapter 4

Weakly damped free surface flows

Everything should be made as simple as possible, but not simpler.

Albert Einstein (1879 – 1955)

Contents

4.1	Introduction	169
4.2	Anatomy of dissipation	172
4.3	Derivation	174
4.3.1	Dissipative KdV equation	179
4.4	Dispersion relation	180
4.4.1	Discussion	182
4.5	Attenuation of linear progressive waves	182
4.6	Numerical results	187
4.6.1	Approximate solitary wave solution	187
4.6.2	Discussion	189
4.7	Conclusion	192

4.1 Introduction

Even though the irrotational theory of free-surface flows can predict successfully many observed wave phenomena, viscous effects cannot be neglected under certain circumstances. Indeed the question of dissipation in potential flows of fluid with a free surface is a very important one. As stated by [LH92], it would be convenient to have equations and boundary

conditions of comparable simplicity as for undamped free-surface flows. The peculiarity here lies in the fact that the viscous term in the Navier–Stokes (NS) equations is identically equal to zero for a velocity deriving from a potential.

The effects of viscosity on gravity waves have been addressed since the end of the nineteenth century in the context of the linearized Navier–Stokes (NS) equations. It is well-known that Lamb [Lam32] studied this question in the case of oscillatory waves on deep water. What is less known is that Boussinesq studied this effect as well [Bou95]. In this particular case they both showed that

$$\frac{d\alpha}{dt} = -2\nu k^2 \alpha, \quad (4.1)$$

where α denotes the wave amplitude, ν the kinematic viscosity of the fluid and k the wavenumber of the decaying wave. This equation leads to the classical law for viscous decay, namely

$$\alpha(t) = \alpha_0 e^{-2\nu k^2 t}. \quad (4.2)$$

The importance of viscous effects for water waves has been realized by numerous experimental studies for at least thirty years. Here we are going to quote a few of them. For example, in [ZG71] one can find

[...] However, the amplitude disagrees somewhat, and we suppose that this might be due to the viscous dissipation [...]

Another author [Wu81] points out this defect of the classical water waves theory:

[...] the peak amplitudes observed in the experiments are slightly smaller than those predicted by the theory. This discrepancy can be ascribed to the neglect of the viscous effects in the theory [...]

And finally in the classical article [BPS81] one finds the following important conclusion:

[...] it was found that the inclusion of a dissipative term was much more important than the inclusion of the nonlinear term, although the inclusion of the nonlinear term was undoubtedly beneficial in describing the observations [...]

Water wave energy can be dissipated by different physical mechanisms. The research community agrees at least on one point: the molecular viscosity is unimportant. Now let us discuss more debatable statements. For example if we take a tsunami wave and estimate its Reynolds number, we find $Re \approx 10^6$. So, the flow is clearly turbulent and in practice it can be modelled by various eddy viscosity models. On the other hand, in laboratory experiments the Reynolds number is much more moderate and sometimes we can neglect this

effect. Then one can think about boundary layers. In this chapter we will deal essentially with the bottom boundary layer. We briefly discuss the free surface boundary layer and explain why we do not take it into account in this study. We have to say that the boundary layer mechanism is especially important for long waves since they “feel” the bottom. Finally, the most important (and the most challenging) mechanism of energy dissipation is wave breaking. This process is extremely difficult from the mathematical but also the physical and numerical points of view since we have to deal with multivalued functions, topological changes in the flow and complex turbulent mixing processes. Nowadays the practitioners can only be happy to model roughly this process by adding ad-hoc diffusive terms when the wave becomes steep enough.

In this work we keep the features of undamped free-surface flows while adding dissipative effects. The classical theory of viscous potential flows [JW04] is based on pressure and boundary conditions corrections due to the presence of viscous stresses. We present here a novel approach.

Currently, potential flows with ad-hoc dissipative terms are used for example in direct numerical simulations of weak turbulence of gravity waves [DKZ03, DKZ04, ZKPD05]. There have also been several attempts to introduce dissipative effects into long wave modelling [Mei94, DD07a, CG07].

The present chapter is a direct continuation of the recent study [DD07b, DDZ07]. In that work the authors considered two-dimensional (2D) periodic waves in infinite depth, while in the present study we remove these two hypotheses and all the computations are done in 3D. This point is important since the vorticity structure is more complicated in 3D. In other words we consider a general wavetrain on the free surface of a fluid layer of finite depth. As a result we obtain a qualitatively different formulation which contains a nonlocal term in the bottom kinematic condition. The inclusion of this term is natural since it represents the correction to potential flow due to the presence of a boundary layer. Moreover, this term is predominant since its magnitude scales with $\mathcal{O}(\sqrt{\nu})$, while other terms in the free-surface boundary conditions are of order $\mathcal{O}(\nu)$. Other researchers have obtained nonlocal corrections but they differ from ours [KM75]. The differences will be explained below.

Recently we discovered that the nonlocal term in exactly the same form was already derived in [LO04]. Unfortunately we made this discovery after publishing our first paper [DD07b] on the subject and, consequently, we could not cite the original work of P. Liu. Even though we try to read the literature on a regular basis, it is impossible to be aware of all papers. Consequently, we sometimes rederive what others did before. It happened to us and we ensure that it was done completely independently.

4.2 Anatomy of dissipation

In this section we are going to discuss the contribution of different flow regions into water wave energy dissipation. We conventionally [Mei94] divide the flow into three regions illustrated on Figure 4.1. On this figure S_f and S_b stand for free surface and bottom respectively. Then, R_i , R_f and R_b denote the interior region, free surface and bottom boundary layers.

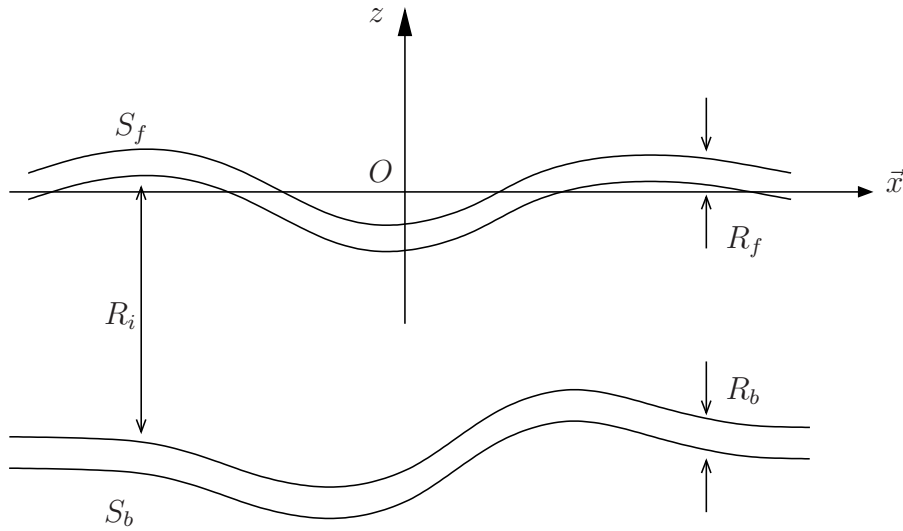


Figure 4.1: Conventional partition of the flow region into interior region and free surface, bottom boundary layers.

In order to make some estimates we introduce the notation which will be used in this section: μ is the dynamic viscosity, $\delta = \mathcal{O}(\sqrt{\mu})$ is the boundary layer thickness characterization, t_0 is the characteristic time, a_0 is the characteristic wave amplitude and ℓ is the wavelength or basin length (in laboratory experiments, for example).

We assume that the flow is governed by the incompressible Navier-Stokes equations:

$$\begin{aligned} \nabla \cdot \vec{u} &= 0, \\ \frac{\partial \vec{u}}{\partial t} + \vec{u} \cdot \nabla \vec{u} + \frac{1}{\rho} \nabla p &= \vec{g} + \frac{1}{\rho} \nabla \cdot \underline{\underline{\tau}}, \end{aligned}$$

where $\underline{\underline{\tau}}$ is the viscous stress tensor

$$\tau_{ij} = 2\mu\varepsilon_{ij}, \quad \varepsilon_{ij} = \frac{1}{2} \left(\frac{\partial u_i}{\partial x_j} + \frac{\partial u_j}{\partial x_i} \right).$$

We multiply the second equation by \vec{u} and integrate over the domain Ω to get the

following energy balance equation:

$$\begin{aligned} \frac{1}{2} \int_{\Omega} \frac{\partial}{\partial t} (\rho |\vec{u}|^2) d\Omega + \frac{1}{2} \int_{\partial\Omega} \rho |\vec{u}|^2 \vec{u} \cdot \vec{n} d\sigma = \\ = \int_{\partial\Omega} (-p\mathbb{I} + \underline{\underline{\tau}}) \vec{n} \cdot \vec{u} d\sigma + \int_{\Omega} \rho \vec{g} \cdot \vec{u} d\Omega - \underbrace{\frac{1}{2\mu} \int_{\Omega} \underline{\underline{\tau}} : \underline{\underline{\tau}} d\Omega}_{\mathcal{T}} . \end{aligned}$$

In this identity each term has a precise physical meaning. The left-hand side is the total rate of energy change in Ω . The second term is the flux of energy across the boundary. On the right-hand side, the first integral represents the rate of work by surface stresses acting on the boundary. The second integral is the rate of work done by the gravity force throughout the volume, and the third integral \mathcal{T} is the rate of viscous dissipation. We will focus our attention on the last one \mathcal{T} . We estimate the order of magnitude of the rate of dissipation in various regions of the fluid.

We start by the interior region R_i . Outside the boundary layers, it is reasonable to expect that the rate of strain is dominated by the irrotational part whose scale is $\frac{a_0}{t_0}$ and the length scale is the wavelength ℓ . The energy dissipation rate is then

$$\mathcal{O}(\mathcal{T}_{R_i}) \sim \frac{1}{\mu} \left(\mu \frac{a}{t_0 \ell} \right)^2 \cdot \ell^3 = \mu \left(\frac{a}{t_0} \right)^2 \ell \sim \mathcal{O}(\mu) .$$

Inside the bottom boundary layer the normal gradient of the solenoidal part of \vec{u} dominates the strain rate, so that

$$\mathcal{O}(\mathcal{T}_{R_b}) \sim \frac{1}{\mu} \left(\mu \frac{a}{t_0 \delta} \right)^2 \cdot \delta \ell^2 = \frac{\mu}{\delta} \left(\frac{a \ell}{t_0} \right)^2 \sim \mathcal{O}(\mu^{\frac{1}{2}}) .$$

A free surface boundary layer also exists. Its importance depends on the free surface conditions. Consider first the classical case of a clean surface. The stress is mainly controlled by the potential velocity field which is of the same order as in the main body of the fluid. Because of the small volume $\mathcal{O}(\delta \ell^2)$ the rate of dissipation in the free surface boundary layer is only

$$\mathcal{O}(\mathcal{T}_{R_f}) \sim \frac{1}{\mu} \left(\mu \frac{a}{t_0 \ell} \right)^2 \cdot \delta \ell^2 = \mu \delta \left(\frac{a}{t_0} \right)^2 \sim \mathcal{O}(\mu^{\frac{3}{2}}) .$$

From the physical point of view it is weaker, since only the zero shear stress condition on the free surface is required.

Another extreme case is when the free surface is heavily contaminated, for example, by oil slicks. The stress in the free surface boundary layer can then be as great as in

the boundary layer near a solid wall. In the present study we do not treat such extreme situations and the surface contamination is assumed to be absent.

The previous scalings suggest the following diagram which represents the hierarchy of dissipative terms:

$$\underbrace{\mathcal{O}(\mu^{\frac{1}{2}})}_{R_b} \leftrightarrow \underbrace{\mathcal{O}(\mu)}_{R_i} \leftrightarrow \underbrace{\mathcal{O}(\mu^{\frac{3}{2}})}_{R_f} \leftrightarrow \dots$$

It is clear that the largest energy dissipation takes place inside the wall boundary layer. We take into account only the two first phenomena from this diagram. Consequently, all dissipative terms of order $\mathcal{O}(\mu^{\frac{3}{2}})$ and higher will be neglected.

4.3 Derivation

Consider the linearized 3D incompressible NS equations describing free-surface flows in a fluid layer of uniform depth h :

$$\frac{\partial \vec{v}}{\partial t} = -\frac{1}{\rho} \nabla p + \nu \Delta \vec{v} + \vec{g}, \quad \nabla \cdot \vec{v} = 0, \quad (4.3)$$

with \vec{v} the velocity vector, p the pressure, ρ the fluid density and \vec{g} the acceleration due to gravity. We represent $\vec{v} = (u, v, w)$ in the form of the Helmholtz–Leray decomposition:

$$\vec{v} = \nabla \phi + \nabla \times \vec{\psi}, \quad \vec{\psi} = (\psi_1, \psi_2, \psi_3). \quad (4.4)$$

After substitution of the decomposition (4.4) into (4.3), one notices that the equations are verified provided that the functions ϕ and $\vec{\psi}$ satisfy the following equations:

$$\Delta \phi = 0, \quad \phi_t + \frac{p - p_0}{\rho} + gz = 0, \quad \frac{\partial \vec{\psi}}{\partial t} = \nu \Delta \vec{\psi}.$$

Next we discuss the boundary conditions. We assume that the velocity field satisfies the conventional no-slip condition at the bottom $\vec{v}|_{z=-h} = \vec{0}$, while at the free surface we have the usual kinematic condition, which can be stated as

$$\eta_t + \vec{v} \cdot \nabla \eta = w.$$

After linearization it becomes simply $\eta_t = w$.

Dynamic condition states that the forces must be equal on both sides of the free surface:

$$[\underline{\underline{\sigma}} \cdot \vec{n}] \equiv -(p - p_0) \vec{n} + \underline{\underline{\tau}} \cdot \vec{n} = 0 \quad \text{at } z = \eta(x, t),$$

where $\underline{\underline{\sigma}}$ is the stress tensor, $[f]$ denotes the jump of a function f across the free surface, \vec{n} is the normal to the free surface and $\underline{\underline{\tau}}$ the viscous part of the stress tensor $\underline{\underline{\sigma}}$. The explicit expressions (in two dimensions for simplicity) of $\underline{\underline{\tau}}$ and \vec{n} are

$$\underline{\underline{\tau}} = \rho\nu \begin{pmatrix} 2\frac{\partial u}{\partial x} & \frac{\partial u}{\partial z} + \frac{\partial w}{\partial x} \\ \frac{\partial u}{\partial z} + \frac{\partial w}{\partial x} & 2\frac{\partial w}{\partial z} \end{pmatrix}, \quad \vec{n} = \frac{1}{\sqrt{1 + (\frac{\partial \eta}{\partial x})^2}} \begin{pmatrix} -\frac{\partial \eta}{\partial x} \\ 1 \end{pmatrix},$$

After linearization the normal vector \vec{n} equals to $(0, 0, 1)$.

Using Fourier–Laplace transforms, which we denote by $\mathcal{L}_{\mathcal{F}} \equiv \mathcal{L} \circ \mathcal{F}$,

$$f(\vec{x}, t) \xrightarrow{\mathcal{L}_{\mathcal{F}}} \hat{f}(\mathbf{k}, s), \quad \mathbf{k} = (k_x, k_y)$$

we can determine the structure of the unknown functions ϕ , $\vec{\psi}$ in the transform space. We assume that all the functions involved in the present computation satisfy the necessary regularity requirements and have sufficient decay at infinity so that the integral transforms can be applied. The solution for ϕ is obtained from the transformed continuity equation

$$\Delta\phi = 0 \xrightarrow{\mathcal{L}_{\mathcal{F}}} \hat{\phi}_{zz} - |\mathbf{k}|^2 \hat{\phi} = 0$$

and $\vec{\psi}$ from the corresponding transformed equation

$$\vec{\psi}_t = \nu\Delta\vec{\psi} \xrightarrow{\mathcal{L}_{\mathcal{F}}} s\hat{\vec{\psi}} = \nu(\hat{\vec{\psi}}_{zz} - |\mathbf{k}|^2 \hat{\vec{\psi}})$$

$$\hat{\phi} = \hat{\phi}_0^+(\mathbf{k}, s)e^{|\mathbf{k}|z} + \hat{\phi}_0^-(\mathbf{k}, s)e^{-|\mathbf{k}|z}, \quad \hat{\psi}_i = \hat{\psi}_{i0}(\mathbf{k}, s)(e^{|\mathbf{k}|z} + C_i(\mathbf{k}, s)e^{-|\mathbf{k}|z}),$$

where $m^2 := |\mathbf{k}|^2 + \frac{s}{\nu}$ and $\hat{\phi}_0^+$, $\hat{\phi}_0^-$, $\hat{\psi}_0$, $\vec{C} := (C_1, C_2, C_3)$ are unknown functions of the transform parameters (\mathbf{k}, s) , determined by the initial and appropriate boundary conditions.

There are three dynamic conditions on the free surface. Let us use first those related to the tangential stresses (the third one will be used later), where $\mu = \rho\nu$:

$$\sigma_{xz} = \mu\left(\frac{\partial w}{\partial x} + \frac{\partial u}{\partial z}\right) = 0, \quad \sigma_{yz} = \mu\left(\frac{\partial w}{\partial y} + \frac{\partial v}{\partial z}\right) = 0, \quad \text{at } z = 0.$$

Substituting decomposition (4.4) into these two identities yields

$$2\frac{\partial^2\phi}{\partial x\partial z} + \frac{\partial^2\psi_2}{\partial x^2} - \frac{\partial^2\psi_1}{\partial x\partial y} + \frac{\partial^2\psi_3}{\partial y\partial z} - \frac{\partial^2\psi_2}{\partial z^2} = 0, \quad z = 0, \quad (4.5)$$

$$2\frac{\partial^2\phi}{\partial y\partial z} + \frac{\partial^2\psi_2}{\partial x\partial y} - \frac{\partial^2\psi_1}{\partial y^2} + \frac{\partial^2\psi_1}{\partial z^2} - \frac{\partial^2\psi_3}{\partial x\partial z} = 0, \quad z = 0. \quad (4.6)$$

The next step consists in taking the Fourier–Laplace transform to these relations. We do not give here the explicit expressions since this operation is straightforward. The combination $(-ik_x)\widehat{(4.5)} + (-ik_y)\widehat{(4.6)}$ gives the important relation

$$ik_y\hat{\psi}_{10}(1+C_1) - ik_x\hat{\psi}_{20}(1+C_2) = -\frac{2|\mathbf{k}|^3}{m^2 + |\mathbf{k}|^2}(\hat{\varphi}_0^+ - \hat{\varphi}_0^-). \quad (4.7)$$

Let us turn to the free-surface kinematic condition

$$\frac{\partial\eta}{\partial t} = w \equiv \frac{\partial\phi}{\partial z} + \frac{\partial\psi_2}{\partial x} - \frac{\partial\psi_1}{\partial y}, \quad z = 0.$$

In transform space it becomes

$$s\hat{\eta} = |\mathbf{k}|(\hat{\varphi}_0^+ - \hat{\varphi}_0^-) + ik_y\hat{\psi}_{10}(1+C_1) - ik_x\hat{\psi}_{20}(1+C_2). \quad (4.8)$$

Equations (4.7) and (4.8) can be rewritten as

$$\frac{|\mathbf{k}|(\hat{\varphi}_0^+ - \hat{\varphi}_0^-)}{\nu(m^2 + |\mathbf{k}|^2)} = \hat{\eta}, \quad (4.9)$$

$$ik_y\hat{\psi}_{10}(1+C_1) - ik_x\hat{\psi}_{20}(1+C_2) = -2\nu|\mathbf{k}|^2\hat{\eta}. \quad (4.10)$$

Using (4.10) one can replace the rotational part in the kinematic free-surface condition:

$$\eta_t = \phi_z + \mathcal{L}_F^{-1}[-2\nu|\mathbf{k}|^2\hat{\eta}] = \phi_z + 2\nu\Delta\eta. \quad (4.11)$$

In order to account for the presence of viscous stresses, we have to modify the dynamic free-surface condition as well. This is done using the balance of normal stresses at the free surface:

$$\sigma_{zz} = 0 \text{ at } z = 0 \Rightarrow p - p_0 = 2\rho\nu\frac{\partial w}{\partial z} \equiv 2\rho\nu\left(\frac{\partial^2\phi}{\partial z^2} + \frac{\partial^2\psi_2}{\partial x\partial z} - \frac{\partial^2\psi_1}{\partial y\partial z}\right).$$

Using (4.10) one can show that $\frac{\partial^2\psi_2}{\partial x\partial z} - \frac{\partial^2\psi_1}{\partial y\partial z} = \mathcal{O}(\nu^{\frac{1}{2}})$, so Bernoulli's equation becomes

$$\phi_t + g\eta + 2\nu\phi_{zz} + \mathcal{O}(\nu^{\frac{3}{2}}) = 0. \quad (4.12)$$

Since we only consider weak dissipation ($\nu \sim 10^{-6} - 10^{-3} \text{ m}^2/\text{s}$), we neglect terms of order $o(\nu)$.

The second step in our derivation consists in introducing a boundary layer correction at the bottom. Obviously, this was not done in the previous study [DDZ07], since the derivation dealt with the infinite depth case. In order to include this modification, we consider a semi-infinite fluid layer as it is usually done in boundary layer theory. The fluid occupies the domain $z > -h$. In this derivation we use the pure Leray decomposition

of the velocity field $\vec{v} = \nabla\phi + \vec{u}$ together with the divergence-free constraint $\nabla \cdot \vec{u} = 0$. Expecting that the rotational part \vec{u} varies rapidly in a distance $\delta = \sqrt{\nu}$,¹ we introduce the boundary-layer coordinate $\zeta \equiv (z + h)/\delta$, so that $\vec{u} = \vec{u}(\vec{x}, \zeta) = (\vec{u}_{\vec{x}}, u_z)(\vec{x}, \zeta)$. The solid boundary is given by $\zeta = 0$, and the potential part of the flow is not subject to this change of variables. With the new scaling, the divergence-free condition becomes

$$\frac{\partial u_z}{\partial \zeta} + \delta \nabla_{\vec{x}} \cdot \vec{u}_{\vec{x}} = 0. \quad (4.13)$$

As done in [Mei94], we expand the unknown functions in powers of the small parameter δ :

$$\phi = \phi_0(\vec{x}, z, t) + \delta\phi_1(\vec{x}, z, t) + \dots, \quad \vec{u} = \vec{q}_0(\vec{x}, \zeta, t) + \delta\vec{q}_1(\vec{x}, \zeta, t) + \dots$$

Substituting the expansion for \vec{u} into (4.13) gives the following relations:

$$\delta^0 : \quad \frac{\partial q_{0z}}{\partial \zeta} = 0, \quad \delta^1 : \quad \frac{\partial q_{1z}}{\partial \zeta} = -\nabla_{\vec{x}} \cdot \vec{q}_{0\vec{x}}, \quad (4.14)$$

where $\vec{q}_{0\vec{x}}$ denotes the first two components of the vector \vec{q}_0 corresponding to the horizontal coordinates \vec{x} . Recall that we would like to determine the correction to the bottom boundary condition

$$\phi_z = -u_z|_{\zeta=0} = -(q_{0z} + \delta q_{1z})|_{\zeta=0} + o(\delta). \quad (4.15)$$

So we only need to compute q_{0z} and q_{1z} at the bottom $\zeta = 0$.

Using the same asymptotic considerations as above, we can write down the following sequence of problems:

$$\begin{aligned} \Delta\phi_0 = 0, \quad \frac{\partial\phi_0}{\partial z}\Big|_{z=-h} = 0, \quad \frac{\partial\vec{q}_0}{\partial t} = \frac{\partial^2\vec{q}_0}{\partial\zeta^2}, \quad \vec{q}_0 = -\nabla\phi_0|_{\zeta=0}, \\ \Delta\phi_1 = 0, \quad \frac{\partial\phi_1}{\partial z}\Big|_{z=-h} = -q_{1z}, \quad \frac{\partial\vec{q}_1}{\partial t} = \frac{\partial^2\vec{q}_1}{\partial\zeta^2}, \quad \vec{q}_1 = -\nabla\phi_1|_{\zeta=0}, \end{aligned}$$

together with the radiation condition $\vec{q} \rightarrow \vec{0}$ as $\zeta \rightarrow \infty$.

This sequence of linear problems can be solved using Fourier transforms. In Fourier space one finds immediately that $\hat{\phi}_0(t, z, \mathbf{k}) = \hat{\varphi}_0(t, \mathbf{k})(e^{|\mathbf{k}|z} + e^{-|\mathbf{k}|z})$. Since we know $\hat{\phi}_0$, we can determine the rotational component $\hat{\vec{q}}_0$.

Analytical solutions to the equation

$$\frac{\partial\hat{\vec{q}}_{0\vec{x}}}{\partial t} = \frac{\partial^2\hat{\vec{q}}_{0\vec{x}}}{\partial\zeta^2} \quad (4.16)$$

¹Of course we should nondimensionalize all quantities in order to define small numbers. One would find that δ is in fact equivalent to $\sqrt{Re^{-1}} \times L$, where Re is the Reynolds number and L a typical length.

are well-known. If we assume that initially the flow is potential and the boundary condition is $\hat{q}_{0\bar{x}} = i\mathbf{k}\hat{\phi}_0(z = -h; \mathbf{k})$, the solution is

$$\hat{q}_{0\bar{x}} = \frac{1}{2\sqrt{\pi}} \int_0^t \frac{\zeta}{(t-\tau)^{\frac{3}{2}}} e^{-\frac{\zeta^2}{4(t-\tau)}} i\mathbf{k}\hat{\phi}_0(\tau, z = -h, \mathbf{k}) d\tau.$$

Let us now integrate the second equation in (4.14) from 0 to ∞ , using the appropriate decay at infinity:

$$\hat{q}_{1z}|_{\zeta=0} = - \int_0^\infty i\mathbf{k} \cdot \hat{q}_{0\bar{x}} d\zeta = \frac{1}{2\sqrt{\pi}} \int_0^\infty \int_0^t \frac{\zeta}{(t-\tau)^{\frac{3}{2}}} e^{-\frac{\zeta^2}{4(t-\tau)}} |\mathbf{k}|^2 \hat{\phi}_0(\tau, z = -h, \mathbf{k}) d\tau d\zeta.$$

One can interchange integral signs and evaluate the inner integral on ζ to obtain:

$$\hat{q}_{1z}|_{\zeta=0} = \frac{1}{\sqrt{\pi}} \int_0^t \frac{|\mathbf{k}|^2 \hat{\phi}_0(\tau, z = -h, \mathbf{k})}{\sqrt{t-\tau}} d\tau.$$

Hence, the bottom boundary condition becomes, at order δ ,

$$\begin{aligned} \left. \frac{\partial \phi}{\partial z} \right|_{z=-h} &= -\sqrt{\frac{\nu}{\pi}} \int_0^t \frac{\mathcal{F}^{-1}(|\mathbf{k}|^2 \hat{\phi}_0(-h, \mathbf{k}))}{\sqrt{t-\tau}} d\tau = \\ &= \sqrt{\frac{\nu}{\pi}} \int_0^t \frac{\nabla_{\bar{x}}^2 \phi_0|_{z=-h}}{\sqrt{t-\tau}} d\tau = -\sqrt{\frac{\nu}{\pi}} \int_0^t \frac{\phi_{0zz}|_{z=-h}}{\sqrt{t-\tau}} d\tau. \end{aligned} \quad (4.17)$$

One recognizes on the right-hand side a half-order integral operator. Summarizing the developments made above and generalizing our equations by including nonlinear terms, we obtain a new set of viscous potential free-surface flow equations:

$$\Delta \phi = 0, \quad (\vec{x}, z) \in \Omega = \mathbb{R}^2 \times [-h, \eta] \quad (4.18)$$

$$\eta_t + \nabla \eta \cdot \nabla \phi = \phi_z + 2\nu \Delta \eta, \quad z = \eta \quad (4.19)$$

$$\phi_t + \frac{1}{2} |\nabla \phi|^2 + g\eta = -2\nu \phi_{zz}, \quad z = \eta \quad (4.20)$$

$$\phi_z = -\sqrt{\frac{\nu}{\pi}} \int_0^t \frac{\phi_{zz}}{\sqrt{t-\tau}} d\tau, \quad z = -h. \quad (4.21)$$

At the present stage, the addition of nonlinear terms is rather a conjecture. However, a recent study by Liu et al. [LPC07] suggests that this conjecture is rather true. The authors investigated the importance of nonlinearity in boundary layer equation (4.16) in the case

of a solitary wave solution. They came to the conclusion that “the nonlinear effects are not very significant”.

Using this weakly damped potential flow formulation and the procedure of Boussinesq equations derivation described in previous chapters (see Chapter 2, for example), one can derive the following system of equations with horizontal velocity \vec{u}_θ defined at the depth $z_\theta = -\theta h$, $0 \leq \theta \leq 1$:

$$\eta_t + \nabla \cdot ((h + \eta)\vec{u}_\theta) + h^3 \left(\frac{\theta^2}{2} - \theta + \frac{1}{3} \right) \nabla^2 (\nabla \cdot \vec{u}_\theta) = 2\nu \Delta \eta + \sqrt{\frac{\nu}{\pi}} \int_0^t \frac{\nabla \cdot \vec{u}_\theta}{\sqrt{t - \tau}} d\tau, \quad (4.22)$$

$$\vec{u}_{\theta t} + \frac{1}{2} \nabla |\vec{u}_\theta|^2 + g \nabla \eta - h^2 \theta \left(1 - \frac{\theta}{2} \right) \nabla (\nabla \cdot \vec{u}_{\theta t}) = 2\nu \Delta \vec{u}_\theta. \quad (4.23)$$

4.3.1 Dissipative KdV equation

In this section we derive a viscous Korteweg-de Vries (KdV) equation from just obtained Boussinesq equations (4.22), (4.23). Since KdV-type equations model only unidirectional wave propagation, our attention is naturally restricted to 1D case. In order to perform asymptotic computations, all the equations have to be switched to nondimensional variables as it is explained in Section 2.2. We find the velocity variable u in this form:

$$u_\theta = \eta + \varepsilon P + \mu^2 Q + \dots$$

where ε and μ are defined in (2.9), P and Q are unknown at the present moment. Using the methods similar to those used in Section 2.9.1, one can easily show that

$$P = -\frac{1}{4}\eta^2, \quad Q = \left(\theta - \frac{1}{6} - \frac{\theta^2}{2} \right) \eta_{xx}.$$

This result immediately yields the following asymptotic representation of the velocity field

$$u_\theta = \eta - \frac{1}{4}\varepsilon\eta^2 + \mu^2 \left(\theta - \frac{1}{6} - \frac{\theta^2}{2} \right) \eta_{xx} + \dots \quad (4.24)$$

Substituting the last formula (4.24) into equation (4.22) and switching again to dimensional variables, one obtains this viscous KdV-type equation:

$$\eta_t + \sqrt{\frac{g}{h}} \left((h + \frac{3}{2}\eta)\eta_x + \frac{1}{6}h^3\eta_{xxx} - \sqrt{\frac{\nu}{\pi}} \int_0^t \frac{\eta_x}{\sqrt{t - \tau}} d\tau \right) = 2\nu\eta_{xx}. \quad (4.25)$$

This equation will be used in Section 4.5 to study the damping of linear progressive waves.

4.4 Dispersion relation

Interesting information about the governing equations can be obtained from the linear dispersion relation analysis. In this section we are going to analyse the new set of equations (4.18)–(4.21) for the complete water wave problem and the corresponding long wave limit (Boussinesq equations) (4.22)–(4.23).

To simplify the computations, we consider the two-dimensional problem. The generalization to higher dimensions is straightforward. Traditionally the governing equations are linearized and the bottom is assumed to be flat. After all these simplifications the new set of equations becomes

$$\phi_{xx} + \phi_{zz} = 0, \quad (x, z) \in \mathbb{R} \times [-h, 0], \quad (4.26)$$

$$\eta_t = \phi_z + 2\nu\eta_{xx}, \quad z = 0, \quad (4.27)$$

$$\phi_t + g\eta + 2\nu\phi_{zz} = 0, \quad z = 0, \quad (4.28)$$

$$\phi_z + \sqrt{\frac{\nu}{\pi}} \int_0^t \frac{\phi_{zz}}{\sqrt{t-\tau}} d\tau = 0, \quad z = -h. \quad (4.29)$$

The next classical step consists in finding solutions of the special form

$$\phi(x, z, t) = \varphi(z)e^{i(kx-\omega t)}, \quad \eta(x, t) = \eta_0 e^{i(kx-\omega t)}. \quad (4.30)$$

From continuity equation (4.26) we can determine the structure of the function $\varphi(z)$:

$$\varphi(z) = C_1 e^{kz} + C_2 e^{-kz}.$$

Altogether we have three unknown constants $\vec{C} = (C_1, C_2, \eta_0)$ and three boundary conditions (4.27)–(4.29) which can be viewed as a linear system with respect to \vec{C} :

$$\mathbf{M}\vec{C} = \vec{0}. \quad (4.31)$$

The matrix \mathbf{M} has the following elements

$$\mathbf{M} = \begin{pmatrix} k & -k & i\omega - 2\nu k^2 \\ i\omega - 2\nu k^2 & i\omega - 2\nu k^2 & -g \\ e^{-kh}(1 + kF(t, \omega)) & e^{kh}(-1 + kF(t, \omega)) & 0 \end{pmatrix}$$

where the function $F(t, \omega)$ can be expressed in terms of the error function of complex argument:

$$F(t, \omega) := \sqrt{\frac{\nu}{\pi}} \int_0^t \frac{e^{i\omega(t-\tau)}}{\sqrt{t-\tau}} d\tau = \sqrt{\frac{\nu}{-i\omega}} \operatorname{Erf}(\sqrt{-i\omega t}).$$

In order to have nontrivial solutions² of (4.26)–(4.29), the determinant of the system (4.31) has to be equal to zero $\det \mathbf{M} = 0$. It gives us a relation between ω and wavenumber k . This relation is called the linear dispersion relation:

$$D(\omega, k) := (i\omega - 2\nu k^2)^2 + gk \tanh(kh) - \sqrt{\frac{i\nu}{\omega}} \operatorname{Erf}(\sqrt{-i\omega t}) ((i\omega - 2\nu k^2) \tanh(kh) + gk) \equiv 0.$$

A similar procedure can be followed for Boussinesq equations (4.22), (4.23). We do not give here the details of the computations but only the final result:

$$D_b(\omega, k) := (i\omega - 2\nu k^2)^2 + b(kh)^2 i\omega (i\omega - 2\nu k^2) + ghk^2 (1 - a(kh)^2) - gk^2 \sqrt{\frac{i\nu}{\omega}} \operatorname{Erf}(\sqrt{-i\omega t}) \equiv 0,$$

where we introduced the following notation: $a := \frac{\theta^2}{2} - \theta + \frac{1}{3}$, $b := \theta(1 - \frac{\theta}{2})$.

Remark 19 *Contrary to the classical water wave problem and, by consequence, standard Boussinesq equations³ where the dispersion relation does not depend on time*

$$\omega^2 - gk \tanh(kh) \equiv 0, \quad (4.32)$$

here we have additionally the dependence of $\omega_t(k)$ on time t as a parameter. It is a consequence of the presence of the nonlocal term in time in the bottom boundary condition (4.21). Physically it means that the boundary layer “remembers” the flow history.

Unfortunately, the relations $D(\omega, k) \equiv 0$ and $D_b(\omega, k) \equiv 0$ cannot be solved analytically to give an explicit dependence of ω on k . That is why we applied Newton-type method to solve numerically these equations with respect to ω . Iterations were initialized with the classical dispersion relation (4.32). The Jacobians can be computed exactly:

$$\begin{aligned} \frac{dD(\omega)}{d\omega} &= 2i(i\omega - 2\nu k^2) - \frac{k}{\omega} \sqrt{\frac{i\nu}{\omega}} ((i\omega - 2\nu k^2)^2 \tanh(kh) + gk) \left(\frac{1}{\sqrt{\pi}} e^{i\omega t} \sqrt{-i\omega t} \right. \\ &\quad \left. - \frac{1}{2} \operatorname{Erf}(\sqrt{-i\omega t}) \right) - 2i \sqrt{\frac{i\nu}{\omega}} k \tanh(kh) (i\omega - 2\nu k^2) \operatorname{Erf}(\sqrt{-i\omega t}), \end{aligned}$$

$$\frac{dD_b(\omega)}{d\omega} = 2i(i\omega - 2\nu k^2) + ib(kh)^2 + \frac{gk^2}{2\omega} \sqrt{\frac{i\nu}{\omega}} \operatorname{Erf}(\sqrt{-i\omega t}) - \frac{gk^2}{\omega} \sqrt{\frac{\nu t}{\pi}} e^{i\omega t}.$$

²Obviously of the special form given by equation (4.30).

³Their dispersion relation is given by (2.50)

4.4.1 Discussion

Numerical snapshots of the nonclassical dispersion relation⁴ at different times for complete and Boussinesq equations are given on Figures (4.2)–(4.6). We will try to make several comments on the results we obtained.

Just at the beginning (when $t = 0$), there is no effect of the nonlocal term. This is why on Figure 4.2 new and classical curves are superimposed. With no surprise, the phase velocity of Boussinesq equations represents well only long waves limit (let us say up to $kh \approx 2$). When time evolves, we can see that the main effect of nonlocal term consists in slowing down long waves (see Figures 4.3–4.5). Namely, in the vicinity of $kh = 0$ the real part of the phase velocity is slightly smaller with respect to the classical formulation. From physical point of view this situation is comprehensible since only long waves “feel” the bottom and, by consequence, are affected by bottom boundary layer. On the other hand, the imaginary part of the phase velocity is responsible for the wave amplitude attenuation. The minimum of $\text{Im } c_p(k)$ in the region of long waves indicates that there is a “preferred” wavelength which is attenuated the most. In the range of short waves the imaginary part is monotonically decreasing. In practice it means that high-frequency components are damped by the model. This property can be advantageous in numerics, for example. On Figure 4.6 we depicted the real part of $c_p(k)$ with zoom made on long and moderate waves. The reader can see that nonlocal complete and Boussinesq equations have similar behaviour in the vicinity of $kh = 0$.

4.5 Attenuation of linear progressive waves

In this Section we investigate the damping rate of linear progressive waves. Thus, the first step consists in linearizing dissipative KdV equation (4.25):

$$\eta_t + \sqrt{\frac{g}{h}} \left(h\eta_x + \frac{1}{6}h^3\eta_{xxx} - \sqrt{\frac{\nu}{\pi}} \int_0^t \frac{\eta_x}{\sqrt{t-\tau}} d\tau \right) = 2\nu\eta_{xx} \quad (4.33)$$

In other words, we can say that we restrict our attention only to small amplitude waves. Equation (4.33) can be called nonlocal dissipative Airy equation.

Now we make the next assumption. We look for a particular form of the solutions:

$$\eta(x, t) = \mathcal{A}(t)e^{ik\xi}, \quad \xi = x - \sqrt{gh}t. \quad (4.34)$$

where k is the wavenumber and $\mathcal{A}(t)$ is called the complex amplitude, since $|\eta(x, t)| = |\mathcal{A}(t)|$. Integro-differential equation governing the temporal evolution of $\mathcal{A}(t)$ can be easily

⁴To be precise, we plot the phase velocity which is defined as $c_p(k) := \frac{\omega(k)}{k}$.

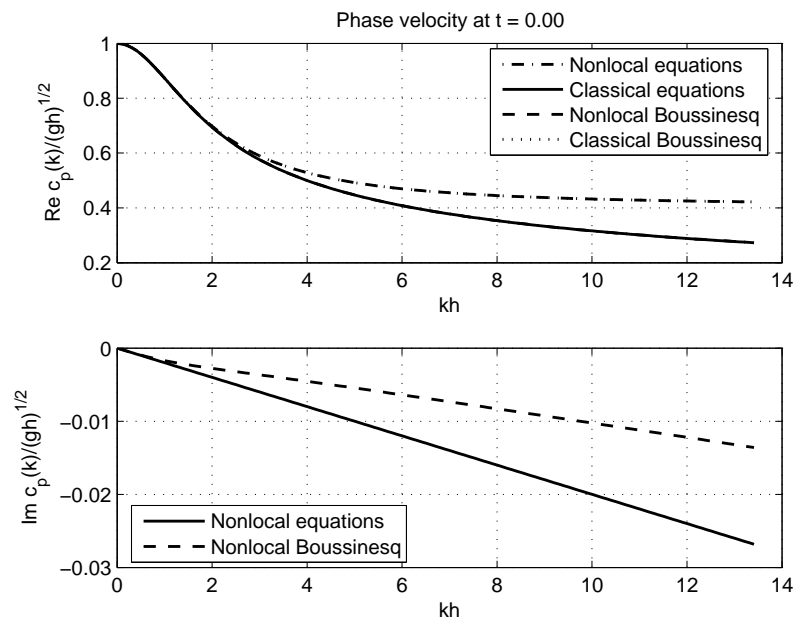


Figure 4.2: Real and imaginary part of dispersion curve at $t = 0$. At the beginning, the nonlocal term has no effect. Thus, the real parts of the classical and new set of equations are exactly superimposed on this figure. The imaginary part represents only local dissipation at this stage.

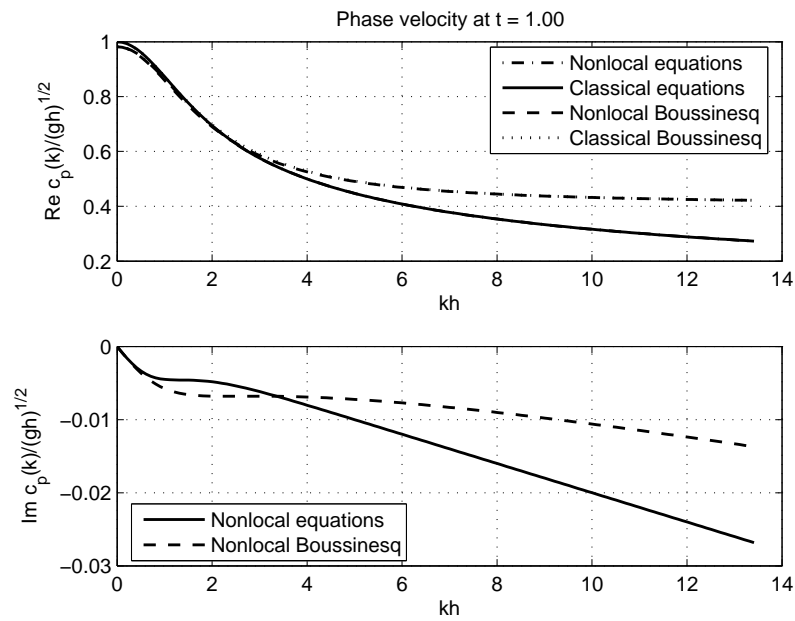


Figure 4.3: Phase velocity at $t = 1$. Boundary layer effects start to be visible: the real part of the velocity slightly drops down and the straight lines of the imaginary part are deformed by the nonlocal term. Within graphical accuracy, the classical and their nonlocal counterparts are superimposed.

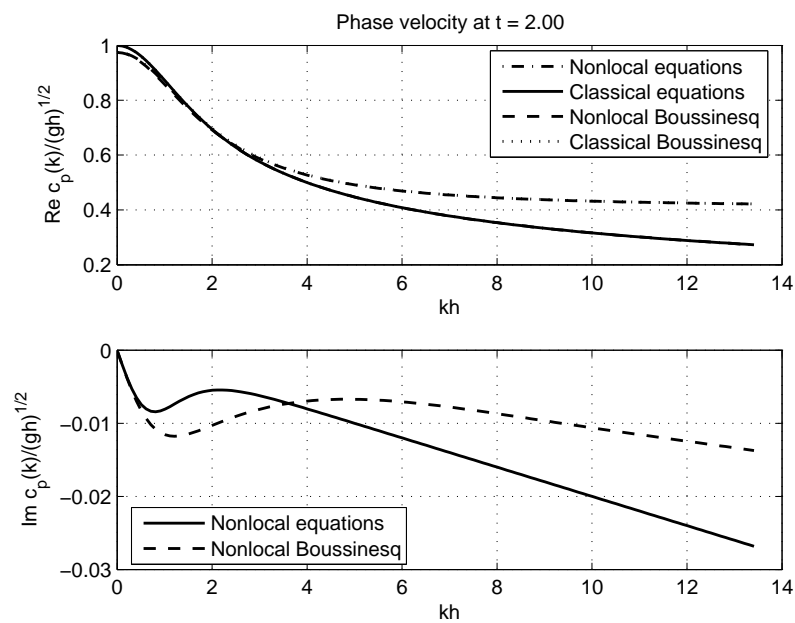


Figure 4.4: Phase velocity at $t = 2$. Nonlocal term slows down long waves since the real part of the phase velocity decreases.

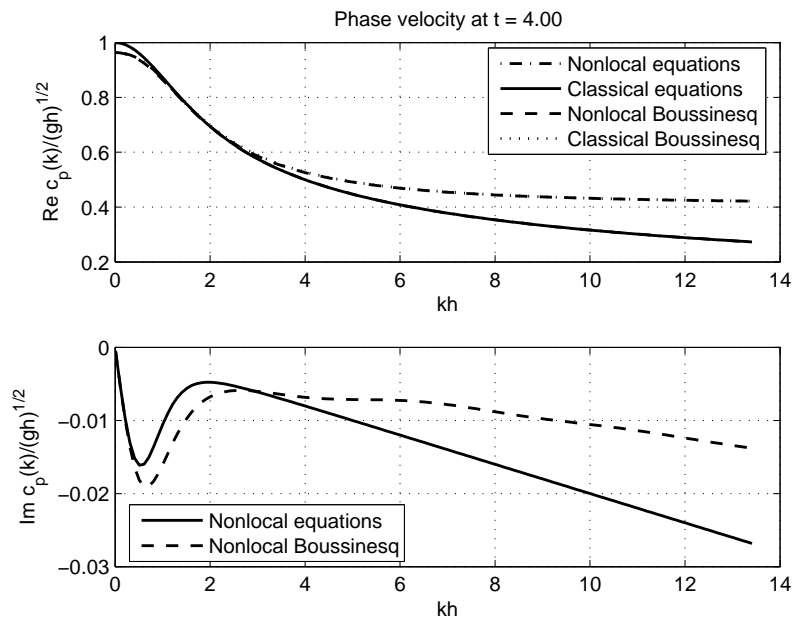
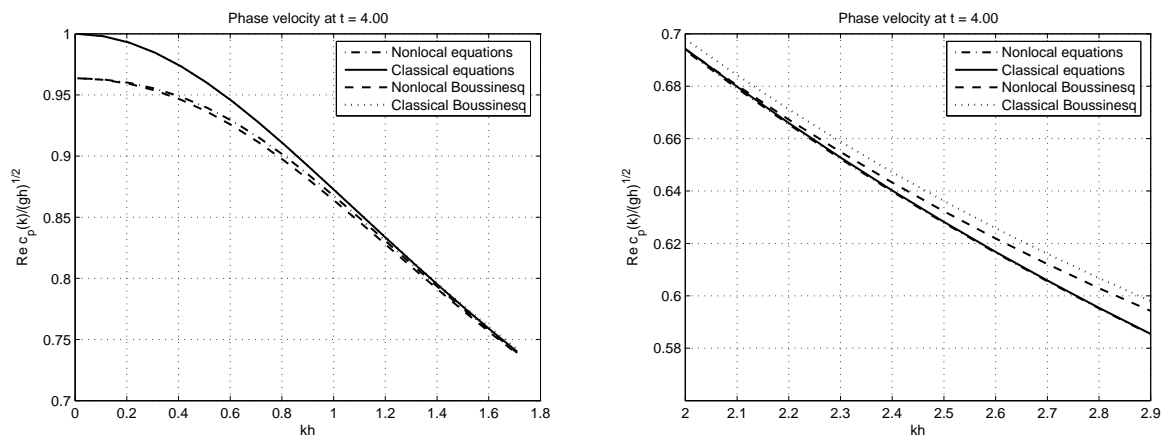


Figure 4.5: Phase velocity at $t = 4$. On Figure 4.6 we plot a zoom on long and moderate waves.



(a) Zoom on long waves. Classical and correspond- (b) Zoom on moderate wavelengths. In this region ing Boussinesq equations are almost superimposed classical and nonlocal complete equations are almost superimposed. In the same time one can notice a little difference in Boussinesq models.

Figure 4.6: Real part of the phase velocity at $t = 4$.

derived by substituting the special representation (4.34) into linearized KdV equation (4.33):

$$\frac{d\mathcal{A}}{dt} - \frac{i}{6}\sqrt{\frac{g}{h}}(kh)^3\mathcal{A}(t) + 2\nu k^2\mathcal{A}(t) - ik\sqrt{\frac{g\nu}{\pi h}}\int_0^t\frac{\mathcal{A}(\tau)}{\sqrt{t-\tau}}d\tau = 0. \quad (4.35)$$

In our applications we are rather interested in temporal evolution of the absolute value $|\mathcal{A}(t)|$. It is straightforward to derive the equation for $|\mathcal{A}(t)|^2$ if we recall that

$$|\mathcal{A}(t)|^2 = \mathcal{A}(t)\bar{\mathcal{A}}(t) \implies \frac{d|\mathcal{A}(t)|^2}{dt} = \frac{d\mathcal{A}(t)}{dt}\bar{\mathcal{A}}(t) + \frac{d\bar{\mathcal{A}}(t)}{dt}\mathcal{A}(t), \quad (4.36)$$

where $\bar{\mathcal{A}}(t)$ means the complex conjugate of $\mathcal{A}(t)$. The last missing ingredient is the time derivative $\frac{d\bar{\mathcal{A}}}{dt}$. This term is easily computed by taking the complex conjugate of (4.35):

$$\frac{d\bar{\mathcal{A}}}{dt} + \frac{i}{6}\sqrt{\frac{g}{h}}(kh)^3\bar{\mathcal{A}}(t) + 2\nu k^2\bar{\mathcal{A}}(t) + ik\sqrt{\frac{g\nu}{\pi h}}\int_0^t\frac{\bar{\mathcal{A}}(\tau)}{\sqrt{t-\tau}}d\tau = 0.$$

By combining just obtained equations according to (4.36), we get required evolution equation for $|\mathcal{A}|^2$:

$$\frac{d|\mathcal{A}|^2}{dt} + 4\nu k^2|\mathcal{A}(t)|^2 - ik\sqrt{\frac{g\nu}{\pi h}}\int_0^t\frac{\bar{\mathcal{A}}(t)\mathcal{A}(\tau) - \mathcal{A}(t)\bar{\mathcal{A}}(\tau)}{\sqrt{t-\tau}}d\tau = 0.$$

If we denote by $\mathcal{A}_r(t)$ and $\mathcal{A}_i(t)$ real and imaginary parts of $\mathcal{A}(t)$ respectively, the last equation can be further simplified:

$$\frac{d|\mathcal{A}|^2}{dt} + 4\nu k^2|\mathcal{A}(t)|^2 + 2k\sqrt{\frac{g\nu}{\pi h}}\int_0^t\frac{\mathcal{A}_r(t)\mathcal{A}_i(\tau) - \mathcal{A}_i(t)\mathcal{A}_r(\tau)}{\sqrt{t-\tau}}d\tau = 0. \quad (4.37)$$

Just derived integro-differential equation represents a generalisation to the classical equation (4.1) by Boussinesq [Bou95] and Lamb [Lam32] for the wave amplitude evolution in a viscous fluid. We recall that novel integral term is a direct consequence of the bottom boundary layer modelling.

Unfortunately, equation (4.37) cannot be used directly for numerical computations since we need to know the following combination of real and imaginary parts $\mathcal{A}_r(t)\mathcal{A}_i(\tau) - \mathcal{A}_i(t)\mathcal{A}_r(\tau)$ for $\tau \in [0, t]$. It represents a new and non-classical aspect of the present theory.

In numerical computations it is advantageous to integrate exactly local terms in equation (4.35). It is done by making the following change of variables:

$$\mathcal{A}(t) = e^{-2\nu k^2 t} e^{\frac{i}{6}\sqrt{\frac{g}{h}}(kh)^3 t} \tilde{\mathcal{A}}(t).$$

<i>parameter</i>	<i>definition</i>	<i>value</i>
ν	eddy viscosity	$10^{-3} \frac{m^2}{s}$
g	gravity acceleration	$9.8 \frac{m}{s^2}$
h	water depth	3600 m
ℓ	wavelength	50 km
k	wavenumber	$= \frac{2\pi}{\ell} \text{ m}^{-1}$

Table 4.1: Values of the parameters used in the numerical computations of the linear progressive waves amplitude. These values correspond to a typical Indian Ocean tsunami.

One can easily show that new function $\tilde{\mathbb{A}}(t)$ satisfies the following equation:

$$\frac{d\tilde{\mathcal{A}}}{dt} = ik\sqrt{\frac{g\nu}{\pi h}} \int_0^t \frac{e^{2\nu k^2(t-\tau)} e^{-\frac{i}{6}\sqrt{\frac{g}{h}}(kh)^3(t-\tau)}}{\sqrt{t-\tau}} \tilde{\mathcal{A}}(\tau) d\tau$$

On Figure 4.7 we plot a solution of integro-differential equation (4.35). All parameters related to this case are given in Table 4.1. These values were chosen to simulate a typical tsunami in Indian Ocean [DD06]. We have to say that the wave amplitude damping is entirely due to the dissipation in boundary layer since local terms are unimportant for sufficiently long waves.

4.6 Numerical results

In this section we would like to show the effect of nonlocal term on the solitary wave attenuation. For simplicity, we will consider wave propagation in a 1D channel.

For numerical computations we use the same Fourier-type spectral method that was described in Section 2.8. Obviously this method has to be slightly adapted because of the presence of nonlocal in time term. We have to say that this term necessitates the storage of $\nabla \cdot \vec{u}^{(n)}$ at previous time steps. Hence, long computations can be memory consuming.

The values of all parameters are given in Table 4.2.

4.6.1 Approximate solitary wave solution

In order to provide an initial condition for equations (4.22), (4.23), we are going to obtain an approximate solitary wave solution for nondissipative 1D version of these equations

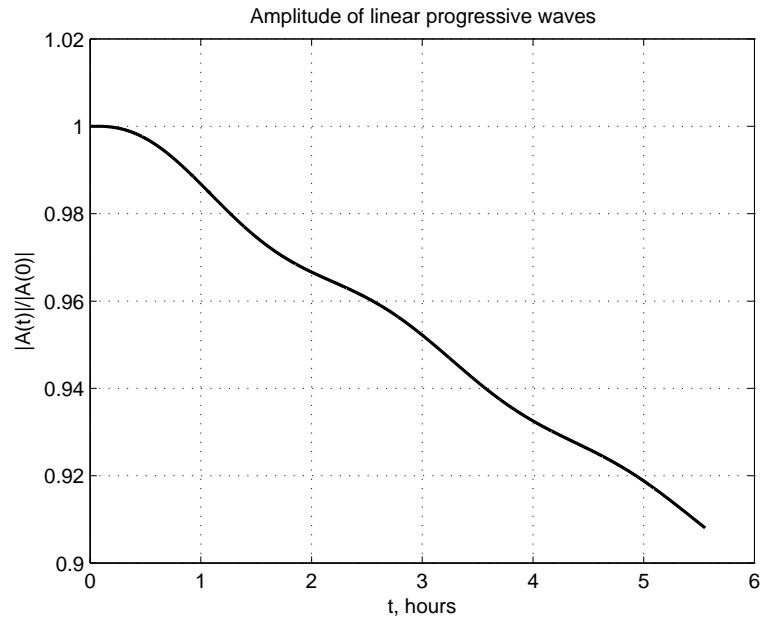


Figure 4.7: Amplitude of linear progressive waves as a function of time. Values of all parameters are given in Table 4.1.

<i>parameter</i>	<i>definition</i>	<i>value</i>
ε	nonlinearity	0.02
μ	dispersion	0.06
ν	eddy viscosity	0.001
c	soliton velocity	1.02
θ	$z_\theta = -\theta h$	$1 - \sqrt{5}/5$
x_0	soliton center at $t = 0$	-1.5

Table 4.2: Values of the parameters used in the numerical computations

over the flat bottom:

$$\begin{aligned}\eta_t + ((1 + \varepsilon\eta)u)_x + \mu^2\left(\frac{\theta^2}{2} - \theta + \frac{1}{3}\right)u_{xxx} &= 0, \\ u_t + \eta_x + \frac{\varepsilon}{2}(u^2)_x - \mu^2\theta\left(1 - \frac{\theta}{2}\right)u_{xxt} &= 0.\end{aligned}$$

Then, we apply the same approach that in Section 2.9.1. We do not provide the computations here since they are simple and can be done without any difficulties. The final result is the following:

$$\eta(x, t) = \frac{2(c-1)}{\varepsilon} \operatorname{sech}^2\left(\frac{\sqrt{6(c-1)}}{2\mu}(x + x_0 - ct)\right)$$

and the velocity is given by this formula:

$$u = \eta - \frac{1}{4}\varepsilon\eta^2 + \mu^2\left(\theta - \frac{\theta^2}{2} - \frac{1}{6}\right)\eta_{xx} + \mathcal{O}(\varepsilon^2 + \varepsilon\mu^2 + \mu^4).$$

In the numerical results presented here, we use $\eta(x, 0)$ and $u(x, 0)$ as initial conditions.

4.6.2 Discussion

On Figures 4.8–4.10 we present three curves. They depict the free surface elevation according to three different formulations. The first corresponds to classical Boussinesq equations without dissipation. The second one to dissipative system with differential terms (for example $\nu\Delta\vec{u}$ in momentum conservation equation) and the third curve corresponds to equations (4.22), (4.23). On Figure 4.11 we made a zoom on the soliton crest.

It can be seen that Boussinesq equations with nonlocal term provide stronger attenuation of the amplitude. In the same time, as it was shown in the previous section, this nonlocal term slightly slows down the solitary wave.

In order to show explicitly the rate of amplitude attenuation, we plot on Figure 4.12 the graph of the following application $t \rightarrow \sup_{-\pi < x < \pi} |\eta(x, t)|$. One can see on this plot little oscillations which are of numerical nature. Our numerical experiments show that their amplitude decreases when $N \rightarrow \infty$. This result shows one more time that nonlocal model provides stronger damping properties. One can have the impression that the amplitude decays linearly but it is only an impression because of (4.2). This behaviour for moderate t can be explained by simple Taylor expansion which is valid when $\nu k^2 t \ll 1$:

$$\alpha(t) = \alpha_0 e^{-2\nu k^2 t} = \alpha_0(1 - 2\nu k^2 t) + \mathcal{O}(\nu^2 k^4 t^2).$$

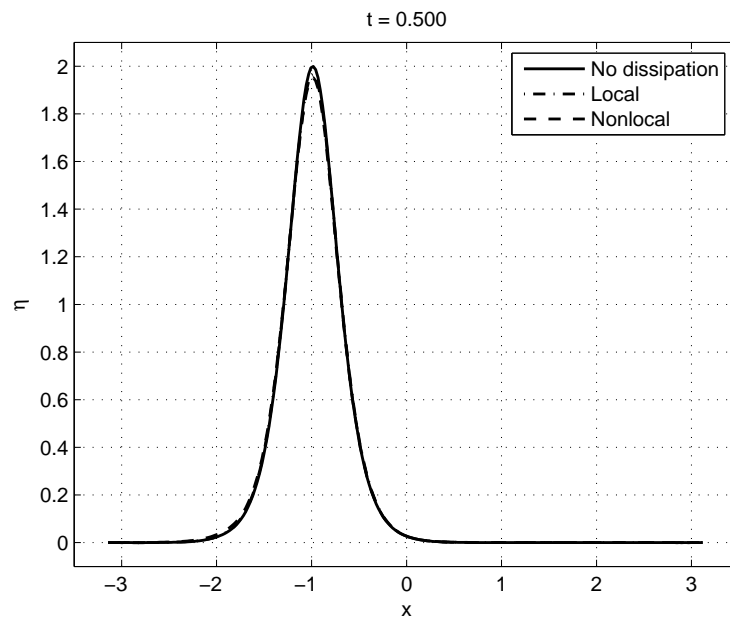


Figure 4.8: Comparison among two dissipative and nondissipative Boussinesq equations. Snapshots of the free surface at $t = 0.5$

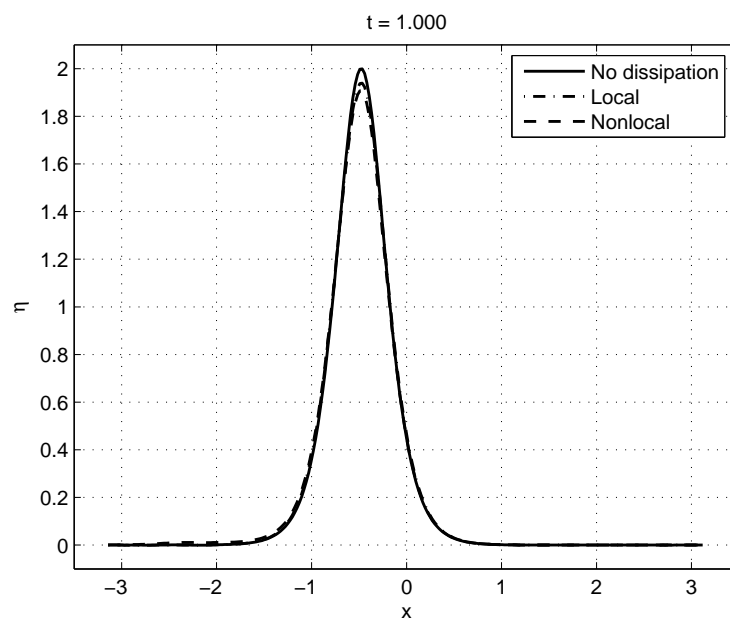


Figure 4.9: Comparison among two dissipative and nondissipative Boussinesq equations. Snapshots of the free surface at $t = 1.0$

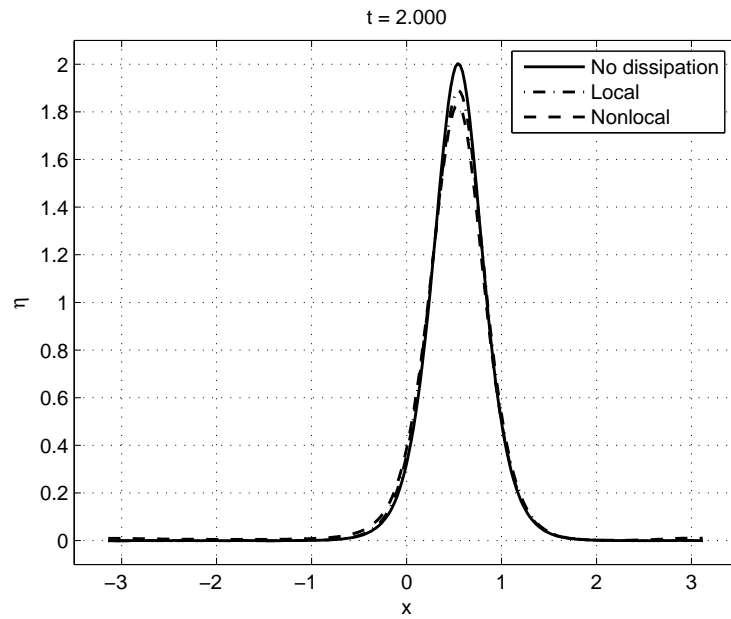


Figure 4.10: Comparison among two dissipative and nondissipative Boussinesq equations. Snapshots of the free surface at $t = 2.0$

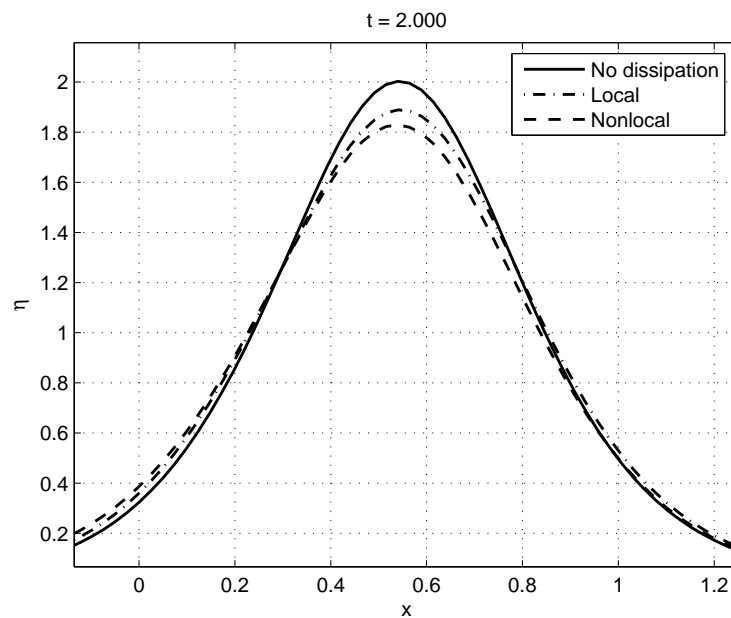


Figure 4.11: Comparison among two dissipative and nondissipative Boussinesq equations. Zoom on the soliton crest at $t = 2.0$

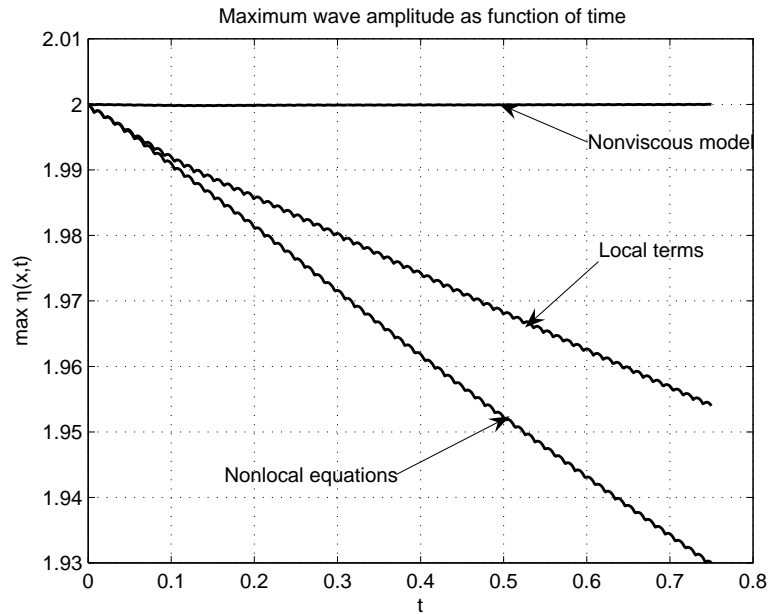


Figure 4.12: Amplitude of the solitary wave as function of time

4.7 Conclusion

In the present chapter we have shown how to express the rotational component of the velocity field in terms of the potential part of Helmholtz–Leray decomposition. This expression contains differential and integral operators. Obviously, this analysis is only linear but we give nonlinear equations. In future work we will try to extend the present derivation to the nonlinear case. A long wave approximation was derived from this new potential flow formulation.

Our results are different from [KM75]. This discrepancy can be explained by a different scaling chosen by Kakutani & Matsuuchi in the boundary layer. Consequently, their governing equations contain a nonlocal term in space. The performance of the present nonlocal term (4.17) was studied in [LSVO06]. The authors carried out in a wave tank a set of experiments, analyzing the damping and shoaling of solitary waves. It is shown that the viscous damping due to the bottom boundary layer is well represented. Their numerical results fit very well with the experiments. The numerical model not only properly predicts the wave height at a given point but also provides a good representation of the changes on the shape and celerity of the soliton. We can conclude that the experimental study by P. Liu [LSVO06] completely validates our theory.

It is interesting to note that local dissipative terms of this form have been used to verify

the theory of weak turbulence of surface gravity waves in deep water⁵ [DKZ03, DKZ04, ZKPD05]. They were added without justification to model dissipation at small scales. Note that a good qualitative agreement was obtained between the Kolmogorov spectrum predicted by weak turbulence theory and the results of DNS. Hence, the present work can be considered as an attempt to justify the inclusion of these terms.

Our final remark concerns the nonlocal term in the kinematic bottom boundary condition. This term can be also considered as a boundary layer correction at the bottom. In modelling viscous effects this term plays the main role, since its magnitude is $\mathcal{O}(\sqrt{\nu})$. Of course, the numerical implementation of this term is another matter. It is interesting to note that the boundary layer effect is not instantaneous but rather cumulative. The flow history is weighted by $(t - \tau)^{-\frac{1}{2}}$ in favour of the current time t . As pointed out in [LO04], this nonlocal term is essential to have an accurate estimation of the bottom shear stress based on the calculated wave field above the bed. Then, this information can be used for calculating sediment-bedload transport fluxes and, in turn, morphological changes.

We would like to mention here a paper of N. Sugimoto [Sug91]. He considered initial-value problems for the Burgers equation with the inclusion of a hereditary integral known as the fractional derivative of order $1/2$. The form of this term was not justified in that work. Note, that from fractional calculus point of view our nonlocal term is a half-order integral.

The dispersion relation associated with a new nonlocal formulation was described. Due to the presence of special functions, we cannot obtain a simple analytical dependence of the frequency ω on the wavenumber k as in classical equations. Consequently the dispersion curve was obtained numerically by a Newton-type method. We made a comparison between the phase velocity of the complete visco-potential problem and the corresponding Boussinesq equations. The effect of the nonlocal term on the solitary wave attenuation was investigated numerically with a Fourier-type spectral method.

What is the value of ν to be taken in numerical simulations? There is surprisingly little published information of this subject. What is clear is that the molecular diffusion is too small to model true viscous damping and one should rather consider the eddy viscosity parameter.

⁵Since the water is considered to be of infinite depth, they do not have the bottom boundary layer phenomenon. Hence, the local viscous terms are very natural choice to model dissipation at Kolmogorov scale.

Direction for future research

*Progress imposes not only new possibilities
for the future but new restrictions.*

Norbert Wiener (1894 – 1964)

A useful direction for future research in the dynamics of tsunami waves is the three-dimensional (3D) simulation of tsunami breaking along a coast. For this purpose, different validation steps are necessary. First more simulations of a two-dimensional (2D) tsunami interacting with a sloping beach ought to be performed. Then these simulations should be extended to the case of a 2D tsunami interacting with a sloping beach in the presence of obstacles. An important output of these computations will be the hydrodynamic loading on obstacles. The nonlinear inelastic behaviour of the obstacles may be accounted for using damage or plasticity models. The development of Boussinesq type models coupled with structure interactions is also a promising task. Finally there is a need for 3D numerical simulations of a tsunami interacting with a beach of complex bathymetry, with or without obstacles. These simulations will hopefully demonstrate the usefulness of numerical simulations for the definition of protecting devices or security zones. An important challenge in that respect is to make the numerical methods capable of handling interaction problems involving different scales: the fine scale needed for representing the damage of a flexible obstacle and a coarse scale needed to quantify the tsunami propagation.

Appendix A

Finite Volumes: Characteristic flux approach

Most of the fundamental ideas of science are essentially simple, and may, as a rule, be expressed in a language comprehensible to everyone.

Albert Einstein (1879 – 1955)

Contents

A.1 Discretization in the finite volume framework	198
A.1.1 The one dimensional case	198
A.1.2 Extension to the multidimensional case	201
A.1.3 On the discretization of source terms	202
A.2 On the discretization of boundary conditions	204

The VFFC¹ approach is based on a discretization of the continuous models through a cell-centered finite volume method. More precisely, we discretize space derivatives using finite volumes and time derivatives by classical finite differences. So at a fixed time step, the solution is represented by a collection of numbers which intend to approximate the mean values of the physical solution on the control volumes. As it is well known, the heart of the matter consists in computing from these degrees of freedom the values of the physical fluxes on the boundaries of the control volumes.

These fluxes are of two different nature: convective fluxes and viscous (or diffusive) fluxes. We know from many instances stemming from single phase fluid flows that the discretization of these fluxes must be adapted to their physical origin. More precisely on

¹Volumes Finis à Flux Caractéristiques

the one hand, discretization of convective fluxes must take into account the wave phenomena associated with convection, that is upwind based methods. On the other hand the discretization of viscous fluxes can rely on centered methods.

In this chapter we are going only to deal with convective fluxes. Moreover we keep the time-variable continuous in order to clearly separate the features of space and time discretizations.

A.1 Discretization in the finite volume framework

In this section we present a method [GKC96, GKC01] for the discretization of hyperbolic systems in the one dimensional case. The extension to the multidimensional case is discussed in Section A.1.2.

A.1.1 The one dimensional case

Let us consider general systems that can be written as follows:

$$\frac{\partial v}{\partial t} + \frac{\partial f(v)}{\partial x} = 0, \quad (\text{A.1})$$

where $v \in \mathbb{R}^m$ and $f : \mathbb{R}^m \mapsto \mathbb{R}^m$. We denote by $A(v)$ the jacobian matrix $\frac{\partial f(v)}{\partial v}$ and we deal first with the case where (A.1) is *smoothly hyperbolic* that is to say: for every v there exists a smooth basis $(r_1(v), \dots, r_m(v))$ of \mathbb{R}^m consisting of eigenvectors of $A(v) : \exists \lambda_k(v) \in \mathbb{R}$ such that $A(v)r_k(v) = \lambda_k(v)r_k(v)$. It is then possible to construct $(l_1(v), \dots, l_m(v))$ such that ${}^t A(v)l_k(v) = \lambda_k(v)l_k(v)$ and $l_k(v) \cdot r_p(v) = \delta_{k,p}$.

Let $\mathbb{R} = \cup_{j \in \mathbb{Z}} [x_{j-1/2}, x_{j+1/2}]$ be a one dimensional mesh. Our goal is to discretize (A.1) by a finite volume method. We set $\Delta x_j \equiv x_{j+1/2} - x_{j-1/2}$, $\Delta t_n \equiv t_{n+1} - t_n$ (we also have $\mathbb{R}_+ = \cup_{n \in \mathbb{N}} [t_n, t_{n+1}]$) and

$$\tilde{v}_j^n \equiv \frac{1}{\Delta x_j} \int_{x_{j-1/2}}^{x_{j+1/2}} v(x, t_n) dx, \tilde{f}_{j+1/2}^n \equiv \frac{1}{\Delta t_n} \int_{t_n}^{t_{n+1}} f(v(x_{j+1/2}, t)) dt.$$

With these notations, we deduce from (A.1) the *exact* relation:

$$\tilde{v}_j^{n+1} = \tilde{v}_j^n - \frac{\Delta t_n}{\Delta x_j} \left(\tilde{f}_{j+1/2}^n - \tilde{f}_{j-1/2}^n \right). \quad (\text{A.2})$$

Since the $(\tilde{f}_{j+1/2}^n)_{j \in \mathbb{Z}}$ cannot be expressed in terms of the $(\tilde{v}_j^n)_{j \in \mathbb{Z}}$, one has to make an approximation. In order to keep a compact stencil, it is more efficient to use a three points scheme: the physical flux $\tilde{f}_{j+1/2}^n$ is approximated by a numerical flux $g_j^n(v_j^n, v_{j+1}^n)$. Let us

show how we construct this flux here. We observe that since $A(v)\frac{\partial v}{\partial t} = \frac{\partial f(v)}{\partial t}$ then according to (A.1),

$$\frac{\partial f(v)}{\partial t} + A(v)\frac{\partial f(v)}{\partial x} = 0. \quad (\text{A.3})$$

This shows that the flux $f(v)$ is advected by $A(v)$ (like v since we also have $\frac{\partial v}{\partial t} + A(v)\frac{\partial v}{\partial x} = 0$). The numerical flux $g_j^n(v_j^n, v_{j+1}^n)$ represents the flux at an interface. Using a mean value $\mu_{j+1/2}^n$ of v at this interface, we replace (A.3) by the linearization:

$$\frac{\partial f(v)}{\partial t} + A(\mu_{j+1/2}^n)\frac{\partial f(v)}{\partial x} = 0. \quad (\text{A.4})$$

It follows that, defining the k -th characteristic flux component to be $f_k(v) \equiv l_k(\mu_{j+1/2}^n) \cdot f(v)$, we have

$$\frac{\partial f_k(v)}{\partial t} + \lambda_k(\mu_{j+1/2}^n)\frac{\partial f_k(v)}{\partial x} = 0. \quad (\text{A.5})$$

This linear equation can be solved explicitly now and we have:

$$f_k(v)(x, t) = f_k(v)(x - \lambda_k(\mu_{j+1/2}^n)(t - t_n), t_n). \quad (\text{A.6})$$

From this equation it is then natural to introduce the following definition.

Definition 2 For the conservative system (A.1), at the interface between the two cells $[x_{j-1/2}, x_{j+1/2}]$ and $[x_{j+1/2}, x_{j+3/2}]$, the characteristic flux g^{CF} is defined by the following formula (we take $\mu_{j+1/2}^n \equiv (\Delta x_j v_j^n + \Delta x_{j+1} v_{j+1}^n) / (\Delta x_j + \Delta x_{j+1})$) : for $k \in \{1, \dots, m\}$,

$$\begin{aligned} l_k(\mu_{j+1/2}^n) \cdot g_j^{CF,n}(v_j^n, v_{j+1}^n) &= l_k(\mu_{j+1/2}^n) \cdot f(v_j^n), \text{ when } \lambda_k(\mu_{j+1/2}^n) > 0, \\ l_k(\mu_{j+1/2}^n) \cdot g_j^{CF,n}(v_j^n, v_{j+1}^n) &= l_k(\mu_{j+1/2}^n) \cdot f(v_{j+1}^n), \text{ when } \lambda_k(\mu_{j+1/2}^n) < 0, \\ l_k(\mu_{j+1/2}^n) \cdot g_j^{CF,n}(v_j^n, v_{j+1}^n) &= l_k(\mu_{j+1/2}^n) \cdot \left(\frac{f(v_{j+1}^n) + f(v_j^n)}{2} \right), \end{aligned} \quad (\text{A.7})$$

when $\lambda_k(\mu_{j+1/2}^n) = 0$.

Remark 20 At first glance, the derivation of (A.3) from (A.1), is only valid for continuous solutions since $A(v)\frac{\partial f(v)}{\partial x}$ is a non conservative product. In fact equation (A.3) can be justified even in the case of shocks as is proved in [Ghi98]. Let us briefly recall here the key point. Assuming that the solution undergoes a discontinuity along a family of disjoint curves, we can focus on one of these curves that we parameterize by the time variable t . Hence, locally, on each side of this curve, $v(x, t)$ is smooth and jumps across the curve $x = \Sigma(t)$. The Rankine-Hugoniot condition implies that $f(v(x, t)) - \sigma(t)v(x, t)$, where $\sigma(t) \equiv \frac{d\Sigma(t)}{dt}$, is smooth across the discontinuity curve and therefore $A(v)\frac{\partial f(v)}{\partial x}$ can be defined as $A(v)\frac{\partial f(v)}{\partial x} \equiv A(v)\frac{\partial(f(v) - \sigma v)}{\partial x} + \sigma\frac{\partial f(v)}{\partial x}$.

Proposition 1 Formula (A.7) can be written as follows: $g_j^{CF,n}(v_j^n, v_{j+1}^n) = g^{CF}(\mu_j^n; v_j^n, v_{j+1}^n)$ where

$$g^{CF}(\mu; v, w) \equiv \sum_{\lambda_k(\mu) < 0} (l_k(\mu) \cdot f(w)) r_k(\mu) + \sum_{\lambda_k(\mu) = 0} \left(l_k(\mu) \cdot \frac{f(v) + f(w)}{2} \right) r_k(\mu) + \sum_{\lambda_k(\mu) > 0} (l_k(\mu) \cdot f(v)) r_k(\mu). \quad (\text{A.8})$$

Proof. This comes from the useful identity valid for all vectors Φ and μ in \mathbb{R}^m : $\Phi = \sum_{k=1}^m (l_k(\mu) \cdot \Phi) r_k(\mu)$. We also observe that (A.8) can be written under the following condensed form:

$$g^{CF}(\mu; v, w) = \frac{f(v) + f(w)}{2} - U(\mu; v, w) \frac{f(w) - f(v)}{2}, \quad (\text{A.9})$$

where $U(\mu; v, w)$ is the sign of the matrix $A(\mu)$ which is defined by

$$\text{sign}(A(\mu))\Phi = \sum_{k=1}^m \text{sign}(\lambda_k) (l_k(\mu) \cdot \Phi) r_k(\mu).$$

The form (A.9) refers to what we have called a numerical flux leading to a flux scheme ([Ghi98]). ■

Remark 21 Let us discuss the relation, in the conservative case, between the characteristic numerical flux g^{CF} and the numerical flux leading to Roe's scheme [Roe81]. This later scheme relies on an algebraic property of the continuous flux $f(v)$ which is as follows. It is assumed that for all admissible states v and w , there exists a $m \times m$ matrix $A^{ROE}(v, w)$ such that $f(v) - f(w) = A^{ROE}(v, w)(v - w)$ (Roe's identity). Then the numerical flux leading to Roe's scheme is given by:

$$g^{ROE}(v, w) = \frac{f(v) + f(w)}{2} - |A^{ROE}(v, w)| \frac{w - v}{2}. \quad (\text{A.10})$$

But using Roe's identity, we obtain that

$$g^{ROE}(v, w) = \frac{f(v) + f(w)}{2} - \text{sign}(A^{ROE}(v, w)) \frac{f(w) - f(v)}{2}, \quad (\text{A.11})$$

which is of the form (A.9): Roe's scheme is also a flux scheme. The characteristic flux proposed in this paper is more versatile than Roe's scheme in the sense that it does not rely on an algebraic property of the flux. Hence for complex systems (like those encountered in the context of two phase flows) this scheme appears like an efficient generalization of

Roe's scheme. Moreover, as we shall see below, this scheme has a natural generalization to arbitrary non conservative systems. Finally, the fact that the numerical flux is a linear combination of the two fluxes induces a quite weak dependance on the state μ which appears in formula (A.8), see [CG00].

Combining (A.2) and (A.7), we arrive to the explicit scheme:

$$v_j^{n+1} = v_j^n - \frac{\Delta t_n}{\Delta x_j} \left(g_j^{CF,n}(v_j^n, v_{j+1}^n) - g_j^{CF,n}(v_{j-1}^n, v_j^n) \right). \quad (\text{A.12})$$

A.1.2 Extension to the multidimensional case

Let us consider a system of m balance equations: ($v = (v_1, \dots, v_m) \in \mathbb{R}^m$)

$$\frac{\partial v}{\partial t} + \nabla \cdot F(v) = 0, \quad (\text{A.13})$$

here $\nabla \cdot F(v) = \sum_{j=1}^{nd} \frac{\partial F^j(v)}{\partial x_j}$, where F^j maps G into \mathbb{R}^m , where G is an open subset of \mathbb{R}^m corresponding to the physically admissible states. This equation is posed in a nd -dimensional domain Ω ($nd = 1, 2$ or 3 in practice).

We assume that the computational domain Ω is decomposed in smaller volumes (the so-called control volumes) $K : \Omega = \cup_{K \in \mathcal{T}} K$ and consider first the case where $\Omega = \cup_{K \in \mathcal{T}} K$ is "conformal" *i.e.* that it is a finite element triangulation of Ω . In practice one can use triangles for $nd = 2$ and tetrahedrons for $nd = 3$. The cell-centered finite volume approach for solving (A.13) consists in approximating the means

$$v_K(t) \equiv \frac{1}{\text{vol}(K)} \int_K v(x, t) dx, \quad (\text{A.14})$$

where $\text{vol}(K)$ denotes the nd -dimensional volume of K and $\text{area}(A)$ stands for the $(nd-1)$ -dimensional volume of an hypersurface A . Integrating (A.13) on K makes the normal fluxes, $F_{\partial K}^\nu$, appear

$$F_{\partial K}^\nu(t) = \int_{\partial K} F(v(\sigma, t)) \cdot \nu(\sigma) d\sigma,$$

where ∂K is the boundary of K , $\nu(\sigma)$ the unit external normal on ∂K and $d\sigma$ denotes the $(nd-1)$ -volume element on this hypersurface.

The heart of the matter in finite volume methods consists in providing a formula for the normal fluxes $F_{\partial K}^\nu$ in terms of the $\{v_L\}_{L \in \mathcal{T}}$. Assuming that the control volumes K are polyhedra, as is most often the case, the boundary ∂K is the union of hypersurfaces $K \cap L$ where L belongs to the set $\mathcal{N}(K)$, the set of $L \in \mathcal{T}$, $L \neq K$, such that $K \cap L$ has positive $(nd-1)$ -measure. We can therefore decompose the normal flux as a sum: $F_{\partial K}^\nu = \sum_{L \in \mathcal{N}(K)} F_{K,L}$, where

($\nu_{K,L}$ points into L): $F_{K,L} = \int_{K \cap L} F(v(\sigma, t)) \cdot \nu_{K,L} d\sigma$. Inspired by the 1D-case, we take an approximation of $F_{K,L}$ in terms of v_K and v_L : $F_{K,L} \approx \text{area}(K \cap L) \Phi(v_K, v_L; K, L)$, where Φ is the numerical flux that we construct by the following formula.

Definition 3 *The numerical flux of the Finite Volume method with characteristic flux is obtained by the formula*

$$\Phi(v, w; K, L) = \frac{F(v) + F(w)}{2} \cdot \nu_{K,L} - U(v, w; K, L) \frac{F(w) - F(v)}{2} \cdot \nu_{K,L}, \quad (\text{A.15})$$

when we take:

$$U(v, w; K, L) = \text{sign}(A_{\nu_{K,L}}(\mu(v, w; K, L))), \quad (\text{A.16})$$

where $\mu(v, w; K, L)$ is a mean between v_K and v_L which only depends on the geometry of K and L :

$$\mu(v, w; K, L) = \frac{\text{vol}(K)v + \text{vol}(L)w}{\text{vol}(K) + \text{vol}(L)}, \quad (\text{A.17})$$

and $A_\nu(v) \equiv \frac{\partial F(v) \cdot \nu}{\partial v}$. ■

This allows us to generalize the explicit scheme (A.12) to the multidimensional case as follows.

Definition 4 *The explicit multidimensional characteristic flux for the approximation of equation (A.13) reads as follows:*

$$v_K^{n+1} = v_K^n - \frac{\Delta t_n}{\text{vol}(K)} \sum_{L \in \mathcal{N}(K)} \text{area}(K \cap L) \Phi(v_K^n, v_L^n; K, L). \quad (\text{A.18})$$

A.1.3 On the discretization of source terms

Let us return to the 1D setting. Instead of (A.1), we want to solve

$$\frac{\partial v}{\partial t} + \frac{\partial f(v)}{\partial x} = S, \quad (\text{A.19})$$

by the numerical scheme:

$$v_j^{n+1} = v_j^n - \frac{\Delta t_n}{\Delta x_j} (f_{j+1/2}^n - f_{j-1/2}^n) + \Delta t_n \Sigma_j^n. \quad (\text{A.20})$$

Equation (A.20) can be obtained by integration of (A.19) on the rectangle $[t_n, t_{n+1}] \times [x_{j-1/2}, x_{j+1/2}]$ and this leads to the following form for Σ_j^n :

$$\Sigma_j^n = \Sigma_j = \frac{1}{\Delta x_j} \int_{x_{j-1/2}}^{x_{j+1/2}} S(x) dx. \quad (\text{A.21})$$

Actually, this formula is not suitable when the source term is large and one must modify (A.21) according to the expression of the numerical flux g_j where $f_{j+1/2}^n = g_j(v_{j+1}^n, v_j^n)$ and

$$g(v, w) = \frac{f(v) + f(w)}{2} - U(v, w) \frac{f(w) - f(v)}{2}, \quad (\text{A.22})$$

where $U(\cdot, \cdot)$ is a matrix to be specified.

Due to the fact that the numerical flux is not centered (upwind bias) one can observe large errors on the permanent solution under investigation. Let us introduce the notion of enhanced consistency as follows. Denoting by

$$\phi = \phi^{\text{conv.}}(x) \equiv \int_0^x S(y) dy, \quad (\text{A.23})$$

we say that Σ_j^n satisfies, with respect to the numerical flux g , the enhanced consistency property when we have: if at some time-step, v_j^n is such that

$$f(v_j^n) = \frac{1}{\Delta x_j} \int_{x_{j-1/2}}^{x_{j+1/2}} \phi^{\text{conv.}}(x) dx, \quad \forall j \in \mathbb{Z}, \quad (\text{A.24})$$

then v_j^{n+1} given by (A.20) must be equal to v_j^n . This condition can be equivalently formulated as

$$\Sigma_j^n = \frac{f_{j+1/2}^n - f_{j-1/2}^n}{\Delta x_j}, \quad (\text{A.25})$$

if v_j^n satisfies (A.24).

In [AGT99], the following results are shown.

Theorem 3 *Let g be given in the form (A.22) and denote by $U_j^n = U(v_j^n, v_{j+1}^n)$. The enhanced consistency will be satisfied if we discretize the forcing term S according to the following formula*

$$\Sigma_j^n = \frac{1}{2\Delta x_j} \left\{ \int_{x_{j-1}}^{x_{j+1}} S(y) dy - U_j^n \int_{x_j}^{x_{j+1}} S(y) dy + U_{j-1}^n \int_{x_{j-1}}^{x_j} S(y) dy \right\}. \quad (\text{A.26})$$

Corollary 1 *Assuming that S is given by a piecewise constant function: $S(x) = S_j$ for $x \in]x_{j-1/2}, x_{j+1/2}[$, the formula (A.26) reads*

$$\Sigma_j^n = \frac{I + U_{j-1}^n}{4} \frac{\Delta x_{j-1}}{\Delta x_j} S_{j-1} + \frac{I - U_j^n + U_{j-1}^n}{2} S_j + \frac{I - U_j^n}{4} \frac{\Delta x_{j+1}}{\Delta x_j} S_{j+1}. \quad (\text{A.27})$$

In order to illustrate this formula, let us show what it means in the case of a single linear equation $v_t + c v_x = S$ where e.g. $c > 0$ and $v \in \mathbb{R}$. Here the usual upwind scheme amounts to take $U_j^n = 1$, i.e. $g(v, w) = c v$ and (A.27) reads as:

$$\Sigma_j^n = \frac{1}{2} \frac{\Delta x_{j-1}}{\Delta x_j} S_{j-1} + \frac{1}{2} S_j. \quad (\text{A.28})$$

These results were one of the key points in the solution to the simulation of a boiling tube (see [TF98]).

A.2 On the discretization of boundary conditions

So far we have not discussed the implementation of boundary conditions. This is a very important topic since they actually determine the solution. Let us consider the space discretization of the system (A.1) by our cell centered finite volume method. For instance for the time explicit discretization we have the scheme (A.18). Of course this formula is not valid when K meets the boundary of Ω . When this occurs, we have to find the numerical flux $\Phi(v_K^n, K, \partial\Omega)$. In practice, this flux is not given by the physical boundary conditions and moreover, in general, (A.1) is an ill-posed problem if we try to impose either v or $F(v) \cdot \nu$ on $\partial\Omega$. This can be understood in a simple way by using the following linearization of this system:

$$\frac{\partial v}{\partial t} + \underline{A}_\nu \frac{\partial v}{\partial \nu} = 0, \quad (\text{A.29})$$

where ν represents the direction of the external normal on $K \cap \partial\Omega$, \underline{A}_ν is the advection matrix:

$$\underline{A}_\nu \equiv \frac{\partial F(v) \cdot \nu}{\partial v} \Big|_{v=\underline{v}}, \quad (\text{A.30})$$

and \underline{v} is the state around which the linearization is performed. When (A.1) is hyperbolic, the matrix \underline{A}_ν is diagonalizable on \mathbb{R} and by a change of coordinates, this system becomes an uncoupled set of m advection equations:

$$\frac{\partial \xi_k}{\partial t} + c_k \frac{\partial \xi_k}{\partial \nu}, \quad k = 1, \dots, m. \quad (\text{A.31})$$

Here the c_k are the eigenvalues of \underline{A}_ν and according to the sign of these numbers, waves are going either into the domain Ω ($c_k < 0$) or out of the domain Ω ($c_k > 0$). Hence we expect that it is only possible to impose p conditions on $K \cap \partial\Omega$ where $p \equiv \#\{k \in \{1, \dots, m\} \text{ such that } c_k < 0\}$.

Let us consider now a control volume K which meets the boundary $\partial\Omega$. We take $\underline{v} = v_K^n$ and write the previous linearization. We denote by x the coordinate along the outer normal so that (A.29) reads:

$$\frac{\partial v}{\partial t} + \underline{A}_\nu \frac{\partial v}{\partial x} = 0, \quad (\text{A.32})$$

which happens to be the linearization of the 1D (*i.e.* when $nd = 1$) system. First we label the eigenvalues $c_k(\underline{v})$ of \underline{A}_ν by increasing order:

$$c_1(\underline{v}) \leq c_2(\underline{v}) \leq \dots \leq c_p(\underline{v}) < 0 \leq c_{p+1}(\underline{v}) \dots \leq c_m(\underline{v}). \quad (\text{A.33})$$

- (i) The case $p = 0$. In this case information comes from inside Ω and therefore we take:

$$\Phi(v_K^n, K, \partial\Omega) = F(v_K^n) \cdot \nu_K. \quad (\text{A.34})$$

In the Computational Fluid Dynamics literature this is known as the “supersonic outflow” case.

- (ii) The case $p = m$. In this case information come from outside Ω and therefore we take:

$$\Phi(v_K^n, K, \partial\Omega) = \Phi_{given}, \quad (\text{A.35})$$

where Φ_{given} are the given physical boundary conditions. In the Computational Fluid Dynamics literature this is known as the “supersonic inflow” case.

- (iii) The case $1 \leq p \leq m - 1$. As already discussed, we need p scalar information coming from outside of Ω . Hence we assume that we have on physical ground p relations on the boundary:

$$g_l(v) = 0, \quad l = 1, \dots, p. \quad (\text{A.36})$$

Remark 22 *The notation $g_l(v) = 0$ means that we have a relation between the components of v . However, in general, the function g_l is not given explicitly in terms of v . For example $g_l(v)$ could be the pressure which is not, in general, one of the components of v .*

Since we have to determine the m components of $\Phi(v_K^n, K, \partial\Omega)$, we need $m - p$ supplementary scalar conditions. Let us write them as

$$h_l(v) = 0, \quad l = p + 1, \dots, m. \quad (\text{A.37})$$

In general (A.36) are named as “physical boundary conditions” while (A.37) are named as “numerical boundary conditions”.

Then we take:

$$\Phi(v_K^n, K, \partial\Omega) = F(v) \cdot \nu_K, \quad (\text{A.38})$$

where v is solution to (A.36)-(A.37) (see however Remark 25 and (A.44)).

Remark 23 *The system (A.36)-(A.37) for the m unknowns $v \in G$ is a $m \times m$ nonlinear system of equations. We are going to study its solvability, see Theorem 4.*

Let us first discuss the numerical boundary conditions (A.37). By analogy with what we did on an interface between two control volumes K and L , we take (recall that $\underline{v} = v_K^n$):

$$\tilde{l}_k(\underline{v}) \cdot (F(v) \cdot \nu_K) = \tilde{l}_k(\underline{v}) \cdot (F(v_K^n) \cdot \nu_K), \quad k = p + 1, \dots, m. \quad (\text{A.39})$$

In other words, we set $h_k(v) \equiv \tilde{l}_k(v_K^n) \cdot (F(v) \cdot \nu_K) - \tilde{l}_k(v_K^n) \cdot (F(v_K^n) \cdot \nu_K)$. We have denoted by $(\tilde{l}_1(\underline{v}), \dots, \tilde{l}_m(\underline{v}))$ a set of left eigenvectors of \tilde{A}_ν : ${}^t\tilde{A}_\nu l_k(\underline{v}) = c_k l_k(\underline{v})$ and by $(r_1(\underline{v}), \dots, r_m(\underline{v}))$ a set of right eigenvectors of \tilde{A}_ν : $\tilde{A}_\nu r_k(\underline{v}) = c_k r_k(\underline{v})$. Moreover the following normalization is taken: $\tilde{l}_k(\underline{v}) \cdot \tilde{r}_p(\underline{v}) = \delta_{k,p}$.

According to [GP05] we have the following result on the solvability of (A.36)-(A.37).

Theorem 4 *In the case $1 \leq p \leq m - 1$, assume that $c_{p+1}(\underline{v}) > 0$, and*

$$\det_{1 \leq k, l \leq p} \left(\sum_{i=1}^m r_k^i(\underline{v}) \frac{\partial g_l}{\partial v_i}(\underline{v}) \right) \neq 0. \quad (\text{A.40})$$

With the choice (A.39) the nonlinear system (A.36)-(A.37) has one and only one solution v , for $v - \underline{v}$ and $g_l(\underline{v})$ sufficiently small.

Remark 24 *In this result we exclude the case where the boundary is characteristic i.e. the case where one of the c_k is equal to 0. This case cannot be dealt at this level of generality. On the other hand, wall boundary conditions belong to this category. They can be discussed and handled directly on the physical system under consideration, see [GP05].*

Remark 25 *In practice, (A.36)-(A.37) are written in a parametric way. We have a set of m physical variables w (e.g. pressure, densities, velocities, ...) and we look for w satisfying:*

$$g_l(w) = 0, \quad l = 1, \dots, p, \quad (\text{A.41})$$

$$\tilde{l}_k(\underline{v}) \cdot \Phi = \tilde{l}_k(\underline{v}) \cdot (F(v_K^n) \cdot \nu_K), \quad (\text{A.42})$$

$$\Phi = F(w) \cdot \nu_K, \quad (\text{A.43})$$

and then we take:

$$\Phi(v_K^n, K, \partial\Omega) = \Phi. \quad (\text{A.44})$$

The system (A.41)-(A.42)-(A.43) is then solved by Newton's method.

Bibliography

- [AG73] A.S. Alekseev and V.K. Gussyakov. *Theory of diffraction and wave propagation*, volume 2, chapter Numerical modelling of tsunami and seismo-acoustic waves generation by submarine earthquakes, pages 194–197. Moscow-Erevan, 1973. in Russian. [3](#)
- [AGT99] F. Alouges, J.-M. Ghiadaglia, and M. Tajchman. On the interaction between upwinding and forcing for hyperbolic systems of conservation laws. Technical report, Centre de Mathématiques et Leurs Applications, 1999. [203](#)
- [AMS04] F. Archambeau, N. Mehitoua, and M. Sakiz. Code Saturne: A finite volume code for turbulent flows. *International Journal On Finite Volumes*, 1, 2004. [140](#)
- [BB73] J.P. Boris and D.L. Book. Flux corrected transport: Shasta, a fluid transport algorithm that works. *J. Comp. Phys.*, 11:38–69, 1973. [143](#)
- [BBM72] T.B. Benjamin, J.L. Bona, and J.J. Mahony. Model equations for long waves in nonlinear dispersive systems. *Philos. Trans. Royal Soc. London Ser. A*, 272:47–78, 1972. [3](#), [106](#)
- [BCL05] J.L. Bona, T. Colin, and D. Lannes. Long wave approximations for water waves. *Arch. Rational Mech. Anal.*, 178:373–410, 2005. [57](#)
- [BCS02] J.L. Bona, M. Chen, and J.-C. Saut. Boussinesq equations and other systems for small-amplitude long waves in nonlinear dispersive media. i: Derivation and linear theory. *Journal of Nonlinear Science*, 12:283–318, 2002. [xxiii](#), [xxv](#), [83](#), [104](#), [105](#)
- [BDM07] J.L. Bona, V.A. Dougalis, and D.E. Mitsotakis. Numerical solution of KdV-KdV systems of Boussinesq equations: I. The numerical scheme and generalized solitary waves. *Mat. Comp. Simul.*, 74:214–228, 2007. [xxvi](#)

- [Ben74] T. B. Benjamin. *Lectures in Appl. Math.*, volume 15, chapter Lectures on nonlinear wave motion, pages 3–47. Amer. Math. Soc., Providence, RI, 1974. [99](#)
- [Ben06] M. Benoit. *Contribution à l'étude des états de mer et des vagues, depuis l'océan jusqu'aux ouvrages cotiers*. 2006. Mémoire d'habilitation à diriger des recherches. [91](#)
- [BF90] T.J. Barth and P.O. Frederickson. Higher order solution of the Euler equations on unstructured grids using quadratic reconstruction. *AIAA*, 90-0013, 1990. [137](#)
- [BH86] N. Bleistein and R.A. Handelsman. *Asymptotic Expansions of Integrals*. Courier Dover Publications, 1986. [29](#)
- [BJ89] T.J. Barth and D.C. Jespersen. The design and application of upwind schemes on unstructured meshes. *AIAA*, 0366, 1989. [133](#), [143](#), [144](#)
- [BMR72] A. Ben-Menahem and M. Rosenman. Amplitude patterns of tsunami waves from submarine earthquakes. *J. Geophys. Res.*, 77:3097–3128, 1972. [36](#)
- [BMSS69] A. Ben-Menahem, S. J. Singh, and F. Solomon. Static deformation of a spherical earth model by internal dislocations. *Bull. Seism. Soc. Am.*, 59:813–853, 1969. [4](#)
- [BMSS70] A. Ben-Mehanem, S. J. Singh, and F. Solomon. Deformation of an homogeneous earth model finite by dislocations. *Rev. Geophys. Space Phys.*, 8:591–632, 1970. [4](#)
- [BO04] T.J. Barth and M. Ohlberger. *Encyclopedia of Computational Mechanics, Volume 1, Fundamentals*, chapter Finite Volume Methods: Foundation and Analysis. John Wiley and Sons, Ltd, 2004. [133](#), [144](#)
- [BOPB07] G. N. Bullock, C. Obhrai, D. H. Peregrine, and H. Bredmose. Violent breaking wave impacts. part 1: Results from large-scale regular wave tests on vertical and sloping walls. *Coastal Engineering*, 54:602–617, 2007. [123](#), [124](#), [125](#)
- [Bou71a] J. V. Boussinesq. Théorie générale des mouvements qui sont propagés dans un canal rectangulaire horizontal. *C. R. Acad. Sc. Paris*, 73:256–260, 1871. [82](#)

- [Bou71b] M.J. Boussinesq. Théorie de l'intumescence liquide appelée onde solitaire ou de translation se propageant dans un canal rectangulaire. *C.R. Acad. Sci. Paris Sér. A-B*, 72:755–759, 1871. [3](#)
- [Bou72] J. Boussinesq. Théorie des ondes et des remous qui se propagent le long d'un canal rectangulaire horizontal, en communiquant au liquide contenu dans ce canal des vitesses sensiblement pareilles de la surface au fond. *J. Math. Pures Appl.*, 17:55–108, 1872. [82](#)
- [Bou95] J. Boussinesq. Lois de l'extinction de la houle en haute mer. *C. R. Acad. Sci. Paris*, 121:15–20, 1895. [83](#), [84](#), [170](#), [186](#)
- [BPS81] J.L. Bona, W.G. Pritchard, and L.R. Scott. An evaluation of a model equation for water waves. *Phil. Trans. R. Soc. Lond. A*, 302:457–510, 1981. [37](#), [84](#), [89](#), [106](#), [110](#), [119](#), [170](#)
- [BPS85] J. L. Bona, W.G. Pritchard, and L.R. Scott. Numerical schemes for a model for nonlinear dispersive waves. *Journal of Computational Physics*, 60:167–186, 1985. [106](#)
- [BQ06] F. Benkhaldoun and L. Quivy. A non homogeneous riemann solver for shallow water and two phase flows. *Flow, Turbulence and Combustion*, 76:391–402, 2006. [70](#), [71](#)
- [BUST06] J. Borrero, B. Uslu, C. Synolakis, and V.V. Titov. Modeling far field tsunamis for california ports and harbors. *Coastal Engineering*, pages 1566–1578, 2006. [78](#)
- [BvdDP73] R.D. Braddock, P. van den Driessche, and G.W. Peady. Tsunamis generation. *J. Fluid Mech.*, 59(4):817–828, 1973. [3](#)
- [Car71] G.F. Carrier. The dynamics of tsunamis. *Mathematical Problems in the Geophysical Sciences. Lectures in Applied Mathematics*, 13:157–187, 1971. [3](#)
- [CG58] G. F. Carrier and H. P. Greenspan. Water waves of finite amplitude on a sloping beach. *Journal of Fluid Mechanics*, 2:97–109, 1958. [xxvii](#)
- [CG00] J. Cortes and J.-M. Ghidaglia. Upwinding at low cost for complex models and flux schemes. In *Trends in Numerical and Physical Modeling for Industrial Multiphase Flows*, 2000. [201](#)

- [CG07] M. Chen and O. Goubet. Long-time asymptotic behaviour of dissipative Boussinesq systems. *Discrete and Continuous Dynamical Systems*, 17:61–80, 2007. [171](#)
- [Cha05] H. Chanson. Le tsunami du 26 décembre 2004: un phénomène hydraulique d’ampleur internationale. premiers constats. *La Houille Blanche*, 2:25–32, 2005. [xvii](#)
- [Che98] M. Chen. Exact traveling-wave solutions to bidirectional wave equations. *International Journal of Theoretical Physics*, 37:1547–1567, 1998. [110](#), [112](#)
- [Chi63] M. A. Chinnery. The stress changes that accompany strike-slip faulting. *Bull. Seism. Soc. Am.*, 53:921–932, 1963. [10](#)
- [CLS04] B. Cockburn, F. Li, and C.-W. Shu. Locally divergence-free discontinuous Galerkin methods for the Maxwell equations. *Journal of Computational Physics*, 194:588–610, 2004. [131](#)
- [Coi94] W.J. Coirier. *An Adaptatively-Refined, Cartesian, Cell-based Scheme for the Euler and Navier-Stokes Equations*. PhD thesis, Michigan Univ., 1994. [144](#)
- [CP92] J. H. E. Cartwright and O. Piro. The dynamics of Runge–Kutta methods. *Int. J. Bifurcation and Chaos*, 2:427–449, 1992. [151](#)
- [CVV99] Y. Coudiere, J.P. Vila, and P. Villedieu. Convergence rate of a finite volume scheme for a two dimensionnal convection diffusion problem. *M2AN*, 33(3):493–516, 1999. [144](#)
- [CWY03] G. F. Carrier, T. T. Wu, and H. Yeh. Tsunami run-up and draw-down on a plane beach. *Journal of Fluid Mechanics*, 475:79–99, 2003. [xxviii](#)
- [DD06] F. Dias and D. Dutykh. *Extreme Man-Made and Natural Hazards in Dynamics of Structures*, chapter Dynamics of tsunami waves, pages 35–60. Springer, 2006. [xvii](#), [187](#)
- [DD07a] D. Dutykh and F. Dias. Dissipative Boussinesq equations. *C. R. Mecanique*, 335:559–583, 2007. [132](#), [171](#)
- [DD07b] D. Dutykh and F. Dias. Viscous potential free-surface flows in a fluid layer of finite depth. *C. R. Acad. Sci. Paris, Ser. I*, 345:113–118, 2007. [171](#)

- [DD07c] D. Dutykh and F. Dias. Water waves generated by a moving bottom. In Anjan Kundu, editor, *Tsunami and Nonlinear waves*. Springer Verlag (Geo Sc.), 2007. [38](#), [64](#), [65](#), [67](#), [91](#)
- [DDK06] D. Dutykh, F. Dias, and Y. Kervella. Linear theory of wave generation by a moving bottom. *C. R. Acad. Sci. Paris, Ser. I*, 343:499–504, 2006. [36](#), [44](#), [52](#), [61](#), [65](#), [67](#), [75](#)
- [DDZ07] F. Dias, A.I. Dyachenko, and V.E. Zakharov. Theory of weakly damped free-surface flows: a new formulation based on potential flow solutions. *Physics Letters A*, to appear, 2007. [85](#), [87](#), [94](#), [171](#), [176](#)
- [DGK06] R. A. Dalrymple, S. T. Grilli, and J. T. Kirby. Tsunamis and challenges for accurate modeling. *Oceanography*, 19:142–151, 2006. [xxiii](#)
- [DKZ03] A.I. Dyachenko, A.O. Korotkevich, and V.E. Zakharov. Weak turbulence of gravity waves. *JETP Lett.*, 77:546–550, 2003. [171](#), [193](#)
- [DKZ04] A.I. Dyachenko, A.O. Korotkevich, and V.E. Zakharov. Weak turbulent Kolmogorov spectrum for surface gravity waves. *Phys. Rev. Lett.*, 92:134501, 2004. [171](#), [193](#)
- [DM04] V.A. Dougalis and D.E. Mitsotakis. *Advances in scattering theory and biomedical engineering*, chapter Solitary waves of the Bona-Smith system, pages 286–294. World Scientific, New Jersey, 2004. [xxvi](#)
- [dSV71] A.J.C. de Saint-Venant. Théorie du mouvement non-permanent des eaux, avec application aux crues des rivières et à l’introduction des marées dans leur lit. *C. R. Acad. Sc. Paris*, 73:147–154, 1871. [82](#)
- [Erd56] A. Erdélyi. *Asymptotic expansions*. Dover publications, 1956. [29](#)
- [ES94] Yu.V. Egorov and M.A. Shubin. *Partial Differential Equations*, volume 2 of *Encyclopaedia of Mathematical Sciences*, chapter Elements of the Modern Theory. Equations with Constant Coefficients. Springer, 1994. [29](#)
- [FB76] L. B. Freund and D. M. Barnett. A two-dimensional analysis of surface deformation due to dip-slip faulting. *Bull. Seism. Soc. Am.*, 66:667–675, 1976. [65](#), [72](#)
- [FD06] C. Fochesato and F Dias. A fast method for nonlinear three-dimensional free-surface waves. *Proc. R. Soc. A*, 462(2073):2715–2735, September 2006. [50](#)

- [FDG05] C. Fochesato, F. Dias, and R. Grimshaw. Generalized solitary waves and fronts in coupled Korteweg–de Vries systems. *Physica D: Nonlinear Phenomena*, 210:96–117, October 2005. [xxvi](#)
- [Fil28] L.N.G. Filon. On a quadrature formula for trigonometric integrals. *Proceedings of the Royal Society of Edinburgh*, 49:38–47, 1928. [3](#), [29](#), [47](#)
- [GBM⁺05] F.I. González, E.N. Bernard, C. Meinig, M.C. Eble, H.O. Mofjeld, and S. Stalin. The NTHMP tsunameter network. *Natural Hazards*, 35:25–39, 2005. [xxix](#), [28](#)
- [GGCCD05] M. Gomez-Gesteira, D. Cerqueiro, C. Crespo, and R. A. Dalrymple. Green water overtopping analyzed with a SPH model. *Ocean Engineering*, 32:223–238, 2005. [xxix](#)
- [GGD01] S. Grilli, P. Guyenne, and F. Dias. A fully non-linear model for three-dimensional overturning waves over an arbitrary bottom. *Int. J. Numer. Meth. Fluids*, 35:829–867, 2001. [50](#)
- [GGD04] M. Gomez-Gesteira and R. A. Dalrymple. Using SPH for wave impact on a tall structure. *Journal of Waterways, Port, Coastal, and Ocean Engineering*, 130:63–69, 2004. [xxix](#)
- [Ghi98] J.-M. Ghidaglia. Flux schemes for solving nonlinear systems of conservation laws. In J.J. Chattot and M. Hafez, editors, *Proceedings of the meeting in honor of P.L. Roe*, Arcachon, July 1998. [199](#), [200](#)
- [Ghi08] J.-M. Ghidaglia. *Finite volumes methods and complex multi-fluid flows*. In preparation, 2008. [126](#)
- [GHM98] M. Guesmia, P.H. Heinrich, and C. Mariotti. Numerical simulation of the 1969 Portuguese tsunami by a finite element method. *Natural Hazards*, 17:31–46, 1998. [50](#)
- [GKC96] J.-M. Ghidaglia, A. Kumbaro, and G. Le Coq. Une méthode volumes-finis à flux caractéristiques pour la résolution numérique des systèmes hyperboliques de lois de conservation. *C. R. Acad. Sci. I*, 322:981–988, 1996. [50](#), [71](#), [198](#)
- [GKC01] J.-M. Ghidaglia, A. Kumbaro, and G. Le Coq. On the numerical solution to two fluid models via cell centered finite volume method. *Eur. J. Mech. B/Fluids*, 20:841–867, 2001. [71](#), [198](#)

- [God59] S.K. Godunov. A finite difference method for the numerical computation of discontinuous solutions of the equations of fluid dynamics. *Mat. Sb.*, 47:271–290, 1959. [134](#), [137](#)
- [GP05] J.-M. Ghidaglia and F. Pascal. The normal flux method at the boundary for multidimensional finite volume approximations in cfd. *European Journal of Mechanics B/Fluids*, 24:1–17, 2005. [151](#), [153](#), [206](#)
- [GR00] I. S. Gradshteyn and M. Ryzhik. *Tables of Integrals, Series, and Products*. Academic Press, Orlando, Florida, 6 edition, 2000. [22](#)
- [GST01] S. Gottlieb, C.-W. Shu, and E. Tadmor. Strong stability-preserving high-order time discretization methods. *SIAM Review*, 43:89–112, 2001. [149](#)
- [GTS06] E.L. Geist, V.V. Titov, and C.E. Synolakis. Tsunami: wave of change. *Scientific American*, 294:56–63, 2006. [36](#)
- [Gus72] V.K. Gussyakov. *Mathematical problems of geophysics*, volume 3, chapter Generation of tsunami waves and ocean Rayleigh waves by submarine earthquakes, pages 250–272. Novosibirsk, VZ SO AN SSSR, 1972. in Russian. [3](#)
- [Gus76] V.K. Gussyakov. *Ill-posed problems of mathematical physics and problems of interpretation of geophysical observations*, chapter Estimation of tsunami energy, pages 46–64. Novosibirsk, VZ SO AN SSSR, 1976. in Russian. [3](#)
- [GV85] J.D. Goodman and R.J. Le Veque. On the accuracy of stable schemes for 2D conservation laws. *Math. Comp.*, 45(171):15–21, 1985. [139](#)
- [GVW02] S. Grilli, S. Vogelmann, and P. Watts. Development of a 3d numerical wave tank for modeling tsunami generation by underwater landslides. *Engng Anal. Bound. Elem.*, 26:301–313, 2002. [51](#)
- [GZI⁺79] S.K. Godunov, A. Zabrodine, M. Ivanov, A. Kraiko, and G. Prokopov. *Résolution numérique des problèmes multidimensionnels de la dynamique des gaz*. Editions Mir, Moscow, 1979. [127](#)
- [HA71] F. Harlow and A. Amsden. *Fluid dynamics*. LANL Monograph LA-4700, 1971. [127](#)
- [Ham73] J. Hammack. A note on tsunamis: their generation and propagation in an ocean of uniform depth. *Journal of Fluid Mechanics*, 60:769–799, 1973. [3](#), [36](#), [50](#), [65](#)

- [Har83] A. Harten. High resolution schemes for hyperbolic conservation laws. *J. Comp. Phys.*, 49:357–393, 1983. [138](#)
- [Has69] N. A. Haskell. Elastic displacements in the near-field of a propagating fault. *Bull. Seism. Soc. Am.*, 59:865–908, 1969. [66](#)
- [HB05] J. Hunt and J. M. Burgers. Tsunami waves and coastal flooding. *Mathematics TODAY*, pages 144–146, October 2005. [xviii](#)
- [HC89] D.G. Holmes and S.D. Connel. Solution of the 2d Navier-Stokes equations on unstructured adaptive grids. In *AIAA 9th Computational Fluid Dynamics Conference*, volume 89-1932-CP, June 1989. [141](#), [146](#), [147](#)
- [HG74] J.R. Houston and A.W. Garcia. Type 16 flood insurance study. Technical Report Report No. H-74-3, USACE WES Report No. H-74-3, 1974. [36](#)
- [HH70] K.L. Heitner and G.W. Housner. Numerical model for tsunami runup. *J. Waterway, Port, Coastal and Ocean Engineering*, 96:701–719, 1970. [85](#)
- [HPHO] F. Hecht, O. Pironneau, A. Le Hyaric, and K. Ohtsuka. *FreeFem++*. Laboratoire JL Lions, University of Paris VI, France. [70](#)
- [HS74] J.L. Hammack and H. Segur. The Korteweg–de Vries equation and water waves. Part 2. Comparison with experiments. *J Fluid Mech*, 65:289–314, 1974. [32](#), [38](#), [40](#)
- [HS78] J.L. Hammack and H. Segur. The Korteweg–de Vries equation and water waves. Part 3. Oscillatory waves. *J Fluid Mech*, 84:337–358, 1978. [32](#)
- [IS79] T. Iwasaki and R. Sato. Strain field in a semi-infinite medium due to an inclined rectangular fault. *J. Phys. Earth*, 27:285–314, 1979. [10](#)
- [Ish75] M. Ishii. *Thermo-Fluid Dynamic Theory of Two-Phase Flow*. Eyrolles, Paris, 1975. [125](#), [162](#)
- [JTSPS96] L. Jiang, C.-L. Ting, M. Perlin, and W.W. Schultz. Moderate and steep Faraday waves: instabilities, modulation and temporal asymmetries. *J. Fluid Mech.*, 329:275–307, 1996. [87](#)
- [JW04] D.D. Joseph and J. Wang. The dissipation approximation and viscous potential flow. *J. Fluid Mech.*, 505:365–377, 2004. [171](#)

- [Kaj63] K. Kajiura. The leading wave of tsunami. *Bull. Earthquake Res. Inst., Tokyo Univ.*, 41:535–571, 1963. [3](#), [36](#)
- [Kaj70] K. Kajiura. Tsunami source, energy and the directivity of wave radiation. *Bull. Earthquake Research Institute*, 48:835–869, 1970. [65](#), [73](#)
- [KCKD00] A.B. Kennedy, Q. Chen, J.T. Kirby, and R.A. Dalrymple. Boussinesq modelling of wave transformation, breaking, and runup. *J. Waterway, Port, Coastal and Ocean Engineering*, 126:39–47, 2000. [85](#)
- [KDD07] Y. Kervella, D. Dutykh, and F. Dias. Comparison between three-dimensional linear and nonlinear tsunami generation models. *Theor. Comput. Fluid Dyn.*, 21:245–269, 2007. [69](#), [70](#)
- [KdV95] D.J. Korteweg and G. de Vries. On the change of form of long waves advancing in a rectangular canal, and on a new type of long stationary waves. *Phil. Mag.*, 39(5):422–443, 1895. [3](#)
- [Kel87] Lord (W. Thomson) Kelvin. *Phil. Mag.*, 23(5):252–257, 1887. [29](#)
- [Kel63] J.B. Keller. Tsunamis: water waves produced by earthquakes. *Int. Un. Geodesy & Geophys. Monograph*, 24:154–166, 1963. [3](#)
- [Kir03] J.T. Kirby. *Advances in Coastal Modeling, V. C. Lakhan (ed)*, chapter Boussinesq models and applications to nearshore wave propagation, surfzone processes and wave-induced currents, pages 1–41. Elsevier, 2003. [57](#), [83](#)
- [KM75] T. Kakutani and K. Matsuuchi. Effect of viscosity on long gravity waves. *J. Phys. Soc. Japan*, 39:237–246, 1975. [171](#), [192](#)
- [KMC03] S.-E. Kim, B. Makarov, and D. Caraeni. A multi-dimensional linear reconstruction scheme for arbitrary unstructured grids. Technical report, Fluent Inc., 2003. [147](#)
- [KML05] E.A. Kulikov, P.P. Medvedev, and S.S. Lappo. Satellite recording of the Indian Ocean tsunami on December 26, 2004. *Doklady Earth Sciences A*, 401:444–448, 2005. [49](#)
- [Kol72] N.E. Kolgan. Application of the minimum-derivative principle in the construction of finite-difference schemes for numerical analysis of discontinuous solutions in gas dynamics. *Uchenye Zapiski TsaGI [Sci. Notes Central Inst. Aerodyn]*, 3(6):68–77, 1972. [137](#), [138](#)

- [Kol75] N.E. Kolgan. Finite-difference schemes for computation of three dimensional solutions of gas dynamics and calculation of a flow over a body under an angle of attack. *Uchenye Zapiski TsAGI [Sci. Notes Central Inst. Aerodyn]*, 6(2):1–6, 1975. [137](#), [138](#)
- [KS06] K. Kanoglu and C. Synolakis. Initial value problem solution of nonlinear shallow water-wave equations. *Phys. Rev. Lett.*, 97:148501, 2006. [xxix](#), [50](#)
- [KWC⁺98] J. T. Kirby, G. Wei, Q. Chen, A. B. Kennedy, and R. A. Dalrymple. Funwave 1.0, fully nonlinear boussinesq wave model documentation and user’s manual. Research Report No. CACR-98-06, 1998. [xxiii](#)
- [Lam32] H. Lamb. *Hydrodynamics*. Cambridge University Press, 1932. [83](#), [170](#), [186](#)
- [Lax73] P.D. Lax. *Hyperbolic Systems of Conservation Laws and the Mathematical Theory of Shock Waves*. SIAM, Philadelphia, Penn., 1973. [138](#)
- [LeV98] R.J. LeVeque. Balancing source terms and flux gradients in high-resolution Godunov methods: the quasi-steady wave-propagation algorithm. *J. Computational Phys.*, 146:346–365, 1998. [50](#)
- [LH74] M. S. Longuet-Higgins. On the mass, momentum, energy and circulation of a solitary wave. *Proc. R. Soc. Lond. A*, 337:1–13, 1974. [xxvii](#)
- [LH92] M.S. Longuet-Higgins. Theory of weakly damped stokes waves: a new formulation and its physical interpretation. *J. Fluid Mech.*, 235:319–324, 1992. [85](#), [169](#)
- [LKA⁺05] T. Lay, H. Kanamori, C. J. Ammon, M. Nettles, S. N. Ward, R. C. Aster, S. L. Beck, S. L. Bilek, M. R. Brudzinski, R. Butler, H. R. DeShon, G. Ekstrom, K. Satake, and S. Sipkin. The great Sumatra-Andaman earthquake of 26 December 2004. *Science*, 308:1127–1133, 2005. [xxi](#), [xxvi](#), [xxvii](#), [3](#), [40](#), [43](#)
- [LL83] P.L.-F. Liu and J.A. Liggett. *Applications of boundary element methods to problems of water waves*, chapter Chapter 3, pages 37–67. 1983. [37](#)
- [LO04] P.L.-F. Liu and A. Orfila. Viscous effects on transient long-wave propagation. *J. Fluid Mech.*, 520:83–92, 2004. [171](#), [193](#)
- [Lov44] A. E. H. Love. *A treatise on the mathematical theory of elasticity*. Dover Publications, New York, 1944. [6](#), [8](#)

- [LPC07] P.L.-F. Liu, Y.S. Park, and E.A. Cowen. Boundary layer flow and bed shear stress under a solitary wave. *J. Fluid Mech.*, 574:449–463, 2007. [178](#)
- [LSVO06] P.L.-F. Liu, G. Simarro, J. Vandever, and A. Orfila. Experimental and numerical investigation of viscous effects on solitary wave propagation in a wave tank. *Coastal Engineering*, 53:181–190, 2006. [192](#)
- [Mad03] R. Madariaga. Radiation from a finite reverse fault in half space. *Pure Appl. Geophys.*, 160:555–577, 2003. [67](#), [72](#)
- [Mar64] T. Maruyama. Statical elastic dislocations in an infinite and semi-infinite medium. *Bull. Earthquake Res. Inst., Tokyo Univ.*, 42:289–368, 1964. [6](#)
- [Mas03] T. Masterlark. Finite element model predictions of static deformation from dislocation sources in a subduction zone: Sensivities to homogeneous, isotropic, poisson-solid, and half-space assumptions. *J. Geophys. Res.*, 108(B11):2540, 2003. [5](#), [65](#)
- [MBS03] P. A. Madsen, H. B. Bingham, and H. A. Schaffer. Boussinesq-type formulations for fully nonlinear and extremely dispersive water waves: derivation and analysis. *Proc. R. Soc. Lond. A*, 459:1075–1104, 2003. [xxiv](#)
- [MBS05] A. Megna, S. Barba, and S. Santini. Normal-fault stress and displacement through finite-element analysis. *Annals Geophys.*, 48:1009–1016, 2005. [65](#), [73](#)
- [MC50] R. D. Mindlin and D. H. Cheng. Nuclei of strain in the semi-infinite solid. *J. Appl. Phys.*, 21:926–930, 1950. [7](#)
- [Mei94] C.C. Mei. *The applied dynamics of ocean surface waves*. World Scientific, 1994. [171](#), [172](#), [177](#)
- [MG96] S. Musferija and D. Gosman. Finite-volume CFD procedure and adaptive error control strategy for grids of arbitrary topology. *J. Comp. Phys.*, 138:766–787, 1996. [140](#)
- [Min36] R. D. Mindlin. Force at a point in the interior of a semi-infinite medium. *Physics*, 7:195–202, 1936. [7](#)
- [Mit07] D.E. Mitsotakis. Boussinesq systems in two space dimensions over a variable bottom for the generation and propagation of tsunami waves. *Mathematics and Computers in Simulation*, submitted, 2007. [4](#)

- [MMS91] P. A. Madsen, R. Murray, and O. R. Sorensen. A new form of the Boussinesq equations with improved linear dispersion characteristics. *Coastal Engineering*, 15:371–388, 1991. [104](#)
- [Mon94] J. J. Monaghan. Simulating free surface flows with SPH. *Physica D*, 110:399–406, 1994. [xxix](#)
- [MS71] L. Mansinha and D. E. Smylie. The displacement fields of inclined faults. *Bull. Seism. Soc. Am.*, 61:1433–1440, 1971. [65](#)
- [MS98] P. A. Madsen and H. A. Schaffer. Higher-order Boussinesq-type equations for surface gravity waves: Derivation and analysis. *Phil. Trans. R. Soc. Lond. A*, 356:3123–3184, 1998. [83](#), [91](#), [100](#)
- [Mur89] R. J. Murray. Short wave modelling using new equations of Boussinesq type. In *Proc., 9th Australian Conf. on Coast. and Oc. Engrg.*, 1989. [104](#)
- [Mur92] J.D. Murray. *Asymptotic Analysis*. Springer, 1992. [29](#)
- [New77] A. C. Newell. Finite amplitude instabilities of partial difference equations. *SIAM Journal of Applied Mathematics*, 33:133–160, 1977. [112](#)
- [NSS⁺05] S. Neetu, I. Suresh, R. Shankar, D. Shankar, S.S.C. Shenoi, S.R. Shetye, D. Sundar, and B. Nagarajan. Comment on “The Great Sumatra-Andaman Earthquake of 26 December 2004”. *Science*, 310:1431a–1431b, 2005. [3](#)
- [Nwo93] O. Nwogu. Alternative form of Boussinesq equations for nearshore wave propagation. *J. Waterway, Port, Coastal and Ocean Engineering*, 119:618–638, 1993. [57](#), [83](#), [91](#), [102](#), [104](#)
- [OK07] Y. Okumura and Y. Kawata. Effects of rise time and rupture velocity on tsunami. *Proceedings of the Seventeenth International Offshore and Polar Engineering Conference*, III, 2007. [66](#)
- [Oka85] Y. Okada. Surface deformation due to shear and tensile faults in a half-space. *Bull. Seism. Soc. Am.*, 75:1135–1154, 1985. [xxiii](#), [4](#), [7](#), [9](#), [10](#), [36](#), [38](#), [65](#), [72](#)
- [Oka92] Y. Okada. Internal deformation due to shear and tensile faults in a half-space. *Bull. Seism. Soc. Am.*, 82:1018–1040, 1992. [7](#), [10](#)
- [Osh84] S. Osher. Riemann solvers, the entropy condition, and difference approximations. *SIAM J. Numer. Anal.*, 21(2):217–235, 1984. [137](#)

- [OTM01] T. Ohmachi, H. Tsukiyama, and H. Matsumoto. Simulation of tsunami induced by dynamic displacement of seabed due to seismic faulting. *Bull. Seism. Soc. Am.*, 91:1898–1909, 2001. [65](#), [66](#)
- [Per66] D.H. Peregrine. Calculations of the development of an undual bore. *J. Fluid Mech.*, 25:321–330, 1966. [3](#)
- [Per67] D. H. Peregrine. Long waves on a beach. *J. Fluid Mech.*, 27:815–827, 1967. [57](#), [83](#), [106](#), [119](#)
- [Per72] D. H. Peregrine. *Waves on Beaches and Resulting Sediment Transport*, chapter Equations for water waves and the approximation behind them, pages 95–121. Academic Press, New York, 1972. [99](#)
- [Per03] D. H. Peregrine. Water-wave impact on walls. *Annu. Rev. Fluid Mech.*, 35:23–43, 2003. [123](#)
- [Pet91] T. Peterson. A note on the convergence of the discontinuous Galerkin method for a scalar hyperbolic equation. *SIAM J. Numer. Anal.*, 28(1):133–140, 1991. [137](#)
- [PL71] G.I. Petrashen' and K.P. Latyshev. *Asymptotic Methods and Stochastic Models in Problems of Wave Propagation*. American Mathematical Society, 1971. [29](#)
- [Pod68] G.S. Podyapolsky. The generation of linear gravitational waves in the ocean by seismic sources in the crust. *Izvestiya, Earth Physics, Akademia Nauk SSSR*, 1:4–12, 1968. [3](#)
- [Pre65] F. Press. Displacements, strains and tilts at tele-seismic distances. *J. Geophys. Res.*, 70:2395–2412, 1965. [7](#)
- [Qui97] J. Quiblier. *Propagation des ondes en géophysique et en géotechnique. Modélisation par méthodes de Fourier*. Paris: Editions Technip, 1997. [67](#)
- [RFF91] K.D. Ruvinsky, F.I. Feldstein, and G.I. Freidman. Numerical simulations of the quasistationary stage of ripple excitation by steep-capillary waves. *J. Fluid Mech.*, 230:339–353, 1991. [85](#), [87](#)
- [Roe81] P. L. Roe. Approximate riemann solvers, parameter vectors and difference schemes. *J. Comput. Phys.*, 43:357–372, 1981. [200](#)

- [Sab86] P. Sabatier. *Encyclopedia of fluid mechanics*, chapter Formation of waves by ground motion, pages 723–759. Gulf Publishing Company, 1986. [3](#)
- [SB06] C.E. Synolakis and E.N. Bernard. Tsunami science before and beyond Boxing Day 2004. *Phil. Trans. R. Soc. A*, 364:2231–2265, 2006. [36](#), [47](#), [69](#)
- [Shu88] C.-W. Shu. Total-variation-diminishing time discretizations. *SIAM J. Sci. Statist. Comput.*, 9:1073–1084, 1988. [149](#)
- [SKP96] C. Skandrani, C. Kharif, and J. Poitevin. Nonlinear evolution of water surface waves: the frequency down-shift phenomenon. *Contemp. Math.*, 200:157–171, 1996. [85](#)
- [SM71] D. E. Smylie and L. Mansinha. The elasticity theory of dislocations in real earth models and changes in the rotation of the earth. *Geophys. J.R. Astr. Soc.*, 23:329–354, 1971. [4](#)
- [SM74] R. Sato and M. Matsu’ura. Strains and tilts on the surface of a semi-infinite medium. *J. Phys. Earth*, 22:213–221, 1974. [10](#)
- [SO88] C.-W. Shu and S. Osher. Efficient implementation of essentially non-oscillatory shock-capturing schemes. *J. Comput. Phys.*, 77:439–471, 1988. [149](#)
- [Sod78] G. A. Sod. A survey of several finite difference methods for systems of nonlinear hyperbolic conservation laws. *J. Comput. Phys.*, 43:1–31, 1978. [153](#)
- [SR02] R. J. Spiteri and S. J. Ruuth. A new class of optimal high-order strong-stability-preserving time discretization methods. *SIAM Journal on Numerical Analysis*, 40:469–491, 2002. [149](#)
- [Ste58] J. A. Steketee. On Volterra’s dislocation in a semi-infinite elastic medium. *Can. J. Phys.*, 36:192–205, 1958. [4](#), [5](#)
- [Sug91] N. Sugimoto. Burgers equation with a fractional derivative; hereditary effects on nonlinear acoustic waves. *J. Fluid Mech.*, 225:631–653, 1991. [193](#)
- [SVBM02] B. Spivak, J.-M. Vanden-Broeck, and T. Miloh. Free-surface wave damping due to viscosity and surfactants. *European Journal of Mechanics B-Fluids*, 21:207–224, 2002. [85](#)
- [Syn87] C. Synolakis. The runup of solitary waves. *J. Fluid Mech.*, 185:523–545, 1987. [xxviii](#)

- [TF98] M. Tajchman and P. Freydier. Schéma VFFC : application à l'étude d'un cas test d'ébullition en tuyau droit représentant le fonctionnement en bouillotte d'un coeur rep. Technical report, Note EDF HT-33/98/033/A, 1998. [203](#)
- [THT02] M.I. Todorovska, A. Hayir, and M.D. Trifunac. A note on tsunami amplitudes above submarine slides and slumps. *Soil Dynamics and Earthquake Engineering*, 22:129–141, 2002. [3](#), [44](#)
- [Tre00] Lloyd N. Trefethen. *Spectral methods in MatLab*. Society for Industrial and Applied Mathematics, Philadelphia, PA, USA, 2000. [106](#)
- [TS94] S. Tadepalli and C. E. Synolakis. The run-up of n -waves on sloping beaches. *Proc. R. Soc. Lond. A*, 445:99–112, 1994. [xxviii](#)
- [TS98] V. V. Titov and C. E. Synolakis. Numerical modeling of tidal wave runup. *J. Waterway, Port, Coastal, and Ocean Engineering*, 124:157–171, 1998. [xxiii](#), [37](#), [47](#), [49](#), [69](#)
- [TT01] M. I. Todorovska and M. D. Trifunac. Generation of tsunamis by a slowly spreading uplift of the seafloor. *Soil Dynamics and Earthquake Engineering*, 21:151–167, 2001. [2](#), [3](#), [37](#), [44](#), [64](#), [65](#)
- [TT05] S. Tinti and R. Tonini. Analytical evolution of tsunamis induced by near-shore earthquakes on a constant-slope ocean. *Journal of Fluid Mechanics*, 535:33–64, 2005. [xxviii](#)
- [Tuc74] E.O. Tuck. The effect of a surface layer of viscous fluid on the wave resistance of a thin ship. *J. Ship Research*, 18:265–271, 1974. [36](#), [62](#), [85](#)
- [Tuc79] E.O. Tuck. Models for predicting tsunami propagation. In L.S. Hwang and Tetra Tech Inc. Y.K. Lee, editors, *NSF Workshop on Tsunamis, California*, pages 43–109, 1979. [37](#), [62](#)
- [Urs53] F. Ursell. The long-wave paradox in the theory of gravity waves. *Proc. Camb. Phil. Soc.*, 49:685–694, 1953. [4](#), [52](#), [91](#)
- [vdD72] R.D. van den Driessche, P. & Braddock. On the elliptic generating region of a tsunami. *J. Mar. Res.*, 30:217–226, 1972. [3](#)
- [vL79] B. van Leer. Towards the ultimate conservative difference scheme v: a second order sequel to Godunov' method. *J. Comput. Phys.*, 32:101–136, 1979. [137](#)

- [vL06] B. van Leer. Upwind and high-resolution methods for compressible flow: From donor cell to residual-distribution schemes. *Communications in Computational Physics*, 1:192–206, 2006. [138](#)
- [Vol07] V. Volterra. Sur l'équilibre des corps élastiques multiples connexes. *Annales Scientifiques de l'École Normale Supérieure*, 24(3):401–517, 1907. [5](#), [6](#)
- [VS93] M. Villeneuve and S.B. Savage. Nonlinear, dispersive, shallow-water waves developed by a moving bed. *J. Hydraulic Res.*, 31:249–266, 1993. [37](#)
- [War01] S.N. Ward. Landslide tsunami. *J. Geophysical Res.*, 106:11201–11215, 2001. [47](#)
- [Wes35] H. M. Westergaard. General solution of the problem of elastostatics of an n -dimensional homogeneous isotropic solid in an n -dimensional space. *Bull. Amer. Math. Soc.*, 41:695, 1935. [7](#)
- [Whi99] G.B. Whitham. *Linear and nonlinear waves*. John Wiley & Sons Inc., New York, 1999. [99](#)
- [Wit84] J. M. Witting. A unified model for the evolution of nonlinear water waves. *J. Comput. Phys.*, 56:203–236, 1984. [105](#)
- [WKGS95] G. Wei, J. T. Kirby, S. T. Grilli, and R. Subramanya. A fully nonlinear Boussinesq model for surface waves. Part 1. Highly nonlinear unsteady waves. *J. Fluid Mech.*, 294:71–92, 1995. [57](#), [83](#), [91](#)
- [Wu81] T.Y. Wu. Long waves in ocean and coastal waters. *Journal of Engineering Mechanics*, 107:501–522, 1981. [170](#)
- [Zel91] J.A. Zelt. The run-up of nonbreaking and breaking solitary waves. *Coastal Engineering*, 15:205–246, 1991. [85](#)
- [ZG71] N.J. Zabusky and C.C.J. Galvin. Shallow water waves, the Korteweg-de Vries equation and solitons. *J. Fluid Mech.*, 47:811–824, 1971. [170](#)
- [ZKPD05] V.E. Zakharov, A.O. Korotkevich, A.N. Pushkarev, and A.I. Dyachenko. Mesoscopic wave turbulence. *JETP Lett.*, 82:487–491, 2005. [171](#), [193](#)
- [ZV97] W. Zhang and J. Vinals. Pattern formation in weakly damped parametric surface waves. *J. Fluid Mech.*, 336:301–330, 1997. [87](#)